**Department**
Address
Address
Address
Coventry CV4 8UW UK
T (0)24 7615 xxxxx
F (0)24 7615 xxxxx
E youremail@warwick.ac.uk
www.warwick.ac.uk

# Synthesis of Glyconanoparticles *via* Emulsion Polymerisation Techniques and Their use to Probe Lectin Interactions and in pH Responsive Drug Delivery

**Andrew Martin Lunn**

A thesis submitted in partial fulfilment of the requirements for the degree of

**Doctor of Philosophy in Chemistry**

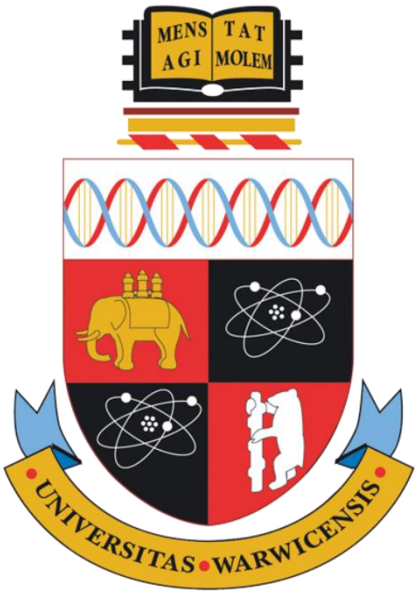


Department of Chemistry

University of Warwick

January 2019

“Ook”

*The Librarian of the Unseen University, T. Pratchett*

# Table of Contents

## List of Figures

## List of Tables



## List of Schemes

## List of Publications

The following publications have been produced from the work presented in this thesis:

**Andrew M. Lunn**; Gurnani, Pratik, and Sébastien Perrier. "Synthesis of mannosylated and PEGylated nanoparticles via RAFT emulsion polymerisation, and investigation of particle-lectin aggregation using turbidimetric and DLS techniques." *Polymer* 106 (2016): 229-237.

**Andrew M. Lunn**, and Sébastien Perrier. "Synthesis of Sub-100 nm Glycosylated Nanoparticles via a One Step, Free Radical, and Surfactant Free Emulsion Polymerization." *Macromolecular rapid communications* (2018): 1800122.

**Andrew M. Lunn**, Meera Unnikrishnan and Sébastien Perrier "Dual pH Responsive Macrophage Targeted Isoniazid Particles for Intracellular Tuberculosis Therapy" *In draft.*

## Abbreviations

A549- Adenocarcinoma human alveolar basal epithelial cells

Abs- Absorption

ACVA- 4,4'-Azobis (4-CyanoValeric Acid)

ADME- Absorption Metabolism Degradation and Excretion

AIBN- 2,2'-Azobis(2-methylprpionitrile)

ANOVA- Analysis of Variance

API- Active Pharmaceutical Ingredient

ATCC- America Type Culture Collection

ATRP- Atom Transfer Radical Polymerisation

*n*BA- *n*-Butyl Acrylate

BBB- Blood Brain Barrier

BCG- Bacilli Calmette Guerin

$BF_3$- Boron trifluoride

C%- conversion of monomer to polymer

$C_{CTA}$ – Chain Transfer Constant

CD- Cluster of Differentiation

CFU- Colony Forming Unit

$C_M$- Chain transfer constant of Monomer

ConA- Concanavalin A

CRD- Carbohydrate Recognition Domain

CREKA- Cysteine-Arginine-Glutamine-Lysine-Alanine

CRP- Controlled Radical Polymerisation

CSIRO- Commonwealth Scientific and Industrial Research Organisation

CT- Computerised Tomography

CTA- Chain Transfer Agent

Cy3- Cyanine 3

Cy3Am- Cyanine 3 Acrylamide

*Đ*- Dispersity

DAAm- Diacetone Acrylamide

DAPI- 4′,6-Diamidino-2-Phenylindole

DCM- Di-Chloro Methane

DC-SIGN- Dendritic Cell-Specific Intercellular Adhesion molecule-3-Grabbing Non-integrin

DI- Deionised

DLS- Dynamic Light Scattering

DMAEMA- 2-(Dimethylamino)Ethyl Methacrylate

DMEM- Dulbecco's Modified Eagle Media

DMF- Dimethyl Formamide

DMSO- Dimethyl Sulfoxide

DP- Degree of Polymerisation

DPAEMA- Di-isoPropyl Amino Ethyl Methcrylate

DRI- Differential Refractive Index

DSC- Differential Scanning Calorimetry

Em- Emission

EPHP- 1-Ethylpiperidine Hypophosphite

EPR- Enhanced Permeability Retention

eV- electron Volt

*f* – Initiator efficiency

FDA- United States Food and Drug Administration

FTIR- Fourier Transform Infrared

GFP- Green Fluorescent Protein

GI- Gastrointestinal

GPC- Gel Permeation Chromatography

HEAm- Hydroxyethyl Acrylamide

HeLa- Henrietta Lacks, cervical cancer cell line

HIV- Human Immunodeficiency Virus

HPLC- High Performance Liquid Chromatography

I – Initiator

INH- Isoniazid

$k_d$- coefficient of initiator decomposition

kDa- kilodalton

$k_p$- coefficient of polymerisation

KPS- Potassium Persulphate

$k_t$- coefficient of termination

LactAm- D-Lactose-1-oxyethyl Acrylamide

LCST- Lower Critical Solution Temperature

M- Monomer

m/z- mass over charge

$M^{\bullet}$ - Propagating radical species

mAb- monoclonal Antibody

ManAm- α-D-Mannopyran-1-oxyethyl Acrylamide

MeOH- Methanol

$M_n$- Number average Molecular weight

MOI- Multiplicity of Infection

MS- Mass Spectrometry

mV- milli Volts

$M_w$- Weight average molecular weight

n/s- non significant

NAT- N-Acryloyl Thiomorpholine

NBMA- 2-Nitrobenzyl Methacrylate

NMM- N-Methyl Morpholine

NMP- Nitroxide Mediated Polymerisation

NMR- Nuclear Magnetic Resonance

OAc- Acetyl

PABTC- 2-(*n*-butyltrithiocarbonylthio)propionic acid

PB- Phosphate Buffer

PBS- Phosphate Buffered Saline

Pdi- Polydispersity index

PEG- Poly(Ethylene Glycol)

PEGA- Poly(Ethylene Glycol) methyl ether Acrylate

pH- potential Hydrogen

PISA- Polymerisation Induced Self-Assembly

PLA- Poly(Lactic Acid)

PLGA- poly(lactic-*co*-glycolic acid)

PMA- Phorbol Myristate Acetate

POx- Poly(2-Oxazoline)

PPA- Particles Per Aggregate

PSA- Prostate Specific Antigen

PVA- Poly(Vinyl Alcohol)

QD- Quantum Dot

RAFT- Reversible Addition Fragmentation chain Transfer (polymerisation)

$RCA_{120}$- Ricinus Communis Agglutinin 120

RDRP- Reversible Deactivation Radical Polymerisation

RGD- Arginylglycylaspartic acid

$R_i$- Rate of initiation

RI- Refractive Index

ROS- Reactive Oxygen Species

$R_p$- Rate of polymerisation

rpm- revolutions per minute

RPMI- Roswell Park Memorial Institute (Media)

$R_t$- Rate of termination

RT- Room Temperature

SD- Standard Deviation

SDS- Sodium Dodecyl Sulphate

SE- Standard Error

SEC- Size Exclusion Chromatography

SEM- Scanning Electron Microscopy

siRNA- short interfering Ribose Nucleic Acid

Sty- Styrene

TB- Tuberculosis

TEM- Transmission Electron Microscopy

TEMPO- (2,2,6,6-Tetramethylpiperidin-1-yl)oxyl

$T_g$- Glass transition Temperature

THP-1- Tamm Horsfal Protein-1, leukaemia monocyte cells

TLC- Thin Layer Chromatography

TRIS- Tris(hydroxymethyl) aminomethane

UV- Ultra Violet

VA-044- 2,2’-Azobis[2-(2-imidazolin-2-yl)propane]dihydrochloride

VEGF- Vascular Endothelial Growth Factor

Vis- Visible

wt%- weight percent

XTT- 2,3-bis-(2-methoxy-4-nitro-5-sulfophenyl)-2H-tetrazolium-5- carboxanilide

ζ- Zeta

## Acknowledgements

So many people who are not immediately obvious have influenced me and helped me over the years towards undertaking my PhD.

First my parents. For as long as I can remember I have been encouraged to take every opportunity to pursue knowledge and education, opportunities that my Mum and Dad did not have. I hope I have achieved in making the most of the opportunities that they have given me, and made them proud. Only now as an adult do I appreciate the sacrifices that they made for me and my siblings to do simple things like going on school trips when money was tight. On the note of money, I would also like to thank them for not being too annoyed that I left a well-paid job to come back to university and undertake both my MSc and PhD. Thank you both for giving me such a strong work ethic and attitude to learning. My siblings need a mention too, mainly because without feeling the need to compete with you all my whole life I never would have achieved so much. I must also thank Stef and Si by name, you gave me a place to live when I started here and have fed me ever since, thank you.

I would not have even gone to university in the first place were it not for inspirational teachers, in particular my chemistry teacher Cathy Webb and my biology teacher Andy Coomber. Not only were you great teachers, you looked after me emotionally and got me to shut up and do some work. Thank you and all (well most) of my other school teachers.

A PhD had never occurred as an option to me were it not for my MPharm supervisor and friend Elsie Gaskell. I owe you a debt in helping me in my first experiences in a research lab, and genuinely inspiring me to the career path I am now on.

I must of course thank Seb, who has given me the opportunity to undertake both my MSc and PhD research in his labs. Other than paying me (thanks), you have taught me about how research should and can be done, kept me on track and allowed me to follow research that you were not sure about at first, some paid off and some didn't. I think it's one of the most important parts to discovery that researchers are allowed to try things out and follow an interesting result. That is something that either, through deliberately ignoring what we are getting up to or through active encouragement, you do consistently. Moreover, I think you are a good person, and I will continue throughout my career to surround myself with good honest people like you.

Working in the Perrier group has been a rewarding experience. I wouldn't have been able to do what I have done without the help of everyone in the group at some point, the post-docs: Guillaume G, Johannes, Sylvain, Matthias, Ed, Ximo, Qiao, Jie, Raoul and Carlos, and the PhD students: Liam, Sophie, Tammie, Caroline, Alex, Majda, Joji, Guillaume, Robert, Julia, Agnes, Andy, Tom, Sean, Fannie and Satu. These people and other visiting students made the time here worthwhile. The one student I haven't mentioned, the man with a hand in my thesis (literally, it's in section 2.3.7.) is Pratik. He has pretty much been a second supervisor for me, and I am grateful for all that he has taught me, not least about star wars and harry potter (even if I didn't want to know it). Seriously, without you Pratik, my PhD would have been tougher and less fun, so thank you.

Finally I need to thank the single most consistent person throughout my PhD, Emily. You have suffered more than I can think of: late nights, "just popping to life science" for hours, proof reading, stress, and at the end of it all me moving away. I cannot imagine having done this without you, you have made the experience easier and been there for me when I needed you. Thank you from the bottom of my heart.

## Declaration

Experimental work contained within this thesis is original research carried out by the author, unless otherwise stated, in the Department of Chemistry at the University of Warwick, between October 2015 and November 2018. No material contained has been submitted for any other degree, or at any other institution.

Results from other authors are referenced in the usual manner.

Signed:_____ Date:_____

Andrew Martin Lunn

# Abstract

The objectives of this thesis are to develop a simple method of synthesising glyconanoparticles, use these particles to explore the impact of particle size and hardness on lectin binding, and to develop a targeted antibiotic delivery system.

Nanoparticles have various properties that can be modified to improve their performance such as: size, morphology and surface charge. They can also be surface functionalised with sugars such that they target a specific location through interaction with cell surface lectins. Glyconanoparticles may be synthesised in a variety of ways. One suitable method of preparation is emulsion polymerisation, a classic emulsion polymerisation being free radical with the addition of surfactant. Methods to improve the biological properties of the resulting latex include RAFT emulsion polymerisation and a classic free radical emulsion polymerisation, without the addition of a surfactant. The former potentially suffers from being prohibitively expensive and time consuming, and the latter from poor size control and lack of surface functionality.

Glycosylated nanoparticles were initially synthesised *via* RAFT emulsion polymerisation; subsequently a simplified free radical surfactant free emulsion polymerisation was used, with the addition of a hydrophilic co-monomer, to improve size control and impart surface functionality. Glyconanoparticles between 50-350 nm in diameter were produced with both methods. The particles were subsequently used to determine the effect of particle size and core glass transition temperature ($T_g$) on lectin induced aggregation. Larger particles, and those with a "soft" core above their $T_g$ were quantitatively shown to aggregate to a greater extent, with more particles per aggregate. The free radical technique was further used to produce a pH responsive, mannosylated nanoparticle, capable of: targeting macrophages, selectively releasing isoniazid intracellularly and breaking up after endocytosis. This system was shown to eradicate intracellular mycobacteria (BCG) *in cellulo* at physiological concentrations.

Overall this thesis presents the facile synthesis of glyconanoparticles suitable for a wide range of applications and uses them to explore the influence of size and hardness on particle-lectin interactions. The same synthetic technique is used to produce a macrophage targeted, dual pH responsive nanoparticle capable of delivering isoniazid intracellularly.

# *Chapter 1*

## Biomedical uses of nanoparticles and their synthesis *via* emulsion polymerisation

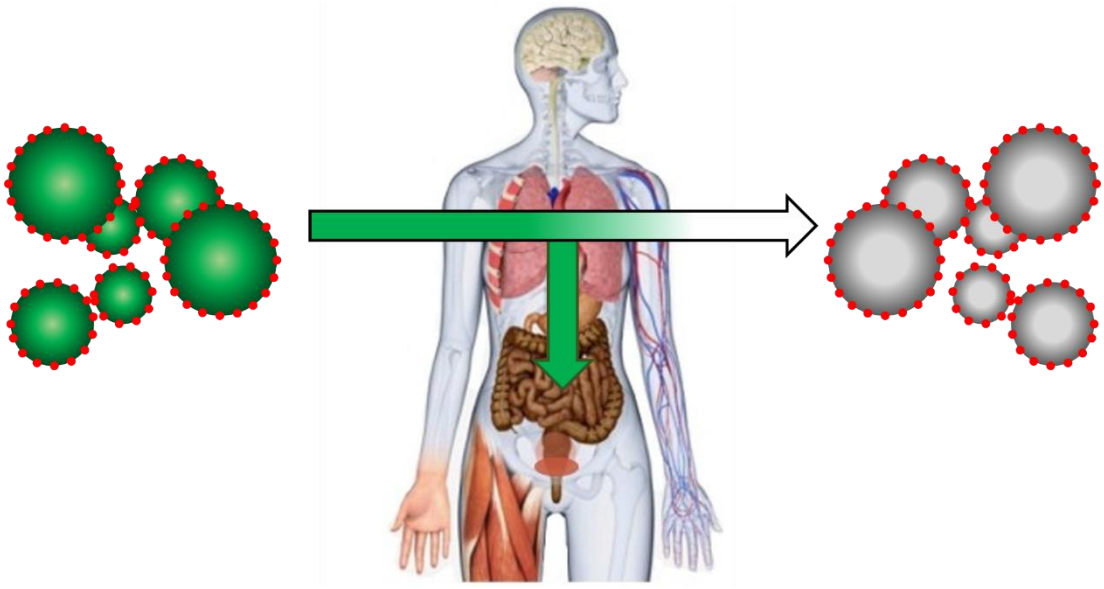

## 1.1 Nanoparticles in Biomedicine

According to the definition from the National Nanotechnology Initiative, a nanoparticle is a system with a diameter between 1-100 nm.[1] Commonly, and in this thesis, the term is applied to particles with diameters below 1000 nm. Nanotechnology has found uses from the oil industry to the production of photonics.[2-4] One area in which it has had a major impact though, is biomedicine.[1] Nanoparticle research in the biomedical arena has, over recent decades become a vastly expanding area of research. Particles of varying composition based on polymers, liposomes, metals or silica have found uses throughout the field.[5-9] Their applications have included use as: imaging agents, diagnostics and drug delivery agents.[10, 11]

### 1.1.1 Nanoparticles as Imaging and Diagnostic Agents

The use of nanoparticles as diagnostic and imaging aids has commonly utilised metal particles such as gold, silver and metal oxides (e.g. $Fe_3O_4$).[12] Gold nanoparticles have received a considerable amount of attention as imaging aids, due to their high X-ray attenuation, low toxicity and ease of synthesis. The synthesis is typically achieved through the reduction of a gold salt (e.g. $HAuCl_4$) with citric acid that further acts as a stabilising agent.[13, 14] The high electron density of gold nanoparticles compared to the standard iodine contrast agents has made them useful in Computerised Tomography (CT) imaging, particularly when entrapped within a polymeric structure such as a dendrimer.[15-17] Non-functionalised gold nanoparticles may be used to show blood pooling, or potentially a tumour environment *via* accumulation from the enhanced permeability and retention (EPR) effect, although the efficiency of the EPR effect for targeting tumours is potentially very low and discussed fully in section 1.3.1.[18] Functionalising their surface however, not only can improve their colloidal stability but direct them to a site of interest for higher contrast imaging *in vivo*.[14] Some examples using this concept include functionalising nanoparticles with "prostate specific antigen" (PSA) in order to obtain a clear image of a prostate tumour, or the use of a targeting peptide to reveal thrombus location.[19, 20] As diagnostics tools for purposes other than in imaging, the relative ease of functionalisation has led to a number of reports using metal nanoparticles in "bio-barcode" assays. In these assays a magnetic microparticle and a metal nanoparticle are coated in separate targeting moieties for a marker of interest (e.g. an antibody). The nanoparticle also has thiolated single strand oligonucleotides (also known as "barcode DNA") attached to it. In the

presence of the marker, an aggregate of magnetic microparticle, receptor and gold nanoparticle forms, which is then isolated. After purification the oligonucleotides are cleaved using a reducing agent such as dithiothreitol and quantified. In this way previously undetectable levels of a specific target may be revealed.[21, 22] This method has further been developed in many ways, including modifications by Nam *et al*. to make the analysis colorimetric.[23] Here, targeted silica nanoparticles with barcode DNA attached are used to capture the target of interest. After isolation, the barcode DNA is cleaved and incubated with gold nanoparticles that target it, causing particle aggregation. The aggregation induces a red to blue colour change due to the difference in surface plasmon resonance of the nanoparticle aggregates (Figure 1.1). This same colorimetric change has since been applied to the detection of bacterial pathogens by the Gibson group, using a microarray of glycosylated gold nanoparticles to create a "QR" like read out specific for pathogenic lectins.[24]

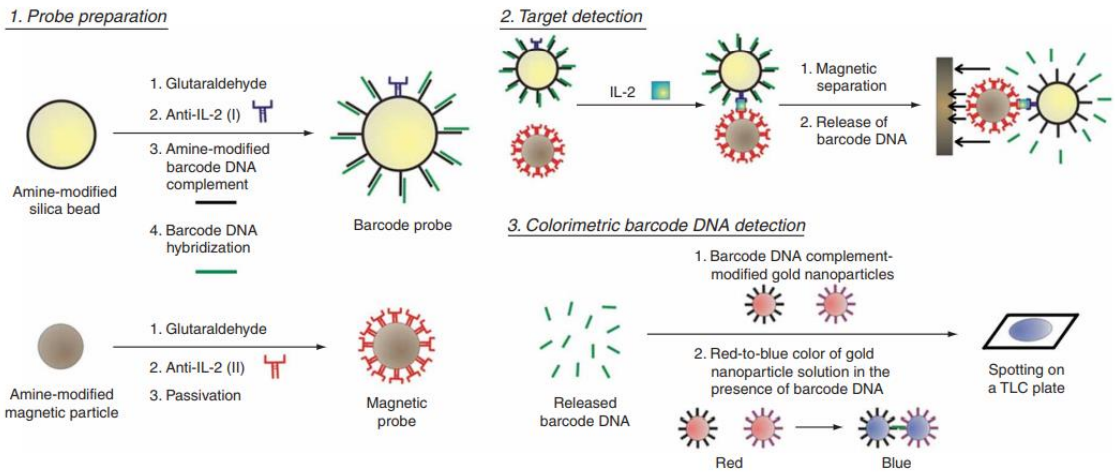


**Figure 1.1:** Visual explanation of the colorimetric "bio-barcode" assay developed by Nam *et al*. for the detection of interleukin-2. Image adapted from Nam *et al*.[23]

Inorganic nanoparticles have also been widely explored in delivering therapeutics, due again, in no small part, to their relative ease of synthesis and high surface area to volume ratio.[12] The volume of loading for an inorganic nanoparticle, though relatively high is limited to the surface area, this may however be enhanced by the use of mesoporous silica.[25, 26] By producing a porous particle, not only is the accessible surface enhanced, properties such as pore size may be modified to further control the particle properties, such as drug release.[27]

### 1.1.2 Nanoparticles as Drug Delivery Agents

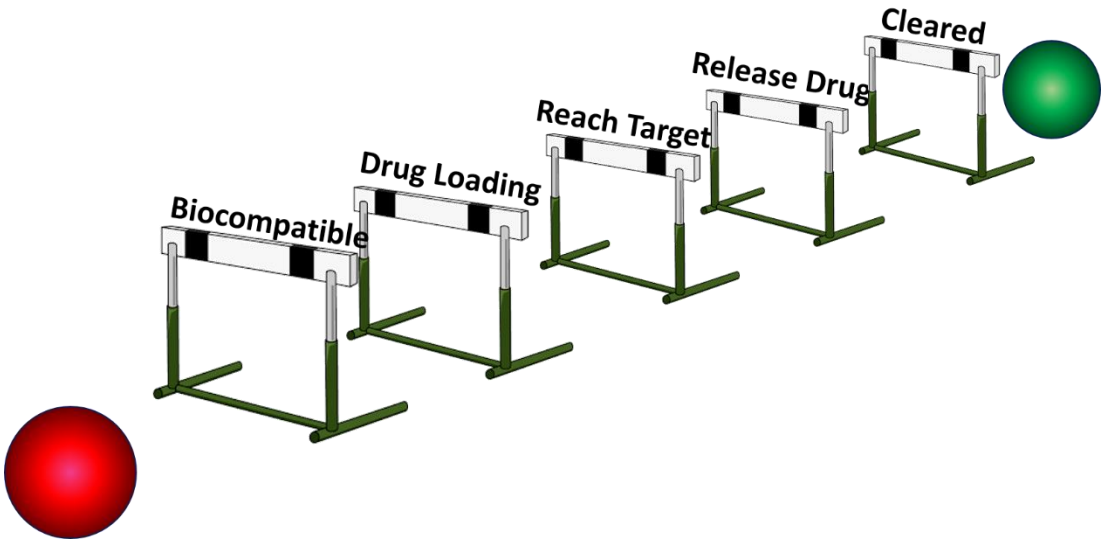


**Figure 1.2:** Representation of challenges in using nanoparticles as drug delivery agents

For use as drug delivery agents, organic nanoparticles of various forms have also been widely studied.[28-30] The reasons for this plethora of research include the ability of organic nanoparticles to have many of their physical characteristics easily modified.[1] The particle properties also allow organic nanoparticles to deliver many potentially effective drugs that cannot be, or are difficult to use due to poor solubility and high toxicity in the body.[10, 31, 32] Ideally, a drug molecule is bound to, or loaded into a biocompatible particle, which transports the drug to its site of action where it is released, and the polymer is subsequently metabolised and/or excreted.[33] Each of these steps poses a challenge in creating a suitable drug delivery nanoparticle, summarised in Figure 1.2.

Clinically the most commonly used organic nanoparticle systems for drug delivery are vesicles, primarily liposomes.[34, 35] First reported in 1965 by Bangham *et al*. vesicles are self-assembled lamella structures surrounding an aqueous core, that resemble the cell membrane phospholipid bilayer.[36] These systems were the first to gain FDA approval, for delivering doxorubicin (Doxil®, an antineoplastic) and Amphoteirin B (an antifungal).[37, 38] They benefit from their facile synthesis (suspension of a suitable surfactant in water), the ease in which multiple drugs may be encapsulated simultaneously and the availability of previously approved materials for use.[34, 39, 40] As such, not only are they one of the most successful nanotherapies, but remain at the forefront of biomedical nanoparticle research.[41, 42] One of the down sides to the use of vesicles is their relatively short half-life in the body due to rapid clearance and immune

recognition. Strategies to overcome this issue have included the use of "self" cell membrane materials as extracellular vesicles and functionalisation with polymers to limit immune recognition.[42-44]

Next to vesicles, protein nanoparticles are one of the most common clinically used nanoparticle formulations.[34, 35] Protein nanoparticles are most commonly composed of a protein conjugated to a drug, in efforts to improve the drug's formulation and pharmacokinetics. These have gained most use for the administration of hydrophobic cancer drugs.[45] One of the earliest and well known examples of such a system is Abraxane® used to deliver paclitaxel.[46] Previously paclitaxel was administered with the formulation vehicle Cremophor, now widely shown as toxic, and requiring co-administration with antihistamines and steroids.[47] Abraxane® combines paclitaxel with human serum albumin to produce a protein bound nanoparticle 130 nm in diameter, which has been shown to eliminate the need for a co-solvent and improve clinical results compared to paclitaxel alone.[48] More recent developments have taken the concept further and produced self-assembling temperature responsive protein nanoparticles.[49] Elastin is a protein known to possess a thermoresponsive self-assembly, a chimeric cyclic peptide derived from it has been shown by McDaniel *et al*. to form nanoparticles in conjugation with hydrophobic drugs.[50] The same group went on to show that a conjugate of the same cyclic peptide with doxorubicin could self-assemble, and showed a phase transition upon heating to between 39-42 °C. This improved its cytotoxicity against cancerous cells upon exposure to mild hyperthermia.[51]

One of the most active areas of research into nanoparticle drug delivery is with polymeric nanoparticles, either as polymer-drug conjugates or polymeric vehicles for the controlled/targeted release of a drug.[52-55] This is an area that at first glance has thus far failed to make a large impact in the clinic, however synthetic polymers in hybrid systems are now commonly on the market, albeit most commonly as poly(ethylene glycol) (PEG) conjugates such as Nuelasta, used to improve drug/biological drug solubility and circulation time.[34, 56-58] The number of these systems only looks set to rise with the patents of many biological drugs expiring, and the FDA approving "bio-similars" such as Fulphila in June 2018, the generic PEGfilgrastim equivalent of Nuelasta.[59, 60] Nevertheless there continues to be a large amount of promising research using polymeric nanoparticles, not least due to the facile synthetic methods such as

emulsion polymerisation and polymerisation induced self-assembly (PISA), and the wide variety of functionalities and physical properties that may be imparted on the particle, which will be explored in depth later.

Crucial to the clinical success of a polymer nanoparticle therapy is its safe and efficient clearance after its cargo has been delivered, and/or it has exerted its biological response. Indeed one of the main drawbacks to polymeric nanoparticles being used in the body is their accumulation. Most studies in the area will report that after injection of a nanoparticle, bioaccumulation occurs majorly in the liver, and also the spleen, lungs and pancreas.[62] Generally speaking a move towards biodegradable and responsive nanoparticles that can be cleared to avoid accumulation, seems necessary for larger polymeric architectures to fulfil their clinical potential in a variety of applications.[63-66] Much of the work in this area has focussed on incorporating hydrolysable esters into the polymer backbone, with polymers such as poly(lactide) and poly(caprolactone).[28, 66, 67] Other studies have focussed on preparing nanoparticles that are held together by responsive cross linkers, such as the work by Zhang *et al*. who reported the synthesis of polymeric nanoparticles based on the photosensitive monomers 2-nitrobenzyl methacrylate (NBMA).[68] After producing a variety of particle morphologies they showed that UV irradiation was able to cleave NMBA moieties, resulting in polymeric carboxylic acid groups. This caused the previously hydrophobic particle core to become hydrophilic, inducing particle break up. The system was subsequently shown to potentially increase drug release in Henrietta Lacks (HeLa) cells. This strategy provides an interesting way of spatiotemporal controlled drug release, the use of UV light poses problems however due to poor tissue penetration, with IR light a more suitable option.[69, 70] A stimulus endogenous to the body that has been explored to trigger particle break up and drug release, is the reactive oxygen species (ROS) hydrogen peroxide, found in increased levels in inflamed or cancerous tissues. Recent work from Sobotta *et al*. showed relevant concentrations of hydrogen peroxide to cause the break-up of particles with an *N*-acryloyl thiomorpholine (NAT) core, due to peroxide induced oxidation (Figure 1.3).[61, 71] Strategies such as this hold promise as release should only be triggered in pathological tissues, however the speed of the response is still slow, with break up occurring over a period of hours to days. Furthermore, many responsive particle systems have utilised pH as a stimulus to trigger particle break up. This may be an acidic pH accelerating ester hydrolysis, or again a solubility switch from hydrophobic to hydrophilic.

Polymers bearing amines are known to exhibit pH responsive behaviour, one specific example being poly(2-(dimethylamino)ethyl methacrylate) P(DMAEMA), known to exhibit a change in solubility from hydrophobic in basic/neutral environments, to hydrophilic in acidic ones due to protonation of its tertiary amine.[72, 73 74] The change in solubility is rapid, proceeding over minutes to hours, and thus would be suitable for particle break-up *in vivo.* Such a pH shift is however found in many cells throughout the body, so without further targeting it would not necessarily confer a directed drug delivery.

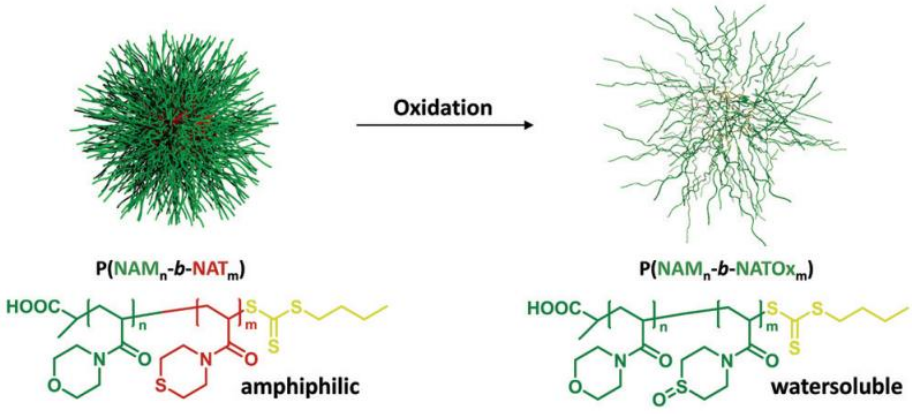


**Figure 1.3:** Graphical representation of the oxidative response of poly(N-acryloyl morpholine)-*b*-poly(N-acryloyl thiomorpholine) micelles switching from amphiphilic to hydrophilic in the presence of hydrogen peroxide. Figure adapted from original paper by Sobotta *et al*.[61]

Nanoparticles present a promising way of delivering a wide range of drugs in a targeted manner. Their use has been widely studied, particularly in the area of cancer therapy. They also hold promise however for other disease states, particularly those where an accumulation of nanoparticles is favoured or where a specific targeting moiety is present.[75, 76]

### 1.1.3 Drug Loading and Release

The effective use of nanoparticles as drug delivery agents requires efficient loading of a drug into the nanocarrier and for the drug to be released at the site of action. The loading of a drug to a nanoparticle will typically be by an incorporative or an absorption/adsorption (ab/adsorption) method.[77] Drug loading is generally characterised as loading content and loading efficiency, determined using Equations 1.1 and 1.2.

$$Drug\ Loading\ (wt\%) = \frac{Mass\ of\ drug\ in\ nanoparticle}{Initial\ mass\ of\ nanoparticle} \times 100$$

**Equation 1.1:** Equation for determining the percentage of drug loading achieved in a nanomedicine

$$Loading\ efficiency = \frac{Mass\ of\ drug\ in\ nanoparticle}{Mass\ of\ drug\ in\ feed} \times 100$$

**Equation 1.2:** Equation for determining the drug loading efficiency achieved in a nanomedicine

The distinction between the two of these expressions is important. Drug loading describes the content of drug that will be found per mass of formulation, and therefore will dictate how much of the formulation will be needed to give a set dose.[78] The loading efficiency however describes how much of the initial drug that was put in will remain in the final formulation. Poor loading efficiency is not necessarily a barrier to high drug loading, but is an important consideration in manufacturing.

Loading of a drug through physical and electrostatic ab/adsorption, either into a polymer matrix or particle surface often gives poor loading efficiency, as the amount of drug that will enter into the nanomedicine is dictated by the partition coefficient between it and the solvent (usually water). As such, loading efficiencies of below 10% are common in the literature.[79, 80] This poses issues with the large volume/mass of particle carrier that consequently has to be administered to achieve a therapeutic concentration of drug, raising questions surrounding toxicity and pharmacokinetic properties. The simple absorption of a drug is however an attractive method of particle loading due to its simplicity and broad applicability. Methods have been explored to improve the loading achievable; for liposomal formulations specifically, increasing the surfactant concentration, and incorporating other molecules such as cholesterol into the structure have been established to improve loading.[81, 82] Work from Taylor *et al*. in the 1990's demonstrated the benefit of incorporating cholesterol in the encapsulation of sodium cromoglycate.[83] They showed a drug loading of 30.7% after 50% cholesterol was added to the liposome particle. This was an increase of 112.7% compared to without the cholesterol. More generally, improving the solubility of the drug in the nanoparticle also enhances the drug loading: charge, pH and co-solvents (subsequently evaporated away) have all been employed in such a manner.[81, 84, 85] To use such a method for the loading of a macromolecule, it has been shown by Calvo *et al*. that encapsulating the macromolecules at their isoelectric point provides for the greatest loading percent.[86] Furthermore highly porous inorganic nanoparticles have been shown to be able to exploit ab/adsorptive methods of drug loading, due to their

extremely large surface area to volume ratio, being able to achieve a drug loading of between 30-60%.[78, 87-89] One recent report from Jiang *et al*. showed quite remarkable drug loading to mesoporous glass.[90] In this study, the mesoporous glass was functionalised with amino groups and subsequently loaded with gentamicin sulfate, the amino functionalisation increasing loading from 49% to 63% when compared to the non-functional equivalent.

In an incorporative method of loading, the drug is added during the particle formation process. This can result in higher loading concentrations through matrix entrapment, and the homogeneous distribution of drug through the carrier also reduces the incidence of burst release.[77] However, depending on the method of particle production, the stability of the drug or drug-conjugate must be considered during the synthetic method, particularly for biomolecules such as proteins that will denature when taken too far out of their natural conditions.[91, 92] Spray drying has been used as a method for producing nano and microparticles where there are sensitive components, due to the short time an elevated temperature is required for solvent evaporation.[93, 94]

Drugs loaded into nanoparticles using the previously described methods, typically suffer from poor spatiotemporal control over drug release, relying on desorption or matrix erosion as release mechanisms. These suffer from being dependant on relative solubility and diffusion rates in various body compartments, and can lead to inappropriate burst release of a drug.[77, 78]

An effective strategy for gaining control over drug release, and retaining high drug loading, is to use a covalent linker to bind a drug to a polymer or particle.[78] The bond used must however be able to break upon a stimulus relevant to the drug target environment, making their use less universal as a loading and release mechanism. The most common of those stimuli is pH, this is partly due to the convenient pH drop found in the cellular lysosome after endocytosis and the number of pH responsive bonds such as: acetals, imines, oximes and hydrazones to name a few.[95, 96] One notable example of a pH responsive release was from Bae *et al*. who demonstrated the targeted delivery of adriamycin to cancer cells using a folate targeted polymeric micelles.[97] Adriamycin was released upon a relevant drop in pH hydrolysing a hydrazone linker. Disulphide bridges have also been explored as covalent linkers for drugs, able to be broken upon exposure to a reducing environment, such as that found in the glutathione rich environment of a cancer cell.[98-100]

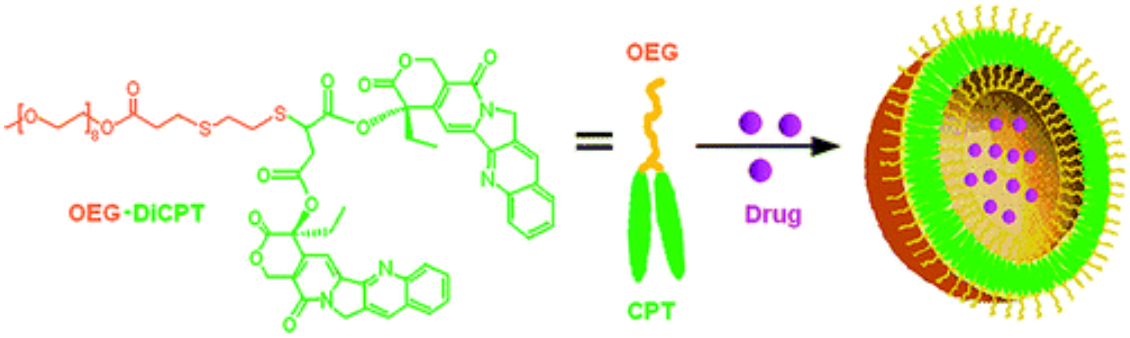


**Figure 1.4:** Graphical representation of the PEG-disulphide-camptothecin linked vesicles prepared by Shen *et al.* co-loaded with doxorubicin, providing a reductive responsive drug delivery agent. Image adapted from original paper.[101]

A good example of a disulphide being used effectively in controlled nanoparticle release is that of Shen *et al.*[101] Either one or two camptothecin moieties were linked to a short PEG chain *via* a disulphide bridge with drug loading of camptothecin up to 58%, and self-assembled into vesicles (Figure 1.4). The vesicles were further loaded with doxorubicin *via* encapsulation up 18.5% w/w. Vesicles with camptothecin alone were shown equivalent to free camptothecin *in vitro*. With co-loaded doxorubicin however a vastly improved cytotoxic effect on ovarian and breast cancer cells was demonstrated. This study showed the potential for efficient drug loading and release using a responsive covalent linker, it further showed *in vitro* the potential to use two different drug loading methods effectively to produce a synergistic biological response.

In summary, the method of loading and release of a drug in a nanoparticle must be considered on a case by case basis. If a prolonged systemic release is desired, then simple ab/adsorption and desorption methods may be best where solubility allows, due to their simplicity and non-specific release profiles. If, however a specific site of release is required, a responsive release may be preferred where there is a stimulus specific to the site of action that can be exploited to cause drug release.

## 1.2 Biological Influence of Nanoparticle Properties

One of the major benefits to using nanoparticles for biomedical applications, is the wide variety of physical properties it is possible to modify on them. Each of these can be used to tailor a nanoparticulate system for a specific use, and an understanding of their biological impact is crucial in designing a successful drug delivery agent.

### 1.2.1 Particle Size

The size of a particle can greatly influence its biological effect, this is most obvious in a simple example such as that of an eye drop. Particles under 10 μm in diameter are not detectable, whilst over that a gritty uncomfortable sensation will be felt on the eye.[102] Particle size is also known to have an influence on deposition in the lungs, with smaller particles being able to deposit further towards the alveoli.[103] Reducing the size of particles has been shown in liposomes and gold nanoparticles (< 10 nm) to increase the efficacy in crossing the blood brain barrier.[104, 105] Moreover, particle size can be changed to modify the bio distribution across all organs and tissues after injection. With particle sizes under 5 nm showing renal clearance, inflamed tissues retaining particles over 80 nm, and ultimately most particles showing accumulation in the liver, spleen and lungs (Figure 1.5).[106-109]

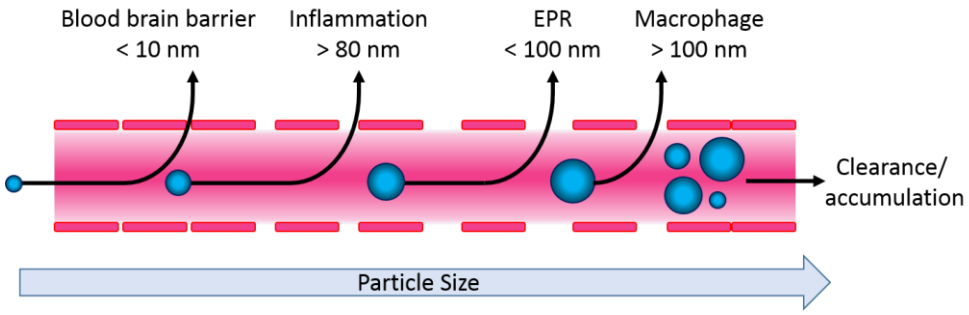


**Figure 1.5:** Representation of the effect particle size has on the biodistribution of a nanoparticle, showing accumulation in certain pathologies/tissues

The influence of particle size on cellular uptake has also been extensively investigated, it is however difficult to come to many firm conclusions regarding the influence of size alone on endocytosis, as the results show great variation between studies and uptake mechanism.[110, 111] Some size limits do recur in the literature, for example immune cell lines have been shown to endocytose larger particles more efficiently (diameter > 100 nm), whereas studies in various non-immune cells (e.g. HeLa) have shown a diameter of 50 nm to be optimal for cell uptake.[110, 112-114] To fully understand the influence of particle size however, it must be considered with particle morphology.

### 1.2.2 Particle Morphology

Nanoparticles are also produced in a variety of different morphologies, including: spheres, vesicles, rods and worms.[115] Non-spherical morphologies, with a high aspect ratio have been shown to exhibit prolonged circulation times. One widely cited study by Geng *et al.* shows the circulation of filamentous particles to be up to a week,

compared to a vesicular equivalent of only two days.[116] They further report enhanced anti-tumour activity when loaded with paclitaxel. One extensive study by Decuzzi *et al*. used spherical, quasi hemi-spherical, discoid and cylindrical silica nanoparticles in mice, and determined the accumulation in various organs.[117] Spheres above 700 nm in diameter were shown to have reduced accumulation with increasing size, interestingly disc shaped particles were shown to have in increased accumulation in all organs except the liver, a phenomenon the authors attribute to the differing rotational inertia and increased adhesion in most organs except to Kupffer cells in the liver. Cylindrical particles were also shown to have the largest increase in deposition in the liver, which may also partly explain the prolonged half-life of cylinders seen *in vivo*. Furthermore, cylindrical nanoparticles may have an advantage in tumour accumulation, due to tumbling in blood flow pushing them towards the blood vessel walls. This results in increased extravasation at sites of increased permeability, such as a tumour.[118, 119]

Morphology has also been shown to influence interaction with cells and internalisation.[111] A spherical morphology has been shown optimal for immune cell uptake, providing further reasons for the increased circulation time that non-spherical morphologies exhibit compared to spherical equivalents.[120, 121] In non-immune cells above 100 nm in diameter, a non-spherical morphology (higher aspect ratio) has been shown to cause an increased cellular uptake. Gratton *et al.* reported that with increasing aspect ratio a corresponding acceleration in particle uptake was seen in HeLa cells.[122] Conversely Qiu *et al.* and Chithrani *et al.* both report that in gold nanoparticles under 100 nm a spherical morphology becomes optimal.[116, 120, 122-124]

### 1.2.3 Particle Surface Charge

The surface charge of nanoparticles has also been widely studied, generally dividing particles into: anionic, neutral and cationic. Broadly speaking cationic particles have been shown by many studies to be internalised into various cell lines to a greater extent than a neutral or anionic equivalent.[125] [110] Perumal *et al.* demonstrated this effect well using poly(amidoamine) dendrimers with different surface functionality, providing positive, neutral and negative charge (amines, hydroxyls and carboxylic acids respectively).[126] The dendrimers were shown, in A549 (lung epithelial carcinoma) cells, to be taken up by distinctly different mechanisms, with anionic dendrimers mainly being internalised *via* clathrin mediated endocytosis and neutral and cationic counterparts *via* non-specific direct interactions. In the case of positive dendrimers and

more generally particles, the increase in uptake is presumed to be due to electrostatic interactions between the cationic particle surface and the anionic cell surface.[127] This same interaction is also responsible however for the widely reported increase in cytotoxicity of cationic nanoparticles (Figure 1.6).[128, 129]

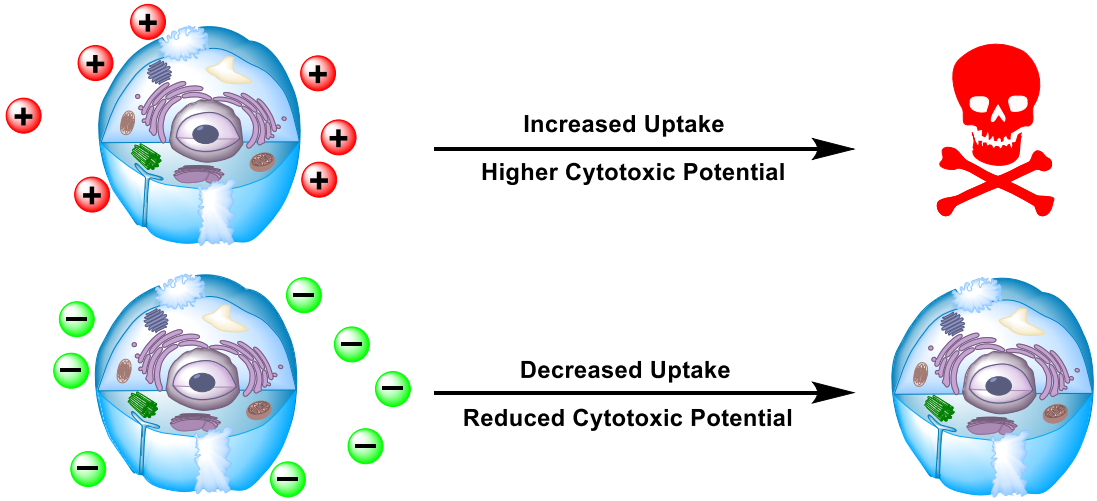


**Figure 1.6:** Graphical representation of the major effects of particle surface charge: neutral and anionic particles with reduced uptake but improved toxicity profiles, cationic particles with increased uptake but poor toxicity profiles

### 1.2.4 "Stealth" Particle Coatings

After administration a nanoparticle must avoid excretion and evade immune clearance, the surface functionalisation of a nanoparticle is an important property in achieving this. Indeed most efforts to evade recognition and capture by the immune system focus on the use of "stealth" polymers.[130-132] First introduced in the 90's, the typical protective or "stealth" polymer that is approved for use is PEG, used coupled to a protein to prolong circulation time (PEGylation) and as a coating for many nanoparticles.[133-136] A study from the Müller group on the effect of the PEG corona thickness and density found that increasing the molecular weight and density of PEG at the particle surface reduced protein adsorption. They further found that they could not completely stop adsorption up to the maximum size and density of PEG tested.[131] More recently, concerns have been raised about the immunogenicity of PEG, with many studies including those from the Kiwada group showing the production of anti-PEG antibodies after injection of PEGylated liposomes.[69, 137, 138] Despite recent concerns, PEG remains the polymer of choice of pharmaceutical companies to produce a "stealth" coating and prolong *in vivo* circulation time of a therapeutic. However, one candidate group of polymers to replace it is poly(2-oxazolines) (POx).[139-144] Research from the Hoogenboom group recently demonstrated the comparative pharmacokinetic

behaviour of radioactively labelled PEG and POx of various molar masses in mice.[145] POx showed similar pharmacokinetic properties, with a cut off for renal clearance at a polymer size of around 40 kDa. It was further shown that polymer chain length was the dominant property affecting biodistribution over polymer molecular weight. Han *et al.* reported the ability of POx based micelles to solubilise a wide range of chemotherapeutics (pactitaxel, docetaxel, 17-allylamino-17-demethoxygeldanamycin, etoposide, and bortezomib) up to 50% w/w drug loading and the enhancement of cytotoxic effect *in vitro*.[146] Studies on POx *in vivo* are still few, He *et al.* published the use of triblock POx based micelles (P($(MeOx)_{33}$-*b*-$(BuOx)_{26}$-*b*-$(MeOx)_{45}$) to solubilise and successfully deliver a variety of taxoids, to nude mice.[147] The study reported modest improvements in reducing tumour growth on current chemotherapeutic formulations, but importantly that the POx polymer was non-toxic.

Even with the concerns over immunogenicity, particle surface functionalisation with PEG represents one of the most successful nanoparticle strategies in biomedicine. It is unlikely to be replaced as a technology until a potential replacement such as POx can show superiority in *in vivo* tests.

## 1.3 Targeted Nanoparticles

Often the rationale for using a nanoparticulate drug delivery agent is to increase the concentration of an active pharmaceutical ingredient (API) at the site of action, relative to the rest of the body. In doing so the API's clinical effect is designed to be increased whilst minimising systemic side effects and overall dose. To do this the API loaded nanoparticle must be able to reach the site of action in a high concentration. As previously explained, a particle system may be coated such that it is protected from clearance to help achieve this. However a particle may also be targeted to direct it to a site of action either through active or passive mechanisms.[148-150]

### 1.3.1 Passive Targeting

The targeting of a site of action with a nanoparticle need not always be an active process, passive targeting mechanisms may first be exploited.[77, 151] Certain disease states lend themselves to the use of nanoparticulate therapy. As previously stated, when injected most nanoparticles will eventually accumulate in the liver.[152, 153] Whilst this is a problem for targeting elsewhere in the body, for delivery of drugs for hepatic disease states such as cirrhosis or cancerous metastases, this is a fortunate

accumulation that has been widely exploited.[154, 155] One example by Canup *et al*. delivered CD98 siRNA to the liver in a simple poly(lactic acid) (PLA)/poly(vinyl alcohol) (PVA) nanoparticle, prepared by a solvent evaporation technique.[156] In this study particle accumulation in the liver led to an *in vivo* reduction in all biomarkers for non-alcoholic fatty liver disease, such as pro-inflammatory cytokines. Another widely discussed and potentially controversial effect nanoparticles can take advantage of for passive targeting is the enhanced permeability and retention (EPR) effect displayed by solid tumours.[31, 157-159] The theory of the EPR effect suggests that fast growing tumours with increased metabolism depletes the surrounding tissue of oxygen. This stimulates the release of growth factors such as vascular endothelial growth factor (VEGF), causing the local over production of blood vessels. The vessels produced have thin walls without the tight endothelial junctions usually seen, and thus provide a sieve that allows the escape of nanoparticles under 100 nm into the tumour environment where they can accumulate (Figure 1.7).[157, 160]

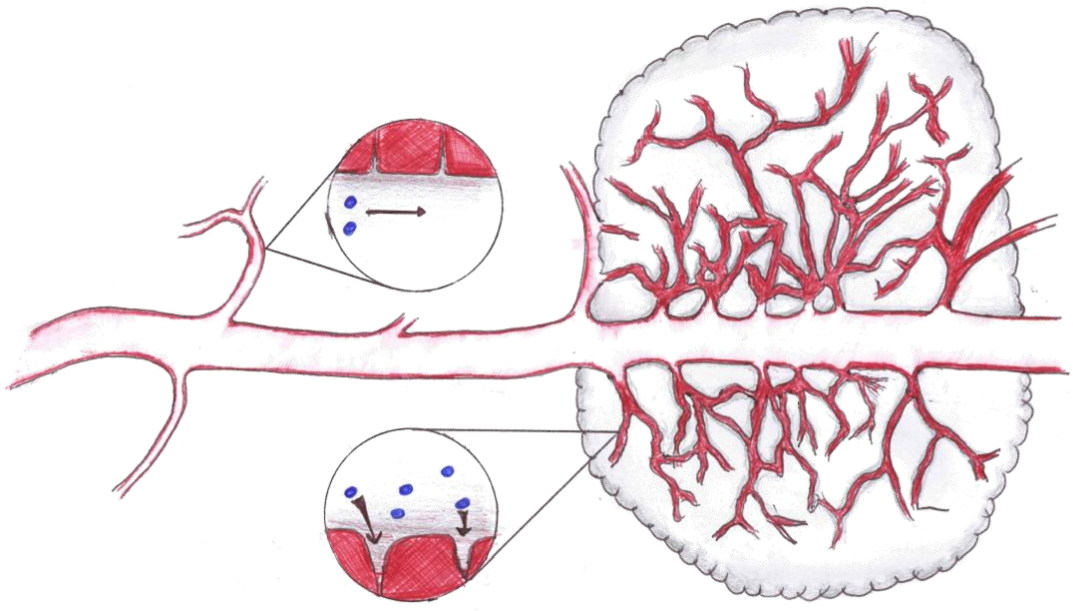

**Figure 1.7:** Graphical representation of the increased tumour vasculature and loose endothelial junctions, causing the EPR effect and the retention of nanomaterials in the tumour environment

The EPR effect had been heralded as a silver bullet for all solid tumours, it now appears however that the benefits of this effect are less pronounced than had been hoped. Indeed work by Chauhan *et al*. showed that repairing the poor tumour vasculature improved the accumulation of nanoparticles under 12 nm in diameter, however reduced the accumulation of 125 nm particles.[161] The effect still holds promise for

certain tumour types such as carcinomas, in particular the passive targeting of the EPR effect may be effectively coupled with an active targeting ligand.[157, 162, 163]

### 1.3.2 Active Targeting

Active targeting is often achieved by decorating the surface of a particle with a targeting ligand. The ligand may be specific for a receptor that is either exclusively expressed, or overexpressed at a site of interest.[164, 165] The targeting groups possible are diverse, including: small molecules and short peptides, to larger targeting groups such as immunoglobulins.[166-172]

The earliest reports of targeted nanomedicines were in 1980 and used monoclonal antibody (mAb) functionalised liposomes.[173, 174] The first, by Heath *et al.* conjugated a mAb to a liposome surface, through an imine bond between primary amines on the mAb and aldehydes on the vesicle.[175] Using these liposomes an 80% association of liposomes to erythrocytes was achieved. Since then mAb's have been licenced in dozens of formulations, perhaps most notably rituximab, targeting CD20 in the treatment of non-Hodgkin's lymphoma, which has gone on to revolutionise other disease states such as rheumatoid arthritis.[176] Monoclonal antibodies are still widely used in research, such as in the recent article from Gu *et al.* who reported the use of a mAb functionalised chitosan nanoparticle to deliver siRNA for the inhibition of HIV replication in astrocytes.[177] This work showed a significant increase in the level of internalised siRNA in relevant astrocytes and blood brain barrier cells, however did not describe any *in vivo* tests to confirm the ability of the particle to cross the blood brain barrier. Nevertheless it shows the continuing potential of mAb's in targeted therapy.

The use of mAb's is not without its drawbacks however, they are large proteins (*ca* 150 kDa and 15 nm diameter) that can be difficult to use in manufacturing processes due to stability issues, and can pose immunogenic issues.[178]

Short peptide sequences, typically 10-15 amino acids in length have been explored as alternative targeting agents, to retain the specificity of mAb's and also address the manufacturing and stability issues.[165] The use of combinatorial libraries has led to the discovery of many peptide sequences that can effectively target specific sites in the body.[179] The most widely reported peptide used for targeting, is arginylglycylaspartic acid (RGD), which binds to αv integrin receptors.[180] There are various types of αv

receptor to which RGD will bind, however αvβ6 and αvβ8 that specifically activate the TGFβ1 pathway have been shown to be upregulated in aggressive cancerous cells.[181-183] Gray *et al*. exploited this over-expression by coating liposomes with the αvβ6 specific peptide H2009.1, and showed a six fold increase in affinity of a tetramer bearing liposome over a monomeric equivalent.[184] Various other targeting peptides have shown promise, one of which is Cys-Arg-Glu-Lys-Ala (CREKA). Zhao *et al*. showed the potential of CREKA, using it to functionalise a polyamidoamine dendrimer, showing enhanced glioblastoma targeting in the brains of nude mice.[185]

Small molecules have also widely been studied for their ability to produce targeted nanoparticles due to their: convenient manufacture and handling, wide range of efficient conjugation chemistries and favourable immunological properties.[165, 186] The most widely used small molecule used for nanoparticle targeting is folic acid and its derivatives.[187] The cell surface folate receptor is an attractive target, as from circulation it is not accessible to targeting ligands, except in certain tumour types such as those in the ovary, kidney and lung.[188, 189] Work from Muraldiharan *et al*. showed the efficient delivery and increased cytotoxic effect of siRNA acting on "human antigen R" in folate receptor overexpressing lung cancer cells, delivered in a folate functionalised liposome.[190] More recently Alibolandi *et al*. reported the dual delivery of doxorubicin and cadmium quantum dots (QD) in the hydrophobic bilayer and aqueous core respectively of a folate conjugated PEG-Poly(lactic-*co*-glycolic acid) polymersome.[191] This study demonstrated the sustained release of doxorubicin and QD's over 12 days and the ability to deliver both an imaging and therapeutic agent together *in vitro*. Further *in vivo* studies however showed only a modest increase in tumour targeting compared to a non-folate equivalent polymersome, with accumulation in multiple organs magnitudes higher than that seen in the tumour.

The other main class of targeting small molecules used is sugars, which are known to be endocytosed after preferential binding to specific cell surface lectins (or carbohydrate binding proteins).[54, 192-194] The presentation of particular sugars or sugar sequences has been shown able to target various disease states including cancer and infection.[195-197] The individual binding of a sugar to a lectin is weak, but the presentation of sugars on a nanoparticle as targeting agents enables them to take advantage of the "cluster glycoside effect" whereby a high density of ligands increases the overall binding affinity.[198] To take advantage of this effect, and for ease of synthesis, sugars are often used as glycopolymers.[199, 200] Ting *et al*. demonstrated the

ability of a glucose functionalised glycopolymer to aggregate with the tetravalent plant lectin concanavalin A.[195] Furthermore the glycoparticles were shown to increase *Escherichia coli* aggregation through interactions with *fim*H when compared to the linear counterpart, showing the potential to target infective bacteria using glycoparticles (Figure 1.8).

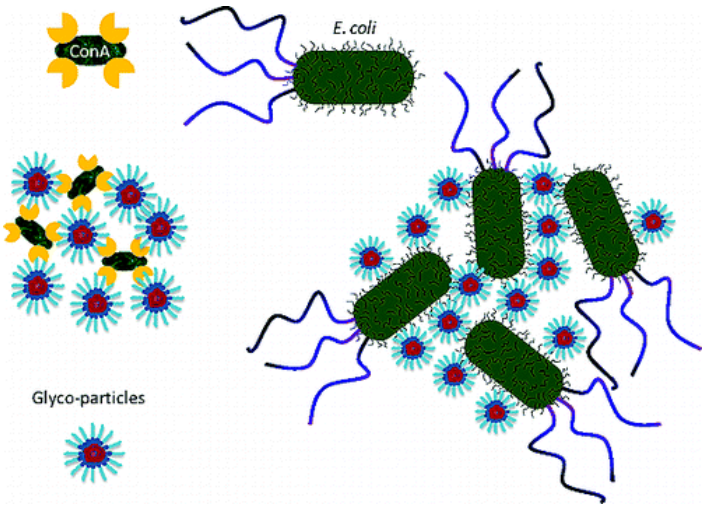


**Figure 1.8:** Graphical abstract showing the aggregation of poly(2-(methylacrylamido)glucopyranose) coated nanoparticles made *via* RAFT emulsion polymerisation with concanvalin A and *E. coli*. Image adapted from original publication by Ting *et al.*[195]

There are various reports of the *in vitro* delivery of small molecules such as doxorubicin and proteins such as insulin using glyconanoparticles.[201-205] Importantly though the presence of sugars at the surface of nanoparticles has been shown to enhance *in vivo* targeting, typically to cancerous or immune cells with mannose, galactose and glucose.[206-214] One study of particular interest when considering the design of a targeted glyconanoparticle is that of Wijagkanalan *et al*. who demonstrated the *in vitro* and *in vivo* effect of varying the density of mannose presented on macrophage cellular uptake.[215] Crucially they showed a statistically relevant increase in macrophage uptake of mannose decorated liposomes over bare liposomes in a concentration and time dependant manner both *in vitro* and *in vivo*. They further show a positive correlation between mannose functionalisation and cellular uptake. Interestingly, there was no statistical difference between bare liposomes and those with only 2.5% mannose functionalisation. This has implications on the design of targeted nanocarriers in general, and more specifically highlights the importance of the cluster glycoside effect in efficient lectin targeting.

In summary, nanoparticles are of considerable interest for a variety of biomedical applications. There remain many issues with their use, particularly in translation from

the lab to the clinic, with toxicity, accumulation and cost issues hampering their progress. Further fundamental studies on the biological effect of different types of nanoparticle are required, and cheaper manufacturing methods, particularly for functional polymeric nanoparticles to progress beyond the simple PEGylation of biomolecules and liposomes.

## 1.4 Emulsion Polymerisation

A simple way of synthesising a variety of nanoparticles and allowing modification of many of the properties previously discussed is *via* emulsion polymerisation. Emulsion polymerisation is a heterogeneous radical polymerisation that is usually performed in water, producing a polymeric latex, and is the most widely used disperse polymerisation technique.[216, 217]

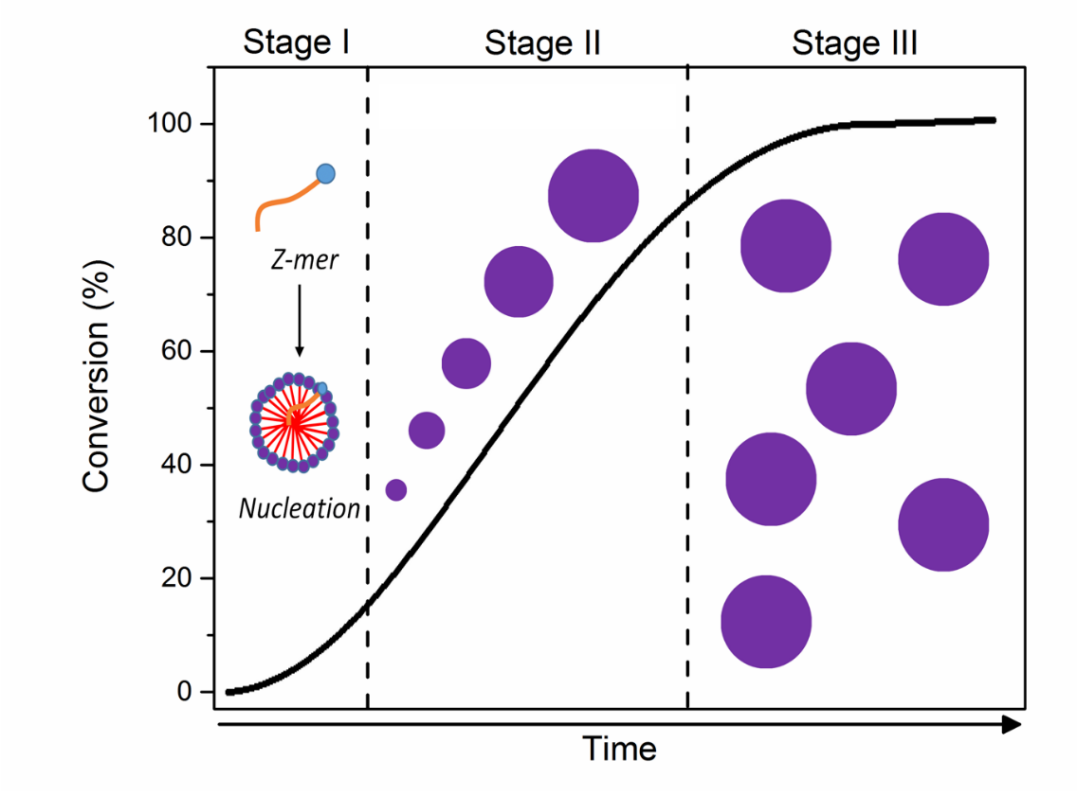


**Figure 1.9:** Example kinetics of a classic emulsion polymerisation, cartoons within depict the major component of each stage. Stage I: particle nucleation, Stage II: polymer and particle growth, Stage III: consumption of remaining monomer and production of final latex

A standard phase emulsion polymerisation takes place with water as the continuous phase and an "oil" as the suspended phase. In the case of an emulsion polymerisation the oil phase will be a liquid monomer that is immiscible with water. Typically the monomer will be suspended through the water with an excess of a surfactant such as sodium dodecyl sulphate (SDS), with only a small concentration of monomer being

dissolved in the aqueous phase. The excess surfactant will self-assemble, usually into a micellar form and crucially, due to their abundance and size, have a surface area far larger than that of the stabilised monomer droplets. A water soluble initiator is also introduced, such as potassium persulphate (KPS). The reaction mix is, under an inert atmosphere and with efficient stirring, heated to produce radicals (Figure 1.9).[218]

### 1.4.1 Emulsion Polymerisation Kinetics

The idea that polymer growth could occur within a growing latex particle was first introduced in the 1940's by Harkins.[219] This was later developed by Smith and Ewart into the eponymously named "Smith-Ewart" theory, which has formed the basis for most mechanistic understandings of emulsion polymerisation ever since.[220-222] Based on this theory, an emulsion polymerisation may be thought of in three stages.

In *stage I* of the emulsion process, particle nucleation occurs. The aqueous radicals polymerise with the small concentration of dissolved monomer, the growing oligomer may terminate in the aqueous phase as a surfactant or grow until it reaches a critical length known as a *Z-mer*. The *Z-mer* is surface active and will insert into a hydrophobic phase usually a surfactant micelle. The *Z-mer* may continue growing in the aqueous phase and reach a length where it will collapse in on itself like a surfactant (self-nucleation) this is a *J-mer*. This is more typical of less hydrophobic monomers. To produce particles with a narrow and monodisperse distribution of diameters, this stage of the emulsion polymerisation is critical, and particle nucleation must be fast, with all particles starting growth at around the same time.[216]

*Stage II* of the emulsion polymerisation is where there is linear growth of particles as monomer in the nucleated particles is consumed by the growing polymer and replenished from the large monomer droplets by diffusion through the aqueous phase. This gives an emulsion polymerisation one of its benefits, the compartmentalisation of the radicals. This allows for a locally high concentration of monomer, producing a pseudo-bulk reaction and a very fast rate of polymerisation. In some systems where the $k_p$ is high and/or the particles very small, the kinetics can be thought of as "one/zero", statistically meaning that half of all particles are growing at any one time. Butyl acrylate typically shows this "on/off" kinetics, where it is only likely for there to be one propagating radical per particle, as upon the insertion of another radical they are in such close proximity they will almost immediately terminate each other. Depending on the system, particles may also grow in this stage by coagulative

nucleation, where primary growing particles aggregate together to form larger secondary particles. If the monomer is too hydrophobic and cannot diffuse fast enough through the water to match the rate of polymerisation, this slows the polymerisation and is deemed "diffusion limited".[216]

The rate of polymerisation per particle at this stage can be determined by Equation 1.3. This assuming that the polymerisation is not diffusion limited where $\bar{n}$ is the average number of radicals per latex particle.[223]

$$R_{p\ particle} = k_p \cdot [M]_p \cdot \left(\frac{\bar{n}}{N_A}\right)$$

**Equation 1.3:** Average rate of polymerisation per particle in an emulsion polymerisation. $k_p$ = rate of polymerisation coefficient, $[M]_p$ = Concentration of monomer in a particle, $\bar{n}$ = average number of radicals per particle and $N_A$ = Avagadro's number

From this equation the average rate of polymerisation at *stage II* for the whole system may be determined by multiplying by the number of particles in the system.[223] (Equation 1.4)

$$R_p = k_p \cdot [M]_p \cdot \left(\frac{\bar{n}}{N_A}\right) \cdot N_p$$

**Equation 1.4:** Average rate of polymerisation in an emulsion polymerisation. $k_p$ = rate of polymerisation coefficient, $[M]_p$ = Concentration of monomer in a particle, $\bar{n}$ = average number of radicals per particle, $N_A$ = Avagadro's number and $N_p$ = number of particles

Although these equations would hold for *stage I* and *III* of an emulsion polymerisation, in practice, due to nucleation, changes in the number of particles and decreasing $[M]_p$, it is difficult to apply them in *stage III*. Many other factors will also affect the kinetics even in *stage II*, such as desorption and chain transfer. However if Smith-Ewart case 2 conditions and "on/off" kinetics are assumed, the rate of polymerisation may be re-arranged to Equation 1.5.[223]

$$R_p = \frac{k_p \cdot [M]_p \cdot N_p}{2N_A}$$

**Equation 1.5:** Average rate of polymerisation in an emulsion polymerisation. $k_p$ = rate of polymerisation coefficient, $[M]_p$ = Concentration of monomer in a particle, $N_A$ = Avagadro's number and $N_p$ = number of particles

If the rate of radical formation in moles is known ($\rho_i$) then the average rate of entry to a particle is determined by Equation 1.6.[223]

$$Rate\ of\ insertion = N_p/\rho_i N_A$$

**Equation 1.6:** Average rate of radical insertion in an emulsion polymerisation. $N_p$ = number of particles, $\rho_i$ = molar radical formation and $N_A$ = Avagadro's number

As the rate of monomer addition to a propagating radical is determined by $k_p[M]_p$, this may be combined with Equation 4 to determine the number average degree of polymerisation ($\bar{x}_n$). This assumes negligible chain transfer and that the radical insertion species is smaller than the existing propagating radical in a particle (Equation 1.7).[223]

$$\bar{x}_n = k_p \cdot [M]_p (N_p / \rho_i N_A)$$

**Equation 1.7:** Number average degree of polymerisation in an emulsion polymerisation ($\bar{x}_n$). $k_p$ = rate of polymerisation coefficient, $[M]_p$ = concentration of monomer in particle, $N_p$ = number of particles, $\rho_i$ = molar rate of radical formation and $N_A$ = Avagadro's number

Looking at Equation 1.6 and 1.7 the only common factor that can be readily manipulated to change both the rate of polymerisation and number average degree of polymerisation is the number of particles. By increasing the number of particles (typically by increasing surfactant concentration) the growing radicals are further compartmentalised reducing the chance of interaction. This both increases the polymerisation rate and the molecular weight of the final polymer.

*Stage III* of an emulsion polymerisation occurs when the monomer droplets have been exhausted and only the monomer that is swelling the particles remains. Further, undesirable particle growth may happen as the remaining monomer is polymerised and coagulation between particles continues to occur, causing a slight drop in number of particles. The polymerisation rate typically plateaus at this stage, particle diameter may show a final rapid increase however, with increased coagulation. The end of this stage results in the final latex.

This technique is widely used on a multi tonne scale across industry and on a smaller scale in many labs. Due to the compartmentalisation of radicals, emulsion polymerisation benefits from fast kinetics and can produce high molecular weight polymers with short reaction times, typically 2-3 hours.[224] One of the other features that makes emulsion polymerisation an attractive process is that it is performed in water. Not only is this cheap and non-toxic, it has a high specific heat capacity making the reactions safer. As the product is dispersed through water, the final product will still have the viscosity of water regardless of polymer chain length (providing that the total solids contents do not exceed 55-60%).[225] The final latex may be used without further modification for many applications, or the water evaporated to obtain the bulk polymer.[220, 226]

However for applications in the medical field the presence of a surfactant such as SDS is undesirable and must be removed, a task that is arduous and requires extensive dialysis. The use of particles made in such a way is also limited, as their surface properties are only modifiable by the initiator used. With the goal of overcoming these issues of surfactant and surface properties, a number of controlled radical emulsion polymerisation techniques have been researched. Controlled radical polymerisation, producing a "pseudo-surfactant free" emulsion system, has been at the forefront of what can be achieved with an emulsion polymerisation. The first instance of a controlled radical emulsion polymerisation utilised nitroxide mediated polymerisation (NMP), more recent efforts however have focussed on the use of reversible addition fragmentation chain-transfer (RAFT) polymerisation.[216, 227-231] Before considering RAFT emulsion polymerisation, RAFT polymerisation will be introduced in more general terms.

### 1.4.2 Reversible Addition Fragmentation Chain-Transfer Polymerisation

Reversible addition-fragmentation chain-transfer (RAFT) polymerisation is a reversible deactivation radical polymerisation (RDRP) technique, developed at the Commonwealth Scientific and Industrial Research Organisation (CSIRO) in Australia, which uses a thioester based CTA known as a RAFT agent, of the general structure shown in Scheme 1.1, which are typically dithioesters, trithiocarbonates or xanthates.[232]

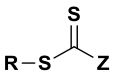


**Scheme 1.1:** The general structure of a RAFT agent, showing stabilising Z-group and re-initiating R-group.

RAFT polymerisation is a standard free radical polymerisation undertaken in presence of a CTA, which can reversibly transfer between growing chains and provide excellent control of polymer dispersity. The degenerative chain transfer process of RAFT agent from chain to chain permits to keep a majority of chains living, with the number of terminated chains, which cannot further chain-extend, being directly linked to the number of initial radicals produced during polymerisation. To ensure optimal polymerisation, producing a polymer with a narrow molecular weight distribution and high chain end fidelity, the choice of RAFT agent is key. The R-group must be a good leaving group able to fragment and re-initiate polymerisation at a similar rate to the monomer being used and as such often resembles the structure of a monomer. The Z-

group is chosen for its ability to stabilise the RAFT intermediate adduct. The RAFT polymerisation process consists of initiation, propagation, chain transfer (as pre-equilibrium, re-initiation and main equilibrium) and minimised termination. The full RAFT reaction scheme is shown in Scheme 1.2.

Initiation, propagation and termination proceed as in a standard free radical polymerisation. During the pre-equilibrium a growing polymer radical reacts with a RAFT agent forming an intermediate adduct, which may fragment towards the original polymer or R-group. If the adduct fragments towards the R-group, this is deemed the re-initiation step, and the R-group will then initiate monomer polymerisation. Once all of the RAFT agent has re-initiated and been consumed, the main equilibrium occurs. All of the growing chains rapidly interchange with the RAFT agents, and spread evenly amongst them, statistically facilitating even chain growth and a narrow molecular weight distribution.[232]

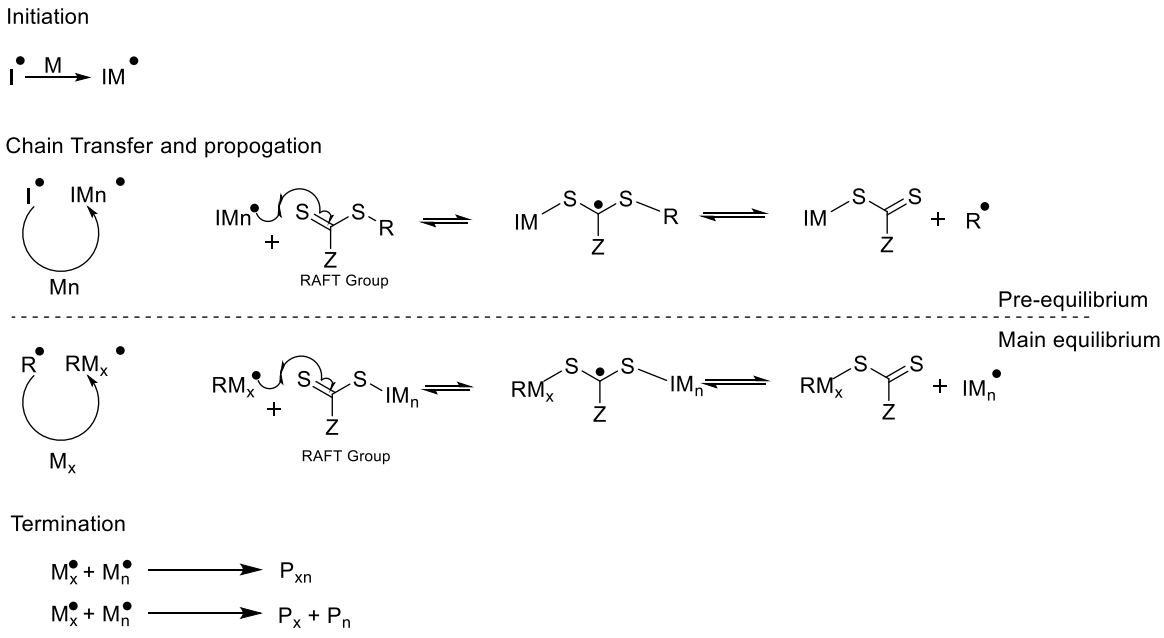


**Scheme 1.2:** General RAFT mechanism, termination shown as bimolecular termination, however disproportionation is also possible

One of the major benefits of RAFT polymerisation, is that it follows kinetics similar to free radical polymerisation, including a relatively fast rate of polymerisation. RAFT polymerisation is also a favoured technique due to its versatility. Polymerisations may be performed in a wide range of solvents, with many vinyl monomer types and it is tolerant to many functional groups. However to minimise termination events the amount of initiator used is reduced as low as is possible without causing excessive slowing the rate of polymerisation. Other considerations when using RAFT

polymerisation include that no one RAFT agent is able to polymerise all monomers and must be carefully matched to the monomer used. Furthermore the resulting polymers contain a RAFT end group that may be undesirable for various applications. It is no surprise then, that various methods for RAFT end group removal have been developed. These have been widely reviewed and include: aminolysis, thermolysis, radical removal and hetero Diels-Alder reactions.[233, 234]

### 1.4.3 RAFT Emulsion Polymerisation

RAFT Emulsion Polymerisation, takes a standard RAFT polymerisation, with its associated benefits, and performs it within the mechanism of an emulsion polymerisation, (Figure 1.10) and was first proposed by Hawket *et al*.[235]

In this technique, a small amphiphilic di-block copolymer, typically less than 30 monomer units long is synthesised *via* RAFT solution polymerisation.[236] The synthesised di-block copolymer after purification is suspended in water, whereupon (due to its amphiphilic nature) it forms micelles with RAFT CTA's embedded within them.[237]

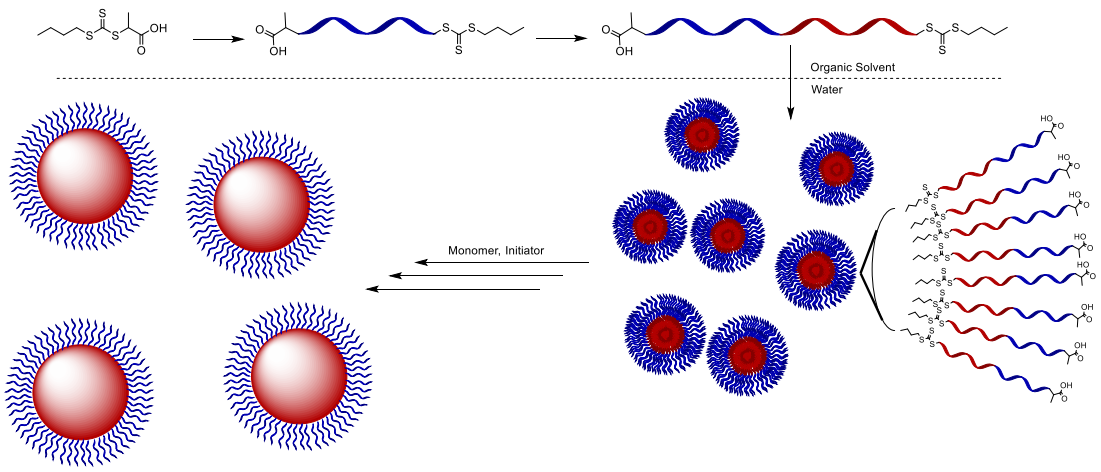


**Figure 1.10:** Simplified representation of RAFT emulsion polymerisation

With the appropriate hydrophilic initiator and hydrophobic monomer, these can then be chain extended using an emulsion polymerization. This results in a colloidally stable particle formation, which can be used as a latex, if desired, or further processed to leave the bulk polymer. Latexes synthesised in this way, should not only have a narrow particle size distribution, but the constituent polymers will also benefit from having controlled molecular weights and a low dispersity ($Đ$), having undergone degenerative chain transfer. As the RAFT di-block acts as the stabilising surfactant, when it is chain extended during the polymerisation it is covalently bound to the

resulting particles.[238, 239] Not only does this eliminate the need to use a charged free surfactant like SDS, it also imparts any functionality from the hydrophilic block of the original di-block onto the surface of the final particles. This allows for modification of the particle shell with any hydrophilic monomer suitable for RAFT polymerisation, and the particle core to be tuned with any monomer suitable for RAFT emulsion polymerisation. A good example of this was shown by Ting *et al*, where a nanoparticle with a glucose shell was produced using a RAFT emulsion polymerisation.[195]

As with any technique, RAFT emulsion polymerisation has its drawbacks.[240] The synthesis of each individual di-block copolymer is relatively time consuming and expensive. This may be improved by starting the emulsion polymerisation from a hydrophilic polymer, forming the di-block *in-situ*, making the reaction one pot and removing intermediate purification. The resulting particle will also have the RAFT agent embedded within its core, something that may pose licencing issues for biomedical applications. On top of these drawbacks, few RAFT agents are being produced in large enough volumes to make a product using them commercially viable. The last of these issues may well change soon with the expiration of many RAFT patents.[240, 241] Strategies to produce controllable and functionalised polymeric nanoparticles in a cheap and scalable way though, still remain a useful area of research.

### 1.4.4 Surfactant Free Emulsion Polymerisation

It is known that if an emulsion polymerisation monomer is hydrophilic enough, it may grow past the length of a *Z-mer* to a *J-mer*.[223] At this increased length the oligomer may act as a surfactant like molecule in its own right with the initiator head group providing the hydrophilic part, and one or many of these chains may self-nucleate without the need for additional surfactant. Work in the 1970's focussing on styrene, before the advent of controlled radical polymerisation techniques, particularly from Goodall, Wilkinson, Hearne and Roe exploited this in what was commonly deemed then "soap free" emulsion polymerisation.[242-244] In this work a classic emulsion polymerisation system was used, however the surfactant was not added, leading to a self-nucleating system of *J-mers*. It was found that the self-nucleation of particles with a sufficiently charged initator head group, such as potassium persulfate, was able to stabilise growing polymer particles. In these surfactant free emulsion polymerisations, particle growth was observed to proceed to a large extent by coagulative nucleation as well as internal polymer growth.[245] The initiators used in this technique to be able to

access particle diameters below 100 nm typically have a very strong charge to improve stability, there may still be concerns surrounding the biocompatibility of these head groups.[246-248] Attempts to use this technique with a less charged initiator typically result in particles over 100 nm up to microns in diameter.[249, 250] Limited work has focussed on using a surfactant free technique with a hydrophilic co-monomer such as acrylic acid to help access sub-100 nm particle diameters.[245, 251-253] The potential for the hydrophilic co-monomer to be incorporated into the final latex particle, potentially providing a facile route to functionalisation remains underexplored, a proposed mechanism for this is summarised in Figure 1.11.

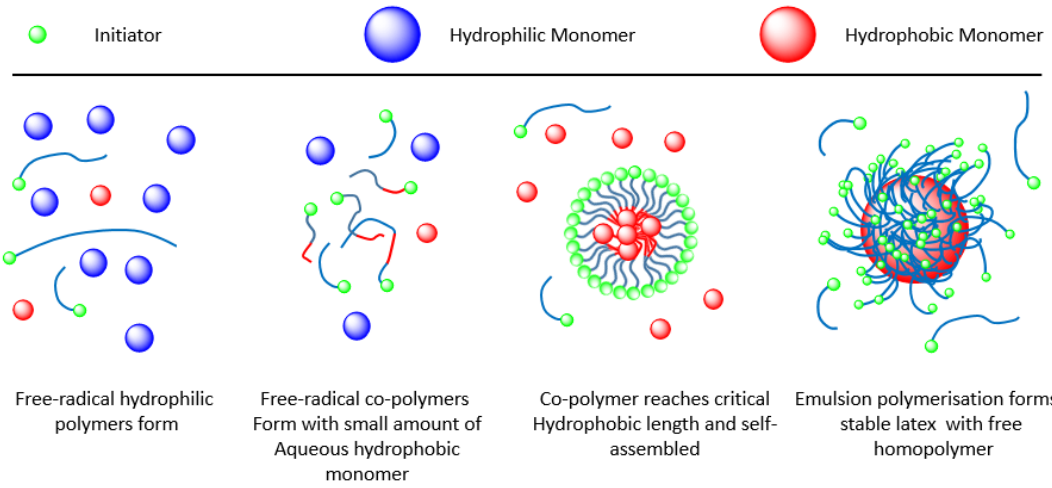


**Figure 1.11:** Proposed emulsion polymerisation mechanism in a free radical surfactant free emulsion polymerisation, including a hydrophilic co-monomer

Given the benefits of functionalised nanoparticles, it is unsurprising that there has been a plethora of research into their use as both diagnostic and drug delivery agents as previously discussed. Most of the nanoparticle based products that are actually being used in a clinical setting are still liposomal formulations.[35] However with the right fundamental study, addressing of current limitations and realistic translation of synthetic techniques, polymeric nanoparticles could still have a positive impact on therapeutics.

## 1.5 Motivation

Nanoparticles represent an interesting avenue of biomedical research, particularly as drug delivery agents. Strategies to synthesise clinically viable polymeric nanoparticles however are still in need of full development. Emulsion polymerisation represents one potential way of addressing that need, as a versatile technique with the potential to produce complex systems to an industrially relevant scale.

Existing strategies to produce functional nanoparticles with controllable size have focussed on controlled radical polymerisation techniques such as RAFT in an emulsion system. These systems are of great use in understanding fundamental properties of nanoparticles, such as the influence of core and shell characteristics on the biological properties of a particle. They are however potentially limited in scale and applicability by cost and challenges in gaining medical approval. Surfactant free emulsion polymerisation techniques may provide a solution to this issue. As a technique however it has until now, mainly been shown to be able to reliably control the size and charge of latex particles, with some reports of their surface functionality.

There is therefore still a need for cheap and scalable techniques to produce functional nanoparticles for a variety of uses. The work presented in this thesis will first focus on the preparation of glycosylated nanoparticles *via* RAFT emulsion polymerisation and use them to develop a DLS based technique to study lectin induced aggregation. Similar particles will be produced *via* a free radical surfactant free emulsion polymerisation, initially to establish if this technique can produce surface functionalised particles with the addition of a functional hydrophilic glycomonomer. The resulting glycoparticles will then be used to investigate the effect of particle core glass transition temperature on lectin induced aggregation. Finally the same surfactant free technique will be used to prepare a macrophage targeted, drug loaded nanoparticle system for the intracellular delivery of isoniazid, and investigated for its ability to kill intracellular mycobacteria as a mimic for *Mycobacteria tuberculosis*.

## 1.6 References


1. Farokhzad, O. C.; Langer, R., Impact of nanotechnology on drug delivery. *ACS Nano* **2009,** *3* (1), 16-20.
2. Priolo, F.; Gregorkiewicz, T.; Galli, M.; Krauss, T. F., Silicon nanostructures for photonics and photovoltaics. *Nature Nanotechnology* **2014,** *9* (1), 19.
3. Cheraghian, G.; Hendraningrat, L., A review on applications of nanotechnology in the enhanced oil recovery part B: effects of nanoparticles on flooding. *International Nano Letters* **2016,** *6* (1), 1-10.
4. Mobasser, S.; Firoozi, A. A., Review of nanotechnology applications in science and engineering. *Journal of Civil Engineering* **2016,** *6* (4), 84-93.
5. Elsabahy, M.; Wooley, K. L., Design of polymeric nanoparticles for biomedical delivery applications. *Chemical Society Reviews* **2012,** *41* (7), 2545-2561.
6. Samad, A.; Sultana, Y.; Aqil, M., Liposomal drug delivery systems: an update review. *Current Drug Delivery* **2007,** *4* (4), 297-305.
7. Liao, H.; Nehl, C. L.; Hafner, J. H., Biomedical applications of plasmon resonant metal nanoparticles. *Future Medicine* **2006**, 201-208.
8. Michalet, X.; Pinaud, F.; Bentolila, L.; Tsay, J.; Doose, S.; Li, J.; Sundaresan, G.; Wu, A.; Gambhir, S.; Weiss, S., Quantum dots for live cells, in vivo imaging, and diagnostics. *Science* **2005,** *307* (5709), 538-544.
9. Slowing, I. I.; Vivero-Escoto, J. L.; Wu, C.-W.; Lin, V. S.-Y., Mesoporous silica nanoparticles as controlled release drug delivery and gene transfection carriers. *Advanced Drug Delivery Reviews* **2008,** *60* (11), 1278-1288.
10. De Jong, W. H.; Borm, P. J., Drug delivery and nanoparticles: applications and hazards. *International Journal of Nanomedicine* **2008,** *3* (2), 133.
11. Gu, Z.; Biswas, A.; Zhao, M.; Tang, Y., Tailoring nanocarriers for intracellular protein delivery. *Chemical Society Reviews* **2011,** *40* (7), 3638-3655.
12. Raliya, R.; Singh Chadha, T.; Haddad, K.; Biswas, P., Perspective on nanoparticle technology for biomedical use. *Current Pharmaceutical Design* **2016,** *22* (17), 2481-2490.
13. Cole, L. E.; Ross, R. D.; Tilley, J. M.; Vargo-Gogola, T.; Roeder, R. K., Gold nanoparticles as contrast agents in x-ray imaging and computed tomography. *Nanomedicine* **2015,** *10* (2), 321-341.
14. Yeh, Y.-C.; Creran, B.; Rotello, V. M., Gold nanoparticles: preparation, properties, and applications in bionanotechnology. *Nanoscale* **2012,** *4* (6), 1871-1880.
15. Wen, S.; Zhao, L.; Zhao, Q.; Li, D.; Liu, C.; Yu, Z.; Shen, M.; Majoral, J.-P.; Mignani, S.; Zhao, J., A promising dual mode SPECT/CT imaging platform based on 99m Tc-labeled multifunctional dendrimer-entrapped gold nanoparticles. *Journal of Materials Chemistry B* **2017,** *5* (21), 3810-3815.
16. Lin, J.; Hu, W.; Gao, F.; Qin, J.; Peng, C.; Lu, X., Folic acid-modified diatrizoic acid-linked dendrimer-entrapped gold nanoparticles enable targeted CT imaging of human cervical cancer. *Journal of Cancer* **2018,** *9* (3), 564.
17. Zhu, J.; Wang, G.; Alves, C. S.; Tomás, H.; Xiong, Z.; Shen, M.; Rodrigues, J.; Shi, X., Multifunctional Dendrimer-Entrapped Gold Nanoparticles Conjugated with Doxorubicin for pH-Responsive Drug Delivery and Targeted Computed Tomography Imaging. *Langmuir* **2018,** *34* (41), 12428-12435.
18. Peng, C.; Zheng, L.; Chen, Q.; Shen, M.; Guo, R.; Wang, H.; Cao, X.; Zhang, G.; Shi, X., PEGylated dendrimer-entrapped gold nanoparticles for in vivo blood pool and tumor imaging by computed tomography. *Biomaterials* **2012,** *33* (4), 1107-1119.

19. Kim, D.; Jeong, Y. Y.; Jon, S., A drug-loaded aptamer− gold nanoparticle bioconjugate for combined CT imaging and therapy of prostate cancer. *ACS Nano* **2010,** *4* (7), 3689-3696.
20. Kim, D. E.; Kim, J. Y.; Sun, I. C.; Park, S. K.; Ahn, C. H.; Kim, K. M., CT contrast medium for detecting thrombus, comprising fibrin-targeted peptide sequence-conjugated glycol chitosan-gold nanoparticles. Google Patents: 2017.
21. Nam, J.-M.; Park, S.-J.; Mirkin, C. A., Bio-barcodes based on oligonucleotide-modified nanoparticles. *Journal of the American Chemical Society* **2002,** *124* (15), 3820-3821.
22. Hill, H. D.; Mirkin, C. A., The bio-barcode assay for the detection of protein and nucleic acid targets using DTT-induced ligand exchange. *Nature Protocols* **2006,** *1* (1), 324.
23. Nam, J.-M.; Jang, K.-J.; Groves, J. T., Detection of proteins using a colorimetric bio-barcode assay. *Nature Protocols* **2007,** *2* (6), 1438.
24. Richards, S.-J.; Otten, L.; Gibson, M. I., Glycosylated gold nanoparticle libraries for label-free multiplexed lectin biosensing. *Journal of Materials Chemistry B* **2016,** *4* (18), 3046-3053.
25. Wang, Y.; Zhao, Q.; Han, N.; Bai, L.; Li, J.; Liu, J.; Che, E.; Hu, L.; Zhang, Q.; Jiang, T., Mesoporous silica nanoparticles in drug delivery and biomedical applications. *Nanomedicine: Nanotechnology, Biology Medicine* **2015,** *11* (2), 313-327.
26. Bharti, C.; Nagaich, U.; Pal, A. K.; Gulati, N., Mesoporous silica nanoparticles in target drug delivery system: a review. *International Journal of Pharmaceutical Investigation* **2015,** *5* (3), 124.
27. Trewyn, B. G.; Giri, S.; Slowing, I. I.; Lin, V. S.-Y., Mesoporous silica nanoparticle based controlled release, drug delivery, and biosensor systems. *Chemical Communications* **2007,** (31), 3236-3245.
28. Hans, M.; Lowman, A., Biodegradable nanoparticles for drug delivery and targeting. *Current Opinion in Solid State Materials Science* **2002,** *6* (4), 319-327.
29. Masood, F., Polymeric nanoparticles for targeted drug delivery system for cancer therapy. *Materials Science Engineering: C* **2016,** *60*, 569-578.
30. Torchilin, V. P., Multifunctional, stimuli-sensitive nanoparticulate systems for drug delivery. *Nature Reviews Drug Discovery* **2014,** *13* (11), 813.
31. Bae, Y. H.; Park, K., Targeted drug delivery to tumors: myths, reality and possibility. *Journal of Controlled Release* **2011,** *153* (3), 198.
32. Gregory, A.; Stenzel, M. H., Complex polymer architectures via RAFT polymerization: From fundamental process to extending the scope using click chemistry and nature's building blocks. *Progress in polymer science* **2012,** *37* (1), 38-105.
33. Longmire, M.; Choyke, P. L.; Kobayashi, H., Clearance properties of nano-sized particles and molecules as imaging agents: considerations and caveats. **2008**.
34. Bobo, D.; Robinson, K. J.; Islam, J.; Thurecht, K. J.; Corrie, S. R., Nanoparticle-based medicines: a review of FDA-approved materials and clinical trials to date. *Pharmaceutical Research* **2016,** *33* (10), 2373-2387.
35. Anselmo, A. C.; Mitragotri, S., Nanoparticles in the clinic. *Bioengineering Translational Medicine* **2016,** *1* (1), 10-29.
36. Bangham, A.; Standish, M. M.; Watkins, J. C., Diffusion of univalent ions across the lamellae of swollen phospholipids. *Journal of Molecular Biology* **1965,** *13* (1), 238-IN27.

37. Vaage, J.; Mayhew, E.; Lasic, D.; Martin, F., Therapy of primary and metastatic mouse mammary carcinomas with doxorubicin encapsulated in long circulating liposomes. *International Journal of Cancer* **1992,** *51* (6), 942-948.
38. Balasegaram, M.; Ritmeijer, K.; Lima, M. A.; Burza, S.; Ortiz Genovese, G.; Milani, B.; Gaspani, S.; Potet, J.; Chappuis, F., Liposomal amphotericin B as a treatment for human leishmaniasis. *Expert Opinion on Emerging Drugs* **2012,** *17* (4), 493-510.
39. Antonietti, M.; Förster, S., Vesicles and liposomes: a self-assembly principle beyond lipids. *Advanced Materials* **2003,** *15* (16), 1323-1333.
40. Riviere, K.; Kieler-Ferguson, H. M.; Jerger, K.; Szoka Jr, F. C., Anti-tumor activity of liposome encapsulated fluoroorotic acid as a single agent and in combination with liposome irinotecan. *Journal of Controlled Release* **2011,** *153* (3), 288-296.
41. Allen, T. M.; Cullis, P. R., Liposomal drug delivery systems: from concept to clinical applications. *Advanced Drug Delivery Reviews* **2013,** *65* (1), 36-48.
42. Vader, P.; Mol, E. A.; Pasterkamp, G.; Schiffelers, R. M., Extracellular vesicles for drug delivery. *Advanced Drug Delivery Reviews* **2016,** *106*, 148-156.
43. Ochyl, L. J.; Bazzill, J. D.; Park, C.; Xu, Y.; Kuai, R.; Moon, J. J., PEGylated tumor cell membrane vesicles as a new vaccine platform for cancer immunotherapy. *Biomaterials Science* **2018,** *182*, 157-166.
44. Kooijmans, S.; Fliervoet, L.; Van Der Meel, R.; Fens, M.; Heijnen, H.; en Henegouwen, P. v. B.; Vader, P.; Schiffelers, R., PEGylated and targeted extracellular vesicles display enhanced cell specificity and circulation time. *Journal of Controlled Release* **2016,** *224*, 77-85.
45. Hawkins, M. J.; Soon-Shiong, P.; Desai, N., Protein nanoparticles as drug carriers in clinical medicine. *Advanced Drug Delivery Reviews* **2008,** *60* (8), 876-885.
46. Green, M.; Manikhas, G.; Orlov, S.; Afanasyev, B.; Makhson, A.; Bhar, P.; Hawkins, M., Abraxane®, a novel Cremophor®-free, albumin-bound particle form of paclitaxel for the treatment of advanced non-small-cell lung cancer. *Annals of Oncology* **2006,** *17* (8), 1263-1268.
47. Gelderblom, H.; Verweij, J.; Nooter, K.; Sparreboom, A., Cremophor EL: the drawbacks and advantages of vehicle selection for drug formulation. *European Journal of Cancer* **2001,** *37* (13), 1590-1598.
48. Miele, E.; Spinelli, G. P.; Miele, E.; Tomao, F.; Tomao, S., Albumin-Bound Formulation of Paclitaxel (Abraxane® ABI-007) in the Treatment of Breast Cancer. *International Journal of Nanomedicine* **2009,** *4*, 99.
49. Hubbell, J. A.; Langer, R., Translating materials design to the clinic. *Nature Materials* **2013,** *12* (11), 963-966.
50. McDaniel, J. R.; Bhattacharyya, J.; Vargo, K. B.; Hassouneh, W.; Hammer, D. A.; Chilkoti, A., Roadmap for the design of drug-loaded thermoresponsive polypeptide nanoparticles. *Angewandte Chemie International Edition* **2013,** *52* (6), 1683.
51. McDaniel, J. R.; MacEwan, S. R.; Dewhirst, M.; Chilkoti, A., Doxorubicin-conjugated chimeric polypeptide nanoparticles that respond to mild hyperthermia. *Journal of Controlled Release* **2012,** *159* (3), 362-367.
52. Soppimath, K. S.; Aminabhavi, T. M.; Kulkarni, A. R.; Rudzinski, W. E., Biodegradable polymeric nanoparticles as drug delivery devices. *Journal of Controlled Release* **2001,** *70* (1-2), 1-20.
53. Chan, J. M.; Valencia, P. M.; Zhang, L.; Langer, R.; Farokhzad, O. C., Polymeric nanoparticles for drug delivery. In *Cancer Nanotechnology*, Springer: 2010; pp 163-175.

54. Cho, K.; Wang, X.; Nie, S.; Shin, D. M., Therapeutic nanoparticles for drug delivery in cancer. *Clinical Cancer Research* **2008,** *14* (5), 1310-1316.
55. Ragelle, H.; Danhier, F.; Préat, V.; Langer, R.; Anderson, D. G., Nanoparticle-based drug delivery systems: a commercial and regulatory outlook as the field matures. *Expert Opinion on Drug Delivery* **2017,** *14* (7), 851-864.
56. Pasut, G.; Veronese, F. M., PEG conjugates in clinical development or use as anticancer agents: an overview. *Advanced Drug Delivery Reviews* **2009,** *61* (13), 1177-1188.
57. Duncan, R., Polymer therapeutics: top 10 selling pharmaceuticals—what next? *Journal of Controlled Release* **2014,** *190*, 371-380.
58. Alconcel, S. N.; Baas, A. S.; Maynard, H. D., FDA-approved poly (ethylene glycol)–protein conjugate drugs. *Polymer Chemistry* **2011,** *2* (7), 1442-1448.
59. Aschenbrenner, D. S., First Pegfilgrastim Biosimilar Approved. *AJN The American Journal of Nursing* **2018,** *118* (10), 19-20.
60. Aladul, M. I.; Fitzpatrick, R. W.; Chapman, S. R., Healthcare professionals' perceptions and perspectives on biosimilar medicines and the barriers and facilitators to their prescribing in UK: a qualitative study. *BMJ Open* **2018,** *8* (11), e023603.
61. Sobotta, F. H.; Hausig, F.; Harz, D. O.; Hoeppener, S.; Schubert, U. S.; Brendel, J. C., Oxidation-responsive micelles by a one-pot polymerization-induced self-assembly approach. *Polymer Chemistry* **2018,** *9* (13), 1593-1602.
62. Takeuchi, I.; Nobata, S.; Oiri, N.; Tomoda, K.; Makino, K., Biodistribution and excretion of colloidal gold nanoparticles after intravenous injection: Effects of particle size. *Bio-Medical Materials Engineering* **2017,** *28* (3), 315-323.
63. De las Heras Alarcón, C.; Pennadam, S.; Alexander, C., Stimuli responsive polymers for biomedical applications. *Chemical Society Reviews* **2005,** *34* (3), 276-285.
64. Martínez-Pérez, B.; Quintanar-Guerrero, D.; Tapia-Tapia, M.; Cisneros-Tamayo, R.; Zambrano-Zaragoza, M. L.; Alcalá-Alcalá, S.; Mendoza-Muñoz, N.; Piñón-Segundo, E., Controlled-release biodegradable nanoparticles: From preparation to vaginal applications. *European Journal of Pharmaceutical Sciences* **2018,** *115*, 185-195.
65. DeMarino, C.; Schwab, A.; Pleet, M.; Mathiesen, A.; Friedman, J.; El-Hage, N.; Kashanchi, F., Biodegradable nanoparticles for delivery of therapeutics in CNS infection. *Journal of Neuroimmune Pharmacology* **2017,** *12* (1), 31-50.
66. Panyam, J.; Labhasetwar, V., Biodegradable nanoparticles for drug and gene delivery to cells and tissue. *Advanced Drug Delivery Reviews* **2003,** *55* (3), 329-347.
67. Esposito, D.; Conte, C.; Dal Poggetto, G.; Russo, A.; Barbieri, A.; Ungaro, F.; Arra, C.; Russo, G.; Laurienzo, P.; Quaglia, F., Biodegradable nanoparticles bearing amine groups as a strategy to alter surface features, biological identity and accumulation in a lung metastasis model. *Journal of Materials Chemistry B* **2018,** *6* (37), 5922-5930.
68. Zhang, W.-J.; Hong, C.-Y.; Pan, C.-Y., Efficient fabrication of photosensitive polymeric nano-objects via an ingenious formulation of RAFT dispersion polymerization and their application for drug delivery. *Biomacromolecules* **2017,** *18* (4), 1210-1217.
69. Ishida, T.; Wang, X.; Shimizu, T.; Nawata, K.; Kiwada, H., PEGylated liposomes elicit an anti-PEG IgM response in a T cell-independent manner. *Journal of Controlled Release* **2007,** *122* (3), 349-355.
70. Cui, S.; Yin, D.; Chen, Y.; Di, Y.; Chen, H.; Ma, Y.; Achilefu, S.; Gu, Y., In vivo targeted deep-tissue photodynamic therapy based on near-infrared light triggered upconversion nanoconstruct. *ACS Nano* **2012,** *7* (1), 676-688.

71. Mittal, M.; Siddiqui, M. R.; Tran, K.; Reddy, S. P.; Malik, A. B., Reactive oxygen species in inflammation and tissue injury. *Antioxidants Redox Signaling* **2014,** *20* (7), 1126-1167.
72. Yuan, W.; Yuan, J.; Zheng, S.; Hong, X., Synthesis, characterization, and controllable drug release of dendritic star-block copolymer by ring-opening polymerization and atom transfer radical polymerization. *Polymer* **2007,** *48* (9), 2585-2594.
73. Bütün, V.; Bennett, C. E.; Vamvakaki, M.; Lowe, A. B.; Billingham, N. C.; Armes, S. P., Selective betainisation of tertiary amine methacrylate block copolymers. *Journal of Materials Chemistry B* **1997,** *7* (9), 1693-1695.
74. Sun, X.; Jiang, G.; Wang, Y.; Xu, Y., Synthesis and drug release properties of novel pH-and temperature-sensitive copolymers based on a hyperbranched polyether core. *Colloid Polymer Science* **2011,** *289* (5-6), 677-684.
75. Pinto-Alphandary, H.; Andremont, A.; Couvreur, P., Targeted delivery of antibiotics using liposomes and nanoparticles: research and applications. *International Journal of Antimicrobial Agents* **2000,** *13* (3), 155-168.
76. Forier, K.; Raemdonck, K.; De Smedt, S. C.; Demeester, J.; Coenye, T.; Braeckmans, K., Lipid and polymer nanoparticles for drug delivery to bacterial biofilms. *Journal of Controlled Release* **2014,** *190*, 607-623.
77. Singh, R.; Lillard Jr, J. W., Nanoparticle-based targeted drug delivery. *Experimental Molecular Pathology* **2009,** *86* (3), 215-223.
78. Shen, S.; Wu, Y.; Liu, Y.; Wu, D., High drug-loading nanomedicines: progress, current status, and prospects. *International Journal of Nanomedicine* **2017,** *12*, 4085.
79. Qin, S.-Y.; Zhang, A.-Q.; Cheng, S.-X.; Rong, L.; Zhang, X.-Z., Drug self-delivery systems for cancer therapy. *Biomaterials* **2017,** *112*, 234-247.
80. Zheng, S.; Xie, Y.; Li, Y.; Li, L.; Tian, N.; Zhu, W.; Yan, G.; Wu, C.; Hu, H., Development of high drug-loading nanomicelles targeting steroids to the brain. *International Journal of Nanomedicine* **2014,** *9*, 55.
81. Eloy, J. O.; de Souza, M. C.; Petrilli, R.; Barcellos, J. P. A.; Lee, R. J.; Marchetti, J. M., Liposomes as carriers of hydrophilic small molecule drugs: strategies to enhance encapsulation and delivery. *Colloids Surfaces B: Biointerfaces* **2014,** *123*, 345-363.
82. Mohammed, A.; Weston, N.; Coombes, A.; Fitzgerald, M.; Perrie, Y., Liposome formulation of poorly water soluble drugs: optimisation of drug loading and ESEM analysis of stability. *International Journal of Pharmaceutics* **2004,** *285* (1-2), 23-34.
83. Taylor, K.; Taylor, G.; Kellaway, I.; Stevens, J., Drug entrapment and release from multilamellar and reverse-phase evaporation liposomes. *International Journal of Pharmaceutics* **1990,** *58* (1), 49-55.
84. Barenholz, Y. C., Doxil®—the first FDA-approved nano-drug: lessons learned. *Journal of Controlled Release* **2012,** *160* (2), 117-134.
85. Govender, T.; Stolnik, S.; Garnett, M. C.; Illum, L.; Davis, S. S., PLGA nanoparticles prepared by nanoprecipitation: drug loading and release studies of a water soluble drug. *Journal of Controlled Release* **1999,** *57* (2), 171-185.
86. Calvo, P.; Remuñan-López, C.; Vila-Jato, J. L.; Alonso, M. J., Chitosan and chitosan/ethylene oxide-propylene oxide block copolymer nanoparticles as novel carriers for proteins and vaccines. *Pharmaceutical Research* **1997,** *14* (10), 1431-1436.
87. Wu, J.; Zhu, Y. J.; Cao, S. W.; Chen, F., Hierachically Nanostructured Mesoporous Spheres of Calcium Silicate Hydrate: Surfactant-Free Sonochemical

Synthesis and Drug-Delivery System with Ultrahigh Drug-Loading Capacity. *Advanced Materials* **2010,** *22* (6), 749-753.
88. Tarn, D.; Ashley, C. E.; Xue, M.; Carnes, E. C.; Zink, J. I.; Brinker, C. J., Mesoporous silica nanoparticle nanocarriers: biofunctionality and biocompatibility. *Accounts of Chemical Research* **2013,** *46* (3), 792-801.
89. Watermann, A.; Brieger, J., Mesoporous silica nanoparticles as drug delivery vehicles in cancer. *Nanomaterials* **2017,** *7* (7), 189.
90. Jiang, S.; Zhang, Y.; Shu, Y.; Wu, Z.; Cao, W.; Huang, W., Amino-functionalized mesoporous bioactive glass for drug delivery. *Biomedical Materials* **2017,** *12* (2), 025017.
91. Mundargi, R. C.; Babu, V. R.; Rangaswamy, V.; Patel, P.; Aminabhavi, T. M., Nano/micro technologies for delivering macromolecular therapeutics using poly (D, L-lactide-co-glycolide) and its derivatives. *Journal of Controlled Release* **2008,** *125* (3), 193-209.
92. Vrignaud, S.; Benoit, J.-P.; Saulnier, P., Strategies for the nanoencapsulation of hydrophilic molecules in polymer-based nanoparticles. *Biomaterials* **2011,** *32* (33), 8593-8604.
93. Lee, G., Spray-drying of proteins. In *Rational design of stable protein formulations*, Springer: 2002; pp 135-158.
94. Faheem, A.; Haggag, Y., Evaluation of nano spray drying as a method for drying and formulation of therapeutic peptides and proteins. *Frontiers in Pharmacology* **2015,** *6*, 140.
95. Liu, J.; Huang, Y.; Kumar, A.; Tan, A.; Jin, S.; Mozhi, A.; Liang, X.-J., pH-sensitive nano-systems for drug delivery in cancer therapy. *Biotechnology Advances* **2014,** *32* (4), 693-710.
96. Gou, P.; Liu, W.; Mao, W.; Tang, J.; Shen, Y.; Sui, M., Self-assembling doxorubicin prodrug forming nanoparticles for cancer chemotherapy: synthesis and anticancer study in vitro and in vivo. *Journal of Materials Chemistry B* **2013,** *1* (3), 284-292.
97. Bae, Y.; Jang, W.-D.; Nishiyama, N.; Fukushima, S.; Kataoka, K., Multifunctional polymeric micelles with folate-mediated cancer cell targeting and pH-triggered drug releasing properties for active intracellular drug delivery. *Molecular BioSystems* **2005,** *1* (3), 242-250.
98. Cheng, R.; Feng, F.; Meng, F.; Deng, C.; Feijen, J.; Zhong, Z., Glutathione-responsive nano-vehicles as a promising platform for targeted intracellular drug and gene delivery. *Journal of Controlled Release* **2011,** *152* (1), 2-12.
99. Balendiran, G. K.; Dabur, R.; Fraser, D., The role of glutathione in cancer. *Cell Biochemistry Function: Cellular Biochemistry its Modulation by Active Agents or Disease* **2004,** *22* (6), 343-352.
100. Huo, M.; Yuan, J.; Tao, L.; Wei, Y., Redox-responsive polymers for drug delivery: from molecular design to applications. *Polymer Chemistry* **2014,** *5* (5), 1519-1528.
101. Shen, Y.; Jin, E.; Zhang, B.; Murphy, C. J.; Sui, M.; Zhao, J.; Wang, J.; Tang, J.; Fan, M.; Van Kirk, E., Prodrugs forming high drug loading multifunctional nanocapsules for intracellular cancer drug delivery. *Journal of the American Chemical Society* **2010,** *132* (12), 4259-4265.
102. Baranowski, P.; Karolewicz, B.; Gajda, M.; Pluta, J., Ophthalmic drug dosage forms: characterisation and research methods. *The Scientific World Journal* **2014,** *2014*.

103. Carvalho, T. C.; Peters, J. I.; Williams III, R. O., Influence of particle size on regional lung deposition–what evidence is there? *International Journal of Pharmaceutics* **2011,** *406* (1-2), 1-10.
104. Agrawal, M.; Tripathi, D. K.; Saraf, S.; Saraf, S.; Antimisiaris, S. G.; Mourtas, S.; Hammarlund-Udenaes, M.; Alexander, A., Recent advancements in liposomes targeting strategies to cross blood-brain barrier (BBB) for the treatment of Alzheimer's disease. *Journal of Controlled Release* **2017,** *260*, 61-77.
105. Gaumet, M.; Vargas, A.; Gurny, R.; Delie, F. J. E. j. o. p.; biopharmaceutics, Nanoparticles for drug delivery: the need for precision in reporting particle size parameters. **2008,** *69* (1), 1-9.
106. Gaumet, M.; Vargas, A.; Gurny, R.; Delie, F., Nanoparticles for drug delivery: the need for precision in reporting particle size parameters. *European Journal of Pharmaceutics Biopharmaceutics & Drug Disposition* **2008,** *69* (1), 1-9.
107. Longmire, M.; Choyke, P. L.; Kobayashi, H., Clearance properties of nano-sized particles and molecules as imaging agents: considerations and caveats. *Future Medicine* **2008**, 703-717.
108. De Jong, W. H.; Hagens, W. I.; Krystek, P.; Burger, M. C.; Sips, A. J.; Geertsma, R. E., Particle size-dependent organ distribution of gold nanoparticles after intravenous administration. *Biomaterials* **2008,** *29* (12), 1912-1919.
109. Choi, H. S.; Liu, W.; Misra, P.; Tanaka, E.; Zimmer, J. P.; Ipe, B. I.; Bawendi, M. G.; Frangioni, J. V., Renal clearance of quantum dots. *Nature biotechnology* **2007,** *25* (10), 1165.
110. He, C.; Hu, Y.; Yin, L.; Tang, C.; Yin, C., Effects of particle size and surface charge on cellular uptake and biodistribution of polymeric nanoparticles. *Biomaterials* **2010,** *31* (13), 3657-3666.
111. Canton, I.; Battaglia, G., Endocytosis at the nanoscale. *Chemical Society Reviews* **2012,** *41* (7), 2718-2739.
112. Chithrani, B. D.; Chan, W. C., Elucidating the mechanism of cellular uptake and removal of protein-coated gold nanoparticles of different sizes and shapes. *Nano Letters* **2007,** *7* (6), 1542-1550.
113. Lu, F.; Wu, S. H.; Hung, Y.; Mou, C. Y., Size effect on cell uptake in well-suspended, uniform mesoporous silica nanoparticles. *Small* **2009,** *5* (12), 1408-1413.
114. Shang, L.; Nienhaus, K.; Nienhaus, G. U., Engineered nanoparticles interacting with cells: size matters. *Journal of Nanobiotechnology* **2014,** *12* (1), 5.
115. Trewyn, B. G.; Nieweg, J. A.; Zhao, Y.; Lin, V. S.-Y., Biocompatible mesoporous silica nanoparticles with different morphologies for animal cell membrane penetration. *Chemical Engineering Journal* **2008,** *137* (1), 23-29.
116. Geng, Y.; Dalhaimer, P.; Cai, S.; Tsai, R.; Tewari, M.; Minko, T.; Discher, D. E., Shape effects of filaments versus spherical particles in flow and drug delivery. *Nature Nanotechnology* **2007,** *2* (4), 249.
117. Decuzzi, P.; Godin, B.; Tanaka, T.; Lee, S.-Y.; Chiappini, C.; Liu, X.; Ferrari, M., Size and shape effects in the biodistribution of intravascularly injected particles. *Journal of Controlled Release* **2010,** *141* (3), 320-327.
118. Toy, R.; Peiris, P. M.; Ghaghada, K. B.; Karathanasis, E., Shaping cancer nanomedicine: the effect of particle shape on the in vivo journey of nanoparticles. *Nanomedicine: Nanotechnology, Biology Medicine* **2014,** *9* (1), 121-134.
119. Lee, S.-Y.; Ferrari, M.; Decuzzi, P., Shaping nano-/micro-particles for enhanced vascular interaction in laminar flows. *Nanotechnology* **2009,** *20* (49), 495101.

120. Chithrani, B. D.; Ghazani, A. A.; Chan, W. C., Determining the size and shape dependence of gold nanoparticle uptake into mammalian cells. *Nano Letters* **2006,** *6* (4), 662-668.
121. Sharma, G.; Valenta, D. T.; Altman, Y.; Harvey, S.; Xie, H.; Mitragotri, S.; Smith, J. W., Polymer particle shape independently influences binding and internalization by macrophages. *Journal of Controlled Release* **2010,** *147* (3), 408-412.
122. Gratton, S. E.; Ropp, P. A.; Pohlhaus, P. D.; Luft, J. C.; Madden, V. J.; Napier, M. E.; DeSimone, J. M., The effect of particle design on cellular internalization pathways. *Proceedings of the National Academy of Sciences* **2008,** *105* (33), 11613-11618.
123. Albanese, A.; Tang, P. S.; Chan, W. C., The effect of nanoparticle size, shape, and surface chemistry on biological systems. *Annual Review of Biomedical Engineering* **2012,** *14*, 1-16.
124. Qiu, Y.; Liu, Y.; Wang, L.; Xu, L.; Bai, R.; Ji, Y.; Wu, X.; Zhao, Y.; Li, Y.; Chen, C., Surface chemistry and aspect ratio mediated cellular uptake of Au nanorods. *Biomaterials* **2010,** *31* (30), 7606-7619.
125. Fröhlich, E., The role of surface charge in cellular uptake and cytotoxicity of medical nanoparticles. *International Journal of Nanomedicine* **2012,** *7*, 5577.
126. Perumal, O. P.; Inapagolla, R.; Kannan, S.; Kannan, R. M., The effect of surface functionality on cellular trafficking of dendrimers. *Biomaterials* **2008,** *29* (24-25), 3469-3476.
127. Foged, C.; Brodin, B.; Frokjaer, S.; Sundblad, A., Particle size and surface charge affect particle uptake by human dendritic cells in an in vitro model. *International Journal of Pharmaceutics* **2005,** *298* (2), 315-322.
128. Hunter, A. C.; Moghimi, S. M., Cationic carriers of genetic material and cell death: a mitochondrial tale. *Biochimica et Biophysica Acta -Bioenergetics* **2010,** *1797* (6-7), 1203-1209.
129. Symonds, P.; Murray, J. C.; Hunter, A. C.; Debska, G.; Szewczyk, A.; Moghimi, S. M., Low and high molecular weight poly (l-lysine) s/poly (l-lysine)–DNA complexes initiate mitochondrial-mediated apoptosis differently. *FEBS letters* **2005,** *579* (27), 6191-6198.
130. Li, S.-D.; Huang, L., Stealth nanoparticles: high density but sheddable PEG is a key for tumor targeting. *Journal of Controlled Release* **2010,** *145* (3), 178.
131. Gref, R.; Lück, M.; Quellec, P.; Marchand, M.; Dellacherie, E.; Harnisch, S.; Blunk, T.; Müller, R., 'Stealth'corona-core nanoparticles surface modified by polyethylene glycol (PEG): influences of the corona (PEG chain length and surface density) and of the core composition on phagocytic uptake and plasma protein adsorption. *Colloids Surfaces B: Biointerfaces* **2000,** *18* (3-4), 301-313.
132. Jokerst, J. V.; Lobovkina, T.; Zare, R. N.; Gambhir, S. S., Nanoparticle PEGylation for imaging and therapy. *Nanomedicine* **2011,** *6* (4), 715-728.
133. Suk, J. S.; Xu, Q.; Kim, N.; Hanes, J.; Ensign, L. M., PEGylation as a strategy for improving nanoparticle-based drug and gene delivery. *Advanced Drug Delivery Reviews* **2016,** *99*, 28-51.
134. Harris, J. M.; Chess, R. B., Effect of pegylation on pharmaceuticals. *Nature Reviews Drug Discovery* **2003,** *2* (3), 214.
135. Veronese, F. M.; Pasut, G., PEGylation, successful approach to drug delivery. *Drug Discovery Today* **2005,** *10* (21), 1451-1458.
136. Perry, J. L.; Reuter, K. G.; Kai, M. P.; Herlihy, K. P.; Jones, S. W.; Luft, J. C.; Napier, M.; Bear, J. E.; DeSimone, J. M., PEGylated PRINT nanoparticles: the

impact of PEG density on protein binding, macrophage association, biodistribution, and pharmacokinetics. *Nano Letters* **2012,** *12* (10), 5304-5310.
137. Verhoef, J. J.; Carpenter, J. F.; Anchordoquy, T. J.; Schellekens, H., Potential induction of anti-PEG antibodies and complement activation toward PEGylated therapeutics. *Drug Discovery Today* **2014,** *19* (12), 1945-1952.
138. Ishida, T.; Ichihara, M.; Wang, X.; Yamamoto, K.; Kimura, J.; Majima, E.; Kiwada, H., Injection of PEGylated liposomes in rats elicits PEG-specific IgM, which is responsible for rapid elimination of a second dose of PEGylated liposomes. *Journal of Controlled Release* **2006,** *112* (1), 15-25.
139. Garay, R. P.; El-Gewely, R.; Armstrong, J. K.; Garratty, G.; Richette, P., Antibodies against polyethylene glycol in healthy subjects and in patients treated with PEG-conjugated agents. Taylor & Francis: 2012.
140. Viegas, T. X.; Bentley, M. D.; Harris, J. M.; Fang, Z.; Yoon, K.; Dizman, B.; Weimer, R.; Mero, A.; Pasut, G.; Veronese, F. M. J. B. c., Polyoxazoline: chemistry, properties, and applications in drug delivery. **2011,** *22* (5), 976-986.
141. Bender, J. C. M. E.; Hoogenboom, R.; Van Hest, J. C. M.; Van Goor, H., Cross-linked polymers and medical products derived from nucleophilically activated polyoxazoline. Google Patents: 2018.
142. Chen, W.; Zhou, S.; Ge, L.; Wu, W.; Jiang, X., Translatable high drug loading drug delivery systems based on biocompatible polymer nanocarriers. *Biomacromolecules* **2018,** *19* (6), 1732-1745.
143. Wilson, P.; Ke, P. C.; Davis, T. P.; Kempe, K., Poly (2-oxazoline)-based micro-and nanoparticles: A review. *European Polymer Journal* **2017,** *88*, 486-515.
144. Bauer, M.; Lautenschlaeger, C.; Kempe, K.; Tauhardt, L.; Schubert, U. S.; Fischer, D., Poly (2-ethyl-2-oxazoline) as Alternative for the Stealth Polymer Poly (ethylene glycol): Comparison of in vitro Cytotoxicity and Hemocompatibility. *Macromolecular Bioscience* **2012,** *12* (7), 986-998.
145. Verbrugghen, T.; Monnery, B. D.; Glassner, M.; Stroobants, S.; Hoogenboom, R.; Staelens, S., μPET imaging of the pharmacokinetic behavior of medium and high molar mass 89Zr-labeled poly (2-ethyl-2-oxazoline) in comparison to poly (ethylene glycol). *Journal of Controlled Release* **2016,** *235*, 63-71.
146. Han, Y.; He, Z.; Schulz, A.; Bronich, T. K.; Jordan, R.; Luxenhofer, R.; Kabanov, A. V., Synergistic combinations of multiple chemotherapeutic agents in high capacity poly (2-oxazoline) micelles. *Molecular Pharmaceutics* **2012,** *9* (8), 2302-2313.
147. He, Z.; Schulz, A.; Wan, X.; Seitz, J.; Bludau, H.; Alakhova, D. Y.; Darr, D. B.; Perou, C. M.; Jordan, R.; Ojima, I., Poly (2-oxazoline) based micelles with high capacity for 3rd generation taxoids: preparation, in vitro and in vivo evaluation. *Journal of Controlled Release* **2015,** *208*, 67-75.
148. Dam, T. K.; Gerken, T. A.; Brewer, C. F., Thermodynamics of Multivalent Carbohydrate− Lectin Cross-Linking Interactions: Importance of Entropy in the Bind and Jump Mechanism. *Biochemistry* **2009,** *48* (18), 3822-3827.
149. Godula, K.; Umbel, M. L.; Rabuka, D.; Botyanszki, Z.; Bertozzi, C. R.; Parthasarathy, R., Control of the molecular orientation of membrane-anchored biomimetic glycopolymers. *Journal of the American Chemical Society* **2009,** *131* (29), 10263-10268.
150. Lehotzky, R. E.; Partch, C. L.; Mukherjee, S.; Cash, H. L.; Goldman, W. E.; Gardner, K. H.; Hooper, L. V., Molecular basis for peptidoglycan recognition by a bactericidal lectin. *Proceedings of the National Academy of Sciences* **2010,** *107* (17), 7722-7727.

151. Sahoo, S. K.; Misra, R.; Parveen, S., Nanoparticles: a boon to drug delivery, therapeutics, diagnostics and imaging. In *Nanomedicine in Cancer*, Pan Stanford: 2017; pp 73-124.
152. Zhang, Y.-N.; Poon, W.; Tavares, A. J.; McGilvray, I. D.; Chan, W. C., Nanoparticle–liver interactions: Cellular uptake and hepatobiliary elimination. *Journal of Controlled Release* **2016,** *240*, 332-348.
153. Almeida, J. P. M.; Chen, A. L.; Foster, A.; Drezek, R., In vivo biodistribution of nanoparticles. *Nanomedicine* **2011,** *6* (5), 815-835.
154. Pulavendran, S.; Rose, C.; Mandal, A. B., Hepatocyte growth factor incorporated chitosan nanoparticles augment the differentiation of stem cell into hepatocytes for the recovery of liver cirrhosis in mice. *Journal of Nanobiotechnology* **2011,** *9* (1), 15.
155. Chiannilkulchai, N.; Ammoury, N.; Caillou, B.; Devissaguet, J. P.; Couvreur, P., Hepatic tissue distribution of doxorubicin-loaded nanoparticles after iv administration in reticulosarcoma M 5076 metastasis-bearing mice. *Cancer Chemotherapy Pharmacology and Therapeutics* **1990,** *26* (2), 122-126.
156. Canup, B. S.; Song, H.; Le Ngo, V.; Meng, X.; Denning, T. L.; Garg, P.; Laroui, H., CD98 siRNA-loaded nanoparticles decrease hepatic steatosis in mice. *Digestive Liver Disease* **2017,** *49* (2), 188-196.
157. Fang, J.; Nakamura, H.; Maeda, H., The EPR effect: unique features of tumor blood vessels for drug delivery, factors involved, and limitations and augmentation of the effect. *Advanced Drug Delivery Reviews* **2011,** *63* (3), 136-151.
158. Torchilin, V., Tumor delivery of macromolecular drugs based on the EPR effect. *Advanced drug delivery reviews* **2011,** *63* (3), 131-135.
159. Acharya, S.; Sahoo, S. K., PLGA nanoparticles containing various anticancer agents and tumour delivery by EPR effect. *Advanced drug delivery reviews* **2011,** *63* (3), 170-183.
160. Maeda, H.; Bharate, G.; Daruwalla, J., Polymeric drugs for efficient tumor-targeted drug delivery based on EPR-effect. *European Journal of Pharmaceutics Biopharmaceutics* **2009,** *71* (3), 409-419.
161. Chauhan, V. P.; Stylianopoulos, T.; Martin, J. D.; Popović, Z.; Chen, O.; Kamoun, W. S.; Bawendi, M. G.; Fukumura, D.; Jain, R. K., Normalization of tumour blood vessels improves the delivery of nanomedicines in a size-dependent manner. *Nature Nanotechnology* **2012,** *7* (6), 383-388.
162. Wilhelm, S.; Tavares, A. J.; Dai, Q.; Ohta, S.; Audet, J.; Dvorak, H. F.; Chan, W. C., Analysis of nanoparticle delivery to tumours. *Nature Reviews Materials* **2016,** *1* (5), 16014.
163. Hansen, A. E.; Petersen, A. L.; Henriksen, J. R.; Boerresen, B.; Rasmussen, P.; Elema, D. R.; Rosenschöld, P. M. a.; Kristensen, A. T.; Kjær, A.; Andresen, T. L., Positron emission tomography based elucidation of the enhanced permeability and retention effect in dogs with cancer using copper-64 liposomes. *ACS Nano* **2015,** *9* (7), 6985-6995.
164. Zununi Vahed, S.; Fathi, N.; Samiei, M.; Maleki Dizaj, S.; Sharifi, S., Targeted cancer drug delivery with aptamer-functionalized polymeric nanoparticles. *Journal of Drug Targeting* **2018,** (just-accepted), 1-22.
165. Kamaly, N.; Xiao, Z.; Valencia, P. M.; Radovic-Moreno, A. F.; Farokhzad, O. C., Targeted polymeric therapeutic nanoparticles: design, development and clinical translation. *Chemical Society Reviews* **2012,** *41* (7), 2971-3010.
166. Steichen, S. D.; Caldorera-Moore, M.; Peppas, N. A., A review of current nanoparticle and targeting moieties for the delivery of cancer therapeutics. *European Journal of Pharmaceutical Sciences* **2013,** *48* (3), 416-427.

167. Liu, Y.; Miyoshi, H.; Nakamura, M., Nanomedicine for drug delivery and imaging: a promising avenue for cancer therapy and diagnosis using targeted functional nanoparticles. *International Journal of Cancer* **2007,** *120* (12), 2527-2537.
168. Tkachenko, A. G.; Xie, H.; Coleman, D.; Glomm, W.; Ryan, J.; Anderson, M. F.; Franzen, S.; Feldheim, D. L., Multifunctional gold nanoparticle− peptide complexes for nuclear targeting. *Journal of the American Chemical Society* **2003,** *125* (16), 4700-4701.
169. Larnaudie, S. C.; Sanchis, J.; Nguyen, T.-H.; Peltier, R.; Catrouillet, S.; Brendel, J. C.; Porter, C. J.; Jolliffe, K. A.; Perrier, S., Cyclic peptide-poly (HPMA) nanotubes as drug delivery vectors: In vitro assessment, pharmacokinetics and biodistribution. *Biomaterials* **2018**.
170. Naito, M.; Yokoyama, T.; Hosokawa, K.; Nogi, K., *Nanoparticle technology handbook*. Elsevier: 2018.
171. Niu, F.; Yan, J.; Ma, B.; Li, S.; Shao, Y.; He, P.; Zhang, W.; He, W.; Ma, P. X.; Lu, W., Lanthanide-doped nanoparticles conjugated with an anti-CD33 antibody and a p53-activating peptide for acute myeloid leukemia therapy. *Biomaterials* **2018,** *167*, 132-142.
172. Cameron, N. R.; Spain, S. G.; Kingham, J. A.; Weck, S.; Albertin, L.; Barker, C. A.; Battaglia, G.; Smart, T.; Blanazs, A., Synthesis of well-defined glycopolymers and some studies of their aqueous solution behaviour. *Faraday Discussions* **2008,** *139*, 359-368.
173. Leserman, L. D.; Barbet, J.; Kourilsky, F.; Weinstein, J. N., Targeting to cells of fluorescent liposomes covalently coupled with monoclonal antibody or protein A. *Nature Materials* **1980,** *288* (5791), 602.
174. Warenius, H.; Galfre, G.; Bleehen, N.; Milstein, C., Attempted targeting of a monoclonal antibody in a human tumour xenograft system. *European Journal of Cancer Clinical Oncology* **1981,** *17* (9), 1009-1015.
175. Heath, T. D.; Fraley, R. T.; Papahdjopoulos, D., Antibody targeting of liposomes: cell specificity obtained by conjugation of F (ab') 2 to vesicle surface. *Science* **1980,** *210* (4469), 539-541.
176. James, J.; Dubs, G., FDA approves new kind of lymphoma treatment. Food and Drug Administration. *AIDS Treatment News* **1997,** (284), 2.
177. Gu, J.; Al-Bayati, K.; Ho, E. A., Development of antibody-modified chitosan nanoparticles for the targeted delivery of siRNA across the blood-brain barrier as a strategy for inhibiting HIV replication in astrocytes. *Drug Delivery Translational Research* **2017,** *7* (4), 497-506.
178. Zhang, X.-X.; Eden, H. S.; Chen, X., Peptides in cancer nanomedicine: drug carriers, targeting ligands and protease substrates. *Journal of Controlled Release* **2012,** *159* (1), 2-13.
179. Brissette, R.; Prendergast, J.; Goldstein, N., Identification of cancer targets and therapeutics using phage display. *Current Opinion in Drug Discovery Development* **2006,** *9* (3), 363-369.
180. Rifkin, D. B.; Sheppard, D., The integrin v 6 binds and activates latent TGF 1: a mechanism for regulating pulmonary inflammation and fibrosis. *Cell* **1999,** *96*, 319-328.
181. Desgrosellier, J. S.; Cheresh, D. A., Integrins in cancer: biological implications and therapeutic opportunities. *Nature Reviews Cancer* **2010,** *10* (1), 9.
182. Ludbrook, S. B.; Barry, S. T.; Delves, C. J.; Horgan, C. M., The integrin alphavbeta3 is a receptor for the latency-associated peptides of transforming growth factors beta1 and beta3. *Biochemical Journal* **2003,** *369* (2), 311-318.

183. Marelli, U. K.; Rechenmacher, F.; Sobahi, T. R. A.; Mas-Moruno, C.; Kessler, H., Tumor targeting via integrin ligands. *Frontiers in Oncology* **2013,** *3*, 222.
184. Gray, B. P.; Li, S.; Brown, K. C., From phage display to nanoparticle delivery: functionalizing liposomes with multivalent peptides improves targeting to a cancer biomarker. *Bioconjugate Chemistry* **2013,** *24* (1), 85-96.
185. Zhao, J.; Zhang, B.; Shen, S.; Chen, J.; Zhang, Q.; Jiang, X.; Pang, Z., CREKA peptide-conjugated dendrimer nanoparticles for glioblastoma multiforme delivery. *Journal of Colloid Interface Science* **2015,** *450*, 396-403.
186. Drabovich, A. P.; Berezovski, M. V.; Musheev, M. U.; Krylov, S. N., Selection of smart small-molecule ligands: the proof of principle. *Analytical Chemistry* **2008,** *81* (1), 490-494.
187. Gu, F. X.; Karnik, R.; Wang, A. Z.; Alexis, F.; Levy-Nissenbaum, E.; Hong, S.; Langer, R. S.; Farokhzad, O. C., Targeted nanoparticles for cancer therapy. *Nano Today* **2007,** *2* (3), 14-21.
188. Brannon-Peppas, L.; Blanchette, J. O., Nanoparticle and targeted systems for cancer therapy. *Advanced Drug Delivery Reviews* **2012,** *64*, 206-212.
189. Lu, Y.; Low, P. S., Immunotherapy of folate receptor-expressing tumors: review of recent advances and future prospects. *Journal of Controlled Release* **2003,** *91* (1-2), 17-29.
190. Muralidharan, R.; Babu, A.; Amreddy, N.; Basalingappa, K.; Mehta, M.; Chen, A.; Zhao, Y. D.; Kompella, U. B.; Munshi, A.; Ramesh, R., Folate receptor-targeted nanoparticle delivery of HuR-RNAi suppresses lung cancer cell proliferation and migration. *Journal of Nanobiotechnology* **2016,** *14* (1), 47.
191. Alibolandi, M.; Abnous, K.; Sadeghi, F.; Hosseinkhani, H.; Ramezani, M.; Hadizadeh, F., Folate receptor-targeted multimodal polymersomes for delivery of quantum dots and doxorubicin to breast adenocarcinoma: In vitro and in vivo evaluation. *International Journal of Pharmaceutics* **2016,** *500* (1-2), 162-178.
192. Minko, T., Drug targeting to the colon with lectins and neoglycoconjugates. *Advanced Drug Delivery Reviews* **2004,** *56* (4), 491-509.
193. Seymour, L. W.; Ferry, D. R.; Anderson, D.; Hesslewood, S.; Julyan, P. J.; Poyner, R.; Doran, J.; Young, A. M.; Burtles, S.; Kerr, D. J., Hepatic drug targeting: phase I evaluation of polymer-bound doxorubicin. *Journal of Clinical Oncology* **2002,** *20* (6), 1668-1676.
194. Yilmaz, G.; Becer, C. R., Glycopolymer code based on well-defined glycopolymers or glyconanomaterials and their biomolecular recognition. *Frontiers in Bioengineering Biotechnology* **2014,** *2*, 39.
195. Ting, S. S.; Min, E. H.; Zetterlund, P. B.; Stenzel, M. H., Controlled/Living ab Initio Emulsion Polymerization via a Glucose RAFT stab: Degradable Cross-Linked Glyco-Particles for Concanavalin A/Fim H Conjugations to Cluster E. coli Bacteria. *Macromolecules* **2010,** *43* (12), 5211-5221.
196. Yilmaz, G.; Becer, C. R., Precision glycopolymers and their interactions with lectins. *European Polymer Journal* **2013,** *49* (10), 3046-3051.
197. Spain, S. G.; Gibson, M. I.; Cameron, N. R., Recent advances in the synthesis of well-defined glycopolymers. *Journal of Polymer Science Part A: Polymer Chemistry* **2007,** *45* (11), 2059-2072.
198. Lundquist, J. J.; Toone, E. J., The cluster glycoside effect. *Chemical Reviews* **2002,** *102* (2), 555-578.
199. Li, X.; Chen, G., Glycopolymer-based nanoparticles: synthesis and application. *Polymer Chemistry* **2015,** *6* (9), 1417-1430.
200. Yilmaz, G.; Becer, C. R., Glyconanoparticles and their interactions with lectins. *Polymer Chemistry* **2015,** *6* (31), 5503-5514.

201. Peng, K.-Y.; Hua, M.-Y.; Lee, R.-S., Amphiphilic polyesters bearing pendant sugar moieties: Synthesis, characterization, and cellular uptake. *Carbohydrate polymers* **2014,** *99*, 710-719.
202. Suriano, F.; Pratt, R.; Tan, J. P.; Wiradharma, N.; Nelson, A.; Yang, Y.-Y.; Dubois, P.; Hedrick, J. L., Synthesis of a family of amphiphilic glycopolymers via controlled ring-opening polymerization of functionalized cyclic carbonates and their application in drug delivery. *Biomaterials* **2010,** *31* (9), 2637-2645.
203. Guo, Q.; Wu, Z.; Zhang, X.; Sun, L.; Li, C., Phenylboronate-diol crosslinked glycopolymeric nanocarriers for insulin delivery at physiological pH. *Soft Matter* **2014,** *10* (6), 911-920.
204. Jin, X.; Zhang, X.; Wu, Z.; Teng, D.; Zhang, X.; Wang, Y.; Wang, Z.; Li, C., Amphiphilic random glycopolymer based on phenylboronic acid: synthesis, characterization, and potential as glucose-sensitive matrix. *Biomacromolecules* **2009,** *10* (6), 1337-1345.
205. Yang, H.; Sun, X.; Liu, G.; Ma, R.; Li, Z.; An, Y.; Shi, L., Glucose-responsive complex micelles for self-regulated release of insulin under physiological conditions. *Soft Matter* **2013,** *9* (35), 8589-8599.
206. Perche, F.; Benvegnu, T.; Berchel, M.; Lebegue, L.; Pichon, C.; Jaffrès, P.-A.; Midoux, P., Enhancement of dendritic cells transfection in vivo and of vaccination against B16F10 melanoma with mannosylated histidylated lipopolyplexes loaded with tumor antigen messenger RNA. *Nanomedicine: Nanotechnology, Biology Medicine* **2011,** *7* (4), 445-453.
207. Geng, F.; Xing, J. Z.; Chen, J.; Yang, R.; Hao, Y.; Song, K.; Kong, B., Pegylated glucose gold nanoparticles for improved in-vivo bio-distribution and enhanced radiotherapy on cervical cancer. *Journal of Biomedical Nanotechnology* **2014,** *10* (7), 1205-1216.
208. Luo, X.; Wang, W.; Dorkin, J.; Veiseh, O.; Chang, P.; Abutbul-Ionita, I.; Danino, D.; Langer, R.; Anderson, D.; Dong, Y., Poly (glycoamidoamine) brush nanomaterials for systemic siRNA delivery in vivo. *Biomaterials Science* **2017,** *5* (1), 38-40.
209. Kim, H. W.; Park, I. K.; Cho, C. S.; Lee, K. H.; Beck, G. R.; Colburn, N. H.; Cho, M. H., Aerosol delivery of glucosylated polyethylenimine/phosphatase and tensin homologue deleted on chromosome 10 complex suppresses Akt downstream pathways in the lung of K-ras null mice. *Cancer Research* **2004,** *64* (21), 7971-7976.
210. Silva, J. M.; Zupancic, E.; Vandermeulen, G.; Oliveira, V. G.; Salgado, A.; Videira, M.; Gaspar, M.; Graca, L.; Préat, V.; Florindo, H. F., In vivo delivery of peptides and Toll-like receptor ligands by mannose-functionalized polymeric nanoparticles induces prophylactic and therapeutic anti-tumor immune responses in a melanoma model. *Journal of Controlled Release* **2015,** *198*, 91-103.
211. Saraogi, G. K.; Sharma, B.; Joshi, B.; Gupta, P.; Gupta, U. D.; Jain, N. K.; Agrawal, G. P., Mannosylated gelatin nanoparticles bearing isoniazid for effective management of tuberculosis. *Journal of Drug Targeting* **2011,** *19* (3), 219-227.
212. Hashida, M.; Nishikawa, M.; Yamashita, F.; Takakura, Y., Cell-specific delivery of genes with glycosylated carriers. *Advanced Drug Delivery Reviews* **2001,** *52* (3), 187-196.
213. Li, X.; Zhou, H.; Yang, L.; Du, G.; Pai-Panandiker, A. S.; Huang, X.; Yan, B., Enhancement of cell recognition in vitro by dual-ligand cancer targeting gold nanoparticles. *Biomaterials* **2011,** *32* (10), 2540-2545.
214. Bergen, J. M.; Von Recum, H. A.; Goodman, T. T.; Massey, A. P.; Pun, S. H., Gold nanoparticles as a versatile platform for optimizing physicochemical

parameters for targeted drug delivery. *Macromolecular Bioscience* **2006,** *6* (7), 506-516.
215. Wijagkanalan, W.; Kawakami, S.; Takenaga, M.; Igarashi, R.; Yamashita, F.; Hashida, M., Efficient targeting to alveolar macrophages by intratracheal administration of mannosylated liposomes in rats. *Journal of Controlled Release* **2008,** *125* (2), 121-130.
216. Fitch, R. M., *Polymer colloids*. Academic Press: 1997.
217. Kreuter, J., Nanoparticles—a historical perspective. *International Journal of Pharmaceutics* **2007,** *331* (1), 1-10.
218. Chern, C., Emulsion polymerization mechanisms and kinetics. *Progress in Polymer Science* **2006,** *31* (5), 443-486.
219. Harkins, W. D.; Stearns, R. S., Loci of Emulsion Polymerization: Diffusion of Organic Molecules from Emulsion Droplets through an Aqueous Phase into Polymer Latex Particles. *The Journal of Chemical Physics* **1946,** *14* (3), 215-216.
220. Smith, W. V.; Ewart, R. H., Kinetics of emulsion polymerization. *The Journal of Chemical Physics* **1948,** *16* (6), 592-599.
221. Smith, W. V., Chain initiation in styrene emulsion polymerization. *Journal of the American Chemical Society* **1949,** *71* (12), 4077-4082.
222. Bovey, F.; Kolthoff, I., Mechanism of emulsion polymerizations. IV. Kinetics of polymerization of styrene in water and detergent solutions. *Journal of Polymer Science* **1950,** *5* (4), 487-504.
223. Young, R. J.; Lovell, P. A., *Introduction to polymers*. CRC press: 2011.
224. Odian, G., Principles of Polymerization. New York: J. Wiley: 1991.
225. Guyot, A.; Chu, F.; Schneider, M.; Graillat, C.; McKenna, T., High solid content latexes. *Progress in Polymer Science* **2002,** *27* (8), 1573-1615.
226. Blackley, D. C., *Emulsion polymerisation: theory and practice*. Applied Science Publishers London: 1975.
227. Manabe, M.; Tatarazako, N.; Kinoshita, M., Uptake, excretion and toxicity of nano-sized latex particles on medaka (Oryzias latipes) embryos and larvae. *Aquatic Toxicology* **2011,** *105* (3-4), 576-581.
228. Manabe, K.; Kobayashi, S., Mannich-type reactions of aldehydes, amines, and ketones in a colloidal dispersion system created by a Brønsted acid− surfactant-combined catalyst in water. *Organic Letters* **1999,** *1* (12), 1965-1967.
229. Charmot, D.; Corpart, P.; Adam, H.; Zard, S.; Biadatti, T.; Bouhadir, G. In *Controlled radical polymerization in dispersed media*, Macromolecular Symposia, Wiley Online Library: 2000; pp 23-32.
230. Farcet, C.; Lansalot, M.; Charleux, B.; Pirri, R.; Vairon, J., Mechanistic aspects of nitroxide-mediated controlled radical polymerization of styrene in miniemulsion, using a water-soluble radical initiator. *Macromolecules* **2000,** *33* (23), 8559-8570.
231. Zetterlund, P. B.; Thickett, S. C.; Perrier, S.; Bourgeat-Lami, E.; Lansalot, M., Controlled/living radical polymerization in dispersed systems: an update. *Chemical Reviews* **2015,** *115* (18), 9745-9800.
232. Barner-Kowollik, C., *Handbook of RAFT polymerization*. John Wiley & Sons: 2008.
233. Semsarilar, M.; Perrier, S., 'Green'reversible addition-fragmentation chain-transfer (RAFT) polymerization. *Nature Chemistry* **2010,** *2* (10), 811.
234. Willcock, H.; O'Reilly, R. K., End group removal and modification of RAFT polymers. *Polymer Chemistry* **2010,** *1* (2), 149-157.

235. Ferguson, C. J.; Hughes, R. J.; Nguyen, D.; Pham, B. T.; Gilbert, R. G.; Serelis, A. K.; Such, C. H.; Hawkett, B. S., Ab Initio Emulsion Polymerization by RAFT-Controlled Self-Assembly §. *Macromolecules* **2005,** *38* (6), 2191-2204.
236. Siauw, M.; Hawkett, B. S.; Perrier, S., Short chain amphiphilic diblock co-oligomers via RAFT polymerization. *Journal of Polymer Science Part A: Polymer Chemistry* **2012,** *50* (1), 187-198.
237. Gurnani, P.; Lunn, A. M.; Perrier, S., Synthesis of mannosylated and PEGylated nanoparticles via RAFT emulsion polymerisation, and investigation of particle-lectin aggregation using turbidimetric and DLS techniques. *Polymer* **2016,** *106*, 229-237.
238. Rieger, J.; Osterwinter, G.; Bui, C.; Stoffelbach, F.; Charleux, B., Surfactant-free controlled/living radical emulsion (co) polymerization of n-butyl acrylate and methyl methacrylate via RAFT using amphiphilic poly (ethylene oxide)-based trithiocarbonate chain transfer agents. *Macromolecules* **2009,** *42* (15), 5518-5525.
239. Zhang, X.; Boissé, S.; Zhang, W.; Beaunier, P.; D'Agosto, F.; Rieger, J.; Charleux, B., Well-defined amphiphilic block copolymers and nano-objects formed in situ via RAFT-mediated aqueous emulsion polymerization. *Macromolecules* **2011,** *44* (11), 4149-4158.
240. Prescott, S. W.; Ballard, M. J.; Rizzardo, E.; Gilbert, R. G., RAFT in emulsion polymerization: what makes it different? *Australian Journal of Chemistry* **2002,** *55* (7), 415-424.
241. Moad, G., The emergence of RAFT polymerization. *Australian Journal of Chemistry* **2006,** *59* (10), 661-662.
242. Egen, M.; Zentel, R., Surfactant-Free Emulsion Polymerization of Various Methacrylates: Towards Monodisperse Colloids for Polymer Opals. *Macromolecular Chemistry and Physics* **2004,** *205* (11), 1479-1488.
243. Roe, C. P., Surface chemistry aspects of emulsion polymerization. *Industrial and Engineering Chemistry* **1968,** *60* (9), 20-33.
244. Goodall, A.; Wilkinson, M.; Hearn, J., Mechanism of emulsion polymerization of styrene in soap-free systems. *Journal of Polymer Science Part A: Polymer Chemistry* **1977,** *15* (9), 2193-2218.
245. Ni, H.; Ma, G.; Nagai, M.; Omi, S., Effects of ethyl acetate on the soap-free emulsion polymerization of 4-vinylpyridine and styrene. II. Aspects of the mechanism. *Journal of Applied Polymer Science* **2001,** *82* (11), 2692-2708.
246. Dire, C.; Magnet, S.; Couvreur, L.; Charleux, B., Nitroxide-mediated controlled/living free-radical surfactant-free emulsion polymerization of methyl methacrylate using a poly (methacrylic acid)-based macroalkoxyamine initiator. *Macromolecules* **2008,** *42* (1), 95-103.
247. Feeney, P. J.; Napper, D. H.; Gilbert, R. G., Surfactant-free emulsion polymerizations: predictions of the coagulative nucleation theory. *Macromolecules* **1987,** *20* (11), 2922-2930.
248. Fan, X.; Liu, Y.; Jia, X.; Wang, S.; Li, C.; Zhang, B.; Zhang, H.; Zhang, Q., Regulating the size and molecular weight of polymeric particles by 1, 1-diphenylethene controlled soap-free emulsion polymerization. *RSC Advances* **2015,** *5* (115), 95183-95190.
249. Appel, J.; Akerboom, S.; Fokkink, R. G.; Sprakel, J., Facile One-Step Synthesis of Monodisperse Micron-Sized Latex Particles with Highly Carboxylated Surfaces. *Macromolecular Rapid Communications* **2013,** *34* (16), 1284-1288.
250. Bao, J.; Zhang, A., Poly (methyl methacrylate) nanoparticles prepared through microwave emulsion polymerization. *Journal of Applied Polymer Science* **2004,** *93* (6), 2815-2820.

251. Chen, S. A.; Lee, S. T., Kinetics and mechanism of emulsifier-free emulsion polymerization: styrene/hydrophilic comonomer (acrylamide) system. *Macromolecules* **1991,** *24* (11), 3340-3351.
252. Adelnia, H.; Pourmahdian, S., Soap-free emulsion polymerization of poly (methyl methacrylate-co-butyl acrylate): effects of anionic comonomers and methanol on the different characteristics of the latexes. *Colloid Polymer Science* **2014,** *292* (1), 197-205.
253. Zhang, J.; Zou, Q.; Li, X.; Cheng, S., Soap-free cationic emulsion copolymerization of styrene and butyl acrylate with comonomer in the presence of alcohols. *Journal of Applied Polymer Science* **2003,** *89* (10), 2791-2797.

# *Chapter 2*

**Synthesis of Glycosylated Nanoparticles *via* RAFT Seeded Emulsion Polymerisation and Investigations into Their Aggregation with Online DLS Measurements**

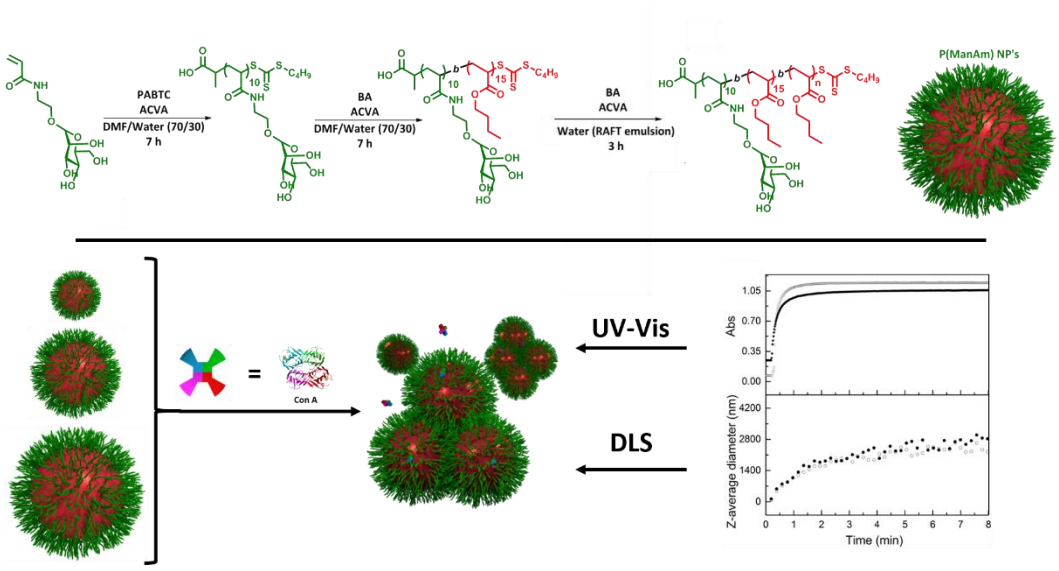

## 2.2 Abstract

This chapter will explore the use of Dynamic Light Scattering (DLS) as a technique to analyse particle aggregation. Polymeric nanoparticles can be prepared by a variety of techniques, with varied and interesting surface functionality now available. One useful technique for preparing polymeric nanoparticles with highly tuneable surfaces is RAFT emulsion polymerisation. Using this technique a range of poly(α-D-mannopyran-1-oxyethyl acrylamide) coated nanoparticles of varying sizes were prepared. The particles were used, along with the lectin concanavalin A, to develop a DLS based system for tracking particle aggregation in real time. The system was validated by equivalent experiments analysed using a standard UV-Vis spectroscopic analysis and was shown to be reliable and robust up to an aggregate diameter of *ca* 500 nm. This system was further used to study the effect of particle size on lectin binding and final aggregate size. Larger particles were found to have a qualitatively enhanced aggregation response by both UV-vis and DLS techniques. The DLS technique however, was able to provide quantitative data on the number of particles per aggregate produced.

## 2.3 Introduction

Within various disciplines, polymeric nanoparticles have found uses that require them to be well defined with reliable size control.[1-3] The most prevalent of these fields, as discussed in Chapter One, is as drug delivery agents, used to improve the performance of a drug that may have an unfavourable absorption metabolism degradation and excretion (ADME) profile.[4-10] In efforts to address these issues for both existing and novel therapeutics, smart drug delivery vectors of various forms have been researched, including the use of polymeric nanoparticles.[5, 11-16]

Many nanoparticle systems for drug delivery currently being researched are polymeric in nature. These systems may be synthesised with a range of functional monomers using techniques such as emulsion polymerisation.[17-20] Emulsion polymerisation provides an industrially applicable and easy way of generating polymeric nanoparticles with narrow size distributions, down to diameters of tens of nanometres.[21, 22] To access small diameters with a narrow particle size distribution, a classical emulsion polymerisation typically requires the addition of a surfactant such as sodium dodecyl sulphate (SDS), resulting in particles that may show poor biocompatibility.[23] In an effort to avoid this toxicity, emulsion polymerisations have been combined with controlled radical polymerisation (CRP) techniques, using a short polymer to provide micelles and particle stabilisation, subsequently becoming covalently bound to the resulting latex.[24-26] Synthesising particles with these methods also allows control of polymer molar mass and architecture, polymer end group, and therefore particle surface functionality.[27] One such method is that of reversible addition-fragmentation chain transfer (RAFT) emulsion polymerisation. In one specific use of this method, a suitable hydrophilic monomer and RAFT agent are polymerised to a low degree of polymerisation (typically under 30 monomer units) and then chain extended with a hydrophobic monomer to produce a short di-block amphiphilic macroRAFT agent. Upon suspension in water these form micelles, and can subsequently be chain extended following an emulsion polymerisation method. RAFT emulsion may also be performed directly from the hydrophilic block, rather than chain extending with a hydrophobic monomer before the emulsion, as initially proposed by Hawkett *et al.*[27] In 2010, Stenzel *et al*.[29] published a paper using this technique to produce nanoparticles with a glycopolymer shell of glucose, and the technique as a whole has been subject to wide study.[24, 28-31]

The ability to functionalise the surface of nanoparticles with moieties such as sugars, opens possibilities for targeting specific receptors in the body directing nanoparticles to a specific site of action. Sugars specifically are able to target lectins on cells including: malignancies, specific tissues, or pathogenic bacteria.[29, 32] Lectins are carbohydrate binding proteins, that are not enzymes or antibodies.[33] They contain carbohydrate recognition domains (CRD's), which show preferential binding to specific carbohydrates or carbohydrate sequences. Lectins can be further divided into types including (although not limited to): C-type, Galectins, Calnexins, L-type, P-type etc. The function of lectins varies between types, for example: C-type lectins are involved in cell adhesion, glycoprotein clearance and innate immunity, whereas galectins are involved in glycan cross linking in the extra cellular matrix.[34, 35] Lectins form a complex with carbohydrates *via* a combination of hydrogen bonding, hydrophobic interactions and (with the involvement of water bridges) co-ordination to a metal ion. Binding may also involve electrostatic interactions in some cases.[2] The process and specificity of lectin-carbohydrate interaction is complex, with many other factors such as: depth of CRD pocket and ability of the lectin structure to deform, enabling lectins to bind to carbohydrate sequences that they are not specific to. The binding then may be thought of as a preference to a certain sequence, with the ability to form a weaker complex with other carbohydrates.[36]

The ability of lectins to show reduced binding to other sugars is important when considering using them as a targeting agent, that even with a specific sequence of sugars, complete specificity may not be achieved. Single interactions between a sugar and a lectin are relatively weak, however it has been shown that where there is a high density of carbohydrates present, the culmination of all of the interactions acts in a non-linear way and results in a strong binding, this is known as the "cluster glycoside effect".[37] Having a high concentration of sugar moieties allows an increased binding as when one interaction breaks, it is highly likely that a proximal sugar will take its place in the binding domain, which can be thought of as a "bind and slide" mechanism.[38, 39] Due to these factors, how the sugar moieties are presented is crucial for lectin binding. Recent work from the Becer group has again highlighted the importance of this, with a system showing improved lectin binding in an assembled state when compared to the same glycopolymer in a linear state.[40]

Functionalised nanoparticles therefore represent a good platform to take advantage of the "cluster glycoside effect", as they are able to present a very high local concentration of a sugar on their surface when engineered properly.[37, 41-44]

Different cell and tissue types are known to express different lectins with a particular specificity. The plant lectin concanavalin A (ConA) is known to bind majorly to alpha mannose and glucose residues (less so to beta), and ricinus communis agglutinin 120 ($RCA_{120}$) to beta galactose residues. The same diversity is found in the mammalian body too, for example some melanoma cell lines have shown increased binding to galactose functional nanoparticles.[45] In rats, galactose has been shown to target the proximal gastro-intestinal (GI) tract, whilst fucose targets the distal GI tract.[46, 47] Furthermore, dendritic cells and macrophages of the human immune system have been shown to express lectins such as dendritic cell-specific intercellular adhesion molecule-3-grabbing non-integrin (DC-SIGN) that exhibit preferential binding to mannose.[48-51]

Various research groups have used glyconanoparticles of many types to probe the ability of lectins for use as diagnostic and targeting agents.[1, 32, 52-54] The ubiquity and specificity of receptors with such a preference for binding to specific carbohydrates therefore represents an attractive target to distinguish between and target different cells and disease states.[2, 55, 56]

Once a targeted latex with a moiety like a sugar has been synthesised, it is important to be able to assess its ability to be recognised and effectively bind to the corresponding receptor, in this case a lectin. One method that is commonly used to study the ability of particles to bind to proteins, and in particular to lectins is turbidimetric UV-Vis analysis, together with a multivalent lectin in solution such as the tetravalent lectin ConA, isolated from the jack bean plant.[57, 58] These tests, that simply require the mixing of two solutions, are quick and easy to perform; typically a lectin in solution will be placed in a UV-Vis spectrometer monitoring absorbance as the particle of interest is added. An increase in absorbance greater than the particles alone would produce indicates aggregation of particles through lectin binding, producing larger particle aggregates with a greater ability to scatter light. Whilst this is a useful tool for quickly determining qualitatively if there is a particle-lectin interaction, without in depth mathematical analysis it does not give any quantitative information. The analysis needed makes many assumptions and does not fully take into account the light

scattering properties of particles, or the dilution effect seen when mixing two solutions together. Another technique used to determine particle size and aggregation is dynamic light scattering (DLS) analysis. Time dependant DLS has been used in determining the thermal stability of metal nanoparticles, but is far less common when applied to particle-lectin binding, as the former simply involves the heating of a sample *in situ*, whereas the latter would require full mixing of lectin and particle during DLS measurements.[22, 54, 59-66] Mixing solutions during DLS measurements is not trivial, due to the nature of DLS analysis, and the practicalities of not being able to open the machine during measurement runs. Online (real time) aggregation analysis however, presents an interesting way of monitoring the lectin binding properties of glyco-nanoparticles, not being affected by dilution effects or particle light scattering properties, but indeed taking advantage of them. As DLS relies as a technique on the Brownian motion of particles in solution, it requires all analysis to be performed on colloidally stable particles and aggregates below a critical size, at which they would sediment out of solution.[67] If DLS is to be used to study glycoparticle-lectin interactions then: the particles analysed must be well defined, with a known amount of sugar residues on their surface and be of a size and at a concentration such as to limit aggregate size and sedimentation out of solution when a lectin is introduced.

With its ability to synthesise well defined particles below 100 nm in diameter, RAFT emulsion polymerisation represents a good method for producing particles to investigate the use of DLS as a technique to study glycoparticle-lectin interactions. It is with this motivation that this chapter will present the synthesis and characterisation of mannosylated glyco-nanoparticles with well controlled diameters, and subsequently use them to precisely investigate and trial the use of real time "online" DLS to track particle-lectin interactions. The same technique will further be used to determine the effect of particle size on lectin binding.

## 2.4 Results and Discussion

### 2.4.1 α-D-Mannopyran-1-oxyethyl Acrylamide Monomer Synthesis

In order to produce a macro-chain transfer agent (CTA) suitable for producing mannosylated nanoparticles *via* RAFT emulsion polymerisation, a monomer suitable for RAFT polymerisation that could be either post functionalised with mannose, or that already bore a mannose moiety was required. It was desirable to have a mannose functionalised monomer before polymerisation, this way it could be ensured that all

monomer units in the polymer chain bore a mannose residue and that the exact mannose concentration was known. Previous research carried out by Cameron *et al.* has shown the synthesis of monosaccharide monomers *via* a coupling reaction of an acetate protected sugar to hydroxyethyl acrylamide (HEAm), and a modification of this method was used to synthesise a α-D-mannopyran-1-oxyethyl acrylamide (ManAm) monomer (Scheme 2.1).[68] Briefly: α-D-mannose pentaacetate underwent a nucleophilic substitution with HEAm at the anomeric carbon using boron trifluoride diethyl etherate ($BF_3$) as a Lewis acid to act as an activating agent. Due to neighbouring group participation from the adjacent acetate protecting group with the anomeric carbon, the resulting monomer produced will majorly be in the α isomer form.[69] This protected sugar monomer was subsequently de-protected with potassium carbonate in methanol and purified by column chromatography with a yield of *ca* 60%. The molecule structure was confirmed by $^{1}H$ and $^{13}C$ NMR spectroscopy, IR spectroscopy, and mass spectrometry (Section 1.5.1.1).

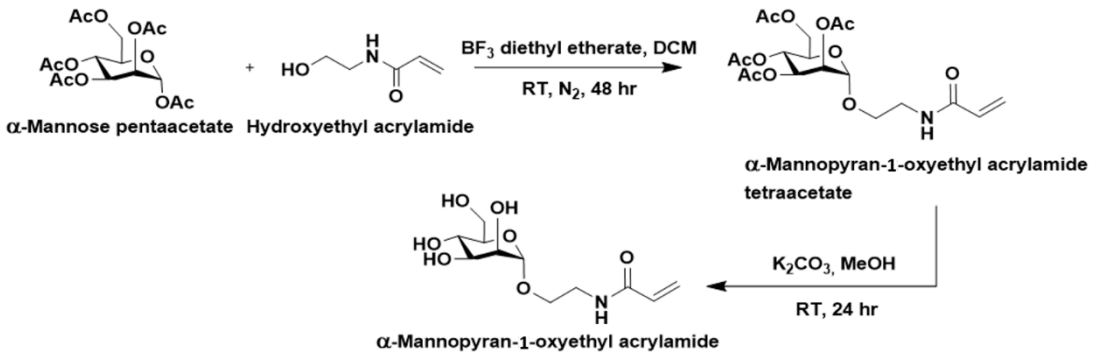


**Scheme 2.1:** Synthetic scheme for α-D-mannopyran-1-oxyethyl acrylamide monomer

### 2.4.2 Synthesis of Poly(α-D-mannopyran-1-oxyethyl acrylamide)$_{10}$-*b*-Poly(n-Butyl Acrylate)$_{15}$

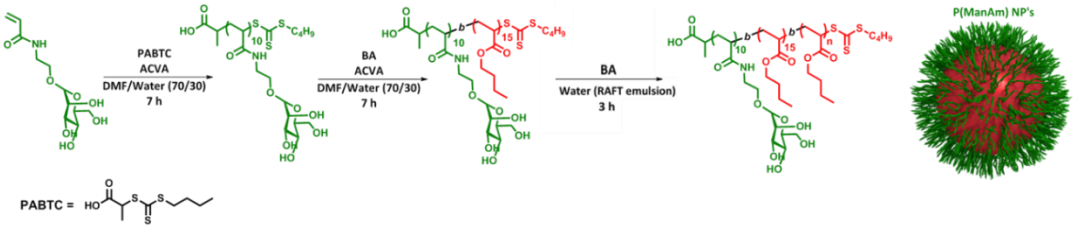


**Scheme 2.2:** Synthetic scheme for RAFT emulsion mediated particle synthesis *via* a poly(α-D-mannopyran-1-oxyethyl acrylamide)$_{10}$-*b*-poly(*n*-butyl acrylate)$_{15}$ di-block copolymer

Previous research has indicated that short chain polymeric oligomers of an amphiphilic nature self-assembled in water act as a sufficient nucleation site and stabiliser for the

formation and growth of polymeric latex particles.[70] By using RAFT polymerisation to synthesise short oligomers of this nature from ManAm and butyl acrylate (BA), an amphiphilic macro-CTA suitable for aqueous self-assembly, and undergoing chain extension in a RAFT emulsion polymerisation was produced (Scheme 2.2). Using a solvent of DMF/Water (70/30 % v/v) to ensure solubility of all monomers at all temperatures, a P(ManAm)$_{10}$-*b*-P(BA)$_{15}$ polymer was synthesised. The addition of water to the DMF solvent was required as α-D-mannopyran-1-oxyethyl acrylamide was found to be thermoresponsive, with lower critical solution temperature (LCST) like behaviour in DMF, precipitating at around 50 °C. 2-(n-butyltrithiocarbonylthio)propionic acid (PABTC) was selected to use as the CTA for this polymerisation as previous work has shown it to be an excellent RAFT agent for both acrylamides and acrylates.[71, 72] In addition to its ability to act as a chain transfer agent for both acrylates and acrylamides, PABTC also possesses a carboxylic acid moiety on its R group, improving aqueous solubility and imparting electrostatic stabilization to the surface of the growing particle thus increasing colloidal stability. α-D-mannopyran-1-oxyethyl acrylamide was polymerised at 70 °C for seven hours at pH 7 using the thermal initiator 4,4'-azobis (4-cyanovaleric acid) (ACVA) as a radical source with >99% conversion of monomer to polymer confirmed by $^1$H NMR spectroscopy. After this seven hour polymerisation only 43% of the ACVA initiator had been consumed, and as the first block had polymerised to completion, the polymerisation of the second block of the polymer was performed without purification. Butyl acrylate, purged of oxygen, was therefore directly added to the reaction vessel to the required concentration, which was then heated to 70 °C again and left stirring for a further seven hours, allowing 97% conversion of butyl acrylate from monomer to polymer. Analysis by $^1$H NMR spectroscopy of side chain protons compared to protons from the $CH_3$ present on the butyl Z-group of PABTC confirmed the polymer structure to be P(ManAm)$_{10}$-*b*-P(BA)$_{15}$ (Section 2.5.1.2). Chromatographic analysis of the polymer using size exclusion chromatography (SEC) indicated a monomodal molecular weight distribution of $M_n$ = 4600 g mol $^{-1}$ ($Đ$ = 1.14) (Section 2.5.1.2).

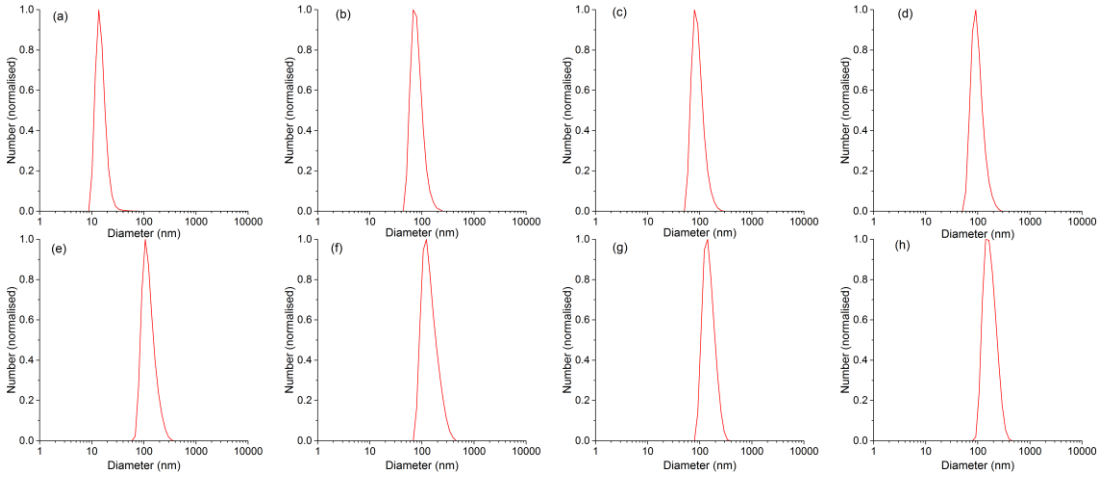


**Figure 2.1:** DLS traces of particles formed from (a) P(ManAm)$_{10}$-*b*-P(BA)$_{15}$ (b) P(ManAm)$_{10}$-*b*-P(BA)$_{15}$-*b*-P(BA)$_{25}$ (c) P(ManAm)$_{10}$-*b*-P(BA)$_{15}$-*b*-P(BA)$_{75}$ (d) P(ManAm)$_{10}$-*b*-P(BA)$_{15}$-*b*-P(BA)$_{100}$ (e) P(ManAm)$_{10}$-*b*-P(BA)$_{15}$-*b*-P(BA)$_{154}$ (f) P(ManAm)$_{10}$-*b*-P(BA)$_{15}$-*b*-P(BA)$_{200}$ (g) P(ManAm)$_{10}$-*b*-P(BA)$_{15}$-*b*-P(BA)$_{300}$ (h) P(ManAm)$_{10}$-*b*-P(BA)$_{15}$-*b*-P(BA)$_{400}$.

To confirm the ability of this di-block to form micelles in water, an aqueous solution of the purified polymer was prepared at a concentration of 15 mg mL$^{-1}$ and the resulting micelle size determined by DLS measurement, displaying a mean hydrodynamic diameter of 10 nm (Pdi 0.06) and a zeta potential of -20 mV (Table 2.1, Figure 2.1).

### 2.4.3 Synthesis of Mannosylated Nanoparticles

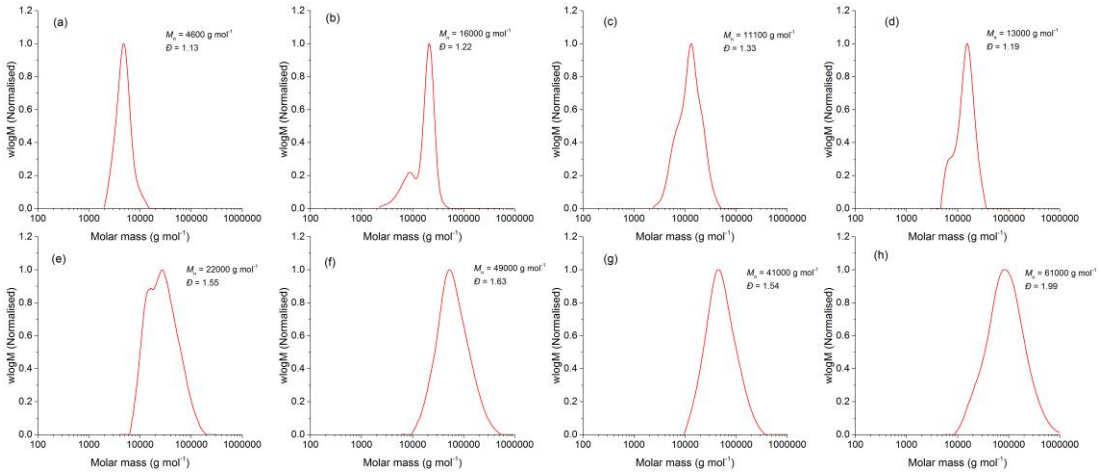


**Figure 2.2:** DMF SEC traces of (a) P(ManAm)$_{10}$-*b*-P(BA)$_{15}$ (b) P(ManAm)$_{10}$-*b*-P(BA)$_{15}$-*b*-P(BA)$_{25}$ (c) P(ManAm)$_{10}$-*b*-P(BA)$_{15}$-*b*-P(BA)$_{75}$ (d) P(ManAm)$_{10}$-*b*-P(BA)$_{15}$-*b*-P(BA)$_{100}$ (e) P(ManAm)$_{10}$-*b*-P(BA)$_{15}$-*b*-P(BA)$_{154}$ (f) P(ManAm)$_{10}$-*b*-P(BA)$_{15}$-*b*-P(BA)$_{200}$ (g) P(ManAm)$_{10}$-*b*-P(BA)$_{15}$-*b*-P(BA)$_{300}$ (h) P(ManAm)$_{10}$-*b*-P(BA)$_{15}$-*b*-P(BA)$_{400}$.

Multiple emulsion polymerisations were performed, using the synthesised P(ManAm)$_{10}$-*b*-P(BA)$_{15}$ macro-CTA following a modified literature procedure (Figure 2).[73] Typically: in a 7 mL vial with a 1 cm magnetic stirrer, P(ManAm)$_{10}$-*b*-P(BA)$_{15}$ was suspended in deionised (DI) water at a concentration of 23 mg mL$^{-1}$ to which a previously prepared solution of ACVA in DI water at a concentration of 5 mg mL$^{-1}$ with 2 eq. of sodium hydroxide was added. The vial was then sealed and the

solution purged of oxygen with nitrogen flow for 10 minutes, following which the required volume of butyl acrylate was added in with a gas tight glass syringe, before heating the reaction to 70 °C and stirring for three hours. In all cases this resulted in the formation of well-defined monodisperse latex particles, with butyl acrylate cores ranging in diameter from 82-180 nm (Pdi ≤0.1) (Figure 2.1, Table 1). To ensure that monomer to polymer conversion was complete (> 99%) $^1$H NMR spectroscopy was performed using a mixed solvent of $d_6$-DMSO/ $CDCl_3$ (80/20 % v/v). No single common deuterated solvent was found to be able to adequately dissolve both the mannose monomer and butyl acrylate parts of the polymer, and the mix of deuterated DMSO and chloroform was found to be the best solvent mix. In all cases tested, monomer to polymer conversion was determined to be >99%, confirming that the emulsion polymerisation was complete after three hours.

| | | $[M]_0/[CTA]_0$ | Average Particle Diameter (nm)[a] | PDi[b] | ζ-Potential (mV) | Conversion (%) | $M_{n,SEC}$ [c] | Đ [d] |
|---|---|---|---|---|---|---|---|---|
| | $P(ManAm)_{10}$-b-$P(BA)_{15}$ | N/A | 11 | 0.060 | -20. | 97 | 4600[c] | 1.13 |
| A | $P(ManAm)_{10}$-b-$P(BA)_{15}$-b-$P(BA)_{25}$ | 25 | 82 | 0.084 | -36 | 99 | 16000[c] | 1.22 |
| B | $P(ManAm)_{10}$-b-$P(BA)_{15}$-b-$P(BA)_{75}$ | 75 | 94 | 0.085 | -34 | 98 | 11000[c] | 1.33 |
| C | $P(ManAm)_{10}$-b-$P(BA)_{15}$-b-$P(BA)_{100}$ | 100 | 100 | 0.088 | -33 | 98 | 13000[c] | 1.19 |
| D | $P(ManAm)_{10}$-b-$P(BA)_{15}$-b-$P(BA)_{154}$ | 154 | 127 | 0.082 | -35 | 93 | 22000[c] | 1.55 |
| E | $P(ManAm)_{10}$-b-$P(BA)_{15}$-b-$P(BA)_{200}$ | 200 | 146 | 0.13 | -32 | 95 | 49000[c] | 1.63 |
| F | $P(ManAm)_{10}$-b-$P(BA)_{15}$-b-$P(BA)_{300}$ | 300 | 153 | 0.073 | -33 | 90 | 41000[c] | 1.54 |
| G | $P(ManAm)_{10}$-b-$P(BA)_{15}$-b-$P(BA)_{400}$ | 400 | 176 | 0.10 | -33 | 99 | 61000[c] | 1.99 |

**Table 2.1:** Synthetic results for mannosylated nanoparticles with butyl acrylate core synthesised via RAFT emulsion polymerisation, and the constituent polymers. [a] determined by DLS (number distribution), [b] Pdi values calculated using Equation 2, [c] determined by DMF-SEC analysis with PMMA standard [d] dispersity values are for all populations in chromatogram

As observed with the block copolymer micelles in solution, the resulting glycoparticles all had negative zeta potentials around -32 mV, due to the carboxylic acid present on the R group from the very first polymerisation on the PABTC RAFT agent. The polymer particles were disassembled into their particle forming polymer unimers by addition of an excess of DMF, and SEC chromatography performed to determine the unimer molecular weight distribution (Figure 2.2). Control of the unimer dispersity can be seen for the smaller particles where the target degree of polymerisation (DP) was lower. However, as the target DP increases a corresponding increase in polymer dispersity can be seen, indicating a loss of control over the chain extension in the growing polymer particle. This is presumably due a large number of initiator derived or "dead" chains that can no longer be chain extended, and RAFT end groups not being readily available in the larger particle due to diffusion limitation, allowing for free radical polymerisation to occur without RAFT group involvement.

### 2.4.4 Size Control of Mannosylated Nanoparticles

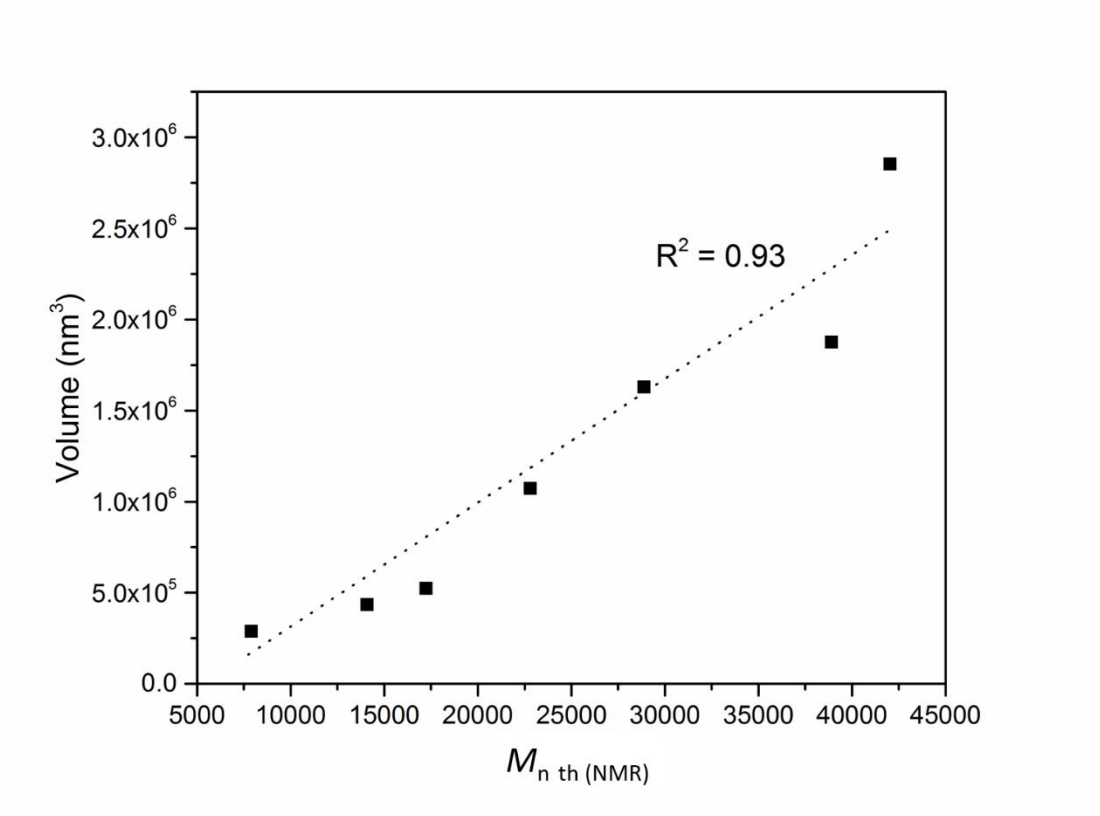


**Figure 2.3:** Size calibration of particles synthesised from: poly(α-D-mannopyran-1-oxyethyl acrylamide)$_{10}$-b-poly(*n*-butyl acrylate)$_{15}$ plotting unimer $M_n$ against the resulting particle volume of particles A, B, C and E, F and G. A near linear relationship can be seen with a linear regression p-value of 0.93

It is important that particle size can be reliably and reproducibly controlled using the RAFT emulsion polymerisation mechanism over a range of sizes. To test this, multiple RAFT emulsion polymerisations were carried out following the same method as in Section 2.4.3 with varying concentrations of butyl acrylate to target a range of degrees of polymerisation to control the final resulting particle size (Table 2.1). The theoretical molecular weight of particle constituent unimers was then plotted against the resulting particle volume for particles A, B, C, E, F and G (Figure 2.3). As expected, a linear relationship can be seen indicating that any particle diameter between 80 and 180 nm can be targeted with a Pdi ≤0.1. To then determine if the particle size was reproducible and produce a particle with a diameter between 100-154 nm (filling a gap in the size calibration between particle C and E), the plot of $M_n$~particle volume was used as a calibration to determine a target DP for a particle 123 nm in diameter. By back calculating from the $M_n$ suggested, a target DP of 154 was then targeted (Table 2.1 particle D). This resulted in a particle with a diameter by DLS of 127 nm, confirming that the calibration produced by these experiments is reliable and that the RAFT

emulsion polymerisation method can reliably be used to target a reproducible range of particle sizes. Such batch to batch consistency is an important factor when considering these particles for biomedical applications, as to be considered for formulation a synthesis method would have to be validated for such parameters.

### 2.4.5 Aggregation Studies

Having synthesised a range of well-defined glyco-nanoparticles with mannosylated shells and shown them to be stable, these could then be taken forward and used in lectin binding studies. Such binding studies are typically carried out in a predominantly qualitative way using UV-vis turbidimetric studies, wherein the absorbance (typically at a wavelength of 500 nm) of a lectin solution is monitored over time after the addition of sugar moieties.[58, 74] This allows for the monitoring of particle aggregation in a straight forward manner, giving information about the time dependant nature of sugar-lectin binding based on the increase in absorbance resulting from aggregation of particles causing turbidity in the solution. In their most simple format, these studies can be used to confirm the presence of a particular moiety at the surface of a particle, or to investigate the colloidal stability of a latex. UV-Vis is not appropriate as a method of determining the relative level of aggregation or stability between particles however due to the nature of light scattering. This is because the change in apparent absorbance between different particle sizes or aggregation over time is non-linear in relation to size.[21] Building on previous work in the field of thermal stability of metal nanoparticles the use of DLS to monitor particle-lectin aggregation was compared to that of UV-Vis.

### 2.4.6 UV-Vis Method Optimisation

UV-Vis studies were performed as an initial test to confirm the presence of mannose on the surface of the latex particles and optimise conditions for the aggregation studies. To probe the effect of order of addition of lectin and sugar, the UV-vis aggregation study was performed adding the particles to a lectin solution and again, with the lectin to a particle solution, with the hypothesis that the order of addition would have no overall effect on the lectin binding. Due to coagulum certain latexes were also found to block the cannula used in the DLS studies, so it was beneficial for future studies that the order of addition did not affect the particle lectin binding, to avoid this issue. This same test was also performed with and without stirring, to determine the effect, if any, this would have on the particle-lectin binding; this was important as for further study by DLS as here the samples could not be mixed.

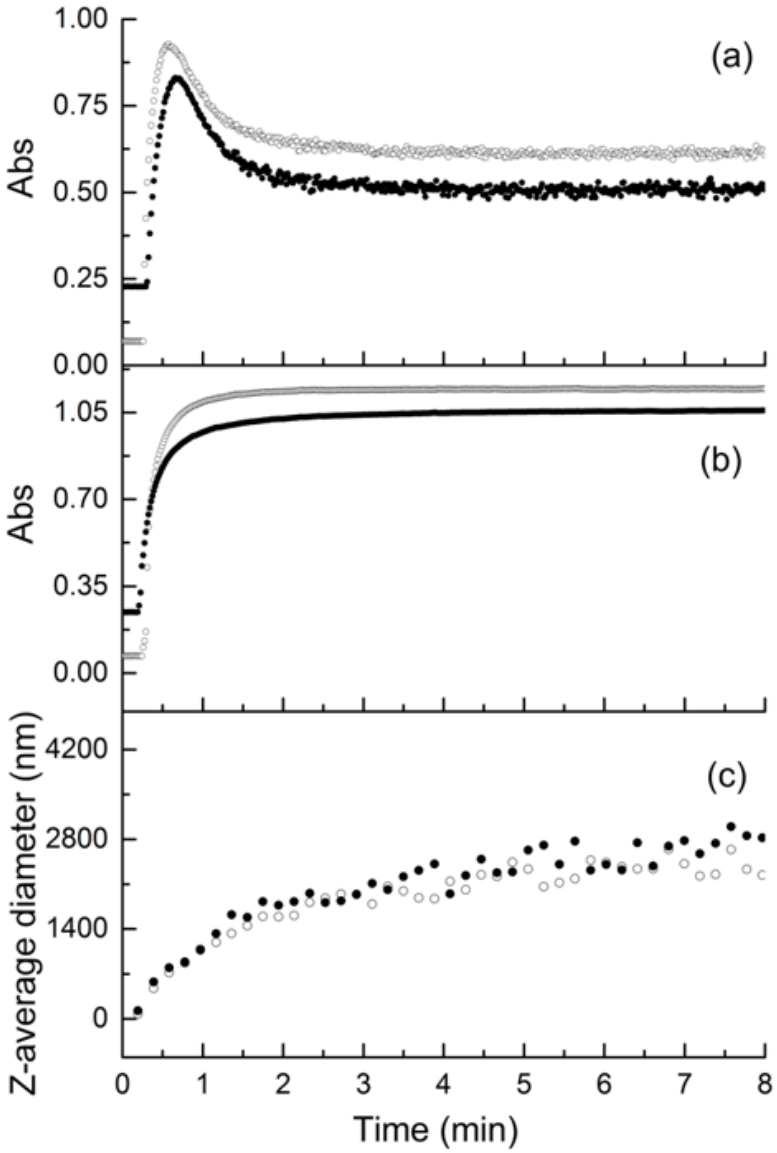


**Figure 2.4:** Effect of stirring and order of addition. a) Stirring UV-Vis (normalised), b) not stirring UV-Vis (normalised), c) not stirring DLS. Hollow circles denote particle solution added into ConA solution, filled circles denote ConA solution into particle solution.

The UV-Vis studies were carried out using an 82 nm α-mannose coated particle with concanavalin A as an alpha mannose and glucose specific lectin. A cuvette loaded with particle solution was loaded into a UV-Vis spectrometer and an absorbance reading was taken every second at 500 nm. After one minute the ConA solution was added using an autopipette. This was repeated with the addition of particle to lectin solution both with and without stirring (Figure 2.4).

The order of addition was shown to have a small effect on final solution turbidity, with particle into lectin solution resulting in a slightly higher absorbance reading than lectin into particles solution, the difference was minimal however, and the aggregation trend for both mixed and non-mixed samples remained unchanged by order of addition.

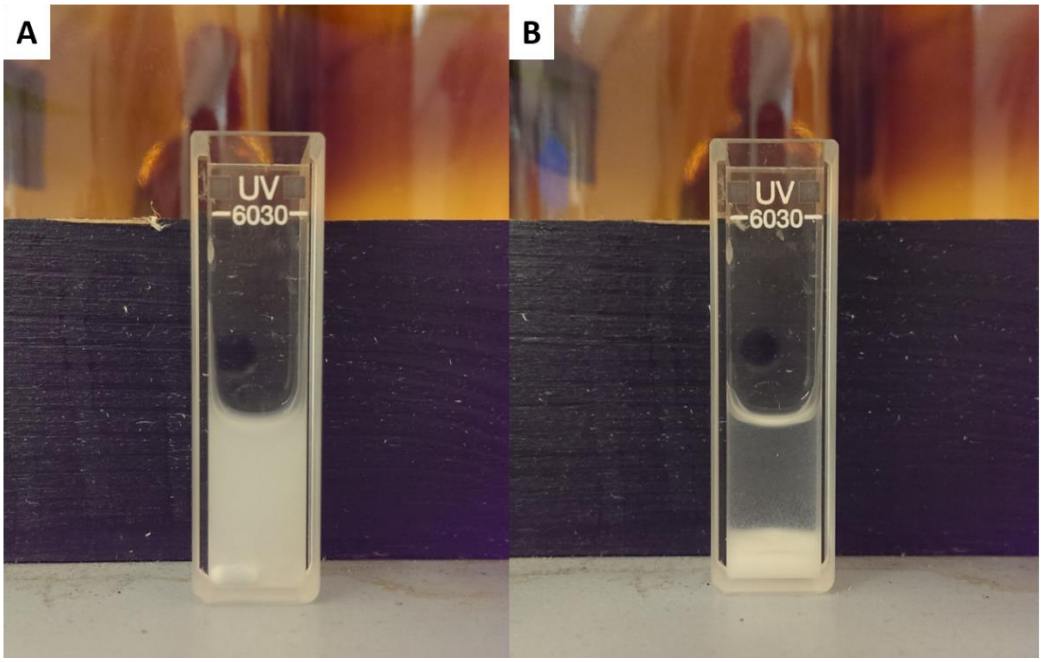


**Figure 2.5:** Showing particle-lectin aggregate sedimentation after stirring. A) α-mannose particle-ConA lectin aggregation stable in solution before mixing, B) five minutes after stirring, showing extensive sedimentation

This difference may be attributed to a slower diffusion of particles through lectin solution, than would be seen from ConA lectin through particle solution. The effect of stirring was however far more pronounced and consistent regardless of order of addition. For both experiments, stirred and not stirred, a sharp increase in absorbance can be seen upon solution mixing due to sugar-lectin interaction. In those experiments without stirring, this then plateaus to an absorbance reading between 0.8-1. With stirring however, the initial sharp increase in absorbance is followed by a subsequent decrease and plateau to a much lower final absorbance value of 0.6. A potential explanation for this phenomenon is that stirring introduces kinetic energy, increasing particle movement, and hence particle-lectin collisions, and thus the chances of a successful binding event between them. This higher successful collision rate may result in larger aggregates to form reaching a critical size, resulting in sedimentation out of solution and a lower absorbance. This hypothesis was supported further visually, by observing the resulting solutions. Those that were stirred were observed to completely sediment from solution after five minutes, whereas those without stirring were stable up to 24 hours. If solutions that were not stirred were later subject to stirring, they were also found to completely sediment from solution after five minutes. (Figure 2.5). Based on these results, if was concluded that aggregation could potentially be monitored by DLS, as when not stirred, successful aggregation occurred and a stable aggregate solution was obtained.

### 2.4.7 DLS Method Development

After optimising test conditions using UV-Vis aggregation the same experiment was performed using DLS to optimise the experimental setup such that real time (online) DLS measurements could be performed to track particle-lectin aggregation.

To enable real time information to be obtained, a setup where solutions could be mixed without interrupting the normal running of the DLS machine was required; to achieve this a cannula injection system was developed. A 4.5 mL plastic cuvette was charged with 1.25 mL of the required solution (particle or lectin) and fitted with a size 23 septum, which was pierced with a cannula attached to a 250 μL glass Hamilton syringe. The cannula was manipulated in such a way that any solution injected through it would flow down the side of the cuvette, rather than being squirted directly into the solution below, this was to minimise interference with Brownian motion and prevent air bubble formation. The cuvette was loaded into the DLS with the cannula exiting through a slit in the side of the sample chamber (Figure 2.6). The software was set up to take a size reading every 10 seconds (each reading actually taking 11.6 s) for one hour. After six readings (69.9 s) had taken place, the required solution of lectin or particles was then injected into the cuvette through the Hamilton syringe. This interrupted only one measurement, recording an artificially low diameter as the particles are induced to move faster than under Brownian motion alone. This allowed real time analysis of the particle aggregates being formed and also allowed the addition of further solutions for later experiments. All experiments were performed at the same concentration of lectin and mannose. In later analysis, particle size for the initial solution was measured by number distribution so as to minimise the influence of any large particles in solution. For clarity of presentation however, and to give an idea of every distribution in the sample, z-average was used for aggregate analysis and is plotted in figures.

As the effect of order of addition was still not clear, initially both orders were trialled to determine any effect and plotted as Z-average diameter for each individual 10 s measurement over time (Figure 2.4). Here, the order of addition was shown to have no effect on final particle aggregate size, with both average aggregate sizes increasing at the same rate and reaching the same final size of *ca* 2400 nm.

**Figure 2.6:** Pictures showing the setup of the DLS with a cannula injection system into the sealed sample holder, allowing injection of solution during measurements

This result confirmed that aggregation experiments could be conducted adding lectin solution to a particle solution without stirring. Having confirmed this, further study into the suitability of DLS for tracking particle-lectin aggregation and in obtaining quantitative information about the aggregation was possible.

### 2.4.8 Effect of Particle Size on Lectin Binding

Having established experimental parameters for UV-Vis and DLS suitable for real time tracking of particle aggregation, the effect of glycoparticle diameter on lectin aggregation was investigated. The hypothesis being that increasing the diameter of the particle would increase the ability for aggregation, producing larger aggregates, formed of more particles. By comparing the same experiment performed by both UV-Vis and DLS, direct comparisons of the two techniques could be made, and conclusions as to the benefits and limitations of each drawn.

Using the previously synthesised nanoparticles, identical aggregation experiments were performed using UV-Vis and DLS measurements. All conditions were kept consistent between different experiments, with a 12.5 μL of latex solution being diluted to 1.25 mL in phosphate buffer (PB) (all latexes at a mannose concentration of 2.608 $x10^{-4}$ M) and 250 μL of 3.125 $x10^{-5}$ M ConA in PB solution mixed either *via* pipetting in the case of UV-Vis, or cannula injection system, for DLS, to induce particle aggregation. An equivalent PEG coated nanoparticle (synthesised by another member of the group) was also tested as a control particle that should not aggregate in the presence of concanavalin A (Figure 2.7).

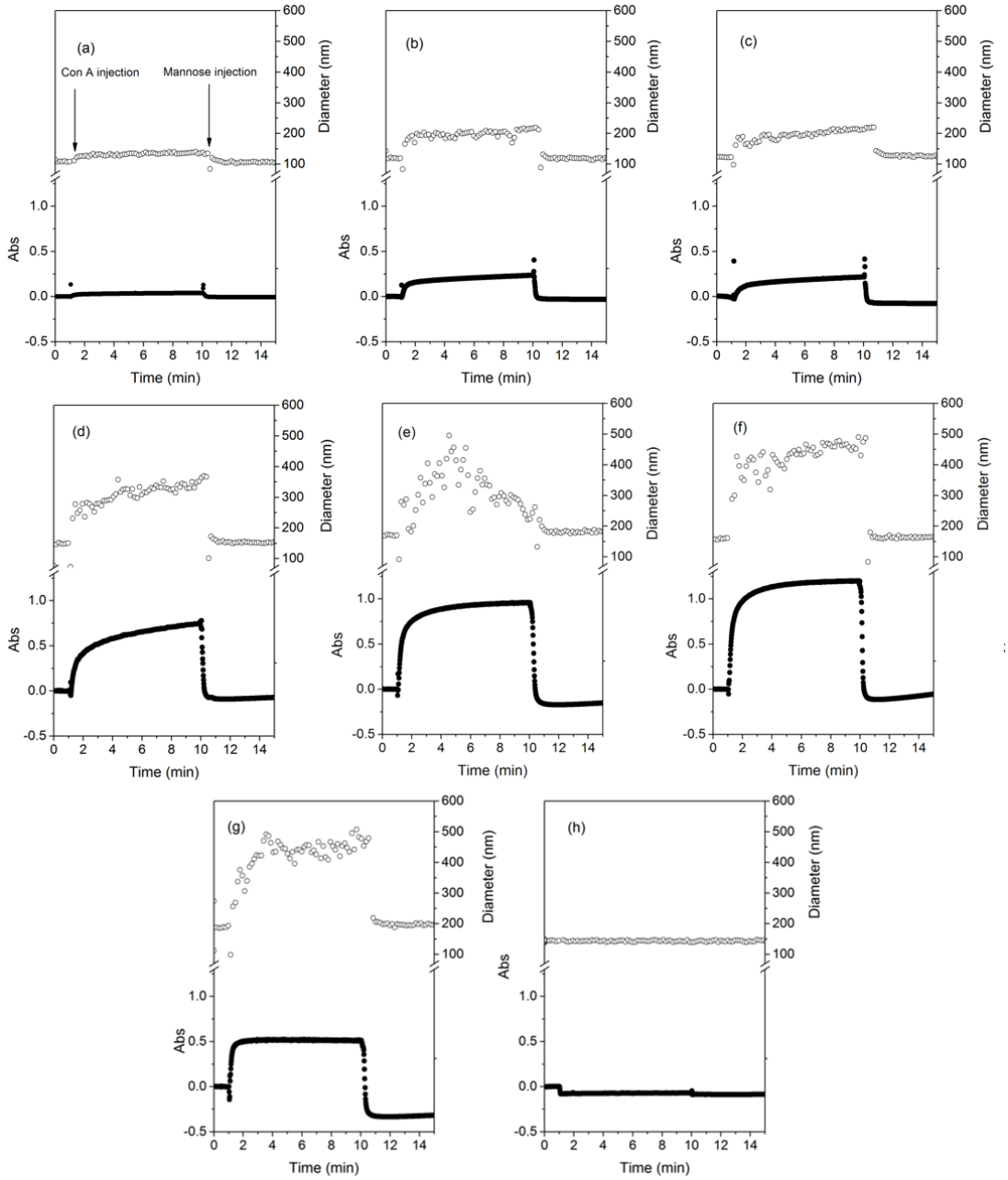


**Figure 2.7:** Nanoparticle-lectin aggregation with both turbidimetric absorbance (filled circles) and DLS Z-average diameter (hollow circles) measurements for P(ManAm) particles (a) 82 nm (b) 94 nm (c) 100 nm (d) 127 nm (e) 146 nm (f) 153 nm (g) 176 nm, and P(PEGA) particle (h) 130 nm. Arrows indicate time of injection for Con A and mannose solutions.

All mannose coated particles resulted in a large increase in diameter and absorbance by DLS and UV-Vis upon the addition of ConA. Subsequent addition of α-mannose (375 mg $mL^{-1}$ in PB) resulted in a drop in aggregate size by DLS to the original particle diameter and a sharp reduction in absorbance by UV-Vis. This was caused by the break-up of aggregates due to competitive inhibition on the ConA binding sites. No response was observed for the PEG control from lectin or sugar addition, confirming the aggregation of mannose particles was due to interaction between the sugar residues and binding sites on the lectin. This control also confirmed that the addition of ConA

does not interfere with DLS measurements, as no size deviation or dilution effect was observed. However, a characteristic drop in absorbance can be seen in the UV-Vis data, due to the dilution effect, reducing the concentration of particles in solution.

The conclusions from the data presented to this point between UV-Vis and DLS studies are broadly similar, showing qualitatively that all mannose coated particles reversibly formed aggregates upon the addition of ConA, and subsequently broke up with the addition of an excess of free α-D-mannose. However, by further analysing the data obtained from DLS it is possible to quantify the results further than is possible with UV-Vis. Firstly, after the initial sharp increase in z-average diameter a second distinct phase of slower aggregation can be seen.

This is particularly visible as a shift to larger diameters for smaller particles (a, b, c, and d) and indicates the slow formation of larger aggregates formed through aggregate-aggregate interaction. This secondary phase of aggregation, though visible in UV-Vis studies, is not able to be quantified as a specific increase in aggregate size.

$$ppa = \left(\frac{aggregate\ volume}{particle\ volume}\right) \times 0.74$$

**Equation 2.1:** Estimation of number of particles forming final particle-lectin aggregate, final aggregate volume divided by the average volume of a single constituent particle, then multiplied by 0.74 as the maximum packing parameter for hard spheres. Aggregate and particle volume determined from radius by DLS

Using the DLS data, an estimation of particles per aggregate (ppa) may be made. To determine this, the average final aggregate volume is divided by the volume of the initial particles forming the aggregate and then multiplied by the maximum packing parameter for hard spheres (0.74) (Equation 2.1).[75] This information can also be compared to a theoretical maximum number of aggregation, a value past which sedimentation would occur. A diameter of over 500 nm, is recognised as an approximate diameter past which polymeric particles start to lose colloidal stability in water and as such was used to determine a theoretical maximum number of aggregation for particle-lectin aggregates (Table 2.2).[58] Aggregate size was determined by taking a mean average diameter after the initial phase of aggregation had completed. A clear increase in aggregate size can be seen as the particle size increases, this could of course simply be due to the aggregates being composed of larger particles. However, by taking the original particle size into account, and determining the number of particles required to form each aggregate, an increase in aggregation number can be seen from 3.6 ppa for 82 nm particles to 30 ppa for particles

146 nm in diameter. Particles above this diameter (153 and 176 nm) were not able to accurately be analysed as they exhibited a large amount of sedimentation. This further supports the previous assertions that for this DLS aggregation analysis to provide quantitative data, aggregates must remain stable in solution, and that a diameter of 500 nm represents a good upper limit for aggregate diameter. It is hypothesised that the observed increase in particle aggregation is related to the surface area of the original particle, containing more mannose residues and therefore more lectins, increasing the chances of a second successful interaction with a mannose residue on another particle. In addition to this, the contact angle between two particles will decrease as particle size increases leading to a corresponding increase in the potential area of interaction where a ConA molecule will be able to bind to residues on both particles.

| Particle Diameter (nm)[a] | Particle Vol ($nm^3$) | Aggregate Diameter (nm) | Aggregate Vol ($nm^3$)[b] | $N_{agg}$ | Max $N_{agg\ Th}$ |
|---|---|---|---|---|---|
| 82 | 290,000 | 138 | 1,400,000 | 3.6 | 167 |
| 94 | 430,000 | 206 | 4,600,000 | 7.9 | 113 |
| 100 | 520,000 | 214 | 5,100,000 | 7.3 | 93 |
| 127 | 1,100,000 | 390 | 31,00,000 | 20.9 | 44 |
| 146 | 1,600,000 | 496 | 64,000,000 | 29.6 | 30 |
| 153 | 1,900,000 | 589 | 107,000,000 | 41.7 | 25 |
| 176 | 2,900,000 | 591 | 108,000,000 | 27.6 | 17 |

**Table 2.2:** Analysis of final particle aggregate, compared to original particle diameter. a- measured by DLS, b- determined using aggregate diameter and formula for the volume of a sphere

The data presented shows that DLS may be used a technique analogous to UV-Vis in the qualitative data obtained for particle aggregation studies. It has also been shown that further quantitative analysis determining the aggregate size and estimating the number of particles forming each aggregate is possible. However, this is only possible where aggregation conditions are controlled such that colloidal stability is maintained, and aggregates formed are small enough to remain governed by Brownian motion.

## 2.5 Conclusions

In conclusion, this chapter has focussed on the preparation of glycosylated nanoparticles by the method of RAFT emulsion polymerisation, and the development of a quantitative DLS based technique for studying particle-lectin aggregation.

Particles of a range of sizes were synthesised from a short amphiphilic di-block copolymer. These particles were further shown to be surface functionalised with mannose from the hydrophilic part of the di-block copolymer.

These particles then had their aggregation properties with ConA studied using UV-Vis and a developed DLS system. Online aggregation measurements using a cannula injection system were shown to be comparable to UV-Vis studies The DLS system was further shown however, to not be affected by the dilution effect and, rather than be hindered by light scattering changes, take advantage of them to provide quantitative information on particle aggregate size and composition.

## 2.6 Experimental

### 2.6.5 Materials

Poly(ethylene glycol) methyl ether acrylate (PEGA, average $M_n$ = 480 g mol$^{-1}$), *n*-butyl acrylate (*n*BA, >99), and *N*-hydroxyethyl acrylamide were obtained from Sigma-Aldrich and all monomers above were passed through basic aluminium oxide to remove inhibitor before use. 1,2,3,4,6-penta-O-acetyl-D-mannopyranose was obtained from Carbosynth Ltd and used as received. Concanavalin A was bought from MP Biomedical SAS. All solvents were bought from commercial sources and were used as received. Dimethyl sulfoxide-$d_6$ (99.9% D atom), chloroform-$d_3$ (99.8% D atom) and deuterium oxide-$d_2$ (99.9% D atom), were obtained from Sigma Aldrich and used for NMR spectroscopy. Thermal initiator 4,4′-azobis(4-cyanovaleric acid) (ACVA) (>98%, Aldrich) was used as received. 0.45 μm syringe filters were obtained from Alpha Laboratories Ltd.

### 2.6.6 Analysis

#### 2.6.6.1 NMR Spectroscopy

$^1$H NMR spectra were recorded on a Bruker DPX-300 spectrometer using deuterated solvent (materials section). Each sample was run with a decay time of 2 s with 16 repeats.

#### 2.6.6.2 Mass Spectrometry

Mass spectrometry measurements were performed on an Agilent 6130B Single Quad for ESI, with a methanol solvent in positive mode.

#### 2.6.6.3 Infrared Spectroscopy

Fourier Transform Infrared Spectroscopy (FTIR) spectra were recorded using a Bruker Vector 22. The contact sampler was a horizontal diamond accessory (ATR) with a resolution of 4 cm$^{-1}$. Scan speed was set at 0.5 cm s$^{-1}$ with 120 scans performed per sample and performed on a dry solid sample.

#### 2.6.6.4 Size Exclusion Chromatography

Chromatograms were performed using an Agilent 390-LC MDS instrument equipped with differential refractive index (DRI), viscometry, dual angle light scatter and dual wavelength UV detectors. The system was equipped with 2 x PLgel Mixed D columns

(300 x 7.5 mm) and a PLgel 5 µm guard column. The eluent was DMF with 5 mmol $NH_4BF_4$ additive. Samples were run at 1 ml $min^{-1}$ at 50°C. Poly(methyl methacrylate) standards (Agilent EasyVials) were used for calibration. Analyte samples were filtered through a nylon membrane with 0.22 µm pore size before injection. Experimental molar mass ($M_n$,SEC) and dispersity ($Đ$) values of synthesised polymers were determined by conventional calibration using Agilent SEC software.

#### 2.6.6.5 Dynamic light scattering, size and ζ-potential

Size and ζ-potential measurements were carried out using a Malvern Zetasizer Nano-ZS at 25°C with a 4 mW He-Ne 633 nm laser at a scattering angle of 173° (back scattering). Measurements were taken assuming the refractive index of hydroxyethylacrylamide for $P(ManAm)_{10}$-*b*-$P(BA)_{15}$ and the refractive index of *n*-butyl acrylate for latex particles. DLS samples of latex particles were prepared by diluting 1000-fold with 1 mL of water filtered through a 0.45 µm RC syringe filter and measured in 1.5 mL polystyrene cuvettes for measuring size and a Malvern DTS-1070 cuvette for ζ-potential. Di-block copolymer samples were measured at the concentration of a typical RAFT emulsion polymerisation. Samples were incubated for 60 seconds at 25°C prior to measurement. Measurements were repeated three times with automatic attenuation selection and measurement position. Results were analysed using Malvern DTS 6.20 software. Pdi values were calculated using the following equation. Measurements of ζ-potential were modelled with the Smoluchowski theory. Number distributions are reported for initial particle size, as previously in the group they have been found to match most closely the diameters obtained through electron microscopy.

$$Pdi = \frac{\sigma^2}{d^2}$$

**Equation 2.2:** Equation to calculate Pdi from standard deviation (σ), and diameter (d).

### 2.6.7 Synthetic Procedures

#### 2.6.7.1 Synthesis of α-D-mannopyran-1-oxyethyl acrylamide

7.5 g (0.0192 mol, 1.13 eq) of α-D-mannopyran-1-oxyethyl acrylamide and 2.01 g (0.017 mol, 1 eq) of hydroxyl ethyl acrylamide were dissolved in 77 mL of anhydrous DCM in a 250 mL round bottomed flask (RBF) equipped with a magnetic stirrer and an appropriately sized rubber septum. The reaction mixture was purged with nitrogen

gas and 13.33 g of boron trifluoride diethyl etherate (0.044 mol, 11.6 mL) was transferred using a gas-tight Hamilton syringe charged with nitrogen. The reaction mixture was consequently subjected to four cycles of 10 min sonication and 5 min rest prior to stirring at ambient temperature for 48 h. The progress of the reaction was monitored with thin layer chromatography (TLC) using a 9:1 chloroform:methanol mixture (v/v), and stained with 5% sulfuric acid in ethanol. Once complete, the reaction mixture was then diluted with two parts DCM and washed thoroughly with brine three times then water in an appropriately sized separating funnel. The organic phase was dried over magnesium sulfate, filtered via vacuum filtration and the solvent removed under reduced pressure at a temperature no higher than 30 °C leaving an orange brown viscous liquid. This was dissolved in 40 mL of potassium carbonate in methanol, purged with nitrogen gas and stirred at ambient temperature for 24 h. The pH was adjusted to pH 7 with a Dowex 50WX4 hydrogen form exchange resin and stirred until the pH was fully adjusted. The Dowex resin was removed with vacuum filtration and solvent removed under reduced pressure at a temperature no higher than 30 °C. The crude product was purified *via* column chromatography on an 80 g silica column and eluted with a 2:8 methanol: chloroform mixture at a flow rate of 1 mL $min^{-1}$, on an auto-column equipped with a UV-Vis detector set to 308 nm. The product was found to elute at around 15 min. Product fractions were combined, the solvent evaporated to less than 10 mL under reduced pressure and subsequently freeze dried to yield the pure monomer as a white powder.

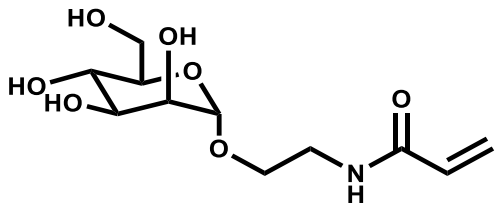


**Scheme 2.3:** Structure of α-D-mannopyran-1-oxyethyl acrylamide

$^{1}$H NMR spectroscopy ($D_2O$, 400 MHz) $\delta_H$: 6.13 (dt, J = 31.0, 13.5 Hz, 2H, C**H**$_2$CH), 5.65 (d, J = 10.0 Hz, 1H, $CH_2$C**H**), 4.74 (s, J = 16.2 Hz, 1H, C**H**$O_2$CH), 3.80 (s, J = 122.4 Hz, 1H, $CH_2$O**H**), 3.76 – 3.28 (m, 9H). $^{13}$C NMR spectroscopy ($D_2O$, 400 MHz): δ 129.75 (s) (**C**H$CH_2$), 121.41 (m) (**C**$H_2$CH), 99.61 (s) (**C**$H_2$OH), 72.71 (s) (**C**HO), 70.39 (s) (**C**HO), 69.92 (s) (**C**HO), 66.52 (s) (**C**HO), 65.69 (s) (**C**HO), 60.76 (m) (**C**H2O), 37.77 (m) (**C**$H_2$NC). (Figures 2.8 and 2.9)

MS *m/z* $[M+Na]^+$: 300.1 ($MS_{th}$: 300.9)

IR spectroscopy ($cm^{-1}$): 3275 (b), 2928 (b), 1656 (n), 1624 (m), 1548 (b), 1409 (m), 1317 (w), 1249 (m), 1131 (m), 1089 (m), 1051 (s), 1023 (s).

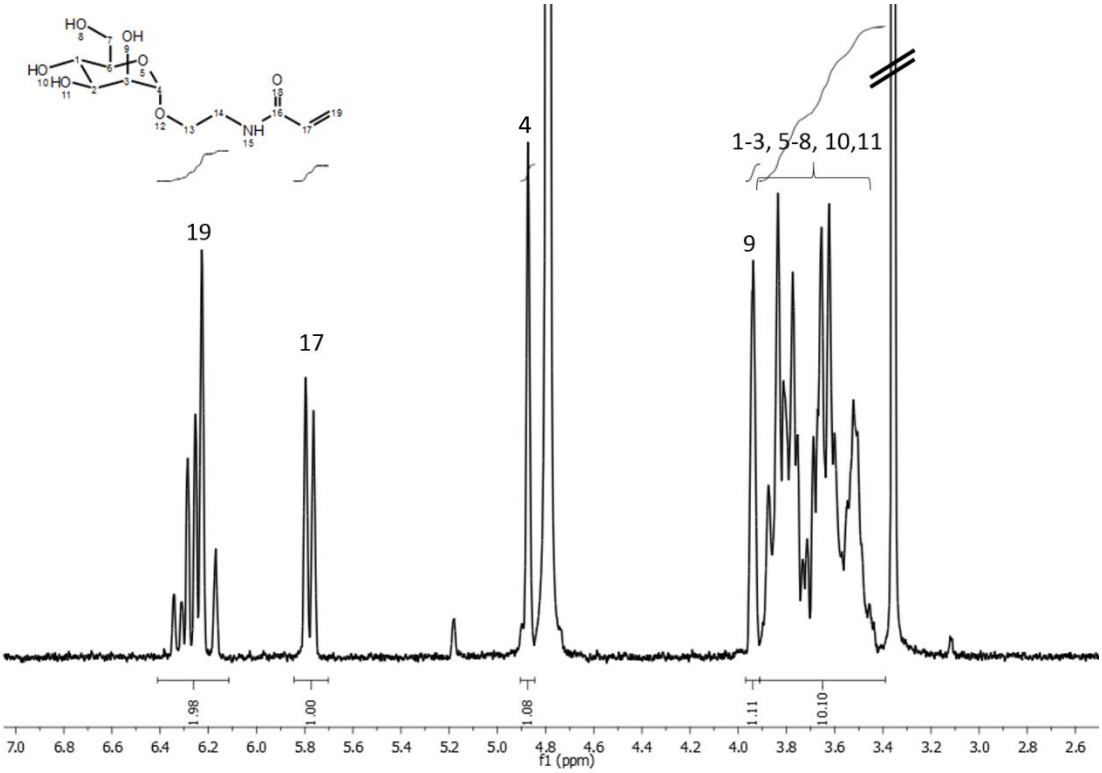


**Figure 2.8:** α-D-mannopyran-1-oxyethyl acrylamide monomer $^1H$ NMR spectrum, solvent $D_2O$

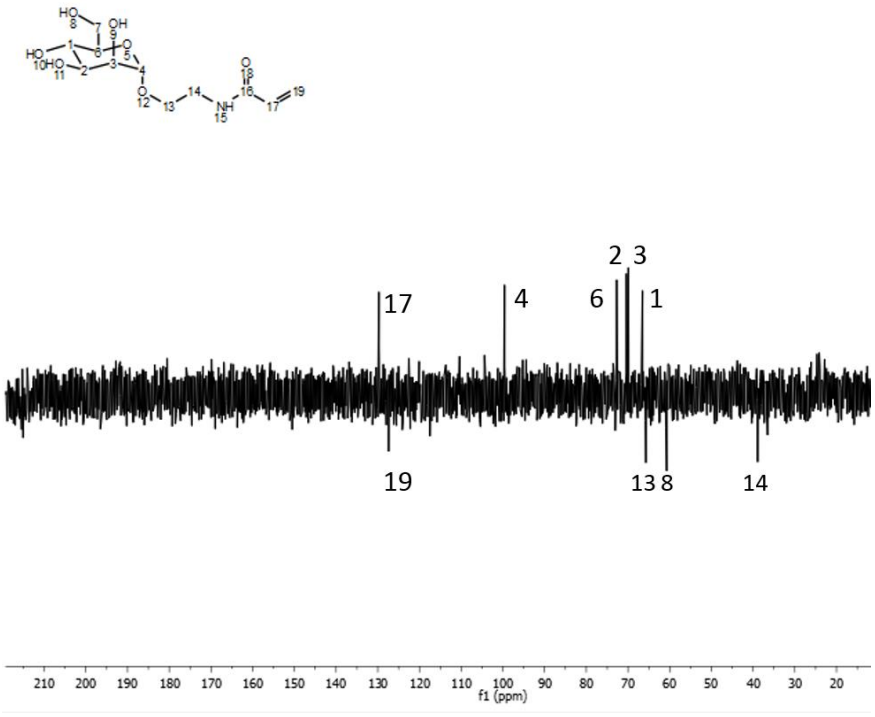


**Figure 2.9:** α-D-mannopyran-1-oxyethyl acrylamide monomer $^{13}C$ NMR spectrum, solvent $D_2O$

### 2.6.7.2 Poly (α-D-Mannopyran-1-oxyethyl Acrylamide)$_{10}$-*b*-Poly(*n*-Butyl Acrylate)$_{15}$ Synthesis

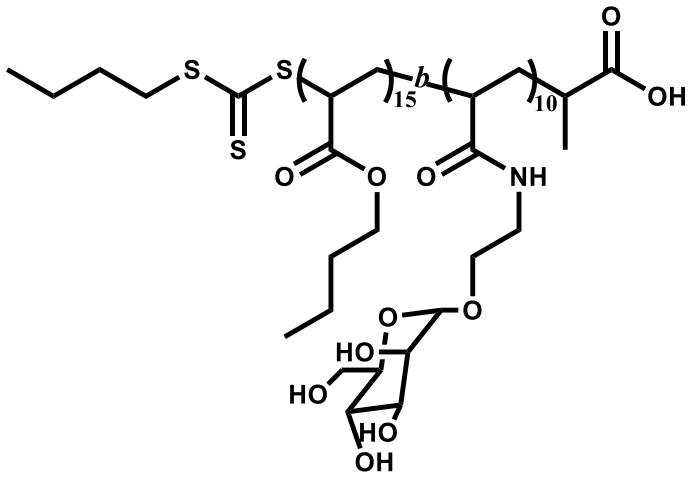


**Scheme 2.10:** Structure of poly(α-D-mannopyran-1-oxyethyl acrylamide)$_{10}$-b-poly(n-butyl acrylate)$_{15}$

α-D-mannopyran-1-oxyethyl acrylamide (1g, 3.62 mmol, 10 eq.), 2-((butylthio) carbonothioyl) thio)propanoic acid (0.0864g, 3.62x10$^{-4}$ mol, 1 eq.), and ACVA (from a pre-made stock solution of 10mg mL$^{-1}$ in DMF:water (70:30) mix) (0.0508g, 1.81x10$^{-4}$ mol) were dissolved in a mixture of DMF:water (70:30) to a total volume of 10.8 mL in a 25 mL round bottomed flask with a magnetic stirrer bar. The flask was sealed with an appropriate rubber septum and purged of oxygen with nitrogen gas for ten minutes before immersing it into a preheated oil bath at 70°C and stirred for seven hours. Monomer conversion was determined by $^1$H NMR spectroscopy in $D_2O$, by comparison of the ratio of the vinyl peak (δ=6.08) and RAFT agent $CH_3$ z-group butyl chain end group peak (δ=0.78). The polymer was analysed by SEC with a DMF eluent at 30°C ($M_{n\ SEC}$=2450 g mol$^{-1}$ $Đ$=1.27) ($M_{n\ th}$ = 3008 g mol$^{-1}$). To chain extend the synthesized P(ManAm)$_{10}$ macro-RAFT agent, *n*-butyl acrylate was purged of oxygen with nitrogen for ten minutes, and 1.3g (1.01x10$^{-2}$ mol, 1.45mL) was injected into the 25 mL round bottomed flask using a dry Hamilton syringe, purged with nitrogen. The round bottomed flask was then immersed in an oil bath set to 70°C and stirred for seven hours. Monomer conversion was determined by $^1$H NMR spectroscopy in $d_6$-DMSO, by comparison of the ratio of vinyl peak (δ=5.94) and RAFT agent/ *n*-BA $CH_3$ z-group butyl chain end group peak (δ=0.83). Polymers were analysed by SEC with a DMF eluent (Figures 2.10 and 2.11).

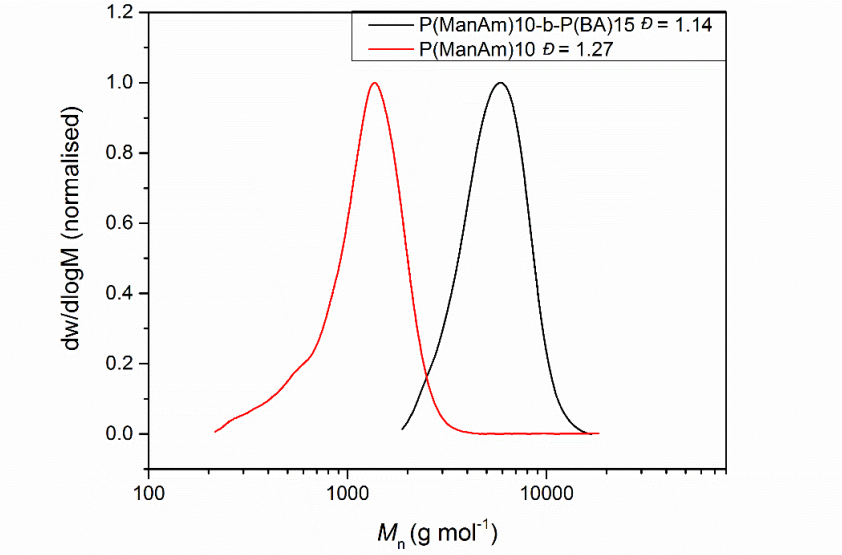


**Figure 2.11:** SEC traces for: red) poly(α-D-mannopyran-1-oxyethyl acrylamide))$_{10}$ $M_n$= 2450 g mol$^{-1}$, $Đ$=1.27; black) of poly(α-D-mannopyran-1-oxyethyl acrylamide)$_{10}$-*b*-poly(*n*-butyl acrylate)$_{15}$ $M_n$= 4600 g mol-1, $Đ$=1.14

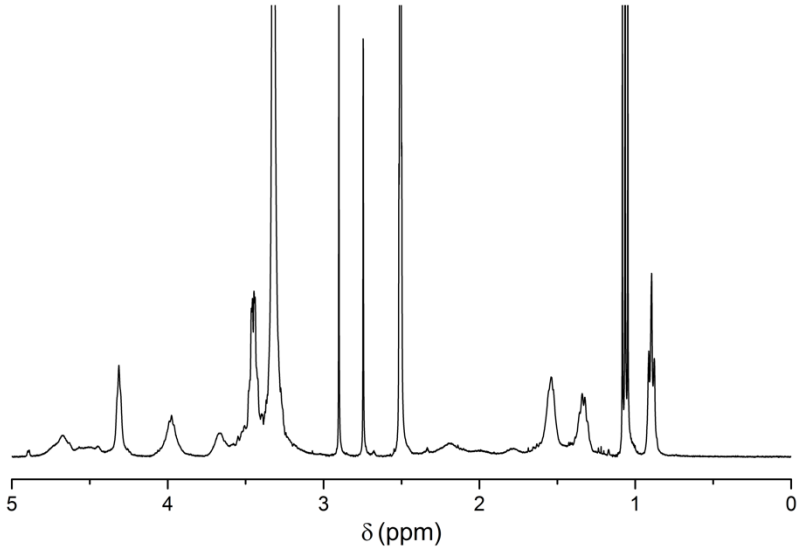


**Figure 2.11:** $^1$H NMR spectrum of P(ManAm)$_{10}$-*b*-P(BA)$_{15}$ in $D_2O$

### 2.6.7.3 General Method for RAFT-Mediated Emulsion Polymerisation

Nanoparticles of different sizes were prepared by altering the ratio of di-block macro-RAFT agent to monomer in an emulsion polymerisation. As an example, P(ManAm)$_{10}$-*b*-P(BA)$_{15}$-*b*-P(BA)$_{400}$ was prepared as follows. NaOH (14.3 mg, 3.6 x 10$^{-4}$ mol) was added to a suspension of ACVA (50 mg, 1.8 x 10$^{-4}$ mol) in water (10 mL) to ensure full solubility. P(ManAm)$_{10}$-*b*-P(BA)$_{15}$ (0.015 g, 3.13 x 10$^{-6}$ mol) was dissolved in 0.645 mL of water, in a 2mL vial fitted with a cap incorporating a rubber septum and equipped with an appropriate magnetic stirrer. 0.175 mL of the above ACVA stock solution was added, and the solution was deoxygenated with nitrogen gas for 20 minutes. A stock of *n*-BA was separately deoxygenated in a vial for 10 minutes.

The macro-RAFT agent solution was immersed in an oil bath set to 70°C, *n*-BA (0.160 g, 1.25 x$10^{-3}$ mol) was injected immediately and the RAFT-emulsion polymerisation was stirred for 3 h at 70°C at 400 rpm. After approximately 10 min, the emulsion turned a milky white as the polymerisation proceeded. Conversion of monomer to polymer was found to be >99% by $^1$H NMR spectroscopy in a mixed solvent of $d_6$-DMSO/ $CDCl_3$ (80/20 % v/v), by comparison of the ratio of vinyl peak (δ=6.14) and $CH_3$ butyl chain end group peak (δ=0.88) (Figure 2.12). The polymer was analysed by SEC with a DMF eluent at 30°C ($M_{n\ SEC}$= 61000 g mol$^{-1}$ $Đ$=1.27) (Figure 2.13), and by DLS to determine particle size (Figure 2.14).

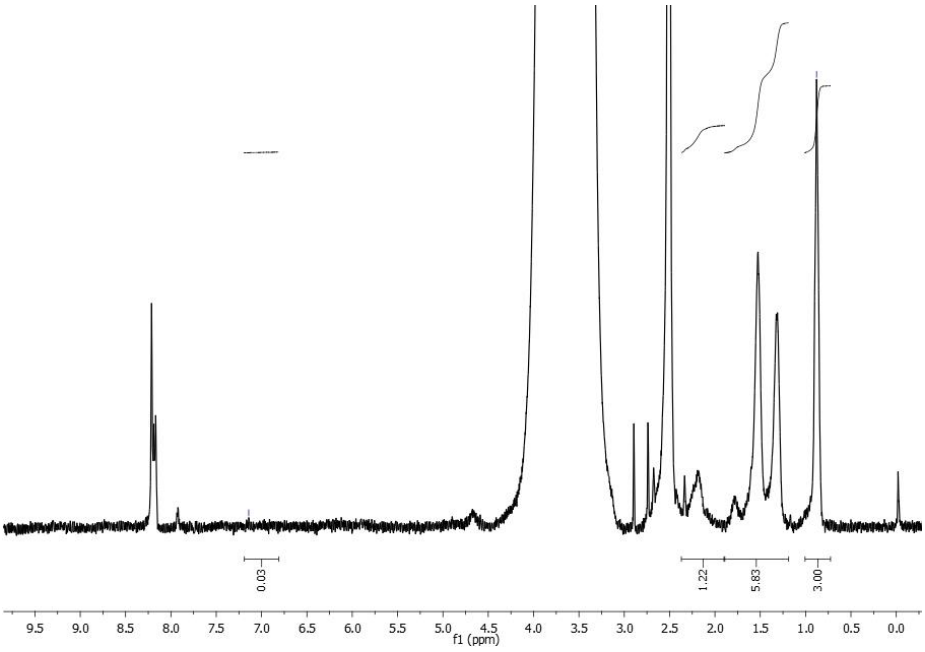


**Figure 2.12:** $^1$H NMR spectrum of P(ManAm)$_{10}$-*b*-P(BA)$_{15}$-*b*-P(BA)$_{400}$ showing no residual monomer

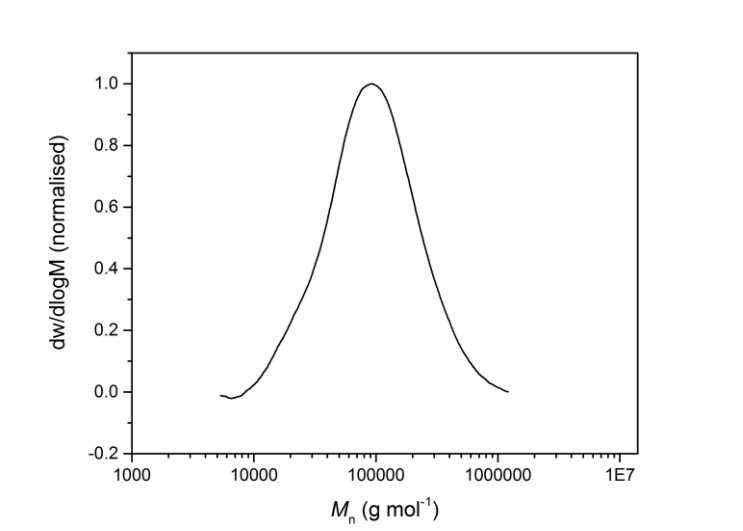


**Figure 2.13:** SEC trace of P(ManAm)$_{10}$-*b*-P(BA)$_{15}$-*b*-P(BA)$_{400}$ using DMF as an eluent, $M_n$= 61000 g mol$^{-1}$ $Đ$ = 1.9

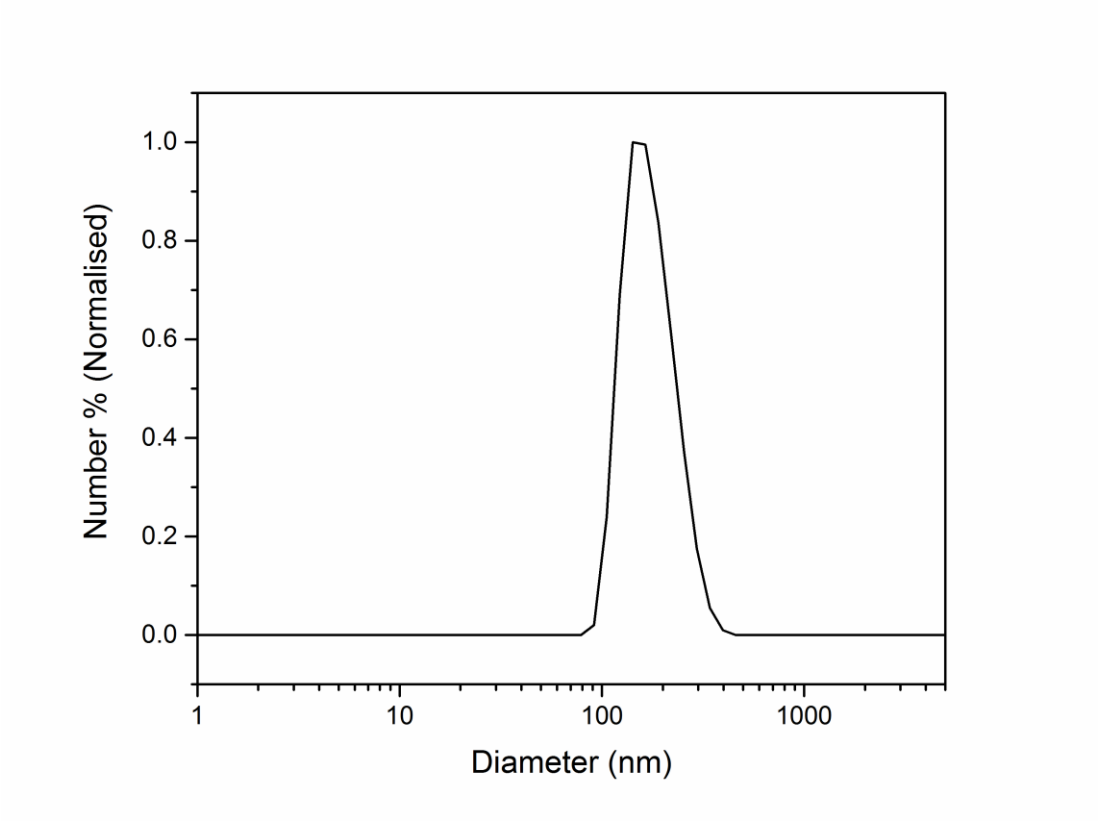


**Figure 2.14:** DLS trace of P(ManAm)$_{10}$-*b*-P(BA)$_{15}$-*b*-P(BA)$_{400}$ in water Diameter = 176 nm, Pdi= 0.1

### 2.6.8 General Method for UV-Vis Aggregation Studies

Turbdimertric studies were conducted by diluting 12.5 µL of undiluted particle solution with 1.3 mL of 10 mM phosphate buffer in a 4.5 mL polystyrene cuvette and placed in a UV-Vis spectrometer. In a separate 4.5 mL polystyrene cuvette a stock solution of 2.027x10$^{-5}$ M Con A in 10mM phosphate buffer was prepared for use. Absorbance readings were taken every second at 500 nm, after 60 seconds 250 µL of Con A in phosphate buffer (2.027x10$^{-5}$ M) was added with an Eppendorf pipette and mixed twice to induce aggregation. After a further 9 minutes 50 µL of α-mannose in phosphate buffer (375 mg mL$^{-1}$) was added with an Eppendorf pipette and mixed twice to induce competitive binding with the glycosylated nanoparticles. The absorbance was monitored for a further 10 minutes. Readings were taken using an Agilent Carey 60 UV-Vis machine with Agilent software and analysed using Origin.

### 2.6.9 DLS Aggregation

DLS measurements were taken using a Malvern instruments Zetasizer Nano at 25 °C with a 4 mW He-Ne 633 nm laser at a scattering angle of 173° (back scattering). For

P(ManAm) particle DLS aggregation studies, 12.5 μL of particle solution was diluted with 1.24 mL of 10 mM phosphate buffer to make a total of 1.25 mL in a 4.5 mL polystyrene cuvette. The cuvette was fitted with a size 23 septum, which was pierced with a cannula attached to a 250 μL Hamilton glass syringe. The cannula was positioned such that, solution ejected through it would run down the side of the cuvette. This prevented the creation of any air bubbles that may have interfered with measurements. The cuvette was placed into the Zetasizer, and the lid closed with the syringe exiting through a slit at the side of the instrument. In a separate 4.5 mL polystyrene cuvette a stock solution of $2.027 \times 10^{-5}$ M Concanavalin A in 10 mM phosphate buffer was prepared for use with P(ManAm) particles. The Zetasizer was set to take a size reading every 10 seconds for 1 hour, however a delay of 1.66 seconds was recorded between each reading, adding 598 seconds to each hour, for which the results have been amended. After the sixth reading, 250 μL of $2.027 \times 10^{-5}$ M Con A stock solution was injected via the cannula giving a final volume of 1.5 mL. The final concentration of Con A and mannose residues was $3.125 \times 10^{-5}$ M and $2.608 \times 10^{-4}$ M respectively. The same technique was then repeated with the addition of 250 μL of 75 mg $mL^{-1}$ α-mannose in phosphate buffer being injected via the syringe cannula after 10 minutes (to allow full de-aggregation). This was performed as a competitive binding assay, to show reversible lectin binding.

## 2.7 References


1. Richards, S.-J.; Otten, L.; Gibson, M. I., Glycosylated gold nanoparticle libraries for label-free multiplexed lectin biosensing. *Journal of Materials Chemistry B* **2016**.
2. Köhn, M.; Benito, J. M.; Ortiz Mellet, C.; Lindhorst, T. K.; García Fernández, J. M., Functional Evaluation of Carbohydrate-Centred Glycoclusters by Enzyme-Linked Lectin Assay: Ligands for Concanavalin A. *ChemBioChem* **2004,** *5* (6), 771-777.
3. Bourne, Y.; van Tilbeurgh, H.; Cambillau, C., Protein-carbohydrate interactions. *Current Opinion in Structural Biology* **1993,** *3* (5), 681-686.
4. Deshpande, A.; Rhodes, C.; Shah, N.; Malick, A., Controlled-release drug delivery systems for prolonged gastric residence: an overview. *Drug Development Industrial Pharmacy* **1996,** *22* (6), 531-539.
5. Maeda, H.; Bharate, G.; Daruwalla, J., Polymeric drugs for efficient tumor-targeted drug delivery based on EPR-effect. *European Journal of Pharmaceutics Biopharmaceutics* **2009,** *71* (3), 409-419.
6. Blix, H. S.; Viktil, K. K.; Moger, T. A.; Reikvam, A., Drugs with narrow therapeutic index as indicators in the risk management of hospitalised patients. *Pharmacy Practice* **2010,** *8* (1), 50.
7. de Leon, J., The crucial role of the therapeutic window in understanding the clinical relevance of the poor versus the ultrarapid metabolizer phenotypes in subjects taking drugs metabolized by CYP2D6 or CYP2C19. *Journal of Clinical Psychopharmacology* **2007,** *27* (3), 241-245.
8. Zolnik, B. S.; Sadrieh, N., Regulatory perspective on the importance of ADME assessment of nanoscale material containing drugs. *Advanced Drug Delivery Reviews* **2009,** *61* (6), 422-427.
9. Levy, G., What are narrow therapeutic index drugs? *Clinical Pharmacology Therapeutics* **1998,** *63* (5), 501-505.
10. Kahan, B. D.; Welsh, M.; Rutzky, L. P., Challenges in cyclosporine therapy: the role of therapeutic monitoring by area under the curve monitoring. *Therapeutic Drug Monitoring* **1995,** *17* (6), 621-624.
11. Moshfeghi, A. A.; Peyman, G. A., Micro-and nanoparticulates. *Advanced Drug Delivery Reviews* **2005,** *57* (14), 2047-2052.
12. Nishiyama, N.; Bae, Y.; Miyata, K.; Fukushima, S.; Kataoka, K., Smart polymeric micelles for gene and drug delivery. *Drug Discovery Today: Technologies* **2005,** *2* (1), 21-26.
13. Charman, W. N.; Charman, S. A., Oral Modified-Release Delivery Systems. In *Modified-Release Drug Delivery Technology*, CRC Press: 2002; pp 25-34.
14. Hamidi, M.; Azadi, A.; Rafiei, P.; Ashrafi, H., A pharmacokinetic overview of nanotechnology-based drug delivery systems: an ADME-oriented approach. *Critical Reviews in Therapeutic Drug Carrier Systems* **2013,** *30* (5).
15. Utama, R. H.; Jiang, Y.; Zetterlund, P. B.; Stenzel, M. H., Biocompatible Glycopolymer Nanocapsules via Inverse Miniemulsion Periphery RAFT Polymerization for the Delivery of Gemcitabine. *Biomacromolecules* **2015,** *16* (7), 2144-2156.
16. Del Pino, P.; Pelaz, B.; Zhang, Q.; Maffre, P.; Nienhaus, G. U.; Parak, W. J., Protein corona formation around nanoparticles–from the past to the future. *Materials Horizons* **2014,** *1* (3), 301-313.

17. Soppimath, K. S.; Aminabhavi, T. M.; Kulkarni, A. R.; Rudzinski, W. E., Biodegradable polymeric nanoparticles as drug delivery devices. *Journal of Controlled Release* **2001,** *70* (1-2), 1-20.
18. Kumari, A.; Yadav, S. K.; Yadav, S. C., Biodegradable polymeric nanoparticles based drug delivery systems. *Colloids Surfaces B: Biointerfaces* **2010,** *75* (1), 1-18.
19. Cho, K.; Wang, X.; Nie, S.; Shin, D. M., Therapeutic nanoparticles for drug delivery in cancer. *Clinical Cancer Research* **2008,** *14* (5), 1310-1316.
20. Singh, R.; Lillard Jr, J. W., Nanoparticle-based targeted drug delivery. *Experimental Molecular Pathology* **2009,** *86* (3), 215-223.
21. Fitch, R. M., *Polymer colloids*. Academic Press: 1997.
22. Tadros, T. F., *Handbook of Colloid and Interface Science: Industrial Applications*. Walter de Gruyter GmbH & Co KG: 2017; Vol. 3.
23. Manabe, M.; Tatarazako, N.; Kinoshita, M., Uptake, excretion and toxicity of nano-sized latex particles on medaka (Oryzias latipes) embryos and larvae. *Aquatic Toxicology* **2011,** *105* (3-4), 576-581.
24. Zhang, X.; Boissé, S.; Zhang, W.; Beaunier, P.; D'Agosto, F.; Rieger, J.; Charleux, B., Well-defined amphiphilic block copolymers and nano-objects formed in situ via RAFT-mediated aqueous emulsion polymerization. *Macromolecules* **2011,** *44* (11), 4149-4158.
25. Charleux, B.; Delaittre, G.; Rieger, J.; D'Agosto, F., Polymerization-induced self-assembly: from soluble macromolecules to block copolymer nano-objects in one step. *Macromolecules* **2012,** *45* (17), 6753-6765.
26. Boyer, C.; Bulmus, V.; Davis, T. P.; Ladmiral, V.; Liu, J.; Perrier, S., Bioapplications of RAFT polymerization. *Chemical Reviews* **2009,** *109* (11), 5402-5436.
27. Zetterlund, P. B.; Kagawa, Y.; Okubo, M., Controlled/living radical polymerization in dispersed systems. *Chemical Reviews* **2008,** *108* (9), 3747-3794.
28. Ferguson, C. J.; Hughes, R. J.; Nguyen, D.; Pham, B. T.; Gilbert, R. G.; Serelis, A. K.; Such, C. H.; Hawkett, B. S., Ab Initio Emulsion Polymerization by RAFT-Controlled Self-Assembly. *Macromolecules* **2005,** *38* (6), 2191-2204.
29. Ting, S. S.; Min, E. H.; Zetterlund, P. B.; Stenzel, M. H., Controlled/Living ab Initio Emulsion Polymerization via a Glucose RAFT stab: Degradable Cross-Linked Glyco-Particles for Concanavalin A/Fim H Conjugations to Cluster E. coli Bacteria. *Macromolecules* **2010,** *43* (12), 5211-5221.
30. Stoffelbach, F.; Tibiletti, L.; Rieger, J.; Charleux, B., Surfactant-free, controlled/living radical emulsion polymerization in batch conditions using a low molar mass, surface-active reversible addition-fragmentation chain-transfer (RAFT) agent. *Macromolecules* **2008,** *41* (21), 7850-7856.
31. Rieger, J.; Osterwinter, G.; Bui, C.; Stoffelbach, F.; Charleux, B., Surfactant-free controlled/living radical emulsion (co) polymerization of n-butyl acrylate and methyl methacrylate via RAFT using amphiphilic poly (ethylene oxide)-based trithiocarbonate chain transfer agents. *Macromolecules* **2009,** *42* (15), 5518-5525.
32. Yilmaz, G.; Becer, C. R., Precision glycopolymers and their interactions with lectins. *European Polymer Journal* **2013,** *49* (10), 3046-3051.
33. Nizet, V.; Varki, A.; Aebi, M., Microbial Lectins: Hemagglutinins, Adhesins, and Toxins. In *Essentials of Glycobiology* 3rd ed.; Varki A, C. R., Esko JD, et al. , Ed. Cold Spring Harbor Laboratory Press: Online, 2017.
34. Ghazarian, H.; Idoni, B.; Oppenheimer, S. B., A glycobiology review: carbohydrates, lectins and implications in cancer therapeutics. *Acta histochemica* **2011,** *113* (3), 236-247.

35. Ohtsubo, K.; Marth, J. D., Glycosylation in cellular mechanisms of health and disease. *Cell* **2006,** *126* (5), 855-867.
36. Publishing, R., *Protein-Carbohydrate Interactions in Infectious Diseases*. RSC Publishing: RSC Publishing, 2006; p 250.
37. Lundquist, J. J.; Toone, E. J., The cluster glycoside effect. *Chemical Reviews* **2002,** *102* (2), 555-578.
38. Godula, K.; Umbel, M. L.; Rabuka, D.; Botyanszki, Z.; Bertozzi, C. R.; Parthasarathy, R., Control of the molecular orientation of membrane-anchored biomimetic glycopolymers. *Journal of the American Chemical Society* **2009,** *131* (29), 10263-10268.
39. Huang, M. L.; Godula, K., Nanoscale materials for probing the biological functions of the glycocalyx. *Glycobiology* **2016,** *26* (8), 797-803.
40. Yilmaz, G.; Uzunova, V.; Napier, R. M.; Becer, C. R., Single-Chain Glycopolymer Folding via Host-Guest Interactions and Its Unprecedented Effect on DC-SIGN Binding. *Biomacromolecules* **2018**.
41. Penadés, S.; Davis, B. G.; Seeberger, P. H., Glycans in Nanotechnology. In *Essentials of Glycobiology*, 3rd ed.; Varki A, C. R., Esko JD, et al., Ed. Cold Spring Harbour Laboratory Press: Online, 2017.
42. Spain, S. G.; Albertin, L.; Cameron, N. R., Facile in situ preparation of biologically active multivalent glyconanoparticles. *Chemical Communications* **2006,** (40), 4198-4200.
43. Munoz-Bonilla, A.; Heuts, J. P.; Fernández-García, M., Glycoparticles and bioactive films prepared by emulsion polymerization using a well-defined block glycopolymer stabilizer. *Soft Matter* **2011,** *7* (6), 2493-2499.
44. Jesús, M.; Penadés, S., Glyconanoparticles: types, synthesis and applications in glycoscience, biomedicine and material science. *Biochimica et Biophysica Acta - General Subjects* **2006,** *1760* (4), 636-651.
45. Kavunja, H. W.; Voss, P. G.; Wang, J. L.; Huang, X., Identification of lectins from metastatic cancer cells through magnetic glyconanoparticles. *Israel Journal of Chemistry* **2015,** *55* (3-4), 423-436.
46. Bies, C.; Lehr, C.-M.; Woodley, J. F., Lectin-mediated drug targeting: history and applications. *Advanced Drug Delivery Reviews* **2004,** *56* (4), 425-435.
47. Bridges, J. F.; Woodley, J. F.; Duncan, R.; Kopeček, J. i., Soluble N-(2-hydroxypropyl) methacrylamide copolymers as a potential oral, controlled-release, drug delivery system. I. Bioadhesion to the rat intestine in vitro. *International Journal of Pharmaceutics* **1988,** *44* (1-3), 213-223.
48. Stahl, P. D., The mannose receptor and other macrophage lectins. *Current Opinion in Immunology* **1992,** *4* (1), 49-52.
49. McGreal, E. P.; Rosas, M.; Brown, G. D.; Zamze, S.; Wong, S. Y.; Gordon, S.; Martinez-Pomares, L.; Taylor, P. R., The carbohydrate-recognition domain of Dectin-2 is a C-type lectin with specificity for high mannose. *Glycobiology* **2006,** *16* (5), 422-430.
50. Ahsan, F.; Rivas, I. P.; Khan, M. A.; Suárez, A. I. T., Targeting to macrophages: role of physicochemical properties of particulate carriers—liposomes and microspheres—on the phagocytosis by macrophages. *Journal of Controlled Release* **2002,** *79* (1-3), 29-40.
51. Zhu, S.; Niu, M.; O'Mary, H.; Cui, Z., Targeting of tumor-associated macrophages made possible by PEG-sheddable, mannose-modified nanoparticles. *Molecular Pharmaceutics* **2013,** *10* (9), 3525-3530.
52. Lehotzky, R. E.; Partch, C. L.; Mukherjee, S.; Cash, H. L.; Goldman, W. E.; Gardner, K. H.; Hooper, L. V., Molecular basis for peptidoglycan recognition by a

bactericidal lectin. *Proceedings of the National Academy of Sciences* **2010,** *107* (17), 7722-7727.
53. Ponader, D.; Maffre, P.; Aretz, J.; Pussak, D.; Ninnemann, N. M.; Schmidt, S.; Seeberger, P. H.; Rademacher, C.; Nienhaus, G. U.; Hartmann, L., Carbohydrate-lectin recognition of sequence-defined heteromultivalent glycooligomers. *Journal of the American Chemical Society* **2014,** *136* (5), 2008-2016.
54. Sánchez-Pomales, G.; Morris, T. A.; Falabella, J. B.; Tarlov, M. J.; Zangmeister, R. A., A lectin-based gold nanoparticle assay for probing glycosylation of glycoproteins. *Biotechnology and Bioengineering* **2012,** *109* (9), 2240-2249.
55. Hartmann, M.; Lindhorst, T. K., The Bacterial Lectin FimH, a Target for Drug Discovery–Carbohydrate Inhibitors of Type 1 Fimbriae-Mediated Bacterial Adhesion. *European Journal of Organic Chemistry* **2011,** *2011* (20-21), 3583-3609.
56. Yilmaz, G.; Becer, C. R., Glyconanoparticles and their interactions with lectins. *Polymer Chemistry* **2015,** *6* (31), 5503-5514.
57. Kalb, A. J.; Levitzki, A., Metal-binding sites of concanavalin A and their role in the binding of α-methyl D-glucopyranoside. *Biochemical Journal* **1968,** *109* (4), 669-672.
58. Tomaszewska, E.; Soliwoda, K.; Kadziola, K.; Tkacz-Szczesna, B.; Celichowski, G.; Cichomski, M.; Szmaja, W.; Grobelny, J., Detection limits of DLS and UV-Vis spectroscopy in characterization of polydisperse nanoparticles colloids. *Journal of Nanomaterials* **2013,** *2013*, 60.
59. Keller, A. A.; Wang, H.; Zhou, D.; Lenihan, H. S.; Cherr, G.; Cardinale, B. J.; Miller, R.; Ji, Z., Stability and aggregation of metal oxide nanoparticles in natural aqueous matrices. *Environmental Science and Technology* **2010,** *44* (6), 1962-1967.
60. Li, Y.; Lubchenko, V.; Vekilov, P. G., The use of dynamic light scattering and Brownian microscopy to characterize protein aggregation. *Review of Scientific Instruments* **2011,** *82* (5), 053106.
61. Phenrat, T.; Saleh, N.; Sirk, K.; Tilton, R. D.; Lowry, G. V., Aggregation and sedimentation of aqueous nanoscale zerovalent iron dispersions. *Environmental Science and Technology* **2007,** *41* (1), 284-290.
62. Rubin, J.; San Miguel, A.; Bommarius, A. S.; Behrens, S. H., Correlating Aggregation Kinetics and Stationary Diffusion in Protein− Sodium Salt Systems Observed with Dynamic Light Scattering. *The Journal of Physical Chemistry B* **2010,** *114* (12), 4383-4387.
63. Trefalt, G.; Szilagyi, I.; Borkovec, M., Measuring particle aggregation rates by light scattering. 2013.
64. Wang, X.; Matei, E.; Gronenborn, A. M.; Ramström, O.; Yan, M., Direct measurement of glyconanoparticles and lectin interactions by isothermal titration calorimetry. *Analytical Chemistry* **2012,** *84* (10), 4248-4252.
65. Wang, X.; Ramström, O.; Yan, M., Dynamic light scattering as an efficient tool to study glyconanoparticle–lectin interactions. *Analyst* **2011,** *136* (20), 4174-4178.
66. Wang, X.; Ramström, O.; Yan, M., Quantitative analysis of multivalent ligand presentation on gold glyconanoparticles and the impact on lectin binding. *Analytical Chemistry* **2010,** *82* (21), 9082-9089.
67. Einstein, A., *Investigations on the Theory of the Brownian Movement*. Courier Corporation: 1956.
68. Cameron, N. R.; Spain, S. G.; Kingham, J. A.; Weck, S.; Albertin, L.; Barker, C. A.; Battaglia, G.; Smart, T.; Blanazs, A., Synthesis of well-defined glycopolymers and some studies of their aqueous solution behaviour. *Faraday Discussions* **2008,** *139*, 359-368.

69. Capon, B., Neighbouring group participation. *Quarterly Reviews, Chemical Society* **1964,** *18* (1), 45-111.
70. Siauw, M.; Hawkett, B. S.; Perrier, S., Short chain amphiphilic diblock co-oligomers via RAFT polymerization. *Journal of Polymer Science Part A: Polymer Chemistry* **2012,** *50* (1), 187-198.
71. Martin, L.; Gody, G.; Perrier, S., Preparation of complex multiblock copolymers via aqueous RAFT polymerization at room temperature. *Polymer Chemistry* **2015,** *6* (27), 4875-4886.
72. Gody, G.; Maschmeyer, T.; Zetterlund, P. B.; Perrier, S. b., Pushing the limit of the RAFT process: multiblock copolymers by one-pot rapid multiple chain extensions at full monomer conversion. *Macromolecules* **2014,** *47* (10), 3451-3460.
73. Poon, C. K.; Tang, O.; Chen, X.-M.; Pham, B. T.; Gody, G.; Pollock, C. A.; Hawkett, B. S.; Perrier, S., Preparation of Inert Polystyrene Latex Particles as MicroRNA Delivery Vectors by Surfactant-Free RAFT Emulsion Polymerization. *Biomacromolecules* **2016,** *17* (3), 965-973.
74. Amin, S.; Barnett, G. V.; Pathak, J. A.; Roberts, C. J.; Sarangapani, P. S., Protein aggregation, particle formation, characterization & rheology. *Current Opinion in Colloid and Interface Science* **2014,** *19* (5), 438-449.
75. Torquato, S.; Truskett, T. M.; Debenedetti, P. G., Is random close packing of spheres well defined? *Physical Review Letters* **2000,** *84* (10), 2064.

# *Chapter 3*

**Synthesis of Glyconanoparticles *via* a Free Radical and Surfactant Free Emulsion Polymerisation Technique, and Investigations into the Effect of Glass Transition Temperature on Lectin Induced Aggregation.**

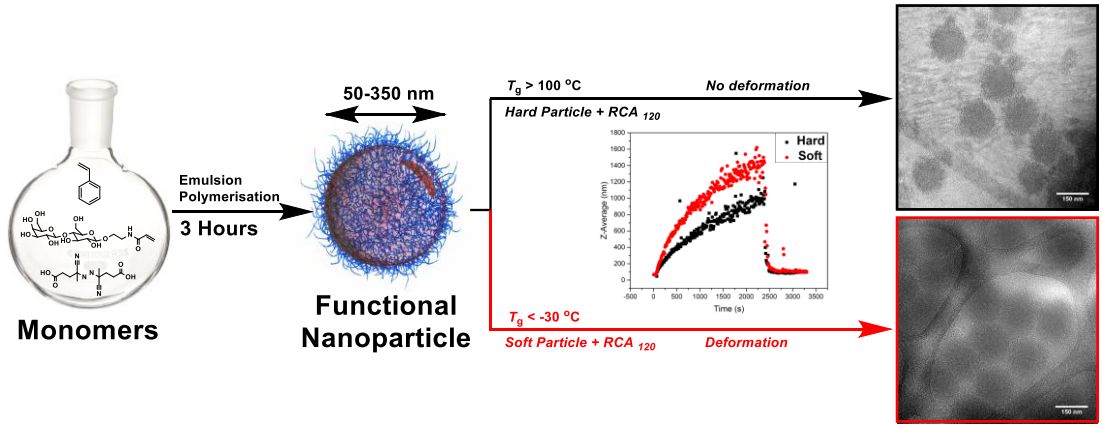

## 3.2 Abstract

Functional nanoparticles with diameters below 100 nm are desirable for biomedical applications and emulsion polymerisation represents an attractive pathway for their synthesis. To access sub-100 nm particles however, traditional emulsion polymerisation strategies rely on the addition of a surfactant that must subsequently be removed. Pseudo-surfactant free emulsion polymerisations, utilising controlled radical polymerisation techniques also provide access to: low diameters, controlled molecular weights and functionalised surfaces. These techniques however are often time consuming and expensive. This chapter will therefore investigate the synthesis of sub-100 nm glyconanoparticles *via* a one step, free radical and surfactant free emulsion polymerization. It is shown that by using sterically large, hydrophilic glycomonomers such as β-D-lactose-1-oxyethyl acrylamide with the charged azo initiator 4,4'-azobis(4-cyanovaleric acid), particles are stabilized sufficiently to reproducibly result in well defined (Pdi $\leq$ 0.1) glycoparticles with diameters below 100 nm. This technique is further used to synthesise a series of "soft" and "hard" glyconanoparticles to probe the effect of changing the particle core glass transition temperature ($T_g$) on lectin induced aggregation. It is shown that "soft" particles, above their $T_g$, form larger aggregates than "hard" equivalents below the core $T_g$. This effect is hypothesised to be due to the ability of the "soft" particles to deform on close packing and form more sugar-lectin interactions, evidence for which is provided using cryo-TEM microscopy.

## 3.3 Introduction

Emulsion polymerisation is an industrially favoured technique for polymer and particle synthesis, with existing infrastructure for manufacture on a multi-ton scale in industries as diverse as glove production to paints.[1] A standard emulsion polymerisation, using water as the solvent phase, is particularly favoured because of its high specific heat capacity, favourable kinetics and low viscosity.[2, 3] These factors make emulsion polymerisation a safe, cheap and easy to process way of producing both bulk polymers and more specialised particles and is explored fully in Chapter One.[2]

A classic emulsion polymerisation utilises a surfactant, which typically is charged, such as sodium dodecyl sulfate to form micelles. The micelles provide nucleation sites of insertion for growing "z-mer" polymer chains and stabilisation to the growing particles, keeping them in suspension.[4] This allows for the synthesis of polymer particles at a high weight percentage with small diameters, routinely below 100 nm. The presence of such a surfactant, though advantageous during the polymerisation, is detrimental for many uses such as in electronics or medicine, and may require extensive purification to be removed; which is typically achieved by extensive dialysis.[5-7] Avoiding the need for surfactant removal is one motivating factor behind the development of "pseudo-surfactant free" controlled radical polymerisation techniques, as outlined and utilised in Chapter Two.[8-13] As the original amphiphilic polymer is bound to the resulting particle, any functionality present is retained by the final product.[14, 15] "Pseudo surfactant free" techniques are also advantageous as they are able to access diameters down to tens of nanometres.[16-19] Such techniques, whilst promising, and incredibly useful for mechanistic studies as demonstrated in Chapter Two, suffer from having a relatively high associated material cost, and in the case of RAFT emulsion, result in particles with an embedded RAFT Z-group.[20, 21]

A technique to produce functional polymer particles without the use of a controlled polymer precursor or surfactant, would then be of interest to produce cheap particles without the need for extensive purification. Research conducted in the 1970's before the advent of controlled radical polymerisation techniques, investigated the use of a classical emulsion polymerisation without the addition of a surfactant to the system.[22-25] This created a self-nucleating "free radical surfactant free" emulsion polymerisation. In such a system one or many of the growing "z-mer" chains nucleate a growing

polymer particle by collapsing in on themselves out of solution, and are stabilised by the water soluble initiator head groups. This produces both polymer in solution, and suspended polymer particles with diameters typically in the hundreds of nanometers to micrometers.[26] It is desirable for applications such as drug delivery however to be able to produce particles with diameters below 100 nm.[7, 27-30] Particles below 100 nm in diameter may be achieved *via* a free radical surfactant free emulsion polymerisation, by using a strongly charged initiator such as potassium persulfate.[31-37] This technique has however not previously been explored for producing functional polymer particles such as glycopolymer particles, nor the influence of co-polymerising them with a hydrophilic monomer on the resulting particle size fully explored.[38]

The biological influence of a number of nanoparticle properties such as surface functionalisation, particle size, shape and charge have been widely studied as discussed in Chapter One.[39-50] The biological influence of the particle core properties however has been less well studied. In particular particle core rigidity, and the biological effects that may have. Some reports have focussed on endocytosis, producing conflicting results, with some studies suggesting that a more fluid particle increases cell uptake and others suggesting a rigid particle is superior.[51-54]

One potential source of the discrepancy seen in these studies, other than the different cell lines used, is the variability in the techniques used to vary particle rigidity. For example: colloidal hydrogels will have their rigidity modified with varying degrees of cross linking.[55-57] This has direct influences on the hydration of the gel and the surface hydrophobicity.

One alternative way of tuning polymer rigidity is by influencing the core polymer glass transition temperature ($T_g$), the temperature at which a polymer changes from glassy and hard to a soft, more liquid state.[58] This physical transition occurs due to changes in the mobility of polymer chains past one another. This approach has been used before by Lorenz *et al*.[59] In this work the $T_g$ of nanoparticles synthesised *via* mini-emulsion polymerisation was modified by changing the polymeric side chain from one carbon to 16 (poly(methyl methacrylate) to poly(stearyl methacrylate)). The results showed that a decrease in $T_g$ and rigidity corresponded to an increased endocytosis in a variety of cell lines. This work again however cannot control against the change in hydrophobicity caused.

The current reported work on the biological influence of particle core $T_g$ leaves various effects unexplored, such as the influence on particle-particle interaction and aggregation, induced by lectins. Neither have previous studies fully negated the effect of changing hydrophobicity. The use of a surface functionalised nanoparticle with varying core properties could potentially overcome some of these issues. By having the same shell chemistry, the differing hydrophobicities of the particle cores should be shielded from influencing results.

This chapter will therefore build on the RAFT emulsion polymerisation synthetic work in Chapter Two, and focus on the synthesis of glyconanoparticles *via* a free radical surfactant free emulsion polymerisation method. The use of a highly charged initiator head group has previously been shown to enable access to particle diameters below 100 nm. To develop this, initiators bearing a carboxylic acid will be investigated for their ability to stabilise the growing latex. Furthermore, the use of a hydrophilic co-monomer in the polymerisation will be investigated, initially to establish if the hydrophilic monomer will be incorporated onto the resulting particle surface, providing a way of simply producing functionalised glyconanoparticles; and the subsequent influence the hydrophilic monomer has on the final particle size. In addition to this, particles made using a free radical and surfactant free emulsion method will be used to investigate the influence of particle core glass transition temperature on lectin binding, using the DLS based aggregation tracking system developed in Chapter Two.

## 3.4 Results and Discussion

### 3.4.1 Free Radical Surfactant Free Emulsion Polymerisation

#### 3.4.1.1 Synthesis of β-D-Lactose-1-oxyethyl Acrylamide

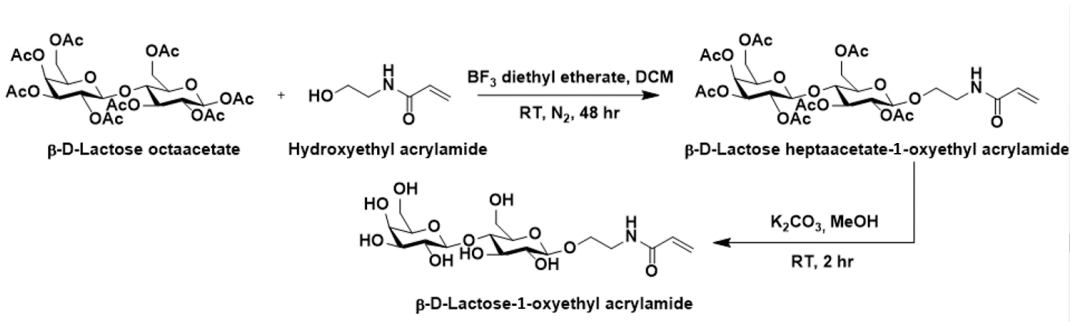


**Scheme 3.1:** Synthesis of β-D-lactose-1-oxyethyl acrylamide via a nucleophilic substitution between lactose octoacetate and hydroxyethyl acrylamide using boron trifluoride di-ethyl etherate as a leaving group. Monomer subsequently de-protected by removal of acetyl groups with potassium carbonate in methanol.

In order to determine the influence of a range of hydrophilic monomers on the free radical and surfactant free emulsion polymerisation method, a disaccharide glycomonomer was synthesised for comparison to the mono-saccharide glycomonomer, mannose acrylamide, described in Chapter Two. For this purpose, β-D-lactose-1-oxyethyl acrylamide was selected, as a readily available acetyl protected disaccharide suitable for modification to an acrylamide monomer *via* a coupling reaction with Hydroxy Ethyl Acrylamide (HEAm) (Scheme 3.1). As for the synthesis of mannose acrylamide, a modification of a method originally published by Cameron *et al.* was used.[60] Briefly: Octa-O-acetyl-β-D-lactose (lactose octaaetate) was subject to a nucleophilic substitution reaction with HEAm at the anomeric carbon of the glucose residue, using boron trifluoride diethyl etherate as a Lewis acid to act as an activating agent. The protected sugar monomer was subsequently de-protected by removal of the acetyl groups with potassium carbonate in methanol. The pure product, free of all acetyl protecting groups was found to precipitate out of the methanol solutions and was easily recovered by filtration, and was further purified by washing with methanol. The monomer structure and purity was confirmed by $^{1}$H NMR spectroscopy, mass spectroscopy and elemental analysis. (Section 3.5.1.1)

### 3.4.1.2 Particle Synthesis and Size Control Using a Free Radical and Surfactant Free Emulsion Polymerisation

It has previously been established in the literature that it is possible to make polymeric nanoparticles simply with the use of a charged initiator and a suitable hydrophobic monomer, such as styrene, in water.

| | Particle Composition | Hydrophilic (μmol) | Hydrophobic (μmol) | ζ Potential (mV) | Diameter - DLS (nm) | Pdi[a] | Diameter-SEM (nm)[b] |
|---|---|---|---|---|---|---|---|
| **A** | $P(LactAm)_1$-*co*-$(BA)_5$ | 228 | 1140 | -31.3 | 85 | 0.1 | - |
| **B** | $P(LactAm)_1$-*co*-$(BA)_{10}$ | 228 | 2280 | -38.1 | 198 | 0.058 | - |
| **C** | $P(LactAm)_1$-*co*-$(BA)_{20}$ | 228 | 4560 | -43 | 260 | 0.051 | - |
| **D** | $P(LactAm)_1$-*co*-$(BA)_{30}$ | 228 | 6840 | -37.3 | 256 | 0.06 | - |
| **E** | $P(LactAm)_1$-*co*-$(BA)_{50}$ | 228 | 11400 | -43.4 | 348 | 0.064 | - |
| **F** | $P(LactAm)_1$-*co*-$(sty)_5$ | 47.11 | 235.5 | -37.1 | 55 | 0.048 | 54 |
| **G** | $P(PEGA)_1$-*co*-$(sty)_5$ | 47.11 | 235.5 | -20.4 | 70 | 0.074 | 69 |
| **H** | $P(ManAm)_1$-*co*-$(sty)_5$ | 47.11 | 235.5 | -14.8 | 88 | 0.02 | 103 |
| **I** | $P(HEAm)_1$-*co*-$(sty)_5$ | 47.11 | 235.5 | -39.2 | 112 | 0.057 | 117 |
| **J** | P(sty) | N/A | 235.5 | -37.3 | 108 | 0.063 | 106 |

**Table 3.1:** Synthetic results for nanoparticles synthesised via a free radical surfactant free emulsion polymerisation, diameters by DLS reported are number distributions [a] Pdi values calculated using eq. 3.2, [b] diameter determined from an average of a minimum of 20 particles imaged by SEM

Less is known however about the influence of adding a hydrophilic co-monomer into the reaction, specifically: if the hydrophilic monomer will be incorporated onto the surface of resulting particles and the influence of the hydrophilic monomer on particle size. In order to understand this, surfactant free emulsion polymerisations were performed with various hydrophilic monomers. Initially a series of polymerisations were carried out using the same LactAm monomer concentration, whilst varying the concentration of hydrophobic butyl acrylate (BA) monomer, effectively changing the ratio of hydrophilic to hydrophobic monomer used. This was to establish whether or not the surfactant free technique would work and if reliable size control could be achieved. The general procedure was typically: LactAm monomer (228 μ mol) and initiator (3.13 μM) were dissolved in water (to a volume such that on addition of BA a total of 2 mL was achieved) in a 7 mL glass vial, charged with a magnetic follower and fitted with a rubber septum. The reaction vessel was purged of oxygen for ten minutes, after which the required volume of BA was injected through the septum using a gas tight syringe purged of oxygen. The reaction was then heated to 70 °C and stirred at 800 rpm for three hours. In all cases this resulted in the formation of monodisperse polymer latexes (Pdi ≤ 0.1).

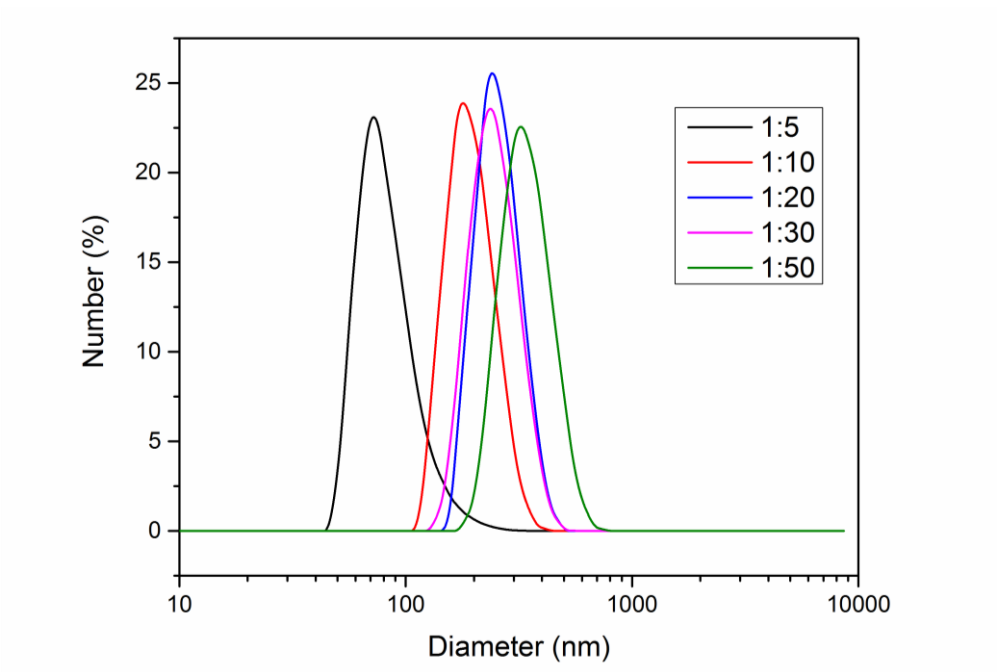


**Figure 3.1:** DLS traces by number for P(LactAm-*co*-*n*BA) particles at the different ratios indicated, used in determining a size calibration and establishing particle size control using a free radical and surfactant free synthetic technique. An expected increase in particle diameter can be observed as the concentration of BA increases, and thus the ratio of BA to LactAm, is also increased.

By varying the ratio of LactAm:BA from 1:5 to 1:50, particles with cores ranging in diameter from 85 - 348 nm were achieved (Table 3.1, A-E, Figures 3.1, 3.2). When the particle volume (derived from the radius by DLS), is plotted against the ratio of BA to LactAm (Figure 3.2), a linear relationship can be seen with a fitted $R^2$ value of 0.963. This confirms that by adjusting the ratio of hydrophilic to hydrophobic monomer in the emulsion a predictable change in diameter can be achieved. This result also confirms that the particles synthesised are reproducible.

All particles also exhibited a zeta potential of between -31 to -43 mV. Whilst this cannot be taken as a quantitative measure of the surface charge of the particle (rather at the slipping plane), this result did show that the surface of the particles was negatively charged from, and stabilised by, the de-protonated carboxylic acid group on the ACVA initiator, confirming it as a suitably charged initiator for use in a surfactant free emulsion polymerisation. All latexes were found to have a pH of *circa* 7 both before and after reaction. A representative sample, when broken up into constituent polymeric unimers by drying and mixing with DMF, along with linear polymer formed in solution, showed a dispersity by SEC of 1.56 ($M_w/M_n$) (Figure 3.2). This figure is consistent with those that would be expected from a free radical polymerisation of this sort in emulsion.[61, 62] Samples were also analysed by $^1$H NMR spectroscopy to ensure complete conversion of monomer to polymer. A mixed solvent of 4 parts *d*-DMSO to 1 part *d*-$CHCl_3$ was used to allow full solubility of all parts, polymerisations were found to go to >99% conversion confirming complete reaction (Section 3.5.1.2).

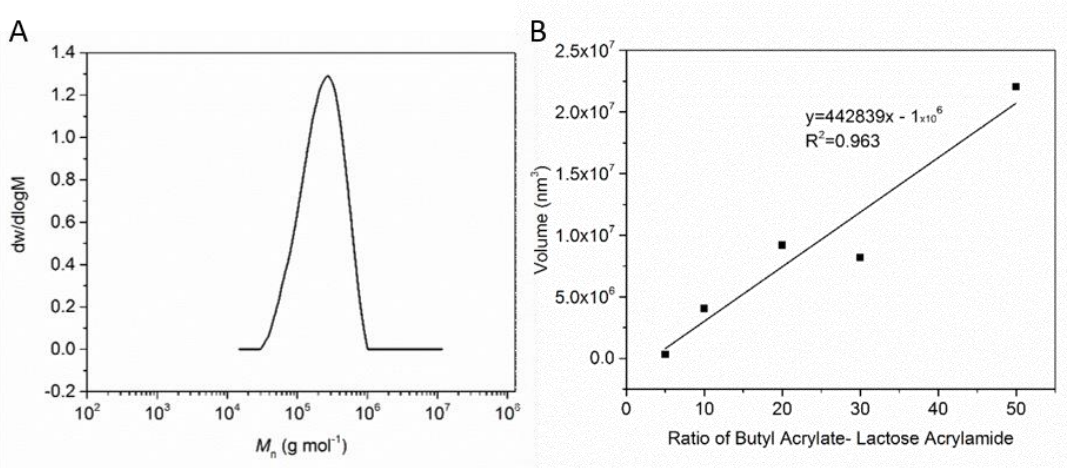


**Figure 3.2:** A) SEC Analysis performed using a DMF eluent , P(LactAm-*co*-*n*BA) latex particle "A" (Table 1) $M_n$= 175000 g mol$^{-1}$ $Đ$=1.56, B) Particle size calibration with varying molar ratios of hydrophobic butyl acrylate monomer to hydrophilic β-D-lactose-1-oxyethyl acrylamide monomer, plotted against the resulting particle volume.

#### 3.4.1.3 Incorporation of Hydrophilic Polymer onto Latex Particle

In order to use a free radical surfactant free emulsion polymerisation technique for producing surface functionalised particles, it was necessary to establish if the hydrophilic monomer would successfully be incorporated onto the resulting latex particles. As the focus of this study was to determine the influence of the hydrophilic monomer on the latex and ultimately to produce glycoparticles, a simple turbidimetric experiment was designed to confirm the particle incorporation of the hydrophilic monomer. A particle was synthesised using the previously described method with: mannose acrylamide (ManAm) as the hydrophilic part and styrene as the hydrophobic part in a ratio of 5:1 styrene to ManAm (Particle H, Table 3.1). This resulted in a particle with a diameter of 88 nm (DLS number distribution). Following a procedure described initially in Chapter Two, turbidimetric studies were then performed on the potentially mannosylated latex using Con A, a tetravalent lectin specific for glucose and mannose, as a cross linker to induce aggregation.[63] Initially the latex was purified of any P(ManAm) not bound to the particles by repeated cycles of particle sedimentation *via* centrifugation at 13,500 rpm for ten minutes. After each cycle the supernatant was removed and the particle pellet re-suspended with clean deionised water, thus removing any free polymer in solution. This purification technique was preferred to dialysis, as it has no upper molecular weight cut off unlike a dialysis membrane that does. This was in efforts to ensure that even the longest polymer not anchored to the particle was removed, which was important, as free radical polymerisation produces polymers of a very high molar mass. Turbidimetric aggregation studies were then performed on both the pure and impure latexes, the latex was diluted with tri(hydroxymethyl) aminomethane (TRIS) buffer (pH 7) in a cuvette and placed within a UV-Vis sprectrometer. The instrument was blanked and reading taken every second at 500 nm, and Con A in TRIS buffer was added (Figure 3.3). The results show that for both the pure and impure latex, aggregation with the Con A occurs, as an increase in turbidity is seen after Con A addition in both cases. The impure latex shows a slow and steady increase in absorbance, due to slow aggregation over 30 minutes. The purified latex however, shows a much faster increase in absorbance from increased aggregation, reaching its maximum in four minutes.

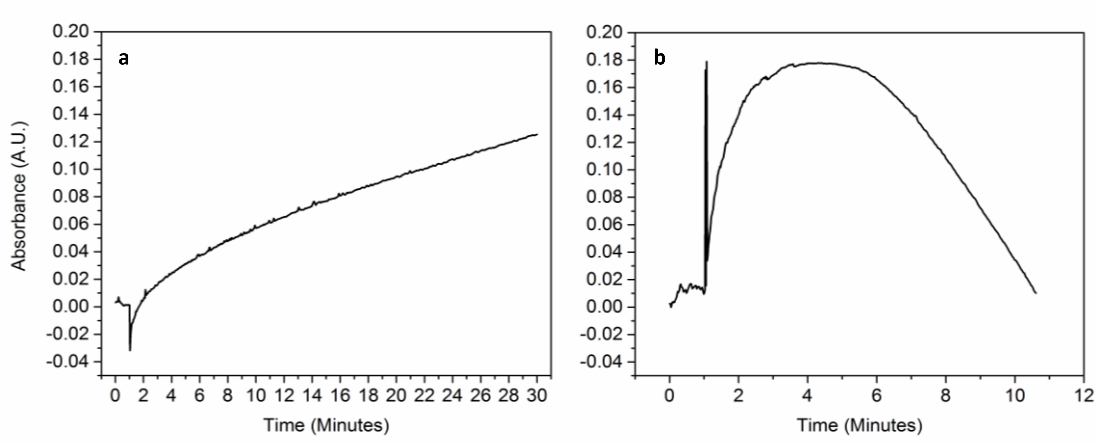


**Figure 3.3:** UV-Vis turbidimetric aggregation tests between mannose coated particles and Con A. a) raw latex with free P(ManAm) in solution, b) purified latex with free P(ManAm) removed from solution *via* centrifugation

After five minutes, the absorbance in the pure latex can also be seen to quickly reduce again, this is hypothesised to be due to the presence of large particulate aggregates sedimenting out of solution, dramatically reducing the suspended particle concentration. This result confirmed that the particles did have a mannose shell, and that the surfactant free emulsion technique successfully incorporated the hydrophilic monomer into the particle structure. It is hypothesised that the difference in aggregation profile between the pure and impure latexes is due to free P(ManAm) homopolymer, present in the impure latex, competing for binding sites on the Con A with the mannosylated particles. Free P(ManAm) is not present in the pure latex and therefore the mannosylated particles have no competition for binding, and can exhibit the faster response seen. A modified turbidimetric test was also performed with the addition of free mannose post aggregation in excess to compete for Con A binding sites and induce aggregate break up, confirming that aggregation was due to sugar-lectin binding (Figure 3.4).

It was not clear however from turbidimetry alone, the extent to which the hydrophilic monomer was incorporated into the particle structure. To quantify the amount of hydrophilic glycopolymer bound to the particles, a simple gravimetric study was performed. The mass of 1 mL of raw latex was compared to the mass of 1 mL of the purified latex, after drying both in solutions in a vacuum oven at 40 °C for 16 hours. The average mass difference after three repeats represented the mass of polymer and initiator in solution. As the mass of initiator was negligible compared to the polymer, the mass difference was used to differentially calculate the amount of polymer bound to the particles, and determined to be 41% incorporation.

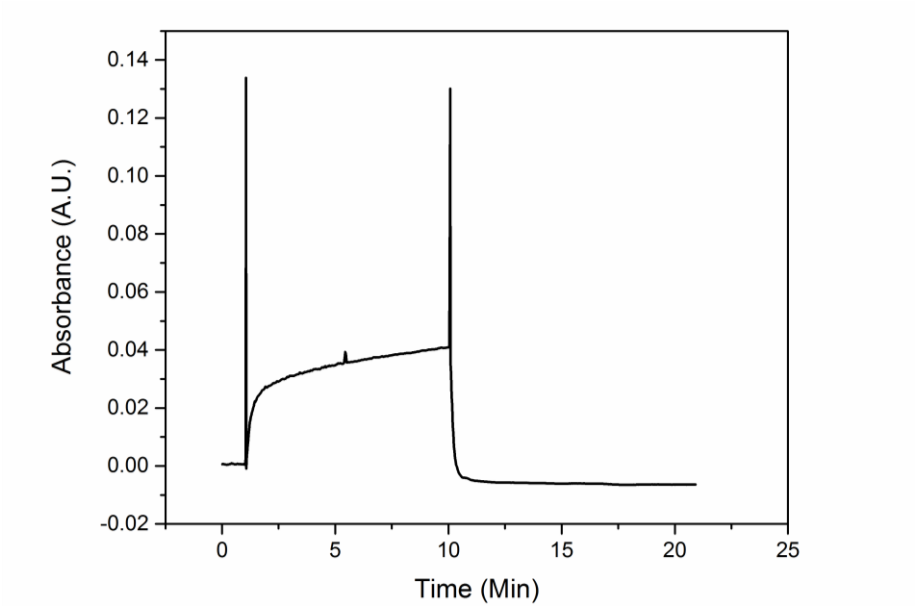


**Figure 3.4:** UV-Vis absorbance trace of P(ManAm)-*co*-P(BA) particles initially aggregated with Con A lectin, causing an increase in absorbance. Aggregation subsequently reversed with the addition of free β-D-lactose sugar, causing a corresponding reduction in absorbance

#### 3.4.1.4 Effect of Hydrophilic Monomer on Resulting Particle Size

Having established that the hydrophilic monomer used in the surfactant free emulsion system was successfully incorporated into the particle structure, the influence the hydrophilic monomer has on the resulting particle size was investigated. The accepted mechanism by which particles are formed in a surfactant free emulsion polymerisation is with the initial polymerisation of small amounts of hydrophobic monomer in the aqueous phase, reaching a critical length (*J-crit*) and then self-nucleating either as single or multiple chains, stabilised by the water soluble initiator head group. These particles then continue as in a standard emulsion polymerisation, growing by internal polymerisation and particle aggregation. It was hypothesised that in the initial phase of polymerisation hydrophilic homopolymer is predominantly formed (as it is fully soluble in the water phase with this initiator), followed by co-polymers of the hydrophilic and hydrophobic monomers. This would form an *in-situ* surfactant like polymer that, upon reaching the *J-crit* would nucleate into particles, driving an emulsion mechanism. The nucleated particles would be stabilised not only by the initiator head group, but also the hydrophilic component of the polymer. The ability of the hydrophilic monomer to stabilise a particle, would therefore have a large impact on the resulting particle size. A monomer with more steric bulk, charge or ability to hydrogen bond would theoretically be better stabiliser, producing a lower apparent number of aggregation and resulting in smaller particles. To test this hypothesis

surfactant free emulsion polymerisations were performed using a variety of hydrophilic vinyl monomers, whilst keeping all other conditions the same. Styrene was used as the hydrophobic part as it is one of the most studied monomers in free radical emulsion polymerisation, and, owing to the high glass transition temperature ($T_g$) of poly(styrene), will produce particles suitable for analysis by electron microscopy. For the hydrophilic part: LactAm, ManAm, hydroxyethyl acrylamide (HEAm) and poly(ethylene glycol) methyl ether acrylate (PEGA) were employed, in order to assess the effect of monomer size and hydrophilicity. The same synthesis was also repeated without the inclusion of any hydrophilic monomer, but with the negatively charged: 4,4′-azobis(4-cyanovaleric acid) (ACVA) initiator as the sole hydrophilic component. The polymerizations all resulted in monodisperse polymer latexes, bearing a negative zeta potential from the inclusion of ACVA as the initiator head group, with a typical polymer displaying an $M_n$ of 74632 g mol$^{-1}$ and a dispersity of 1.78 by DMF SEC (Figure 3.5). Varying the hydrophilic monomer led to a range of particles which size varied from largest to smallest in the order: HEAm ≥ ACVA > ManAm > PEGA > LactAm (Table 3.1 F-J; and Figure 3.6).

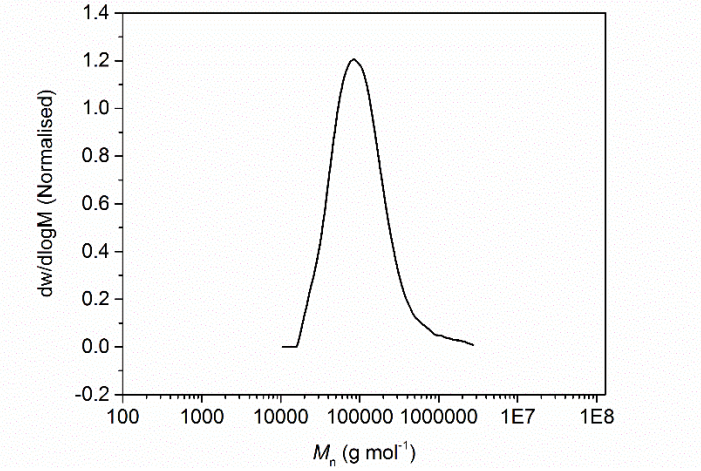


**Figure 3.5:** DMF SEC trace for particle "F" (Table 1), P(LactAm)$_1$-*co*-(sty)$_5$ $M_n$= 74600 g mol$^{-1}$ $Đ$= 1.78

This result primarily confirmed that the hydrophilic monomer used plays a large part in the stabilization of this emulsion system and can be used to influence the size of any resulting particle. This further adds evidence towards confirming the inclusion of the hydrophilic part in the resulting particle structure. The trend in diameter change between the monomers further supports the hypothesis that those monomers with a larger steric bulk stabilise the resulting particles more efficiently than a smaller monomer, producing the smallest particles. The number of hydroxyl groups on the hydrophilic monomer, and the ability to hydrogen bond with water can also be seen to

have an influence on particle size and stabilisation, shown when LactAm and PEGA particles are compared directly. Both monomers LactAm and PEGA monomers are of a similar molecular weight (439 and 480 g $mol^{-1}$ respectively), however LactAm has seven free hydroxyl groups and is able to form more hydrogen bonds with water than PEGA. Consequently LactAm is able to stabilise a growing particle more efficiently than with steric bulk alone, and produced particles 55 nm in diameter compared to PEGA, which produced particles 70 nm in diameter. A similar trend is also seen when comparing ManAm to HEAm, with ManAm producing a diameter of 88 nm and HEAm 112 nm. This direct comparison is less valid however due to the difference in molecular weight (277 and 115 g $mol^{-1}$ for ManAm and HEAm respectively).

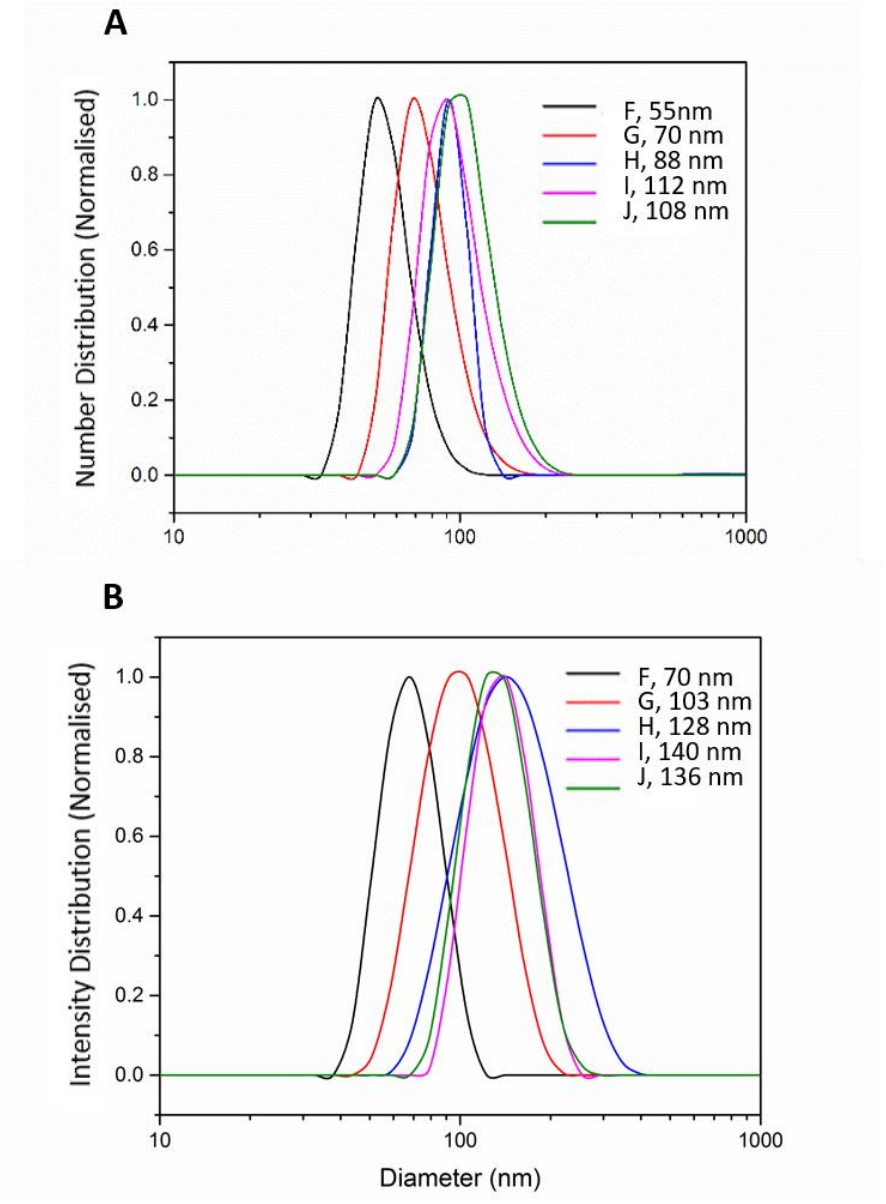


**Figure 3.6:** Particle diameter by DLS with varying hydrophilic monomer: Normalised DLS traces by number for particles F-J (Table 1) showing A) number average particle diameter (normalised) B) intensity average (normalised). Traces F-J represent: LactAm, PEGA, ManAm, HEAm, ACVA respectively

It is also noteworthy that the emulsion polymerisation using only the ACVA initiator as the hydrophilic component, produced well-defined particles of 108 nm in diameter. The stabilisation in this case is solely due to the charged carboxylic acid group of ACVA, having been deprotonated by sodium hydroxide used to ensure complete dissolution of ACVA in water. That such a small, well defined particle was achieved with only the head group shows the importance of charge, and the initiator choice, in stabilising the growing particles. In the case of HEAm particles, the ACVA potentially provided the majority of stabilisation, as both particles stabilised by HEAm and ACVA alone showed equivalent sizes and zeta potentials (c. 110 nm and -37 to -39 mV respectively). The diameters and morphology of the particles was also confirmed by scanning electron microscopy (SEM) and was broadly found to be in agreement with the number distribution determined by DLS (Figure 3.7, Table 3.1).

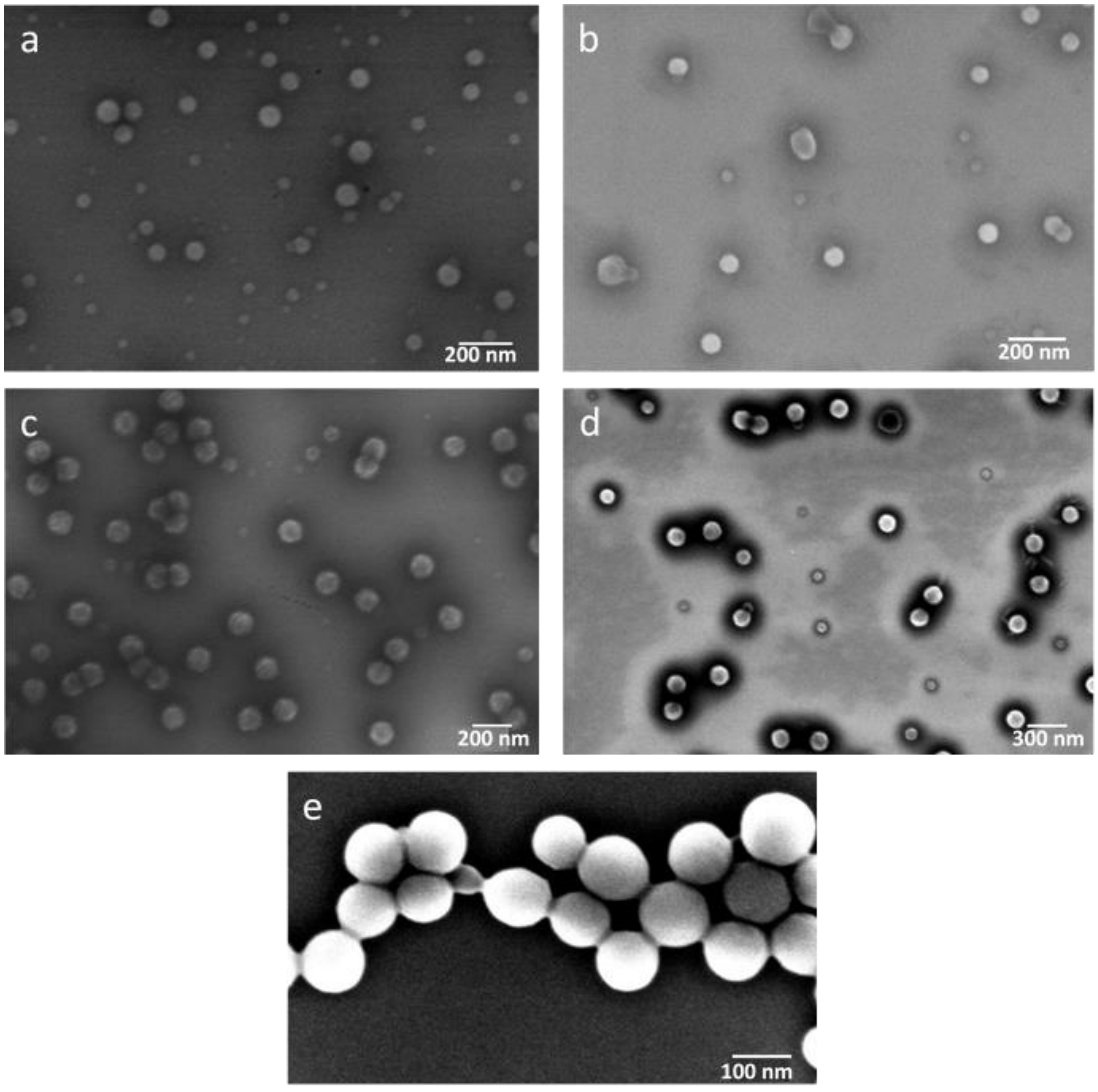


**Figure 3.7:** SEM images showing particle size and morphology. Pictures a, b, c, d and e correspond to styrene particles with shells of β-D-lactose-1-oxyethyl acrylamide, PEGA, mannose acrylamide, hydroxyethyl acrylamide and no hydrophilic monomer respectively. Average diameter for each can be found in Table 3.1

SEM analysis also showed evidence on the mechanism of particle growth in a free radical surfactant free emulsion polymerisation. In images a, b, c, and d of Figure 3.7, a smaller population of proto-particles can be seen in addition to the larger particle population, indicating the inclusion of multiple particles. These findings suggest that proto-particle aggregation is a significant means of growth, along with the accepted particle size increase through radical insertion and internal polymer growth. The smallest particles produced were those using LactAm as the hydrophilic monomer, resulting in a diameter of 55 nm (determined by DLS and confirmed by scanning electron microscopy (SEM), giving an average size of 54 nm). This suggested that the lactose monomer provides superior stabilization when compared to all other hydrophilic co-monomers tested. The improved stabilisation is hypothesised to be due to its seven hydroxyl groups, which increase the number of potential hydrogen bonds and thus its number of hydration and water solubility, as well as good steric stabilization from its bulky disaccharide structure. These results are remarkable as surfactant free polymerization does not typically provide access to particle diameters under 100 nm, due to insufficient stabilization causing particle aggregation. Indeed, most examples to date use the initiator potassium persulfate (KPS) to provide sufficient stabilization, e.g., in the emulsion polymerization of styrene and methyl methacrylate.[23, 32] This work however, has shown that styrene particles made with ACVA initiator and either lactose monomer, PEGA, or mannose acrylamide as a hydrophilic co-monomer provide access to particles of diameter 55, 70, and 88 nm, respectively. Being able to reliably produce particles under 100 nm in diameter without the use of a surfactant or initial polymer di-block shows the potential for using a charged initiator with sterically large or charged monomers, particularly glycomonomers, for their ability at stabilizing a latex and to produce functional nanoparticles.

#### 3.4.1.5 Maximum Weight Percentage

One major drawback to a surfactant free system, relying on *in situ* stabilisation is the low weight percentage of polymer that can be used, typically around 5%, if a particle diameter below 100 nm is desired. To further explore the limits of the surfactant free system described here, we experimentally determined the maximum particle concentration possible by repeating an emulsion polymerisation of LactAm and styrene at a ratio of 1:10 at varying weight percentages of: 10, 15, 20 and 30 wt% (Figure 3.8).

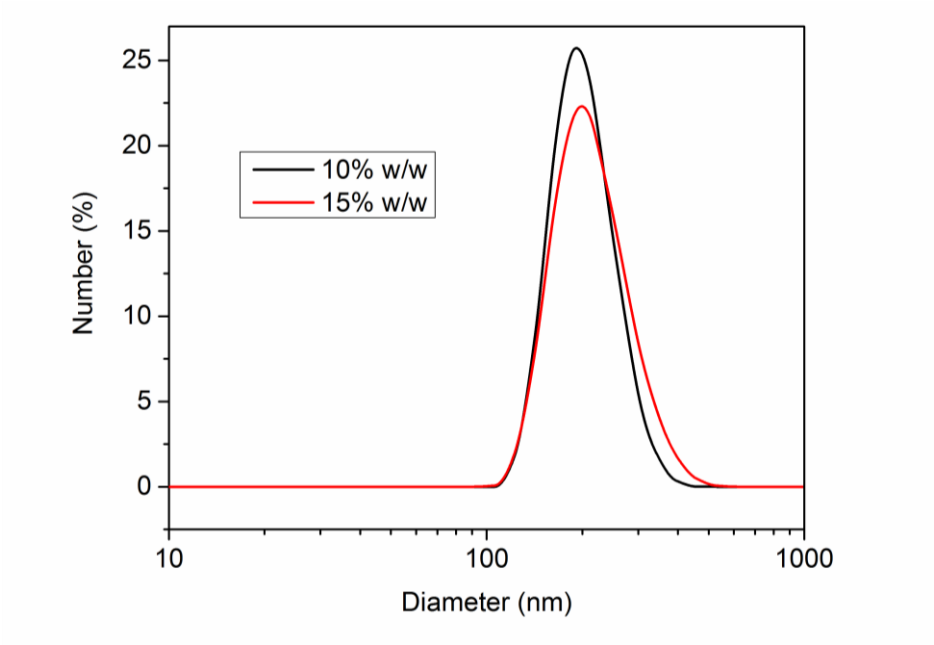


**Figure 3.8:** DLS traces by number of LactAm:Styrene 1:10 particles at both 10 and 15 wt%. 10% diameter = 230 nm Pdi = 0.062, 15% diameter = 210 nm, Pdi = 0.048

The maximum solids percent was determined to be <20 wt% of monomer, as well-defined particles were produced up to 15 wt%. At 20 wt% and above, defined particles were not obtained and aggregated to such an extent that a reliable size could not be obtained by DLS.

### 3.4.2 Effect of Particle Core $T_g$ on Lectin Binding

Having shown the potential for synthesising surface functionalised particles using a free radical surfactant free emulsion polymerisation, and for DLS to be used in real time qualitative analysis of particle-lectin aggregation, the two techniques were used together to determine the effect of particle core glass transition temperature ($T_g$) on lectin induced particle aggregation. When particles aggregate, they are brought into very close proximity to each other by multiple lectin-sugar interactions, the force of which individually may be small, but cumulatively may be enough to deform particles, if the constituent polymer is above its $T_g$ and able to flow. Conversely a particle in which the core forming polymer is below the $T_g$ and hard, particle deformation would be less likely to occur, requiring far larger forces. For this reason it is hypothesised that those particles below their $T_g$ will be able to deform, increasing their packing density above the maximum for a hard sphere (74%), and the area and number of particle-lectin interactions, resulting in larger aggregates, when compared to an equivalent particle below its $T_g$.

#### 3.4.2.1 Synthesis of "Soft" and "Hard" Particles with Varying Core Glass Transition Temperatures

To investigate the effect of particle core $T_g$ a series of lactose and mannose coated particles with equivalent butyl acrylate or styrene cores were synthesised, representing particles with a low and high $T_g$ (*ca* -30 °C and 100 °C respectively). Using the developed surfactant free emulsion polymerisation was of benefit here, as each particle could be made readily from the monomers alone, with no need for separate polymer di-block synthesis of each particle composition. As the DLS aggregation tracking technique is limited by the colloidal stability of the final particle aggregate, smaller particles that were able to be aggregated in a controlled way were required. For this reason LactAm coated particles were chosen to study using the DLS aggregation method, as LactAm produced the smallest particles using a surfactant free emulsion polymerisation. Lactose coated particles were also able to be aggregated using the bivalent lectin ricinus communis rgglutinin $(RCA)_{120}$, which is known to bind specifically to β-galactose terminal residues.[64] This is in preference to the tetravalent Con A, preferential towards mannose and glucose), as the interactions from a bivalent lectin were hypothesised to be fewer and thus produce a smaller aggregate. Conversely for analysis by cryo-Transmission Electron Microscopy (TEM) larger particles and aggregates are easier to analyse. For this purpose P(ManAm) coated particles were synthesised to be larger in diameter, and form larger aggregates with the tetravalent lectin Con A.

| | Particle Composition | Hydrophilic (μmol) | Hydrophobic (μmol) | $T_g$ (°C) | Diameter by DLS (nm) | PDi[a] |
|---|---|---|---|---|---|---|
| **A** | $P(LactAm)_1$-*co*-$(Sty)_5$ | 47 | 235 | 103 | 55 | 0.1 |
| **B** | $P(LactAm)_1$-*co*-$(BA)_{4.5}$ | 47 | 212 | -42 | 60 | 0.058 |
| **C** | $P(ManAm)_1$-*co*-$(Sty)_5$ | 55 | 275 | 103 | 145 | 0.1 |
| **D** | $P(ManAm)_1$-*co*-$(BA)_{2.8}$ | 55 | 154 | -42 | 150 | 0.09 |

**Table 3.2:** Synthetic results for nanoparticles synthesised *via* a free radical surfactant free emulsion polymerisation, for use in determining the effect of particle core $T_g$ on lectin induced aggregation [a] Pdi values calculated using Equation 3.2

Initially equivalent particles with a LactAm shell were synthesised, using the previously described surfactant free emulsion polymerisation method, with poly(butyl acrylate) (BA) and poly(styrene) (Sty) cores producing diameters of 60 and 55 nm respectively (Table 3.2). Differential scanning calorimetry (DSC) was performed on the particles, and revealed a core $T_g$ of -42 °C for P(BA) and 103 °C for P(Sty);

confirming that in the bulk phase at least, particles with P(BA) cores are above their $T_g$ and can be considered "soft" and fluid at room temperature, whereas P(Sty) particles are not and can be considered as "hard" spheres at room temperature. (Figure 3.9) Particles with a P(ManAm) shell and equivalent P(BA) and P(Sty) cores were then synthesised using the same synthetic method, producing particles with diameters of 150 and 145 nm, and core $T_g$'s of -42 and 102 °C respectively (Table 3.2, Figure 3.10). LactAm coated particles were then purified by dialysis against deionised water using a membrane with a 100 kD molecular weight cut off (efficient centrifugation was not possible due to the small particle size), and filtration through a 200 nm syringe filter. This was to remove free P(LactAm) in solution and any large particles. ManAm coated particles were purified by three cycles of centrifugation and particle re-suspension in clean de-ionised water to remove P(ManAm) homopolymer.

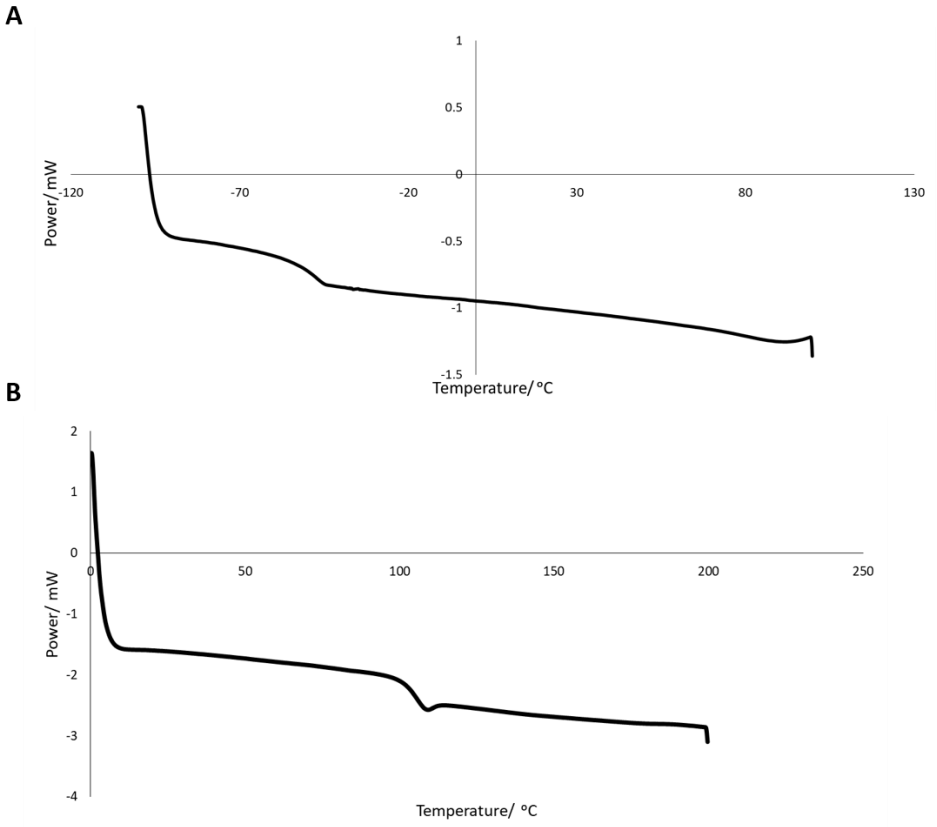


**Figure 3.9:** DSC traces for P(LactAm) coated particles with: A) poly(butyl acrylate) and B) poly(styrene) core, synthesised *via* a free radical surfactant free emulsion polymerisation showing glass transition temperatures of -42 and 103 °C for butyl acrylate and styrene respectively.

### 3.4.2.2 Particle-Lectin DLS Aggregation Determining Effect of Glass Transition Temperature

In order to determine the effect, if any, of changing the particle core $T_g$ on lectin induced aggregation, the P(BA) and P(Sty) particles had their lectin induced

aggregation analysed by the real time DLS technique outlined in Chapter Two. This was to reveal any difference in apparent number of particles per aggregate, with the hypothesis that P(BA) particles will form larger aggregates than equivalent P(Sty) particles, comprising more particles due to deformation allowing more simultaneous sugar-lectin interactions. Both the impure and purified P(LactAm) coated particles were analysed using the bivalent lectin $RCA_{120}$, following a modified protocol described in Chapter Two (Section 2.3.7). Briefly, each latex was diluted with TRIS buffer, and placed into a cuvette in the DLS instrument, having been fitted with a septum and cannula to a glass syringe. A series of consecutive ten second measurements were performed for an hour, and after 60 s, $RCA_{120}$ in TRIS buffer was injected to induce aggregation. After 40 minutes 75 mg $mL^{-1}$ β-D-lactose in TRIS buffer was injected to competitively inhibit aggregation and induce aggregate break up (Figure 3.11). Particle aggregation can be seen in all cases as an increase in Z-average diameter after the injection of $RCA_{120}$.

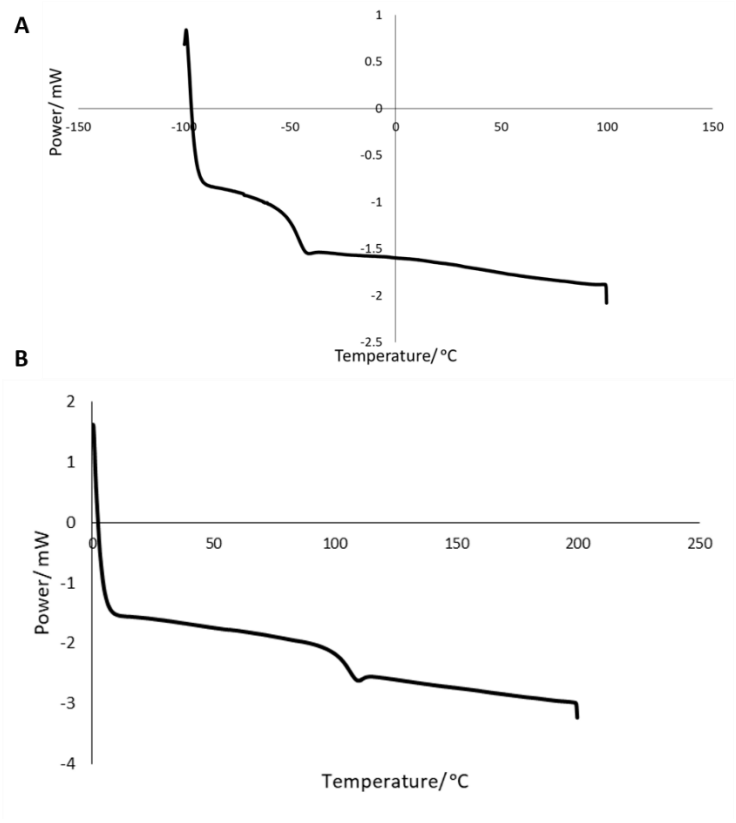


**Figure 3.10:** DSC traces of P(ManAm) coated particles with: A) P(BA) core showing a major $T_g$ of -42 °C, B) P(Sty) core showing a major $T_g$ of 102 °C

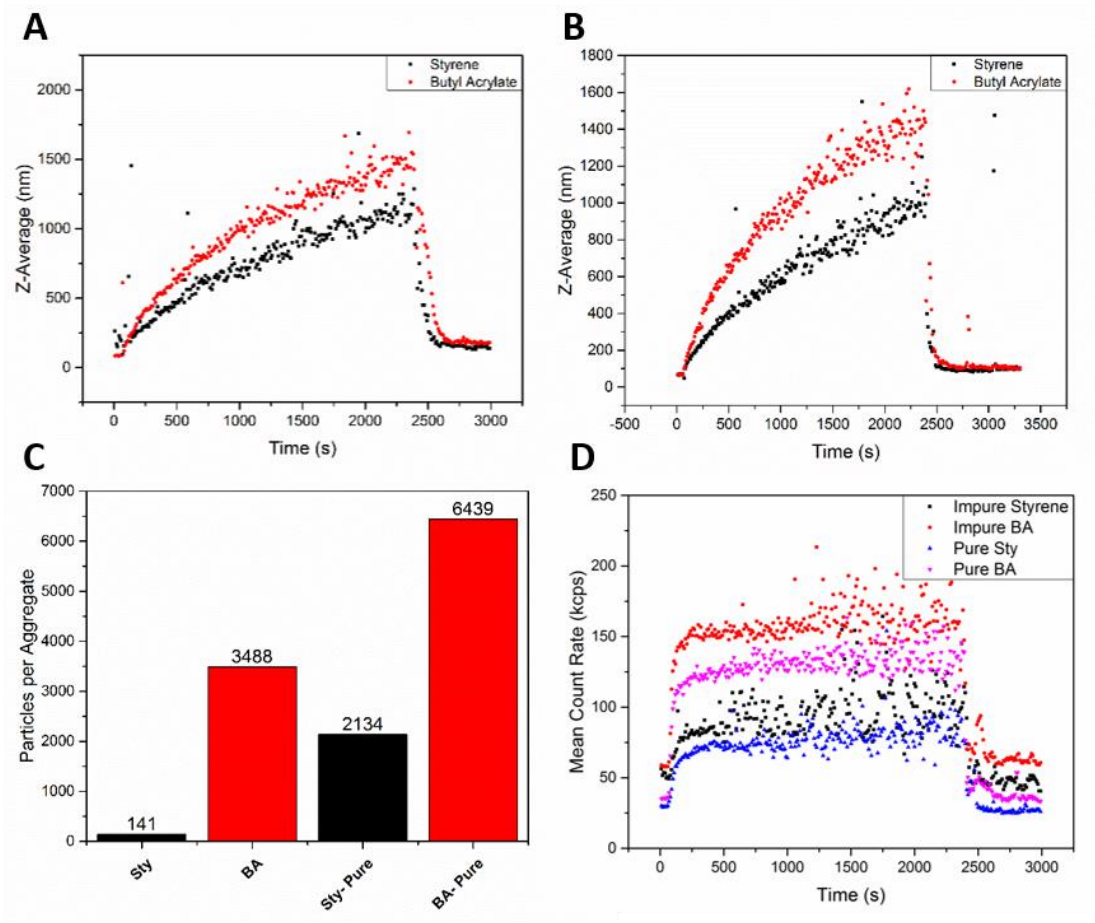


**Figure 3.11:** Results for lectin induced aggregation of lactose coated particles with the lectin $RCA_{120}$, showing differences between particles with a "hard" P(Sty) core in black and a "soft" P(BA) in red. Initial increase in diameter where lectin introduced, subsequent reduction in aggregate size induced by free β-D-lactose sugar. A) Aggregation of raw latexes followed in DLS showing larger aggregate size for P(BA) particles, B) experiment "A" repeated with a purified latex, removing free P(LactAm) from solution, thus increasing the aggregation response, C) number of particles per aggregate determined using Equation 1, D) Mean count rate for all experiments, showing a steady increase suggesting no major sedimentation of aggregates from solution.

Furthermore, this aggregation was confirmed as being due to reversible sugar-lectin interactions by the fast reversal of aggregation induced by the introduction of an excess of free β-D-lactose, seen as a return to the original Z-average diameter. The increase in aggregate diameter was reduced when using impure particle latexes with both P(BA) and P(Sty) aggregates showing a lower number of aggregation when impure. This reduced aggregation is due to competition for lectin binding sites from free P(LactAm) homopolymer in solution. In the pure particles, where free P(LactAm) has been removed by dialysis, a much larger number of particles per final aggregate can be seen. In both cases (pure and impure) latexes composing a "soft" core of P(BA) showed an increased aggregate size, in the case of the pure particles, P(BA) showing a number of aggregation of 6439, compared to P(Sty) showing 2134 particles per aggregate when determined using Equation 3.1, dividing the aggregate by the particle volume and multiplying by the ideal packing parameter of hard spheres, 0.7404.

$$ppa = \left({}^{Aggregate\ Vol.}/_{Particle\ Vol.}\right) \times 0.74$$

**Equation 3.1:** Used to determine number of particles per aggregate from DLS

As both P(Sty) and P(BA) possess the same P(LactAm) concentration (before purification) and similar particle diameter, this increase in aggregate size may be attributed to the difference in particle core $T_g$. Suggesting that a particle with a "soft" core is able to form larger particle aggregates than a "hard" equivalent, which is hypothesised to be due to the ability of its core to deform, packing above the hard sphere limit of 74% and creating more simultaneous sugar-lectin interactions. In order for the data revealed by aggregation in DLS to be reliable, it is important that the aggregates formed are colloidally stable in solution and do not sediment. In order to track this the mean count rate was also monitored over time (Figure 3.11). An increase in count rate can be seen upon introducing the lectin to the latex, due to increased light scattering from particle aggregates. The intensity does not decrease again until the injection of free β-D-lactose sugar, suggesting that the aggregates formed are not growing large enough to sediment out of solution, thus validating the results obtained in this part.

Having shown that the particles above their core $T_g$ have an increased lectin induced aggregation, a cryo-Transmission Electron Microscopy (TEM) experiment was designed to try and elucidate the mechanism by which increased aggregation occurred. Images were obtained by the University of Warwick Advanced Bioimaging Research Technology Platform. It was hypothesised that the increased aggregation was due to the ability of the "soft" particles being able to deform and pack closer together, forming more simultaneous sugar-lectin interactions. In order to be visualised by cryo-TEM it was necessary to perform the aggregation experiment at a far higher concentration.

Therefore the aggregation experiment was repeated at the same particle to lectin ratio, however with the concentrated latex solution. At this high concentration, particle aggregation was immediate, therefore 20 μL of the aggregated solution was immediately placed onto a lacey carbon TEM grid after mixing and flash frozen in liquid ethane before being imaged (Figure 3.12). The results from this test were inconclusive, with potential deformation being seen in the P(BA) particles, however this was not clear.

In order to try and improve the resolution of the microscopy, and the extent to which the particles may deform, a larger particle system with higher valence lectin was required.

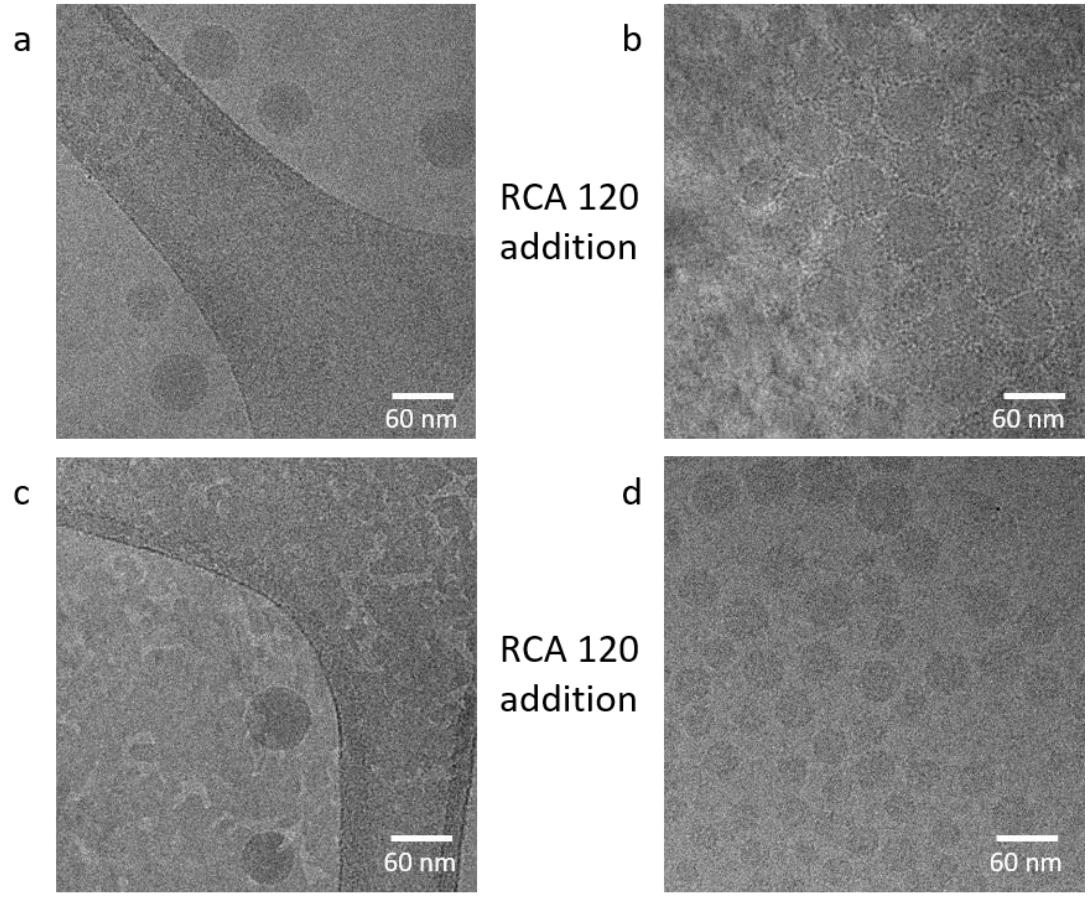


**Figure 3.12:** Cryo-TEM images of P(LactAm) coated particles with "soft" P(BA) and "hard" P(Sty) cores, a) P(BA) particles before aggregation, b) P(BA) after lectin induced aggregation with $RCA_{120}$, c) P(Sty) particles before aggregation, d) P(Sty) after lectin induced aggregation with $RCA_{120}$. All samples were flash frozen before imaging, in the case of aggregated samples, this was done immediately after lectin aggregation of concentrated latex

For this purpose P(ManAm) coated P(BA) and P(Sty) cored particles were used. Purified particles were initially analysed by DLS aggregation with the tetravalent lectin Con A, to confirm that they aggregated as expected before performing cryo-TEM. Both particles showed an expected increase in diameter after Con A injection, with the "soft" P(BA) particles showing a limited increase in aggregate size compared to the equivalent P(Sty) particles, showing 170 and 51 particles per aggregate respectively; this confirmed them as suitable for subsequent cryo-TEM experiments. The results from this DLS experiment alone were however not reliable for confirming that particles with a "soft" core aggregate more than "hard" equivalents, due to sedimentation of aggregates out of solution in both cases, shown in the reduced count rates over time after Con A addition (Figure 3.13).

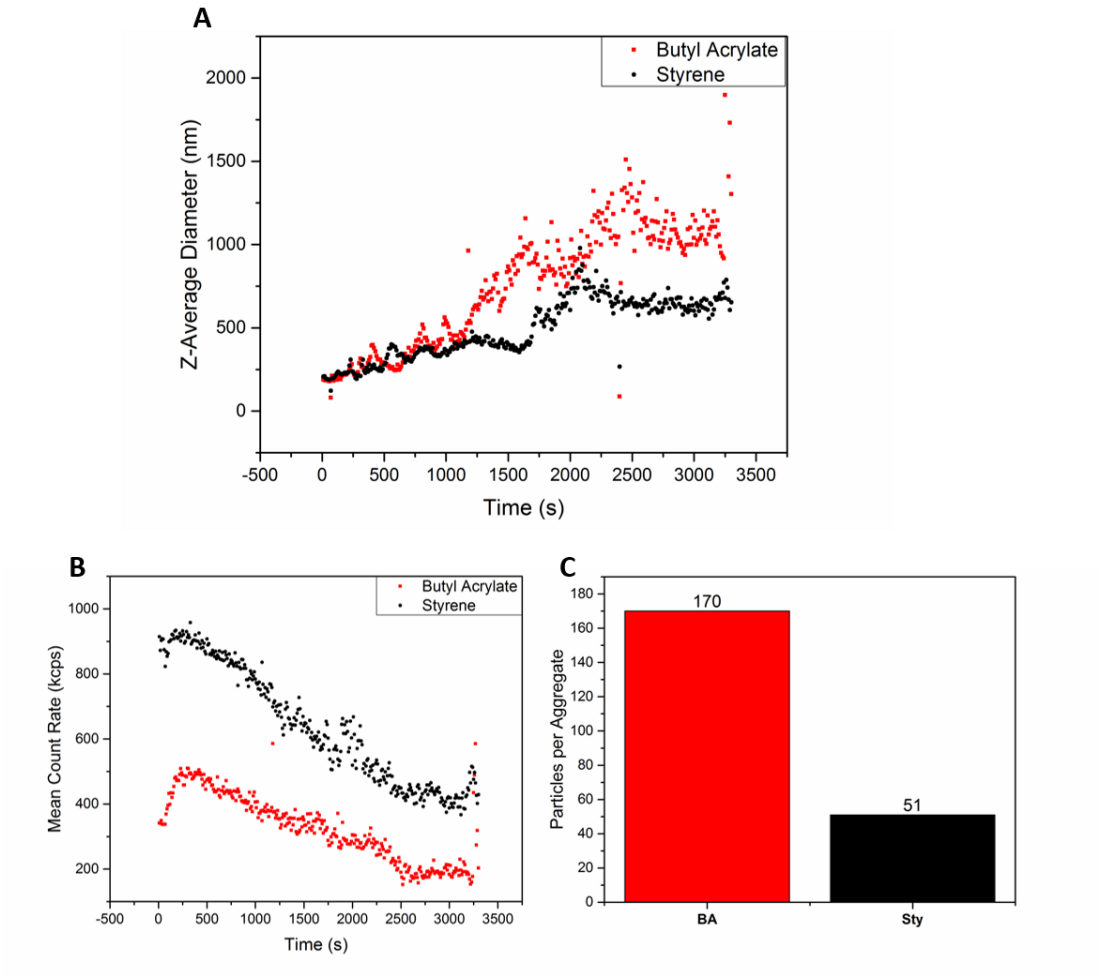


**Figure 3.13:** Results for lectin induced aggregation of mannose coated particles with the lectin Con A showing differences between particles with a "hard" P(Sty) core in black and a "soft" P(BA) in red, initial increase in diameter where lectin introduced. A) Aggregation of purified latexes followed in DLS showing larger aggregate size for P(BA) particles, B) mean count rate for all experiments, showing an initial increase and subsequent drop, suggesting sedimentation of aggregates from solution, C) number of particles per aggregate determined using Equation 3.1

This sedimentation was however expected, due to the large particle size and increased interaction with the tetravalent Con A. When the same experiment was performed on the concentrated latex and analysed using cryo-TEM a clear difference between the "soft" P(BA) and the "hard" P(Sty) particles was seen (Figure 3.14). P(BA) particles could be seen to show significant deformation only when aggregated, conversely no deformation could be seen at all with the P(Sty) particles either before or after aggregation. This result, taken together with the increase in apparent aggregate size when analysed by DLS, provides evidence for the hypothesis that particles with a "soft" core undergo increased lectin induced aggregation, where the polymer is above its $T_g$. The appearance of visual particle deformation after aggregation seen in P(BA) particles suggests that the reason for this may be the ability of the core forming "soft" polymer being able to flow. This enables the particles to deform and pack above the

theoretical limit for a hard sphere (74%), allowing more simultaneous sugar-lectin interactions and thus the formation of larger aggregates.

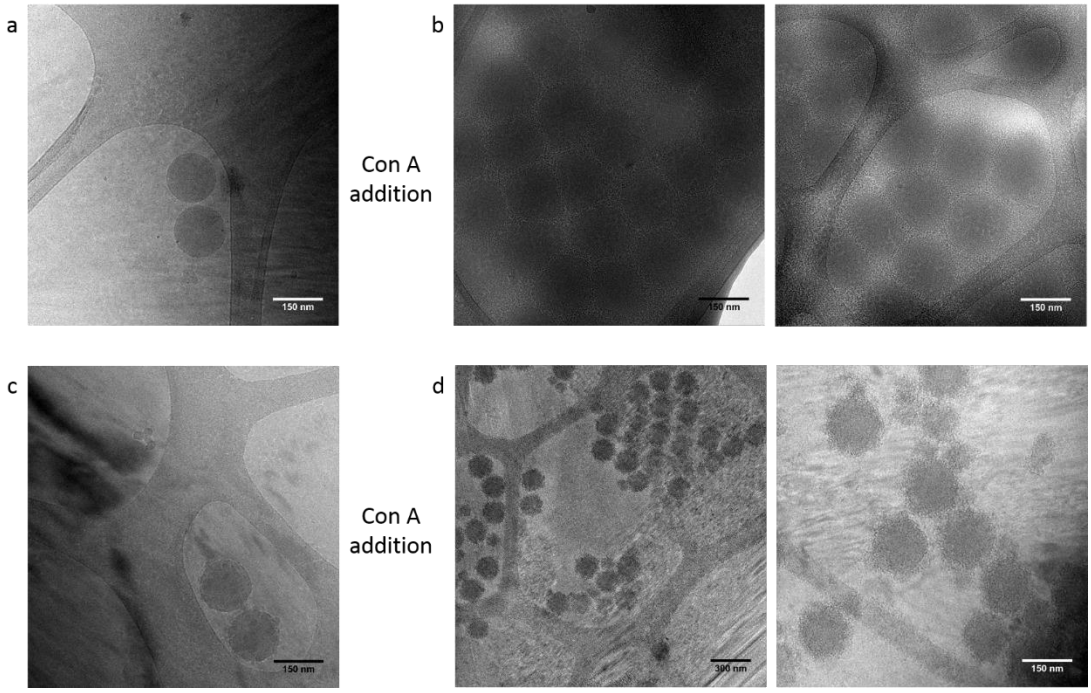


**Figure 3.14:** Cryo-TEM images of P(ManAm) coated particles with "soft" P(BA) and "hard" P(Sty) cores, a) P(BA) particles before aggregation, b) P(BA) after lectin induced aggregation with ConA showing deformation and close packing, c) P(Sty) particles before aggregation, d) P(Sty) after lectin induced aggregation with ConA showing no deformation and loose packing. All samples were flash frozen before imaging, in the case of aggregated samples, this was done immediately after lectin aggregation of concentrated latex

## 3.5 Conclusions

In this chapter it has been shown that a surfactant free emulsion polymerisation method can reliably produce nanoparticles between 50 and 350 nm in diameter in a one-step synthesis, with little or no purification necessary. The use of a hydrophilic co-monomer has been shown to influence the resulting particle size through improved particle stabilisation, and shown to be incorporated into the final particle structure. The initiator ACVA and glycomonomers, particularly disaccharide monomers with a large number of hydration such as β-D-lactose-1-oxyethyl acrylamide, have been shown to be extremely good at stabilizing emulsion polymerizations; and provide a useful tool for synthesizing low diameter, well-defined carbohydrate coated nanoparticles suitable for biological use. The versatility and reproducibility of this technique has also been shown by synthesising a range of P(LactAm) and P(ManAm) particles with "soft" and "hard" cores of P(BA) and P(Sty) respectively of equivalent diameter. Furthermore these particles were used to study the effect of particle core forming polymer $T_g$ on lectin induced aggregation using both DLS and cryo-TEM techniques. Particles with a "soft" core above the $T_g$, of P(BA) were shown to form larger aggregates than a

"hard" P(Sty) equivalent when aggregated using identical conditions, showing a larger number of particles per aggregate. Cryo-TEM experiments, visualising the particle-lectin aggregates and showing only P(BA) particles deforming from spherical after lectin induced aggregation were also performed. These provided evidence to support the hypothesis that the increase in aggregation shown by P(BA) particles over a P(Sty) equivalent was due to the ability of the P(BA) particle to deform above its $T_g$, packing closer than the theoretical maximum for a hard sphere (74%), and being able to form more simultaneous sugar-lectin interactions.

## 3.6 Experimental

### 3.6.1 Materials

Poly(ethylene glycol) methyl ether acrylate (PEGA, average $M_n$ = 480 g mol$^{-1}$), n-butyl acrylate (BA, >99%), bromo-propionic acid (>99%), 1-butanethiol (99%) and carbon disulphide (>99%), and *N*-hydroxyethyl acrylamide were obtained from Sigma-Aldrich and all monomers above were passed through basic aluminium oxide to remove inhibitor before use. 1,2,3,4,6-penta-O-acetyl-D-mannopyranose and β-D-lactose octaacetate was obtained from Carbosynth Ltd and used as received. concanavalin A and $RCA_{120}$ was bought from MP Biomedical SAS. All solvents were bought from commercial sources and were used as received. Dimethyl sulfoxide-$d_6$ (99.9% D atom), chloroform-$d_3$ (99.8% D atom) and deuterium oxide-$d_2$ (99.9% D atom), were obtained from Sigma Aldrich and used for $^1$H NMR spectroscopy. Thermal initiator 4,4′-azobis(4-cyanovaleric acid) (ACVA, >98%, Aldrich) was used as received. 0.45 μm syringe filters were obtained from Alpha Laboratories Ltd. Super smooth silicon wafers and lacey carbon (on copper) TEM grids were purchased from Agar Scientific and used as received.

### 3.6.2 Analysis

#### 3.6.2.1 NMR Spectroscopy

$^1$H NMR spectra were recorded on a Bruker DPX-300 spectrometer using a mixed deuterated solvent of 4 parts *d*-DMSO to 1 part *d*-$CHCl_3$. Each sample was run with a decay time of 2 s with 16 repeats.

#### 3.6.2.2 Mass Spectrometry

Mass spectrometry measurements were performed on an Agilent 6130B Single Quad for ESI, with a methanol solvent.

#### 3.6.2.3 Elemental Analysis

Samples were sent to Warwick Analytical Services (WAS) for analysis, all values are reported as received from WAS.

#### 3.6.2.4 Scanning Electron Microscopy (SEM)

Polymer latex particles were first synthesised as described above. Raw latex was diluted by a factor of 500 with filtered de-ionised water, 5 μL was spotted onto a super

smooth silicon wafer and left to dry overnight in a laminar flow cabinet to ensure no sample contamination. Acheson silver DAG 1415M was painted onto the corners of each silicon wafer to as electrostatic screening. Samples were visualised using a Zeiss Gemini SEM- field emission scanning electron microscope. Particle diameter was determined using images obtained from SEM using Image J software with the FIJI macro. A minimum of 20 particles for each sample were manually measured and a mean average taken of the resulting diameters.

#### 3.6.2.5 Cryo-Transmission Electron Microscopy (TEM)

Cryo-TEM samples were analysed by the Warwick Advanced Bioimaging Research Technology Platform (RTP). Samples were prepared by mixing the required amount of lectin-buffer solution with concentrated particle latex. 20 μL of the particle-lectin solution was immediately placed onto a lacey carbon TEM grid (on mesh copper) using an autopipette, and flash frozen by submerging in liquid ethanol. Images were then acquired by Warwick RTP using a Jeol 2200FS and processed using ImageJ software. The University of Warwick Advanced Bioimaging Research Technology Platform supported by BBSRC ALERT14 award BB/M01228X/1 are acknowledged for help with obtaining these images.

#### 3.6.2.6 Differential Scanning Calorimetry

Glass transition temperatures were determined by differential scanning colorimetry using a Mettler-Toledo DSC1 with autosampler under nitrogen at a heating rate of two degrees per minute in capped 40 μL aluminium crucibles, with pierced lids.

#### 3.6.2.7 Size Exclusion Chromatography

Chromatograms were recorded using an agilent 390-LC MDS instrument equipped with differential refractive index (DRI), viscometry (VS), dual angle light scatter (LS) and UV detectors. The system was equipped with 2 x PLgel Mixed D columns (300 x 7.5 mm) and a PLgel 5 μm guard column. The eluent is DMF with 5 mmol $NH_4BF_4$ additive. Samples were run at 1ml $min^{-1}$ at 50'C. Poly(methyl methacrylate) standards (Agilent EasyVials) were used for calibration between 955,000 – 550 $gmol^{-1}$. Experimental molar mass ($M_{n,SEC}$) and dispersity ($Đ$) values of synthesized polymers were determined by conventional calibration and universal calibration using Agilent GPC/SEC software.

#### 3.6.2.8 Dynamic light scattering, size and ζ-potential

Size and ζ-potential measurements were carried out using a Malvern Zetasizer Nano-ZS at 25°C with a 4 mW He-Ne 633 nm laser at a scattering angle of 173° (back scattering). Pdi values were calculated using Equation 3.2.

$$Pdi = \frac{\sigma^2}{d^2}$$

**Equation 3.2:** Equation to calculate Pdi from standard deviation (σ), and diameter (d).

### 3.6.3 Synthetic Procedures

#### 3.6.3.1 Synthesis of β-D-Lactose-1-oxyethyl Acrylamide

β-D-lactose-1-oxyethyl acrylamide monomer was synthesised following modification of the same procedure used to synthesise α-D-mannose-1-oxyethyl acrylamide in Chapter Two (Section 2.3.1). However, column chromatography was not utilised for the final purification of the monomer. Removal of the acetyl protecting groups was performed by evaporating DCM from the crude protected monomer and dissolving in 250 mL of 0.3 M potassium carbonate in dry methanol in a 500 mL round bottom flask, which was charged with a 2.5 cm magnetic stirrer and sealed with a size 49 septum. The flask was then purged of oxygen by bubbling nitrogen through it for 20 minutes. This was then stirred at 400 rpm for 2 hours. The fully de-protected β-D-lactose-1-oxyethyl acrylamide precipitated out of solution and was isolated by Buchner filtration, removing the excess solvent through a 2 μM filter. The resulting crude product was then washed with an excess of dry methanol under vacuum pumping. The structure of the monomer was confirmed by $^{1}$H NMR spectroscopy, Mass Spectroscopy and elemental analysis. (Table 3.3, Figure 3.15)

| Element | Theoretical % | Analysed % |
|---|---|---|
| C | 0.464692483 | 0.46 |
| H | 0.066059226 | 0.0659 |
| O | 0.031890661 | 0.031 |

**Table 3.3:** Elemental analysis for β-D-lactose-1-oxyethyl acrylamide monomer, showing theoretical and observed (analysed) percentage.

MS *m/z* $[M+Na]^+$: 462 (MSth:462.16), $[M+K]^+$:478 (MSth:478.13)

$^1$H NMR spectroscopy (400 MHz, $D_2O$) δ 6.29 – 5.99 (m, 2H), 5.69 (d, *J* = 9.9 Hz, 1H), 4.45 – 4.34 (m, 2H), 4.02 – 3.35 (m, 23H), 3.31 – 3.20 (m, 1H).

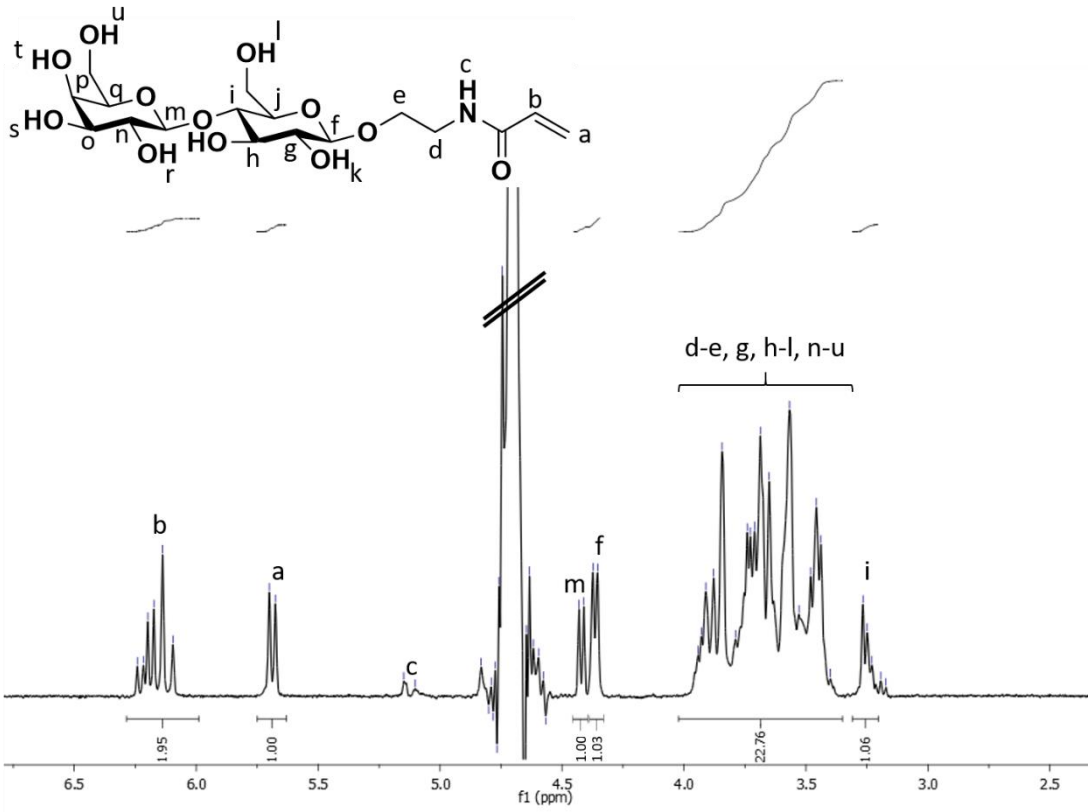


**Figure 3.15:** $^1$H NMR spectrum for β-D-lactose-1-oxyethyl acrylamide monomer

### 3.6.3.2 General Method for Free Radical Surfactant Free Emulsion Polymerisation

Nanoparticles of various sizes (diameters between 50-500 nm) were synthesised by varying the ratio of hydrophilic to hydrophobic monomer in the reaction mixture. The general method by which nanoparticles were prepared is represented by the following: 14.3 mg NaOH ($3.6 \times 10^{-4}$ mol) was added to 10 mL of deionised water, into which 50 mg of ACVA ($1.8 \times 10^{-4}$ mol) was dissolved, the 2 eq. of NaOH is to ensure full solubility of ACVA in water. 10 mg of β-D-lactose acrylamide powder ($2.276 \times 10^{-4}$ M) was weighed into a tared 7.5 mL glass vial, 1.6327 mL of deionised water was then added into the glass vial using an auto-pipette, to which 0.351 mL of the previously described stock solution of ACVA was added. The glass vial was then charged with a 1 cm magnetic stirrer bar, sealed with a size 21 septum and purged of oxygen by bubbling nitrogen through the solution for 10 minutes. In a separate 20 mL glass vial, sealed with a size 33 septum, *n*-butyl acrylate was purged of oxygen by bubbling nitrogen through the liquid monomer for 10 minutes. After both solutions had been

purged, 0.01459 mg of BA ($1.139x10^{-3}$ moles, 0.0163 mL)) was transferred into the 7.5 mL glass vial using a gas tight Hamilton syringe that has been purged of oxygen. The 7.5 mL vial was placed into an oil bath set to 70 °C and stirred at a rate of 800 rpm for three hours. After approximately 5-10 minutes the reaction mixture turned a uniform white milky colour as the particles nucleated and the polymerisation proceeded. At the end of three hours the reaction was quenched by removing the vial from the oil bath and exposing it to oxygen by removing the septum. The latex was analysed by $^{1}$H NMR spectroscopy to confirm complete conversion of monomer to polymer (>99%) (Figure 3.16), SEC to determine polymer molecular weight and dispersity ($M_n$ = 174608 g mol$^{-1}$, $Đ$= 1.56, Figure 3.17), and DLS to determine particle diameter (Figure 3.18)

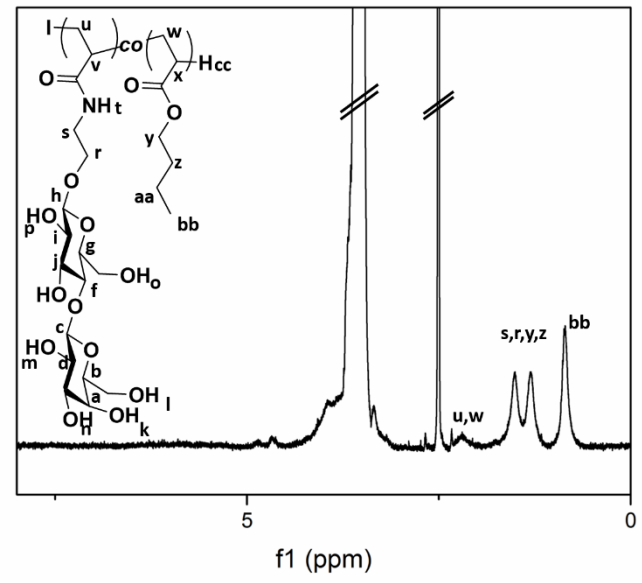


**Figure 3.16:** $^{1}$H NMR spectrum for particle "A" (Table 3.1), P(LactAm)$_1$-*co*-(BA)$_5$ showing no residual monomer

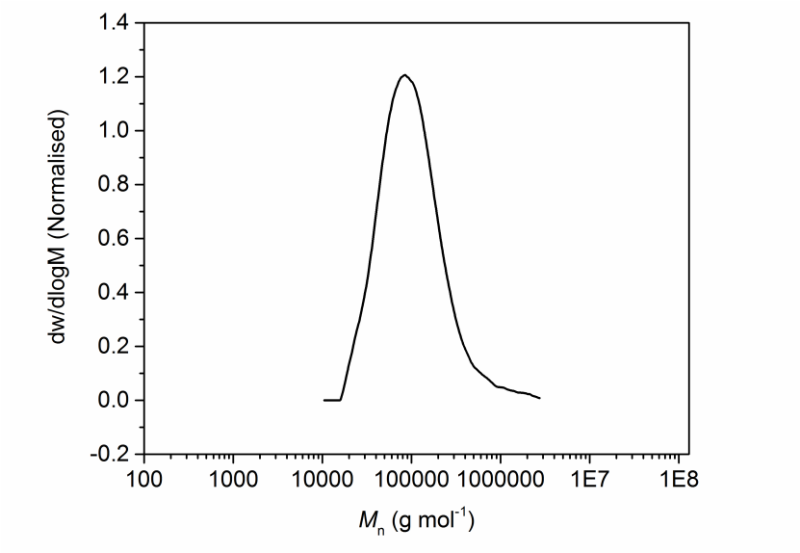


**Figure 3.17:** DMF SEC trace for particle "A" (Table 3.1), P(LactAm)$_1$-*co*-(BA)$_5$ $M_n$= 174600 g mol$^{-1}$, $Đ$= 1.56

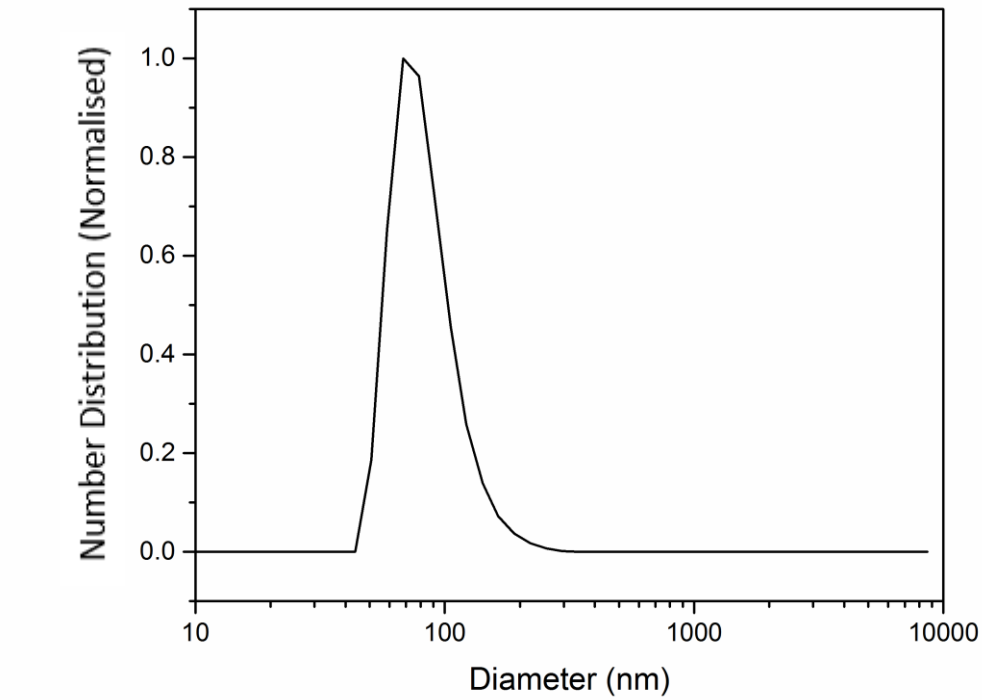


**Figure 3.18:** DLS number distribution for particle "A" (Table 1), P(LactAm)$_1$-*co*-(BA)$_5$ Diameter = 85 nm Pdi= 0.1

### 3.6.3.3 General Method for UV-Vis Aggregation Studies

Turbidimetric studies were conducted by diluting 12.5 µL of undiluted particle solution with 1.25mL of 10 mM TRIS buffer in a 4.5 mL polystyrene cuvette, and placed in the UV-Vis spectrometer. In a separate 4.5 mL polystyrene cuvette, a stock solution of 2.027x10$^{-5}$ M Con A in 10 mM TRIS buffer was prepared for use with

P(ManAm), P(LactAm) and P(GalAm) particles. Absorbance readings were taken every second at 500 nm, with 185.5 μL of Con A stock solution being added after 60 seconds at which point 250 μL of Con A in TRIS buffer ($2.027x10^{-5}$ M) was added with an Eppendorf pipette, and mixed twice to induce aggregation. In the case of de-aggregation experiments the same protocol was followed with the following modifications: the initial 12.5 μL particle solution was diluted with 2.5 mL of 10 mM TRIS buffer (rather than 1.25 mL) and a further 9 minutes after Con A solution addition, 250 μL of mannose in phosphate buffer (150 mg $mL^{-1}$) was added with an Eppendorf pipette and mixed twice to induce competitive binding with the glycosylated nanoparticles. The absorbance was monitored for a further 10 minutes. Readings were taken using an Agilent Cary 60 UV-Vis machine with Agilent software and analysed using Origin.

#### 3.6.3.4 General Method for DLS Aggregation Studies

DLS measurements were taken using a Malvern instruments Zetasizer Nano at 25°C with a 4 mW He-Ne 633 nm laser at a scattering angle of 173° (back scattering). For P(LactAm) particle DLS aggregation studies, 10 μL of particle solution was diluted with 1.24 mL of 0.1 mM TRIS buffer in a 4.5 mL polystyrene cuvette. The cuvette was fitted with a size 23 septum, which was pierced with a cannula attached to a 250 μL Hamilton glass syringe. The cannula was positioned such that, solution ejected through it would run down the side of the cuvette. This prevented the creation of any air bubbles that may have interfered with measurements. The cuvette was placed into the Zetasizer, and the lid closed with the syringe exiting through a slit at the side of the instrument. In a separate 4.5 mL polystyrene cuvette a stock solution of 15 μg $mL^{-1}$ $RCA_{120}$ in 0.1 mM TRIS buffer was prepared. The Zetasizer was set to take a size reading every 10 seconds for 1 hour, however a delay of 1.66 seconds was recorded between each reading, adding 598 seconds to each hour, for which the results have been amended. After the sixth reading, 250 μL of 15 μg $mL^{-1}$ $RCA_{120}$ stock solution was injected via the cannula giving a final volume of 1.5 mL. The final concentration of $RCA_{120}$ and side chain sugar residue was 3 μg $mL^{-1}$ and $1.14x10^{-4}$M respectively. The same technique was then repeated with the addition of 250 μL of 75 mg $mL^{-1}$ β-D-lactose in TRIS buffer being injected *via* the syringe cannula after 40 minutes (to allow full aggregation). This was performed as a competitive binding assay, to show reversible lectin binding. The same technique was repeated for P(ManAm) particles

using 5 μL of particle latex with a stock solution of $2.027x10^{-5}$ M ConA in 0.1 mM TRIS buffer. This gave a final concentration of Con A and side chain residue of $3.125x10^{-5}$M and $1.37x10^{-4}$M respectively.

An estimation of aggregate volume was made by using the average final aggregate radius obtained by DLS in the formula for the volume of a sphere. Further, by dividing this by the initial volume of particles forming the aggregate multiplied by 0.74 (the ideal packing parameter of spheres) an estimation of aggregation number as particles per aggregate (ppa) was be made, summarised in Equation 3.1.

## 3.7 References


1. Anderson, C. D.; Daniels, E. S., *Emulsion polymerisation and latex applications*. Smithers Rapra Publishing: 2003; Vol. 14.
2. Fitch, R. M., *Polymer colloids*. Academic Press: 1997.
3. Chern, C., Emulsion polymerization mechanisms and kinetics. *Progress in Polymer Science* **2006,** *31* (5), 443-486.
4. Chern, C.; Lin, S.; Chang, S.; Lin, J.; Lin, Y., Effect of initiator on styrene emulsion polymerisation stabilised by mixed SDS/NP-40 surfactants. *Polymer* **1998,** *39* (11), 2281-2289.
5. Robertson, J. D.; Rizzello, L.; Avila-Olias, M.; Gaitzsch, J.; Contini, C.; Magoń, M. S.; Renshaw, S. A.; Battaglia, G., Purification of Nanoparticles by Size and Shape. *Scientific Reports* **2016,** *6*, 27494.
6. Luo, Z.; Zou, C.; Syed, S.; Syarbaini, L. A.; Chen, G., Highly monodisperse chemically reactive sub-micrometer particles: polymer colloidal photonic crystals. *Colloid and Polymer Science* **2012,** *290* (2), 141-150.
7. Mahapatro, A.; Singh, D. K., Biodegradable nanoparticles are excellent vehicle for site directed in-vivo delivery of drugs and vaccines. *Journal of Nanobiotechnology* **2011,** *9* (1), 55.
8. Siauw, M.; Hawkett, B. S.; Perrier, S., Short chain amphiphilic diblock co-oligomers via RAFT polymerization. *Journal of Polymer Science Part A: Polymer Chemistry* **2012,** *50* (1), 187-198.
9. Rieger, J.; Zhang, W.; Stoffelbach, F. o.; Charleux, B., Surfactant-free RAFT emulsion polymerization using poly (N, N-dimethylacrylamide) trithiocarbonate macromolecular chain transfer agents. *Macromolecules* **2010,** *43* (15), 6302-6310.
10. Prescott, S. W.; Ballard, M. J.; Rizzardo, E.; Gilbert, R. G., Successful use of RAFT techniques in seeded emulsion polymerization of styrene: living character, RAFT agent transport, and rate of polymerization. *Macromolecules* **2002,** *35* (14), 5417-5425.
11. Poon, C. K.; Tang, O.; Chen, X.-M.; Pham, B. T.; Gody, G.; Pollock, C. A.; Hawkett, B. S.; Perrier, S., Preparation of Inert Polystyrene Latex Particles as MicroRNA Delivery Vectors by Surfactant-Free RAFT Emulsion Polymerization. *Biomacromolecules* **2016,** *17* (3), 965-973.
12. Ferguson, C. J.; Hughes, R. J.; Nguyen, D.; Pham, B. T.; Gilbert, R. G.; Serelis, A. K.; Such, C. H.; Hawkett, B. S., Ab Initio Emulsion Polymerization by RAFT-Controlled Self-Assembly §. *Macromolecules* **2005,** *38* (6), 2191-2204.
13. Chiefari, J.; Chong, Y.; Ercole, F.; Krstina, J.; Jeffery, J.; Le, T. P.; Mayadunne, R. T.; Meijs, G. F.; Moad, C. L.; Moad, G., Living free-radical polymerization by reversible addition− fragmentation chain transfer: the RAFT process. *Macromolecules* **1998,** *31* (16), 5559-5562.
14. Ting, S. S.; Min, E. H.; Zetterlund, P. B.; Stenzel, M. H., Controlled/Living ab Initio Emulsion Polymerization via a Glucose RAFT stab: Degradable Cross-Linked Glyco-Particles for Concanavalin A/Fim H Conjugations to Cluster E. coli Bacteria. *Macromolecules* **2010,** *43* (12), 5211-5221.
15. Eissa, A. M.; Abdulkarim, A.; Sharples, G. J.; Cameron, N. R., Glycosylated nanoparticles as efficient antimicrobial delivery agents. *Biomacromolecules* **2016,** *17* (8), 2672-2679.
16. Gurnani, P.; Lunn, A. M.; Perrier, S., Synthesis of mannosylated and PEGylated nanoparticles via RAFT emulsion polymerisation, and investigation of particle-lectin aggregation using turbidimetric and DLS techniques. *Polymer* **2016,** *106*, 229-237.

17. Jacobs, J.; Gathergood, N.; Heuts, J. P.; Heise, A., Amphiphilic glycosylated block copolypeptides as macromolecular surfactants in the emulsion polymerization of styrene. *Polymer Chemistry* **2015,** 6(25), 4634-4640.
18. Dire, C.; Magnet, S.; Couvreur, L.; Charleux, B., Nitroxide-mediated controlled/living free-radical surfactant-free emulsion polymerization of methyl methacrylate using a poly (methacrylic acid)-based macroalkoxyamine initiator. *Macromolecules* **2008,** *42* (1), 95-103.
19. Delaittre, G.; Nicolas, J.; Lefay, C.; Save, M.; Charleux, B., Surfactant-free synthesis of amphiphilic diblock copolymer nanoparticles via nitroxide-mediated emulsion polymerization. *Chemical Communications* **2005,** (5), 614-616.
20. Boyer, C.; Bulmus, V.; Davis, T. P.; Ladmiral, V.; Liu, J.; Perrier, S., Bioapplications of RAFT polymerization. *Chemical Reviews* **2009,** *109* (11), 5402-5436.
21. Nurumbetov, G.; Engelis, N.; Godfrey, J.; Hand, R.; Anastasaki, A.; Simula, A.; Nikolaou, V.; Haddleton, D. M., Methacrylic block copolymers by sulfur free RAFT (SF RAFT) free radical emulsion polymerisation. *Polymer Chemistry* **2017,** *8* (6), 1084-1094.
22. Roe, C. P., Surface chemistry aspects of emulsion polymerization. *Industrial and Engineering Chemistry* **1968,** *60* (9), 20-33.
23. Goodall, A.; Wilkinson, M.; Hearn, J., Mechanism of emulsion polymerization of styrene in soap-free systems. *Journal of Polymer Science Part A: Polymer Chemistry* **1977,** *15* (9), 2193-2218.
24. Fan, X.; Liu, Y.; Jia, X.; Wang, S.; Li, C.; Zhang, B.; Zhang, H.; Zhang, Q., Regulating the size and molecular weight of polymeric particles by 1, 1-diphenylethene controlled soap-free emulsion polymerization. *RSC Advances* **2015,** *5* (115), 95183-95190.
25. Appel, J.; Akerboom, S.; Fokkink, R. G.; Sprakel, J., Facile One-Step Synthesis of Monodisperse Micron-Sized Latex Particles with Highly Carboxylated Surfaces. *Macromolecular Rapid Communications* **2013,** *34* (16), 1284-1288.
26. Egen, M.; Zentel, R., Surfactant-Free Emulsion Polymerization of Various Methacrylates: Towards Monodisperse Colloids for Polymer Opals. *Macromolecular Chemistry and Physics* **2004,** *205* (11), 1479-1488.
27. Maeda, H.; Wu, J.; Sawa, T.; Matsumura, Y.; Hori, K., Tumor vascular permeability and the EPR effect in macromolecular therapeutics: a review. *Journal of Controlled Release* **2000,** *65* (1-2), 271-284.
28. Fang, J.; Nakamura, H.; Maeda, H., The EPR effect: unique features of tumor blood vessels for drug delivery, factors involved, and limitations and augmentation of the effect. *Advanced Drug Delivery Reviews* **2011,** *63* (3), 136-151.
29. Carvalho, T. C.; Peters, J. I.; Williams III, R. O., Influence of particle size on regional lung deposition–what evidence is there? *International Journal of Pharmaceutics* **2011,** *406* (1-2), 1-10.
30. Troendle, E. P.; Khan, A.; Searson, P. C.; Ulmschneider, M. B., Predicting Drug Delivery Efficiency into Tumor Tissues through Molecular Simulation of Transport in Complex Vascular Networks. *Biophysical Journal* **2018,** *114* (3), 679a.
31. Tauer, K.; Deckwer, R.; Kühn, I.; Schellenberg, C., A comprehensive experimental study of surfactant-free emulsion polymerization of styrene. *Colloid and Polymer Science* **1999,** *277* (7), 607-626.
32. Rao, J. P.; Geckeler, K. E., Polymer nanoparticles: preparation techniques and size-control parameters. *Progress in Polymer Science* **2011,** *36* (7), 887-913.

33. Bao, J.; Zhang, A., Poly (methyl methacrylate) nanoparticles prepared through microwave emulsion polymerization. *Journal of Applied Polymer Science* **2004,** *93* (6), 2815-2820.
34. Thickett, S. C.; Gilbert, R. G., Emulsion polymerization: state of the art in kinetics and mechanisms. *Polymer* **2007,** *48* (24), 6965-6991.
35. Telford, A. M.; Pham, B. T.; Neto, C.; Hawkett, B. S., Micron-sized polystyrene particles by surfactant-free emulsion polymerization in air: Synthesis and mechanism. *Journal of Polymer Science Part A: Polymer Chemistry* **2013,** *51* (19), 3997-4002.
36. Peach, S., Coagulative nucleation in surfactant-free emulsion polymerization. *Macromolecules* **1998,** *31* (10), 3372-3373.
37. Feeney, P. J.; Napper, D. H.; Gilbert, R. G., Surfactant-free emulsion polymerizations: predictions of the coagulative nucleation theory. *Macromolecules* **1987,** *20* (11), 2922-2930.
38. Juang, M. S. D.; Krieger, I. M., Emulsifier-free emulsion polymerization with ionic comonomer. *Journal of Polymer Science Part A: Polymer Chemistry* **1976,** *14* (9), 2089-2107.
39. Dam, T. K.; Roy, R.; Das, S. K.; Oscarson, S.; Brewer, C. F., Binding of Multivalent Carbohydrates to Concanavalin A and Dioclea grandiflora Lectin Thermodynamic Analysis of the "Multivalency Effect". *Journal of Biological Chemistry* **2000,** *275* (19), 14223-14230.
40. Weis, W. I.; Drickamer, K., Structural basis of lectin-carbohydrate recognition. *Annual Review of Biochemistry* **1996,** *65* (1), 441-473.
41. Pieters, R. J., Maximising multivalency effects in protein–carbohydrate interactions. *Organic and Biomolecular Chemistry* **2009,** *7* (10), 2013-2025.
42. Kitov, P. I.; Bundle, D. R., On the nature of the multivalency effect: a thermodynamic model. *Journal of the American Chemical Society* **2003,** *125* (52), 16271-16284.
43. He, C.; Hu, Y.; Yin, L.; Tang, C.; Yin, C., Effects of particle size and surface charge on cellular uptake and biodistribution of polymeric nanoparticles. *Biomaterials* **2010,** *31* (13), 3657-3666.
44. Ma, N.; Ma, C.; Li, C.; Wang, T.; Tang, Y.; Wang, H.; Mou, X.; Chen, Z.; He, N., Influence of nanoparticle shape, size, and surface functionalization on cellular uptake. *Journal of Nanoscience Nanotechnology* **2013,** *13* (10), 6485-6498.
45. Huang, X.; Teng, X.; Chen, D.; Tang, F.; He, J., The effect of the shape of mesoporous silica nanoparticles on cellular uptake and cell function. *Biomaterials* **2010,** *31* (3), 438-448.
46. Champion, J. A.; Katare, Y. K.; Mitragotri, S., Particle shape: a new design parameter for micro-and nanoscale drug delivery carriers. *Journal of Controlled Release* **2007,** *121* (1-2), 3-9.
47. Fröhlich, E., The role of surface charge in cellular uptake and cytotoxicity of medical nanoparticles. *International Journal of Nanomedicine* **2012,** *7*, 5577.
48. Ho, L. W. C.; Yung, W.-Y.; Sy, K. H. S.; Li, H. Y.; Choi, C. K. K.; Leung, K. C.-F.; Lee, T. W.; Choi, C. H. J., Effect of Alkylation on the Cellular Uptake of Polyethylene Glycol-Coated Gold Nanoparticles. *ACS Nano* **2017,** *11* (6), 6085-6101.
49. Kulkarni, S. A.; Feng, S.-S., Effects of particle size and surface modification on cellular uptake and biodistribution of polymeric nanoparticles for drug delivery. *Pharmaceutical Research* **2013,** *30* (10), 2512-2522.
50. Albanese, A.; Tang, P. S.; Chan, W. C., The effect of nanoparticle size, shape, and surface chemistry on biological systems. *Annual Review of Biomedical Engineering* **2012,** *14*, 1-16.

51. Anselmo, A. C.; Zhang, M.; Kumar, S.; Vogus, D. R.; Menegatti, S.; Helgeson, M. E.; Mitragotri, S., Elasticity of nanoparticles influences their blood circulation, phagocytosis, endocytosis, and targeting. *ACS Nano* **2015,** *9* (3), 3169-3177.
52. Sun, H.; Wong, E. H.; Yan, Y.; Cui, J.; Dai, Q.; Guo, J.; Qiao, G. G.; Caruso, F., The role of capsule stiffness on cellular processing. *Chemical Science* **2015,** *6* (6), 3505-3514.
53. Hartmann, R.; Weidenbach, M.; Neubauer, M.; Fery, A.; Parak, W. J., Stiffness-dependent in vitro uptake and lysosomal acidification of colloidal particles. *Angewandte Chemie International Edition* **2015,** *54* (4), 1365-1368.
54. Liu, W.; Zhou, X.; Mao, Z.; Yu, D.; Wang, B.; Gao, C., Uptake of hydrogel particles with different stiffness and its influence on HepG2 cell functions. *Journal of Soft Matter* **2012,** *8* (35), 9235-9245.
55. Raemdonck, K.; Demeester, J.; De Smedt, S., Advanced nanogel engineering for drug delivery. *Soft Matter* **2009,** *5* (4), 707-715.
56. Anseth, K. S.; Bowman, C. N.; Brannon-Peppas, L., Mechanical properties of hydrogels and their experimental determination. *Biomaterials* **1996,** *17* (17), 1647-1657.
57. Anselmo, A. C.; Mitragotri, S., Impact of particle elasticity on particle-based drug delivery systems. *Advanced Drug Delivery Reviews* **2017,** *108*, 51-67.
58. Ngai, K.; Plazek, D., Identification of different modes of molecular motion in polymers that cause thermorheological complexity. *Rubber Chemistry Technology* **1995,** *68* (3), 376-434.
59. Lorenz, S.; Hauser, C. P.; Autenrieth, B.; Weiss, C. K.; Landfester, K.; Mailänder, V., The softer and more hydrophobic the better: influence of the side chain of polymethacrylate nanoparticles for cellular uptake. *Macromolecular Bioscience* **2010,** *10* (9), 1034-1042.
60. Cameron, N. R.; Spain, S. G.; Kingham, J. A.; Weck, S.; Albertin, L.; Barker, C. A.; Battaglia, G.; Smart, T.; Blanazs, A., Synthesis of well-defined glycopolymers and some studies of their aqueous solution behaviour. *Faraday Discussions* **2008,** *139*, 359-368.
61. Krstina, J.; Moad, G.; Rizzardo, E.; Winzor, C. L.; Berge, C. T.; Fryd, M., Narrow polydispersity block copolymers by free-radical polymerization in the presence of macromonomers. *Macromolecules* **1995,** *28* (15), 5381-5385.
62. DeGraff, A. W.; Poehlein, G. W., Emulsion polymerization of styrene in a single continuous stirred-tank reactor. *Journal of Polymer Science Part A-2: Polymer Physics* **1971,** *9* (11), 1955-1976.
63. Köhn, M.; Benito, J. M.; Ortiz Mellet, C.; Lindhorst, T. K.; García Fernández, J. M., Functional Evaluation of Carbohydrate-Centred Glycoclusters by Enzyme-Linked Lectin Assay: Ligands for Concanavalin A. *ChemBioChem* **2004,** *5* (6), 771-777.
64. Ting, S. S.; Chen, G.; Stenzel, M. H., Synthesis of glycopolymers and their multivalent recognitions with lectins. *Polymer Chemistry* **2010,** *1* (9), 1392-1412.

# *Chapter 4*

## Dual pH Responsive Macrophage Targeted Isoniazid Particles for Intracellular Tuberculosis Therapy

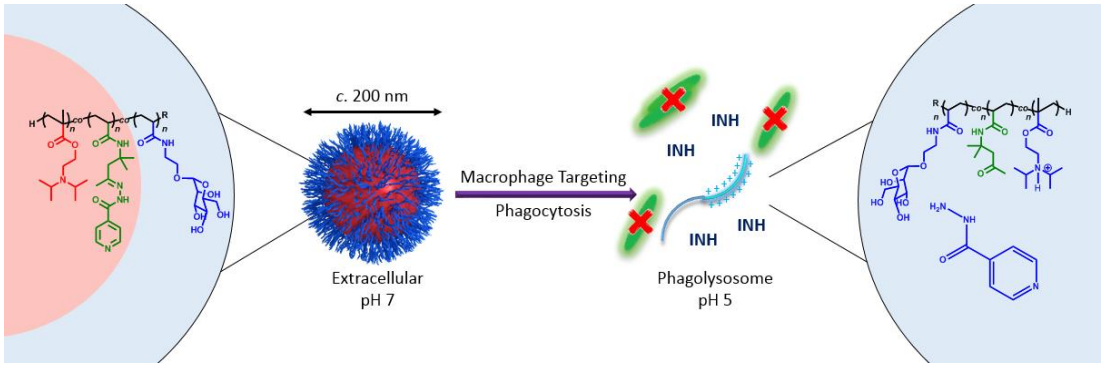

## 4.1 Abstract

Tuberculosis (TB) is a global epidemic, killing 1.7 million people in 2016 alone, particularly those in poorer communities. *Mycobacterium tuberculosis*, the most common causative bacteria of TB, is difficult to treat due in part to its ability to survive and replicate within the host macrophage. New treatment options leading to better tolerated, shorter antibiotic courses targeting intracellular bacteria are of great interest. The development of a novel, pH responsive, mannosylated nanoparticle, covalently loaded with isoniazid, a first line TB antibiotic, is presented. This nanoparticle drug delivery agent is shown to have an increased macrophage uptake and, upon exposure to the acidic phagolysosome, release isoniazid through hydrolysis of a hydrazone bond, and disintegrate into linear polymer. Full antibiotic activity is shown to be retained in cell tests, with mannosylated isoniazid particles being the only treatment exhibiting complete bacterial eradication of intracellular bacteria, compared to an equivalent PEGylated system and free isoniazid.

## 4.2 Introduction

Tuberculosis (TB), a bacterial infection mainly caused by *Mycobacterium tuberculosis*, is a global epidemic, being one of the top 10 causes of death in the world and killing 1.7 million people in 2016 alone.[1, 2] Most infections affect the lungs, and it is generally contracted *via* prolonged inhalation of aerosols containing the bacteria from a person with an active infection coughing or sneezing. Infection typically occurs whilst living in close quarters, with the majority of deaths associated with TB occur in people who live in countries with low or middle incomes.[3,4]

One of the most widely used and important antibiotics in the treatment of TB is isoniazid, which is commonly in combination with: rifampicin, pyrazinamide or ethambutol for a minimum of six months.[5-7] Such long drug regimens are required partly as TB is a slowly dividing bacteria that is able to survive and grow inside immune macrophage cells.[8-12] It is difficult to target and eradicate the bacteria that are able to survive in immune cells, this coupled with antibiotic courses not being finished contribute to ineffective therapy.[13, 14] New therapeutics, capable of targeting intracellular bacteria would therefore be an invaluable weapon in combatting tuberculosis.

Many strategies exist to improve tuberculosis therapy, including the development of new small molecule antibiotics such as bedaquiline.[15-18] Another strategy, with potential to quickly improve the efficacy and longevity of current antibiotics, is to deliver them to the site of action bound to a targeted nanocarrier, the use of which is fully explored in Chapter One.[19-21] In this manner an increased concentration of antibiotic may be achieved at the infection site, in this case the macrophage, from a smaller overall administered dose, potentially reducing systemic exposure and minimising associated side effects. The nanocarrier must be able to be effectively loaded with a drug and release it intracellularly in the macrophage. Covalently loading a drug to a nanocarrier is one way of ensuring high drug loading with minimal unwanted release. If this strategy is employed, the drug must either remain active when tethered to the nanocarrier or the covalent bond must be cleavable at the site of action. A release trigger of considerable interest is pH, particularly when targeting the macrophage. Upon phagocytosis any carrier would experience an acidic shift of environment from extracellular pH 7 to lysosomal pH 5.[22, 23] This change would

quickly hydrolyse a bond such as an imine, oxime or hydrazone, and consequently release any drug tethered by it e.g. isoniazid.[24-26]

Such a change in pH could also be used to address one further issue when using polymeric nanoparticles as drug delivery agents, the accumulation of the injected particles in organs such as the liver and spleen.[27] Particles that are able to break up into their constituent polymers upon a stimulus would be able to be cleared thus avoiding accumulation, pH is a good candidate stimulus for producing such a response.[28, 29] A pH change, such as that experienced when moving from the extracellular to the phagolysosomal environment, can be used to induce assembly or disassembly through modified polymer solubility.[30-32] Both Sun *et al.* and Bütün *et al*. have shown that Poly(2-(Dimethylamino)ethyl methacrylate) (P(DMAEMA)) exhibits a change from hydrophobic to hydrophilic upon pH reduction, due to protonation of the tertiary amine.[33-35] It is reasonable to assume that similar polymers such as poly(2-(di-isopropylamino)ethyl methacrylate) (P(DPAEMA)) would exhibit similar behaviour. If this solubility change could be induced at pH 5, such polymers could be used to produce the required particle break-up for clearance upon phagocytosis.

Another property that can be exploited in improving macrophage targeting is particle size. Macrophages are known to preferentially phagocytose particles ≥100 nm in diameter, ensuring that any nanocarrier that is over this diameter will further improve the macrophage uptake and intracellular concentration of any drug associated with it.[36-39] Macrophages also express certain cell surface lectins such as dendritic cell-specific intercellular adhesion molecule-3-grabbing non-integrin (DC-SIGN), which bind to the sugar mannose, a property that can be taken advantage of by having the surface of a nanocarrier functionalised with mannose.[40-42] Lectin-sugar interactions have previously been shown to be enhanced by the close packing of sugars such as on a particle surface, the "cluster glycoside effect".[43-46] Such properties are achievable using a nanoparticle system synthesised using techniques such as those demonstrated in both Chapter Two and Three. Thus mannose coated polymeric nanoparticles are good candidates for targeting the macrophage.

Using the free-radical surfactant free emulsion polymerisation method for synthesising functional nanoparticles developed in Chapter Three as a simple and scalable process; this chapter will explore the synthesis of isoniazid loaded nanoparticles with a novel

hydrazone linked, pH responsive isoniazid vinyl monomer (DAAm-*hydrazone*-INH), together with DPAEMA and mannose acrylamide (ManAm).[47] It is demonstrated that particles with a mannose shell are capable of preferential endocytosis into macrophage cells, and upon endocytosis, release their antibiotic cargo as a result of acidic hydrolysis of the hydrazone linker. Furthermore, to stop bioaccumulation, the same reduction in pH causes the particles to break down into their constituent linear polymers for clearance. Finally, bacterial killing assays show the retention of full antibiotic effect after intracellular release, with full bacterial eradication only being achieved by mannose coated pH responsive isoniazid nanocarrier.

## 4.3 Results and Discussion

### 4.3.1 Monomer Syntheses

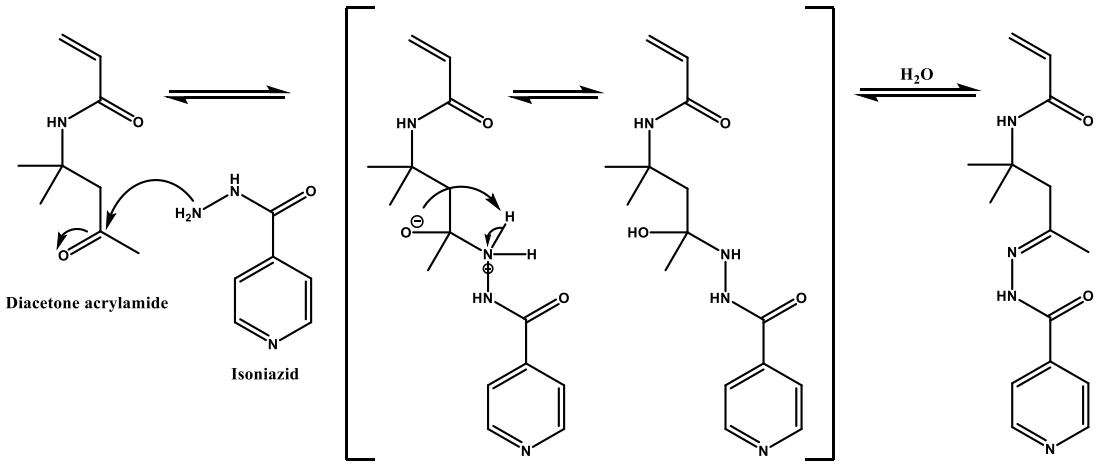


**Scheme 4.1:** Proposed synthetic mechanism for hydrazone formation between diacetone acrylamide and isoniazid

To achieve intracellular release of isoniazid with a high drug loading and efficiency, a responsive monomer was required that was suitable for use during emulsion polymerisation, and able to release isoniazid upon phagocytosis. The pH change from the extracellular to phagoloysosomal environment is from around pH 7 to 5. As isoniazid bears a hydrazine group, a convenient bond that this can form with an aldehyde or ketone is a hydrazone, which is stable at pH 7 and hydrolyses around pH 5. To achieve this hydrazone linked monomer, a condensation reaction was performed between the hydrazine group on isoniazid, and the ketone on the commercially available monomer, diacetone acrylamide (Scheme 4.1). Using stoichiometric conditions, the reaction yielded in full conversion the expected structure of the diacetone acrylamide-isoniazid imine linked monomer (DAAm-*hydrazone*-INH)

product. The structure was confirmed by $^{1}$H NMR spectroscopy, mass spectrometry and elemental analysis (Section 4.5.2).

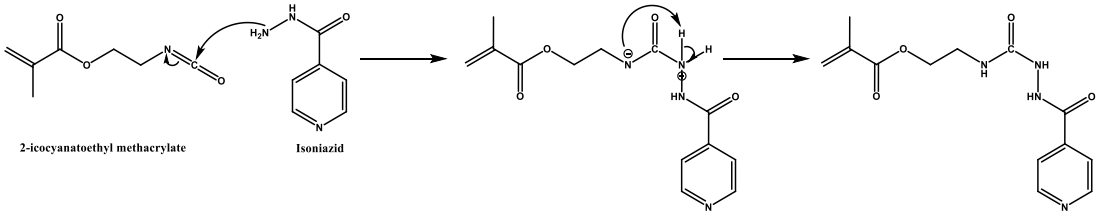


**Scheme 4.2:** Proposed synthetic mechanism for urea formation between 2-icocyanatoethyl methacrylate and isoniazid

To assess the pH-responsive isoniazid release of the DAAm-*hydrazone*-INH monomer, a non-responsive control was also synthesised that would not release isoniazid at the reduced phagolysosomal pH. This was achieved by coupling the hydrazine group on isoniazid with 2-isocyanatoethyl methacrylate, forming a urea linked isoniazid monomer (*urea*-INH). (Scheme 4.2) The pure monomer was found to precipitate out of methanol when cooled to 2-8 °C, and was recovered by filtration and further purified by recrystallization in methanol. The structure and purity were confirmed by $^{1}$H NMR spectroscopy, mass spectrometry and elemental analysis. (Section 4.5.3). By having both a pH and non-pH responsive monomer, particles could then be made that were suitable for assessing the ability of a hydrazone linked isoniazid for intracellular release.

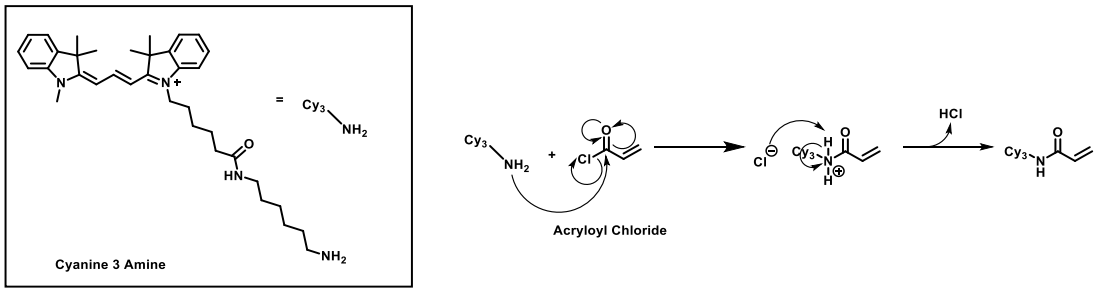


**Scheme 4.3:** Proposed mechanism for the synthesis of cyanine 3 acrylamide, from cyanine 3 amine and acryloyl chloride

In order to determine particle uptake by macrophages however, a fluorescent particle analogue was required to track the particles by fluorescence microscopy and using a fluorescence plate reader. To produce fluorescent particle analogues, a cyanine 3 acrylamide (Cy3Am) monomer was synthesised to be used as a co-monomer in a low molar percentage during particle synthesis. (Scheme 4.3) To achieve this, cyanine 3 amine was reacted with acryloyl chloride; mass spectrometry and HPLC analysis revealed that this resulted in a pure Cy3Am monomer suitable for use as a hydrophilic

co-monomer during emulsion polymerisation. (Section 4.5.4). Having synthesised all required monomers, both pH responsive and non-pH responsive isoniazid loaded particles could be synthesised with their fluorescent analogues.

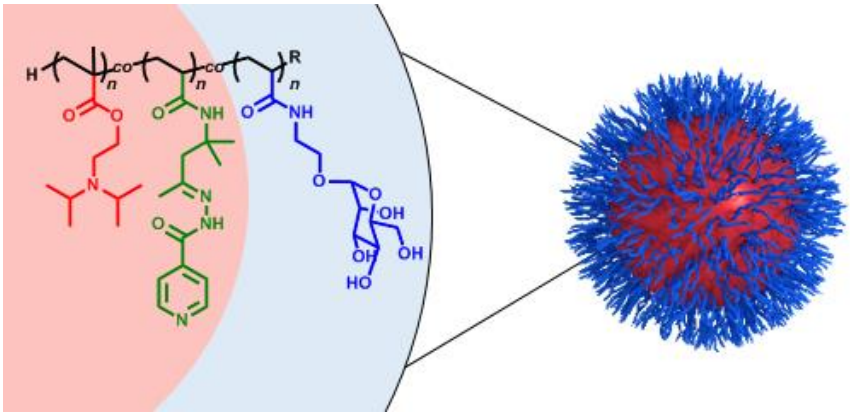

**Figure 4.1:** Graphical representation of the nanoparticle system produced showing the three components: poly(mannose acrylamide) in blue, poly(diisopropylamino)ethyl methacrylate)) in red and poly(diacetone acrylamide-*hydrazone*-isoniazid) in green

### 4.3.2 Particle Synthesis

To produce controlled drug delivery to macrophages, nanoparticles around 200 nm in diameter and coated in mannose were targeted. This was in order to exploit both the propensity of macrophages to phagocytose particles over 100 nm in diameter, and to target the cell surface lectins known to preferentially bind to mannose, such as DC-SIGN.[40-42, 48, 49] The particles were synthesised using the free radical surfactant free emulsion polymerisation method outlined in Chapter Three.[47] In addition to the investigative system of mannose coated particles with cleavable isoniazid (P(ManAm)-*co*-P(DAAm-*hydrazone*-INH)-*co*-P(DPAEMA)) (Figure 4.1), control particles of: mannose with no antibiotic (P(ManAm)-*co*-P(DPAEMA)), mannose and a non-cleavable isoniazid (P(ManAm)-*co*-P(*urea*-INH)-*co*-P(DPAEMA)), PEGA shell with no antibiotic (P(PEGA)-*co*-P(DPAEMA)), and PEGA with cleavable isoniazid (P(PEGA)-*co*-P(DAAm-*hydrazone*-INH)-*co*-P(DPAEMA)) were also synthesised. This was to determine the source of any antimicrobial activity. Fluorescent analogues of P(ManAm)-*co*-(DAAm-*hydrazone*-INH)-*co*-P(DPAEMA)-*co*-P(Cy3Am), P(PEGA)-*co*-P(DAAm-*hydrazone*-INH)-*co*-P(DPAEMA)-*co*-P(Cy3Am) and P(ManAm)-*co*-P(DPAEMA)-*co*-P(Cy3Am) particles were also synthesised with 1% Cy3Am co-monomer as a molar ratio to DPAEMA content.

| Particle | Hydrophilic Monomer (mol) | DPAEMA (mol) | Isoniazid monomer (mol) | Cy3 Am (mol) | Diameter (nm) | Pdi[c] | w/w% pro-drug loading[d] |
|---|---|---|---|---|---|---|---|
| P(ManAm)-*co*-P(DPAEMA) | $4.69x10^{-5}$ | $6.33x10^{-5}$ | n/a | n/a | 210[a] | 0.08 | n/a |
| P(ManAm)-*co*-P(*urea*-INH)-*co*-P(DPAEMA) | $4.69x10^{-5}$ | $8.44x10^{-5}$ | $4.69x10^{-5}$ | n/a | 280[a] | 0.04 | 48 |
| P(ManAm)-*co*-P(DAAm-*hydrazone*-INH)-*co*-P(DPAEMA) | $4.69x10^{-5}$ | $8.44x10^{-5}$ | $4.69x10^{-5}$ | n/a | 212[a] | 0.1 | 44 |
| P(PEGA)-*co*-P(DPAEMA) | $4.69x10^{-5}$ | $8.44x10^{-5}$ | n/a | n/a | 212[a] | 0.14 | n/a |
| P(PEGA)-*co*-P(DAAm-*hydrazone*-INH)-*co*-P(DPAEMA) | $4.69x10^{-5}$ | $8.44x10^{-5}$ | $4.69x10^{-5}$ | n/a | 225[a] | 0.07 | 33 |
| P(ManAm)-*co*-(DAAm-*hydrazone*-INH)-*co*-P(DPAEMA)-*co*-P(Cy3Am) | $4.69x10^{-5}$ | $8.44x10^{-5}$ | $4.69x10^{-5}$ | $8.44x10^{-7}$ | 175[b] | 0.1 | 43 |
| P(PEGA)-*co*-P(DAAm-*hydrazone*-INH)-*co*-P(DPAEMA)-*co*-P(Cy3Am) | $4.69x10^{-5}$ | $8.44x10^{-5}$ | $4.69x10^{-5}$ | $8.44x10^{-7}$ | 205[b] | 0.04 | 33 |
| P(ManAm)-*co*-P(DPAEMA)-*co*-(P(Cy3Am) | $4.69x10^{-5}$ | $6.33x10^{-5}$ | n/a | $6.33x10^{-7}$ | 131[b] | 0.03 | n/a |

**Table 4.1:** Characterisation of all particles synthesised *via* surfactant free emulsion polymerisation, all reactions used a VA-044 initiator at a concentration of 0.75 mg $mL^{-1}$. [a] determined using DLS number distribution, [b] determined using SEM with an average of 20 particles measured, [c] determined using Equation 4.1. Original DLS traces see A4.1-4.4, SEM images A4.5-4.7, [d] determined using Equation 1.1.

All non-fluorescent latexes were analysed for particle size by DLS. Fluorescent latexes were analysed using SEM as DLS was not suitable due to absorption at the wavelength of the laser used (633 nm) (Table 4.1). The absorption/emission maxima of the Cy3Am particles was determined as 554/565 nm (Figure 4.2). There was some size discrepancy between particles, with the majority showing diameters of around 200 nm. Crucially the (P(ManAm)-*co*-P(DAAm-*hydrazone*-INH)-*co*-P(DPAEMA)), (P(ManAm)-*co*-P(DPAEMA)), (P(PEGA)-*co*-P(DAAm-*hydrazone*-INH)-*co*-P(DPAEMA)) and (P(PEGA)-*co*-P(DPAEMA)) particles were all within 15 nm diameter of each other (210-225 nm). This is important as these particles will be directly compared to each other for their antibiotic activity in cell tests. Using this emulsion polymerisation method for isoniazid loading ensured 100% encapsulation efficiency (assuming full conversion of monomer to polymer), significantly higher than possible using entrapment methods, typically showing 40-80%.[50-52] Furthermore the pro-drug loading of DAAm-*hydrazone*-INH achieved in the investigative system of (P(ManAm)-*co*-P(DAAm-*hydrazone*-INH)-*co*-P(DPAEMA)) was 33 % calculated using eq. 1.1. When considered as the total amount of active drug released this reduces to 17% (pro-drug loading was used for continuity of calculation between systems and to account for change in mass of conjugate product). Both of these represent a high percentage of drug loading, compared to the commonplace loading percent achieved in the literature of around 10%.[53]

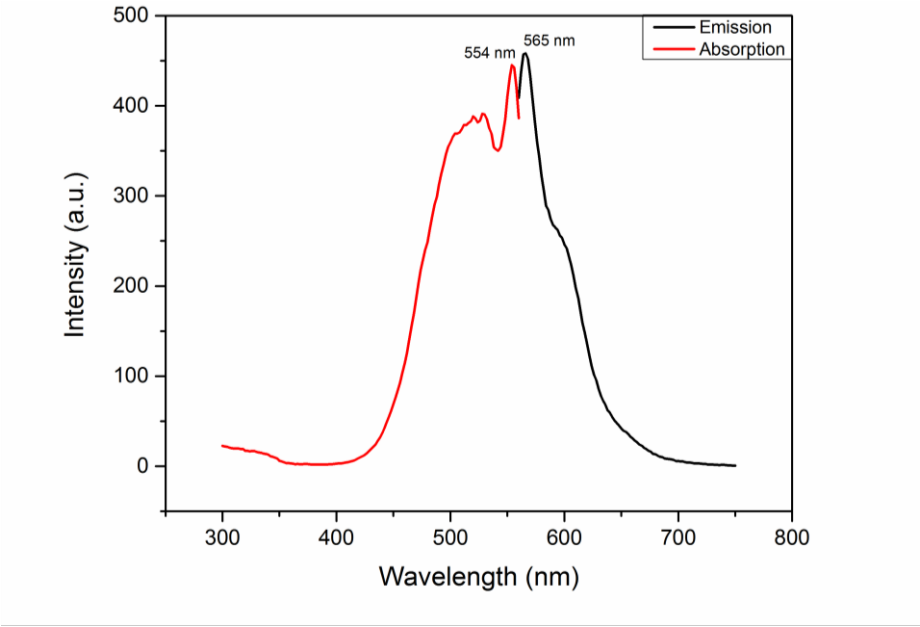


**Figure 4.2:** Fluorescent absorption and emission spectrum of mannose-(DAAm-*hydrazone*-Iso)-DPAEMA-Cy3Am particles in water, absorption/emission maxima λ = 554/565 nm

This produced a latex with a final active isoniazid concentration of 6.5 mg $mL^{-1}$, which is potentially too low for clinical applications, however if the solids content of this emulsion were increased to the maximum of 15% (as established in Chapter Three), a concentration of 44 mg $mL^{-1}$ could be achieved whilst still keeping a stable latex. This concentration would be clinically relevant for both injectable and inhalable formulations with 6.8 mL providing a standard dose of 300 mg isoniazid.[54]

### 4.3.3 Particle Disintegration and Isoniazid Release pH Studies

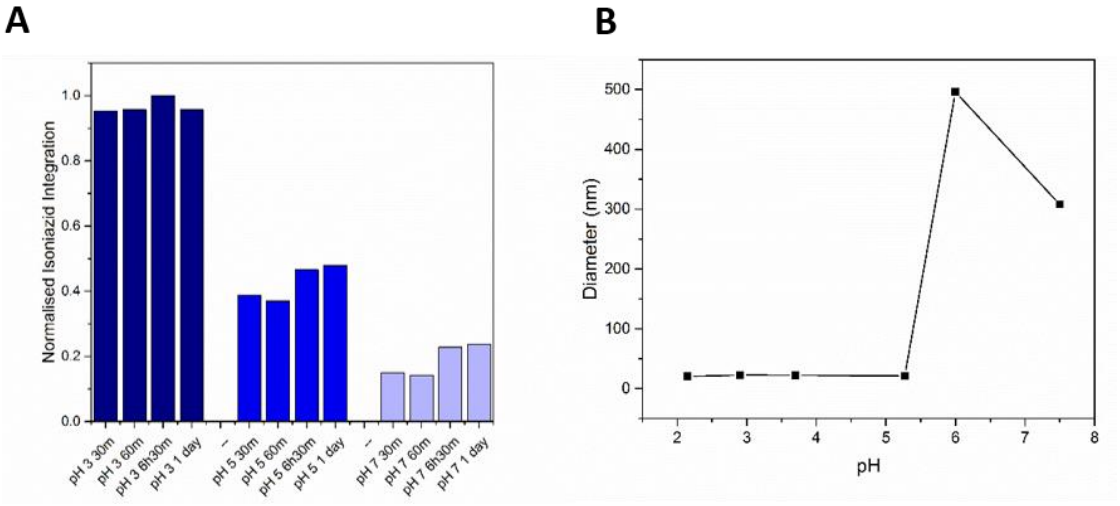


**Figure 4.3:** A) Normalised level of isoniazid released from P(ManAm)-*co*-P(DAAm-*hydrazone*-INH)-*co*-P(DPAEMA) particles over 24 hours at pH 3, 5 and 7, determined using HPLC (Original traces A4.9), B) Average diameter by DLS of P(ManAm)-*co*-P(DAAm-*hydrazone*-INH)-*co*-P(DPAEMA) particles at pH: 2.1, 2.9, 3.7, 5.3, 6 and 7.5, showing stability at pH 7 and particle break up as a large drop in diameter below pH 6, count rate data A4.8

For the synthesised particles to selectively release isoniazid intracellularly, it is necessary for the hydrazone bonding the isoniazid to be selectively cleaved, in response to a relevant drop in pH. To assess this and the ability of the particles to disassemble at reduced pH values, their physical characteristics at a range of pHs were first assessed. To determine if isoniazid would be released from the particles at a relevant pH, P(ManAm)-*co*-P(DAAm-*hydrazone*-INH)-*co*-P(DPAEMA) particles were diluted in phosphate buffered saline (PBS) to 1 mg $mL^{-1}$ at pH: 3, 5 and 7 and analysed by HPLC over 24 hours, comparing peak integrations for isoniazid. HPLC samples were prepared by centrifugation to remove polymer particles (where still present) and filtration to remove as much polymer as possible. This purification was necessary as the acidic conditions of the HPLC eluent would cause hydrolytic release of isoniazid bound to any polymer left, producing an artificially increased release profile (Figure 4.3, A4.9). The results confirmed the release of isoniazid at reduced pH values, with the largest release of isoniazid being seen at pH 3, reducing to half at pH 5. Some limited release can be seen at pH 7; this is believed to be caused by residual particles/polymer in solution, releasing isoniazid in the acidic conditions of the HPLC eluent. These results confirmed that the DAAm-*hydrazone*-INH monomer was stable at neutral pH, releasing isoniazid *via* hydrolysis at reduced pH values. These results were in line with recent literature: Hwang *et al.* showed isoniazid release from a silica particle using a similar hydrazone linker to be stimulated with reduced pH, and minimal release at pH 7. More recently Nkanga *et al.* showed in two publications, nearly full isoniazid release from a hydrazone linker in 12 hours below pH 5.4.[55-57]

A 5 mg $mL^{-1}$ solution of the non-responsive *urea*-INH monomer was also tested for isoniazid release at pH 3 by mass spectrometry to ensure it was hydrolytically stable and a suitable control (A4.10). After 24 hours, a characteristic peak for the *urea*-INH monomer at m/z 315.2 $[mass + Na]^+$ was still observed, with no trace of a peak for isoniazid. This result confirmed that the non-responsive control monomer did not release isoniazid under acidic physiological conditions.

Due to the tertiary amine becoming protonated in acidic conditions, P(DPAEMA) is known to exhibit pH responsive behaviour, switching from hydrophobic to hydrophilic in an acidic environment.[32, 58, 59] For this reason it was chosen as a co-monomer for particle synthesis, in order to cause particle disintegration after endocytosis and avoid

particle bioaccumulation. Dilutions of P(ManAm)-*co*-P(DAAm-*hydrazone*-INH)-*co*-P(DPAEMA) particles were prepared to pHs of: 2.1, 2.9, 3.7, 5.3, 6 and 7.5, and their diameter analysed by DLS to determine the pH at which particle break up occurred (Figure 4.3). The particles were shown to be stable from pH 7.5-6, below which the particles swelled and disintegrated; this can be seen as an increase and subsequent drop in diameter by DLS. The point of disassembly at pH 6, which represents the $pK_b$ of the P(DPAEMA) is a useful value biologically, as the synthesised particles will be stable at extracellular pH 7 and break up in phagolysosomal conditions (around pH 5). The pH at which these particles break up is as expected and matches that reported by Xu *et al.* who used the same response to trigger the assembly of a polymeric tri-block.[58]

These results confirmed the ability of this particle system to both break down into linear polymer and release isoniazid in response to a biologically relevant pH drop, and thus the suitability of the system for further biological testing as an intracellular drug delivery vector for isoniazid.

### 4.3.4 Cytotoxicity

In order for this particle system to be of use in delivering isoniazid to kill infective bacteria, it must itself be biocompatible and non-toxic to the host cells. To ensure the particles were biocompatible, cell viability tests were performed to determine the cytotoxicity of the responsive particles synthesised. The equivalent concentration of isoniazid loaded into the particles was used as a control. A 2,3-bis-(2-methoxy-4-nitro-5-sulfophenyl)-2H-tetrazolium-5-carboxanilide (XTT) assay was performed to determine cell viability by mitochondrial activity against a healthy cell control (Figure 4.4). Particles were tested against a lung epithelial cell line (A549) and PMA activated THP-1 macrophages, representative of the typical pulmonary environment. The particles were shown to be non-toxic up to 0.5 mg $mL^{-1}$ of polymer against A549 cells and 0.1 mg $mL^{-1}$ in macrophages. The equivalent dose of isoniazid showed a similar, but less pronounced trend in both cell lines; it may then be concluded that any cytotoxic effect seen from the isoniazid particles is predominantly due to the presence of polymer and partially isoniazid. This matches well with the literature, one useful example from Hwang *et al.* in 2016 tested a range of polymeric nanoparticles against A549 and THP-1 cells specifically and also reported significant toxicity above 0.1 mg

$mL^{-1}$.[60] Taken together with the previous physical tests, these results suggested that the particles were suitable for further biological testing.

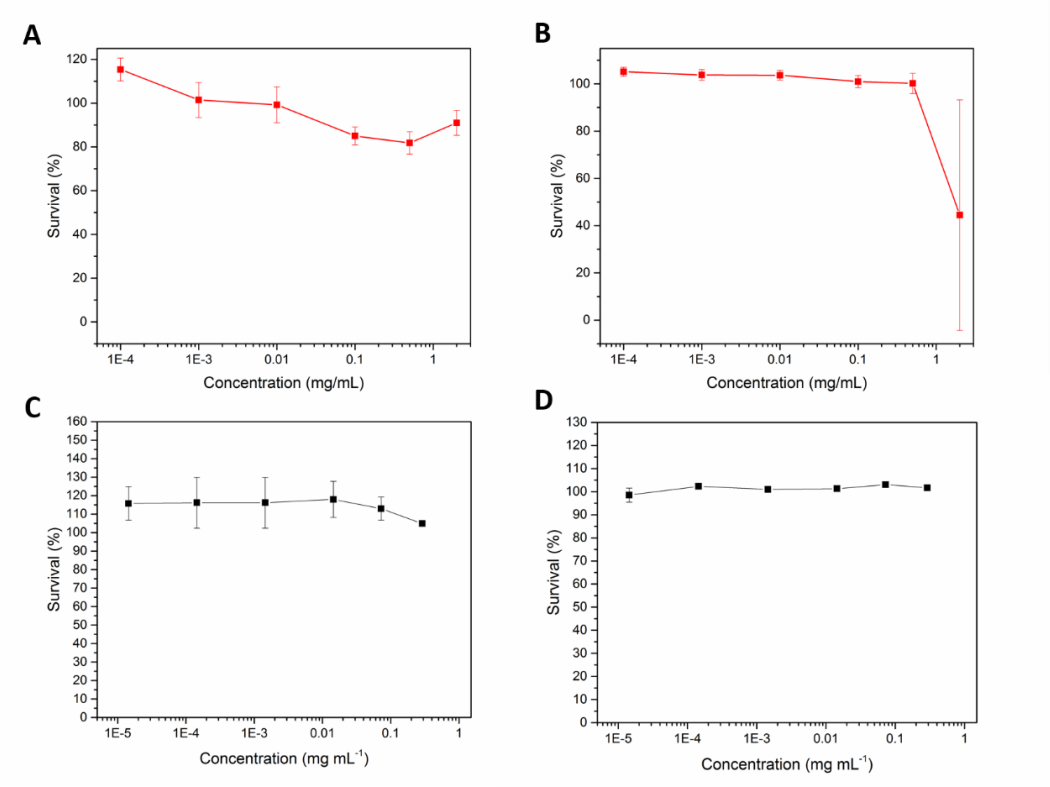


**Figure 4.4:** Cytotoxicity tests, cell viability determined over 24 hours using an XTT assay. P(ManAm)-*co*-P(DAAm-*hydrazone*-INH)-*co*-P(DPAEMA) particles tested against: A) THP-1 derived macrophages and B) lung epithelial (A549) cells. The equivalent concentrations of isoniazid delivered by the particle system tested against: C) THP-1 derived macrophages and D) lung epithelial (A549) cells

### 4.3.5 Cellular Uptake

It is important for the mechanism of particle break up and drug release that the particles are endocytosed *via* a lysosomal pathway, exposing the particles to an acidic environment. This has been previously demonstrated by Kalluru *et al.* who showed polylactide nanoparticles were trafficked to the phagolysosome of macrophages.[61] It was also hypothesised that the presence of mannose on the particle surface would confer a preferential endocytosis, and demonstrate macrophage targeting. In order to test this hypothesis, a fluorescent cell uptake assay was performed using a cytation 3 plate reader, with equivalent experiments performed using confocal fluorescence microscopy. It was first necessary however to ensure that the previously synthesised fluorescent particle analogues were purified to ensure they had no free dye present that would interfere with the experiment.

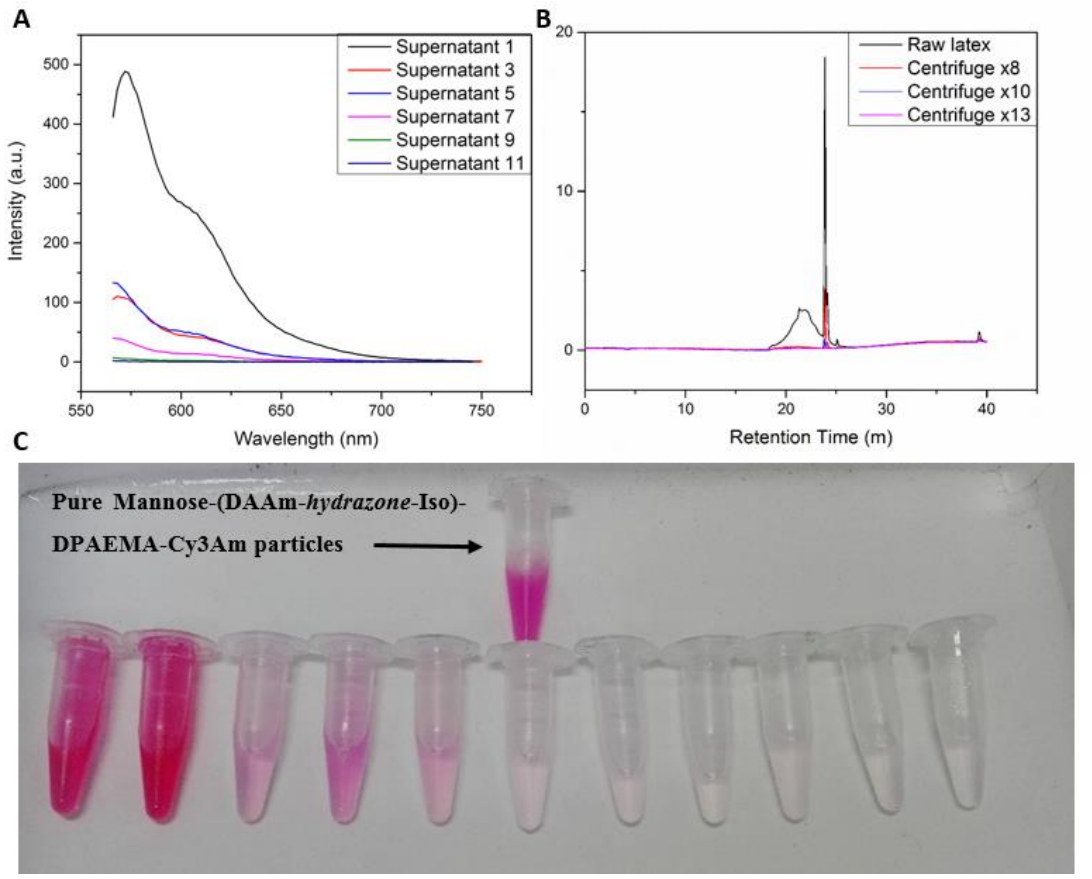


**Figure 4.5:** A) Fluorescence spectra of mannose-(DAAm-*hydrazone*-Iso)-DPAEMA-Cy3Am particle supernatant after centrifugation (excitation λ = 554 nm), showing disappearance of fluorescence indicative of all free dye having been removed, B) Fluorescence HPLC (absorption/emission λ = 554/565 nm) of mannose-(DAAm-*hydrazone*-Iso)-DPAEMA-Cy3Am particles showing disappearance of free fluorescent polymer and monomer in solution indicative of complete removal, C) Image showing loss of colour from free Cy3Am and poly(Cy3Am) in the supernatants of mannose-(DAAm-*hydrazone*-Iso)-DPAEMA-Cy3Am

To achieve this, P(ManAm)-*co*-(DAAm-*hydrazone*-INH)-*co*-P(DPAEMA)-*co*-P(Cy3Am) and P(PEGA)-*co*-P(DAAm-*hydrazone*-INH)-*co*-P(DPAEMA)-*co*-P(Cy3Am) particles were purified by repeated cycles of centrifugation and replacement of supernatant with clean, deionised water. Both visually and using fluorescence spectroscopy, the removed supernatants showed an eventual loss of fluorescence, and HPLC analysis of the purified particles showed loss of free fluorescent polymer and monomer after purification. This confirmed the successful removal of all free dye. (Figure 4.5). The purified particles were then used in a fluorescence uptake assay. Particles were incubated at 0.1 mg $mL^{-1}$ with THP-1 macrophage cells for two, six and 24 hours. The level of intracellular fluorescence was analysed on a fluorescent plate reader, taking an average reading of fluorescence per cell as an indication of the level of endocytosis (A4.11). The relative fluorescence of the two latexes were normalised to each other using the extinction coefficient of each,

obtained from calibration curves of fluorescence by concentration (Figure 4.6). The results were then analysed by means of a separate Student's T-test between ManAm and PEGA particles at each time point (Figure 4.7). (Normality of distribution was verified with a Kolmogorov-Smirnov non-parametrical test).

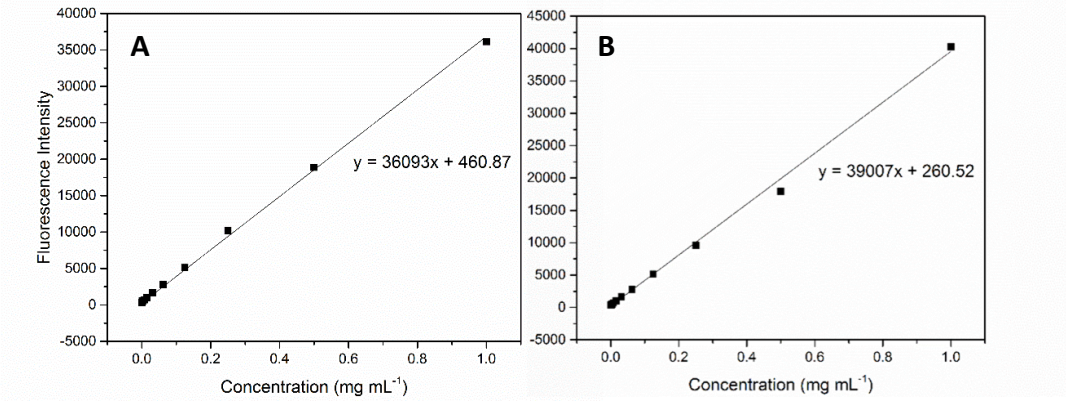


**Figure 4.6:** Fluorescence calibration of A) mannose-(DAAm-*hydrazone*-Iso)-DPAEMA-Cy3Am particles and B) PEGA-(DAAm-*hydrazone*-Iso)-DPAEMA-Cy3Am particles

The results showed that the particles were taken up in a time dependent manner and that, at six and 24 hours, a significantly increased fluorescence was observed for the mannose coated particles. This confirmed that a mannose shell conferred a preferential endocytosis over PEGA equivalent. These statistical analyses were supplemented with confocal microscopy images of the mannose coated particles in THP-1 macrophages, showing punctuated fluorescence increasing in intensity over the same two, six and 24 hour time course. (Figure 4.7). This result is key in providing evidence that the presence of a mannosylated shell does confer a preferential uptake into macrophage cell lines. The increase, though statistically significant is modest however, as those with a PEG shell also show a time dependant increase in uptake. This effect has been reviewed in the literature, and the results presented here are broadly in line with previously reported data, with mannosylated liposomes having been shown to have an increased macrophage uptake when compared to a "bare" liposomal equivalent.[62] The relative increase in mannosylated particle uptake, compared to a PEG equivalent in the environment of a well plate with a cell monolayer, is not surprising however. In this artificial environment the macrophages are left with particles simply placed on them in a perfect environment for their growth. The situation *in vivo* though is rather more complex, as the targeting of mannose receptors may give a far more pronounced increase in macrophage uptake. Reports regarding the *in vivo* uptake of a mannosylated compared to non-mannosylated particles all show an increased macrophage uptake of

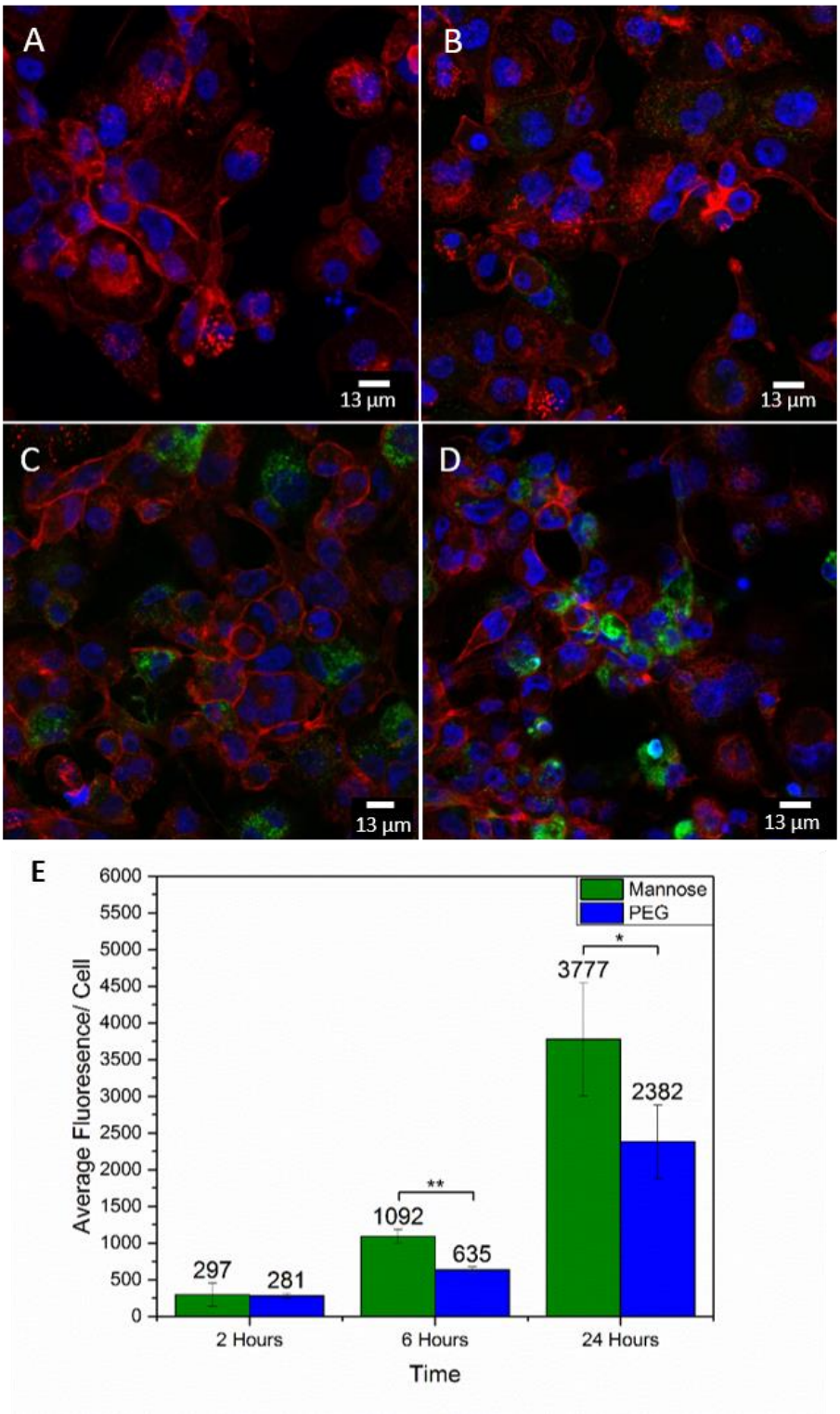


**Figure 4.7:** Cellular uptake of fluorescent analogues of P(ManAm)-*co*-(DAAm-*hydrazone*-INH)-*co*-P(DPAEMA)-*co*-P(Cy3Am) particles at 0.1 mg mL$^{-1}$ by THP-1 derived macrophages tracked in A-D by confocal microscopy with particle incubation for B) two hours, C) six hours, D) 24 hours and A) as a control with no particles. Particles are shown in green with a Cy3 fluorophore, Actin in red with a DyLight 650 phalloidin stain, and the cell nucleus in blue with a DAPI stain. E) Comparative uptake of fluorescent ManAm and PEGA particles. Average intracellular fluorescence determined using a fluorescence plate reader as an indicator of endocytosis. Error bars show standard error, * = $p < 0.05$, ** = $p < 0.01$ determined by a Student's T-test. Example images taken by citation plate reader shown in A4.12.

mannosylated particles, although the extent to which that effect is seen varies greatly between reports.[42, 63, 64] Indeed some studies, such as that from the Hashida group report a *circa* two fold increase in alveolar macrophages,[37] with others including those from the Morimoto group showing almost a three-fold concentration increase, again in macrophages.[36, 41]

### 4.3.6 BCG Invasion and Intracellular Killing

*Mycobacterium tuberculosis* is known to enter the macrophage, evading detection, replicating and ultimately bursting out of the macrophage cell.[8-10] Therapies able to target and kill bacteria intracellularly are crucial in improving outcomes for TB therapy. Using *Mycobacterium bovis* Bacilli Calmette Guerin (BCG) as a mimic, intracellular killing assays were performed to assess the efficacy of synthesised P(ManAm)-*co*-P(DAAm-*hydrazone*-INH)-*co*-P(DPAEMA) particles (performed without purification). These were performed against the control of free isoniazid at 7.2 μg $mL^{-1}$, Poly(Ethylene Glycol) Acrylate (PEGA) coated particles with cleavable isoniazid, mannose coated particles with no isoniazid and mannose coated particles with non-cleavable isoniazid: (P(PEGA)-*co*-P(DAAm-*hydrazone*-INH)-*co*-P(DPAEMA), P(ManAm)-*co*-P(DPAEMA), and P(ManAm)-*co*-P(*urea*-INH)-*co*-P(DPAEMA) respectively. An isoniazid concentration of 7.2 μg $mL^{-1}$ was used as this is equivalent to the concentration of particle bound isoniazid at experimental concentration. In order to determine the antimicrobial activity, THP-1 macrophages were infected with *M. bovis* BCG by incubation at a multiplicity of infection (MOI) of one, with extracellular BCG subsequently washed off and killed. Infected macrophages were incubated for 20 hours with treatment or control at 0.1 mg $mL^{-1}$ polymer concentration or equivalent isoniazid concentration (7.2 μg $mL^{-1}$). This concentration was selected as it provides an isoniazid concentration within the normal therapeutic range in serum (4.3-8.1 μg $mL^{-1}$).[65, 66] After incubation, macrophage cells were lysed to release intracellular bacteria and Colony Forming Unit (CFU) counts were performed to determine the number of bacteria present in each well. Results were analysed for significance using an ANOVA with a post-hoc Tukey's range test. (Figure 4.8, A4.12). The results showed that all treatments containing either free isoniazid or isoniazid bound by a cleavable hydrazone bond, exhibited significant bacterial killing compared to every other treatment group and positive controls.

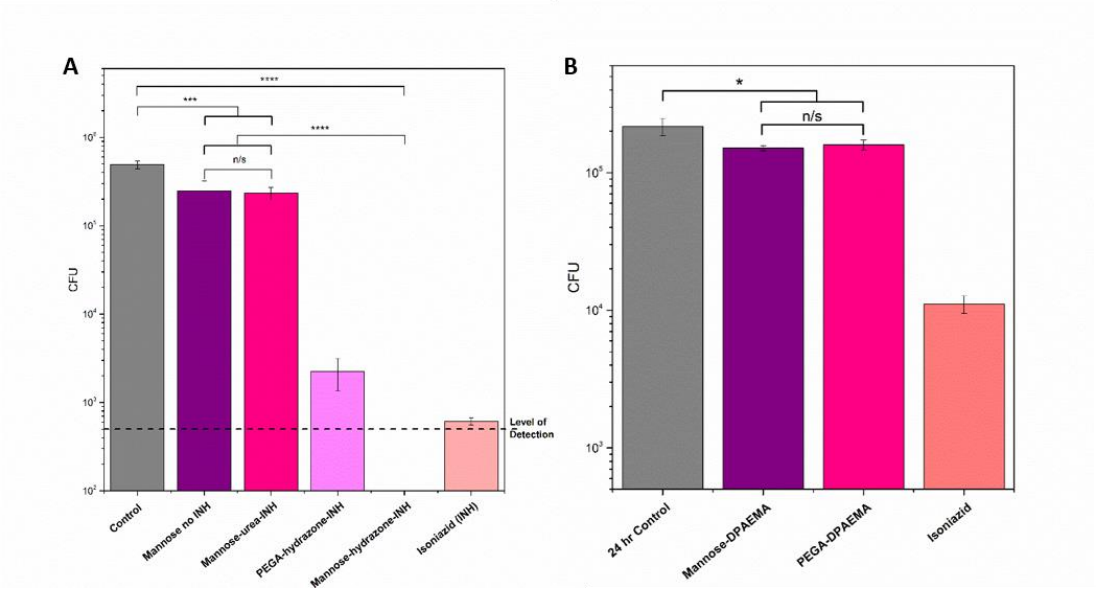


**Figure 4.8:** Intracellular BCG killing determined as number of viable bacteria *via* CFU counts after treatment, with positive controls of infected cells receiving no treatment at four and 24 hours. A) CFU counts comparing mannose-(DAAm-*hydrazone*-INH)-DPAEMA particles against controls of PEGA-(DAAm-*hydrazone*-INH)-DPAEMA, mannose-(DAAm-urea-INH)-DPAEMA and mannose-DPAEMA particles, and equivalent free isoniazid. B) Comparing mannose-DPAEMA particles to PEGA-DPAEMA particles and free isoniazid. Error bars show standard error, * = $p < 0.05$, ** = $p < 0.01$, *** = $p < 0.001$, **** = $p < 0.0001$ (Full statistical analysis A4.12-4.13)

Furthermore, delivery *via* a mannosylated particle improved the activity of the delivered dose of isoniazid, with P(ManAm)-*co*-P(DAAm-*hydrazone*-INH)-*co*-P(DPAEMA) being the only treatment showing complete bacterial eradication. As the bacterial level observed for these treatments was so close to the minimum level of detection for this method, statistical significance could not be shown between the mannosylated particle and the PEG equivalent or free isoniazid. Nevertheless, this result was remarkable when compared to similar tests in the literature; with the particulate systems retaining as a minimum, full antimicrobial activity, and achieving complete bacterial eradication in 20 hours at a typical therapeutic serum concentration.[61, 65, 66] Studies, such as that from Horvati *et al*. used a similar analytical method and found that isoniazid conjugated poly(lactic-*co*-glycolic acid) (PLGA) particles, whilst having a greater antimicrobial effect than free isoniazid, still showed 50-100 bacterial colonies per well after three days treatment time.[67]

Treatments without isoniazid, or where isoniazid had been introduced *via* a non-cleavable linker: P(ManAm)-*co*-P(DPAEMA) and P(ManAm)-*co*-P(*urea*-INH)-*co*-P(DPAEMA), showed a far reduced antimicrobial activity, with no statistical difference between the two treatments. This revealed that for the isoniazid to be active it must first be released from the polymer, and gave further evidence that the

responsive systems were effectively releasing isoniazid. Both control particles did however show statistically significant antimicrobial activity compared to the 24 hours control group. It was not clear though if this activity was an immunological response to the mannose present, or antimicrobial activity of the DPAEMA component that has recently been reported.[68-71] The most relevant of these recent reports being that of Phillips *et al.* who showed that poly(dimethylaminoethyl methacrylate) was active against *Mycobacterium smegmatis*, a bacterium of the same family as tuberculosis and BCG, but faster growing.[72] This study was limited to extracellular bacteria in MIC testing. Interestingly, further work from the same group has revealed the antimicrobial effect of a polycation against *M. smegmatis* is bacteriostatic and not membrane lysing.[73]

To determine which component was the cause of the activity in this case, intracellular bacterial killing assays were performed with the P(ManAm)-*co*-P(DPAEMA) particle against controls of P(PEGA)-*co*-P(DPAEMA) and isoniazid (Figure 4.8, Table 4.1). Again, isoniazid showed good antimicrobial activity, with significantly reduced CFU counts against all other treatment groups and controls, validating the experiment. Both mannose and PEG coated particles showed limited, but statistically significant antimicrobial activity when compared to the 24 hour positive control. There was no significant difference shown between mannose and PEG coated particles however; this indicates that the antimicrobial activity shown is from the DPAEMA content of the particles. Positive polymers are known to exhibit antimicrobial activity, it was therefore hypothesised that protonation of the tertiary amine on DPAEMA in the acidic environment of the phagolysosome is responsible for the activity shown.[74] This suggests limited co-localisation within the macrophage between the polymer and bacteria, either through lysosomal fusion or escape.

### 4.3.7 Particle-Bacteria Co-Localisation Confocal Microscopy

To test the hypothesis of intracellular co-localisation between particles and bacteria, THP-1 macrophages were infected with eGFP fluorescent BCG following the same protocol used in the bacterial killing assays. The infected macrophages were then treated with a fluorescent P(ManAm)-*co*-P(DPAEMA)-*co*-P(Cy3Am) particle, bearing no isoniazid so as not to eradicate BCG. Upon imaging using a Zeiss 880 confocal microscope, limited co-localisation could be seen between BCG (shown in

magenta) and polymer (shown in green) (Figure 4.9). This would suggest that there is the potential for the now positively charged polymer to directly interact with BCG intracellularly, providing a plausible explanation for antimicrobial activity.

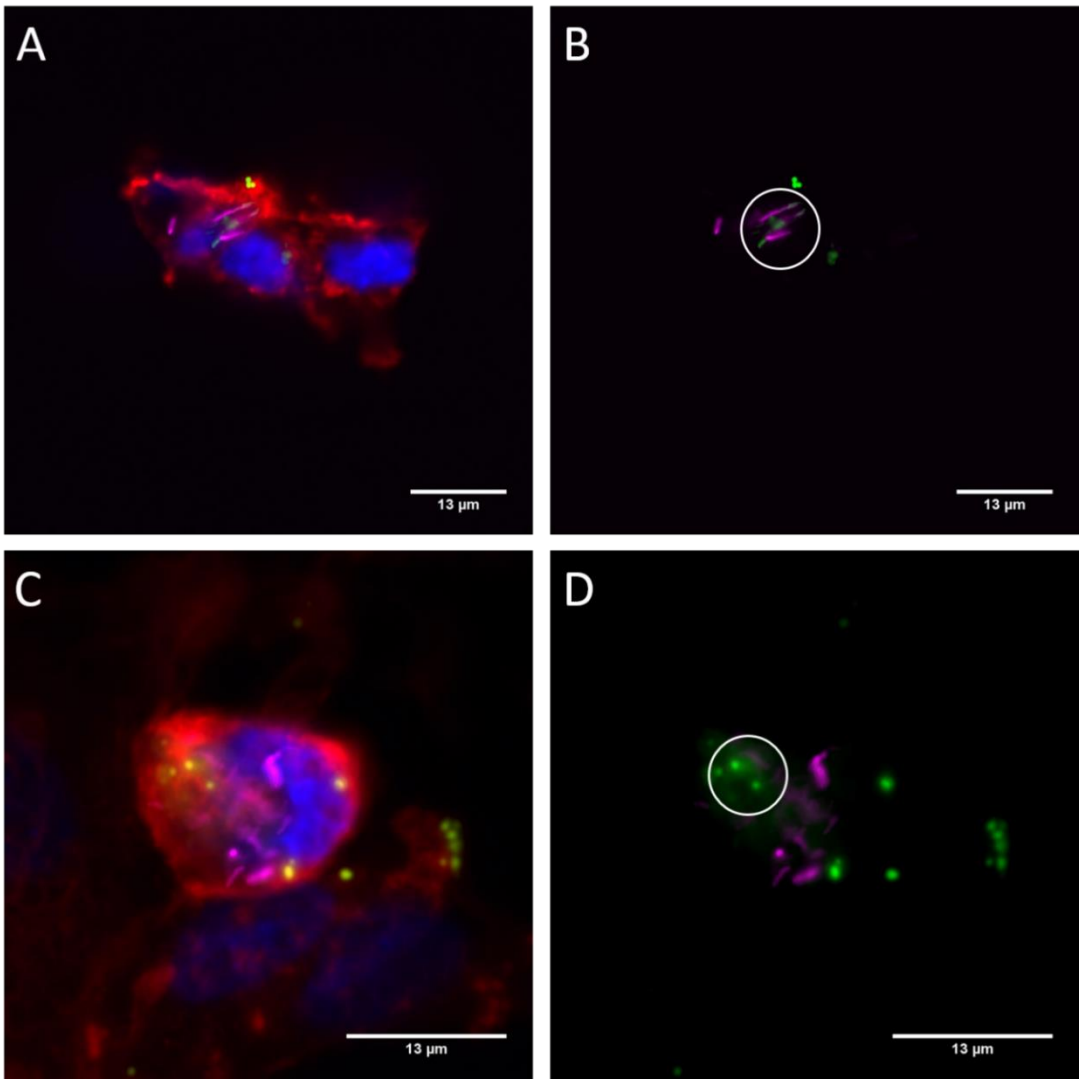


**Figure 4.9:** Confocal microscopy showing co-localisation between investigative ManAm-DPAEMA-Cy3Am particle and BCG bacteria, areas of interest denoted by white circle. Green = ManAm-DPAEMA-Cy3Am particles, magenta = eGFP BCG, red = DyLight 650 phalloidin stained actin, blue = DAPI stained nucleus. Figures A and B show the same image with B only showing channels for particles and BCG for clarity; figures C and D show the same image with D only showing channels for particles and BCG for clarity.

The limited nature of the co-localised fluorescence, together with the likely bacteriostatic antimicrobial mechanism would further explain the very modest antimicrobial activity that the particles exhibit.[73] Where there is fluorescence from polymer and bacteria, the polymer fluorescence can be seen to be diffuse, and not clearly punctuated, suggesting that interaction is made possible through particle lysosomal escape rather than the fusion of separate compartments. Lysosomal escape would match with previous findings that nanoparticles and mycobacteria are found in

different compartments of the macrophage, the phagosome and phagolysosome respectively. The tertiary amine also provides a mechanism by which escape may occur, with its buffering capacity potentially triggering the "proton sponge" effect causing phagolysosome rupture.[75] This provides a reasonable, but not conclusive explanation for interaction between bacteria and polymer, and thus the displayed antimicrobial activity of the particles not bearing isoniazid.

## 4.4 Conclusions

A novel isoniazid monomer has been described, utilising the hydrazine group of isoniazid to form a hydrazone bond with the ketone present on diacetone acrylamide. This monomer was shown to be suitable for emulsion polymerisation. The hydrazone linker was demonstrated to be cleavable by a biologically relevant drop in pH from 7 to 5, yielding the active isoniazid compound. This monomer was co-polymerised with mannose acrylamide and DPAEMA in a free radical surfactant free emulsion polymerisation. Dual pH responsive nanoparticles with diameters of *c.* 200 nm were synthesised, breaking apart and releasing the covalently bound isoniazid at a clinically relevant pH of 5 in PBS. Fluorescence uptake studies showed preferential endocytosis of mannosylated particles *via* sugar-lectin interactions, over a PEGylated control.

These particles were subsequently shown to be effective at killing intracellular *M. bovis* BCG bacteria in THP-1 macrophages, releasing their isoniazid cargo and exhibiting at least equivalent activity to free isoniazid in the artificial environment of a well plate, with P(ManAm)-*co*-P(DAAm-*hydrazone*-INH)-*co*-P(DPAEMA) particles being the only treatment to show complete bacterial eradication. This improved activity is hypothesised to be due to the increased cellular uptake of mannose coated particles, causing a higher intracellular isoniazid concentration compared to the controls. Furthermore, limited antimicrobial activity of the DPAEMA component of the particle was demonstrated, potentially contributing to the enhanced antimicrobial activity of the P(ManAm)-*co*-P(DAAm-*hydrazone*-INH)-*co*-P(DPAEMA) particle.

Taken together these results show that *in vitro,* such macrophage targeted particles increase intracellular isoniazid concentration, showing an increased antimicrobial activity against intracellular mycobacterium, and leave the possibility for an enhanced effect *in vivo* to be studied.

## 4.5 Experimental

### 4.5.1 Materials

Magnesium sulphate, isoniazid (≥ 99%), diacetone acrylamide (99%), poly(ethylene glycol) methyl ether acrylate (PEGA, average $M_n$= 480 g mol$^{-1}$), 2-(diisopropylamino) ethyl methacrylate (97 %), acryloyl chloride (97%), 2-isocyanatoethyl methacrylate (98%), paraformaldehyde powder (95%), sodium hydroxide (≥ 97%), N-methylmorpholine (99%) phorbol myristate acetate (PMA, ≥ 99%), trifluoro acetic acid (>98%), Middlebrook 7H10 agar base, Middlebrook 7H10 broth base, glycerol (≥ 99%), hygromycin B from *Streptomyces hygroscopius*, amikacin (European pharmacopoeial standard), phenazine methosulfate (PMS) (≥ 90%) and 2,3-Bis(2-methoxy-4-nitro-5-sulfophenyl)-2H-tetrazolium-5-carboxanilide inner salt (XTT) were purchased from Sigma-Aldrich and used as received except for all monomers that were passed through basic aluminium oxide to remove inhibitor. Thermal initiator VA-044 2,2'-azobis[2-(2-imidazolin-2-yl)propane] dihydrochloride was purchased from Alpha Laboratories, Cyanine3 amine (95%) was purchased from Lumiprobe, Middlebrook OADC growth supplement was purchased from Agar Scientific, RPMI 1640 Medium, GlutaMAX™ Supplement, DMEM, Hoechst 33342 and fetal bovine serum (FBS) was purchased from ThermoFisher, Phalloidin DyLight 650 Phalloidin (300 unit) was purchased from New England Bioloabs, ProLong Gold Antifade Reagent with DAPI was purchased from Vector Laboratories, super smooth silicon wafers, adhesive copper tape were purchased from Agar Scientific and LabTek II 4-well microscopy culture slides were purchased from Thermo Scientific and all were used as purchased. THP-1 (ATCC® TIB-202™), A549 (ATCC® CCL-185™), *Mycobacterium bovis* Karlson and Lessel (ATCC® 35737™) and cells were taken from frozen stocks originally purchased from ATCC, eGFP BCG bacteria was taken from stocks previously engineered and used by the group.

### 4.5.2 Analysis

#### 4.5.2.1 NMR Spectroscopy

$^1$H NMR spectra were recorded on a Bruker DPX-300 spectrometer using deuterated solvent (materials section). Each sample was run with a decay time of 2 s with 16 repeats.

#### 4.5.2.2 Mass Spectrometry

ESI mass spectrometry measurements were performed using an Agilent 6130B single quad in methanol as a solvent in positive mode.

#### 4.5.2.3 Melting Point

Melting point temperatures were determined using a Stuart SMP10 digital melting point apparatus with a small amount of monomer placed into capillary tubing and repeated in triplicate, the average of all three readings reported in all cases.

#### 4.5.2.4 Dynamic Light Scattering

Size measurements were carried out using a Malvern Zetasizer Nano-ZS at 25°C with a 4 mW He-Ne 633 nm laser at a scattering angle of 173° (back scattering). Measurements were taken assuming the refractive index of di-isopropyl aminoethyl methacrylate. Pdi values were calculated using Equation 4.1. Measurements of ζ-potential were modelled with the Smoluchowski theory.

$$\text{Pdi} = \frac{\sigma^2}{d^2}$$

**Equation 4.1:** Equation to calculate Pdi from standard deviation (σ), and diameter (d).

#### 4.5.2.5 Scanning Electron Microscopy

SEM analysis was performed to determine the size and morphology of fluorescent particles as the fluorophore absorbed the laser used in DLS. Samples were prepared by diluting raw latex by a factor of 500 in previously filtered deionised water. A 5 μL drop of this diluted sample was then spotted onto a super smooth silicon wafer and left to dry for 12 hours in a laminar flow cabinet to ensure no sample contamination. The particles were visualised using a Zeiss Gemini SEM field emission scanning electron microscope at an accelerating voltage of 5 keV. Particle size and standard deviation was determined by taking an average of 20 particle diameters using Image J software, Pdi was determined using Equation 4.1.

#### 4.5.2.6 High Performance Liquid Chromatography (HPLC)

HPLC samples were prepared by centrifuging the latex using an Eppendorf MiniSpin5452 at 13500 rpm for five minutes. The supernatant was aspirated off and filtered using a 0.2 μM PVC syringe filter. The filtered sample was then diluted by a

factor of 100 into HPLC water eluent (0.05 TFA) at an injection volume of 100 μL. Chromatograms were obtained using an Agilent 1260 Infinity series equipped with an Agilent 1260 variable wavelength detector. The HPLC was fitted with a Phenomenex Luna® C18 (250 × 4.6 mm) with 5 μm packing (100 Å) column. Mobile phase A: water (+0.05 % TFA), mobile phase B: methanol (+0.05 % TFA). The gradient used for HPLC analysis was increased from 5% to 95 % B in 30 minutes. Detection for isoniazid release was achieved *via* monitoring at 270 nm. To detect Cy3 or Cy3Am the same procedure was carried out, with monitoring of fluorescence at excitation/emission wavelengths of 554/565 nm.

#### 4.5.2.7 Cell Culture

A549 (lung epithelial carcinoma) cells were grown in Dulbecco's modified Eagle's medium (DMEM) supplemented with 10% (v/v) fetal bovine serum (FBS) and 2 mM of glutamine and pen/strep at 37°C in a sterile, humid 5% $CO_2$ environment. Tamm-Horsfall Protein (THP)-1 cells were grown in Roswell Park Memorial Institute (RPMI) 1640 GlutaMAX Medium supplemented with 20% (v/v) FBS at 37°C in a sterile, humid 5% CO2 environment.

#### 4.5.2.8 2,3-Bis-(2-Methoxy-4-Nitro-5-Sulfophenyl)-2H-Tetrazolium-5-Carboxanilide (XTT) Cell Viability Assay

THP-1 monocytes were seeded at a density of $2.5x10^5$ cells per mL into a 96 well plate in RPMI Glutamax media supplemented with 20% FBS and 100 ng $mL^{-1}$ PMA in order to differentiate the cells to adherent macrophages and incubated for 72 hours at 37°C. Alternatively; A549 cells were seeded at a density of $5x10^5$ cells per mL of DMEM (supplemented with 10% FBS, 1% glutamine and 1% pen/strep) into a 96 well plate and incubated for 24 hours at 37°C. In both cases after incubation, fresh media was replaced in all of the wells. The cells were then incubated with serial dilutions of the particles at 0.1 μg $mL^{-1}$, 1 μg $mL^{-1}$, 10 μg $mL^{-1}$, 0.1 mg $mL^{-1}$, 0.5 mg $mL^{-1}$ and 2 mg $mL^{-1}$ for 72 hours. To determine the cell viability a standard XTT assay was used.[44] The cell media was replaced with 100 μL fresh media and 100 μL of a 0.0083 mM phenazine methosulfate (PMS)/ 0.33 mg $mL^{-1}$ XTT solution in media and left to incubate at 37°C for 24 hours. Each well then had its absorbance recorded using a BioTek Cytation3 plate reader at 450 nm and 650 nm (background). The relative absorbance compared to a control of healthy cells as 100% cell viability was recorded

and used to show the percentage cell viability in each case. The experiments were carried out with three technical replicates in triplicate.

#### 4.5.2.9 Macrophage Particle Uptake Assay

THP-1 cells were seeded at a density of $2.5x10^5$ cells per mL into a 96 well plate in RPMI Glutamax media supplemented with 20% FBS, and 100 ng $mL^{-1}$ PMA in order to differentiate the cells to adherent THP macrophages and incubated for 72 hours at 37°C to form adherent monolayers. The media was then replaced and cells were inoculated for either 24, six or two hours with either PEG or mannose coated fluorescent particles at a concentration of 0.1 mg $mL^{-1}$. At 23 hours and 30 minutes incubation time, 10 μL of a 50 μg $mL^{-1}$ Hoescht 33342 in PBS stock solution was added to the wells and incubated at 37°C for a further 30 minutes to stain the nucleus of the cells. The media was then removed and any extra cellular particles removed by with PBS three times. The cells were incubated in phenol red free media and placed into a BioTek Citation3 plate reader, to determine the level of fluorescence in each cell. The nucleus of each cell was imaged as a reference, set at absorption/emission detection of 377/477 nm for Hoechst 33342, and the fluorescence of cyanine 3 labelled particles at an absoption/emission of 531/593 nm. From the nucleus a representative cell size cut off of 13 μm was applied and using a rolling ball algorithm for background calculation, particle fluorescence per cell over hundreds of cells was determined and an average taken. This was repeated with three technical replicates in duplicate. To ensure any difference in fluorescence was due to changes in uptake, and not differing fluorescence intensity, a fluorescence calibration for both PEG and mannose particles was then produced. This was determined by serially diluting a 1 mg $mL^{-1}$ stock of each particle by half repeatedly 15 times and taking a fluorescence reading of each, this was repeated in triplicate. The difference in relative fluorescence intensities was then determined by comparing the extinction co-efficient for each calibration. The relative fluorescence for both particles was found to be at a ratio of 1:0.97, and as such, within error of each other. However to ensure that differing fluorescence did not contribute to any observed differences in uptake, the readings for PEG particles were multiplied by 0.97 (Figure 4.6).

#### 4.5.2.10 Confocal Microscopy Cell Uptake

THP-1 derived macrophage cells were cultured on LabTek II 4-well microscopy culture slides as described for a 96 well plate in section "Macrophage Particle Uptake Assay". After incubating with fluorescent mannose particles for two, six and 24 hours at 0.1 mg $mL^{-1}$ the cells were washed three times with PBS and fixed by incubation with 1 mL of a cooled 4% PFA solution at room temperature for ten minutes. This was then washed three times with PBS. Cells were permeabilized in 1 mL of a 1% saponin, 0.5% Triton X-100 solution in PBS for 20 minutes at room temperature, then blocked with 0.5 mL of a 3% bovine serum albumin (BSA) solution in PBS for 30 minutes at room temperature. Culture slides were then washed with 0.5 mL of 1% BSA in PBS. F-actin was then stained by adding 0.2 mL of a 2.5 μg $mL^{-1}$ solution of phalloidin 650 in 1% BSA for 40 minutes in the dark at room temperature. Chamber slides were then washed with 1 mL of PBS three times and chambers removed from the culture slides. A cover slip was then secured using 10 μL of DAPI mounting medium per well, also staining the nuclei of the cells. Slides were then kept in the dark between 2-8 °C until imaging. Confocal images were taken on a Zeiss 880 at 37 °C using a 40x objective lens and sequential scanning for each channel. Excitation/emission used for imaging was as follows: nucleus DAPI 405/410-480 nm, Cy3 particles 561/567-620 nm, DyLight 650 phalloidin 633/639-759 nm. Images were overlaid and processed using Image-J software.

#### 4.5.2.11 BCG Invasion and Intracellular Killing Assays

Intracellular infection was performed on THP-1 derived macrophages. Cells were seeded at a density of $2.5x10^5$ cells per mL into a 24 well plate in RPMI Glutamax media supplemented with 20% FBS, and 100 ng $mL^{-1}$ PMA in order to differentiate the cells to adherent macrophages and incubated for 72 hours at 37°C. A single colony of BCG bacteria was inoculated in Middlebrook 7H10 broth supplemented with 10% (v/v) OADC enrichment. The inoculum was grown to an $OD_{600}$=0.8, so to be in the log phase, and diluted ten-fold into cell culture medium (RPMI GlutMAX + 20% FBS). Media was then removed from each well of macrophages and replaced with the inoculated media. This was incubated for three hours at 37 °C giving an MOI of 1:1. Extracellular bacteria were then removed with PBS three times and the macrophages incubated with 1 mL solution of 200 ng $mL^{-1}$ amikacin in media for one hour to ensure

no viable extracellular BCG. Cells were then further washed with 1 mL of PBS twice. Four hour controls incubated at room temperature with cold water for 5 minutes followed by vigorous pipetting to disrupt the mammalian cell membrane, and immediately diluted by a factor of ten into warm PBS twice. 20 µL of each dilution was pipetted onto Middlebrook 7H10 ADC agar petri dishes and incubated at 37 °C for 14-21 days to allow bacterial growth. The remaining wells were incubated for 20 hours at 37 °C with 1 mL media containing particle or control. After 20 hours the cells were washed with PBS, lysed, plated and incubated as described for the four hour control wells. After two weeks CFU counts for all dilutions were performed and the total number of CFU's per well determined using Equation 4.2.

$$CFU_{Total} = CFU_{Counted} \times (50 \times Dilution\ Factor)$$

**Equation 4.2**. Calculation performed to determine viable number of colony forming units (CFU) using dilute 20 µL sample from a 1 mL well

#### 4.5.2.12 Confocal Microscopy of Particle/Bacteria Co-Localisation

THP-1 derived M0 macrophage cells were cultures on LabTek II 4-well microscopy culture slides as described for 24 well plates in the section "Intracellular BCG Killing Assays", and fixed as described in "Confocal Microscopy, Cell Uptake", with the addition of the excitation/emission of eGFP BCG at 490/500-540 nm. Images were overlaid and processed using Image-J software.

#### 4.5.2.13 Statistical Analysis

All analyses were performed using IBM SPSS Statistics 24. The test used for comparison of the means of particle uptake at 2, 6 and 24 hours for PEG versus mannose coated particles was a Student's T-test. The test performed to compare all CFU count data after intracellular BCG killing was a one-way ANOVA test with a Tukey post-hoc analysis. The assumptions for the tests were: normality of distribution (verified with a Kolmogorov-Smirnov non-parametrical test), homogeneity of variances (evaluated using a Levene test). Analysis was performed on two or three biological repeats performed with three technical repeats in all cases.

### 4.5.3 Synthetic Procedures

#### 4.5.3.1 Isoniazid-Diacetone Acrylamide Hydrazone, pH Responsive Monomer ((E)-N-(4-(2-isonicotinoylhydrazineylidene)-2-methylpentan-2-yl) acrylamide) Synthesis

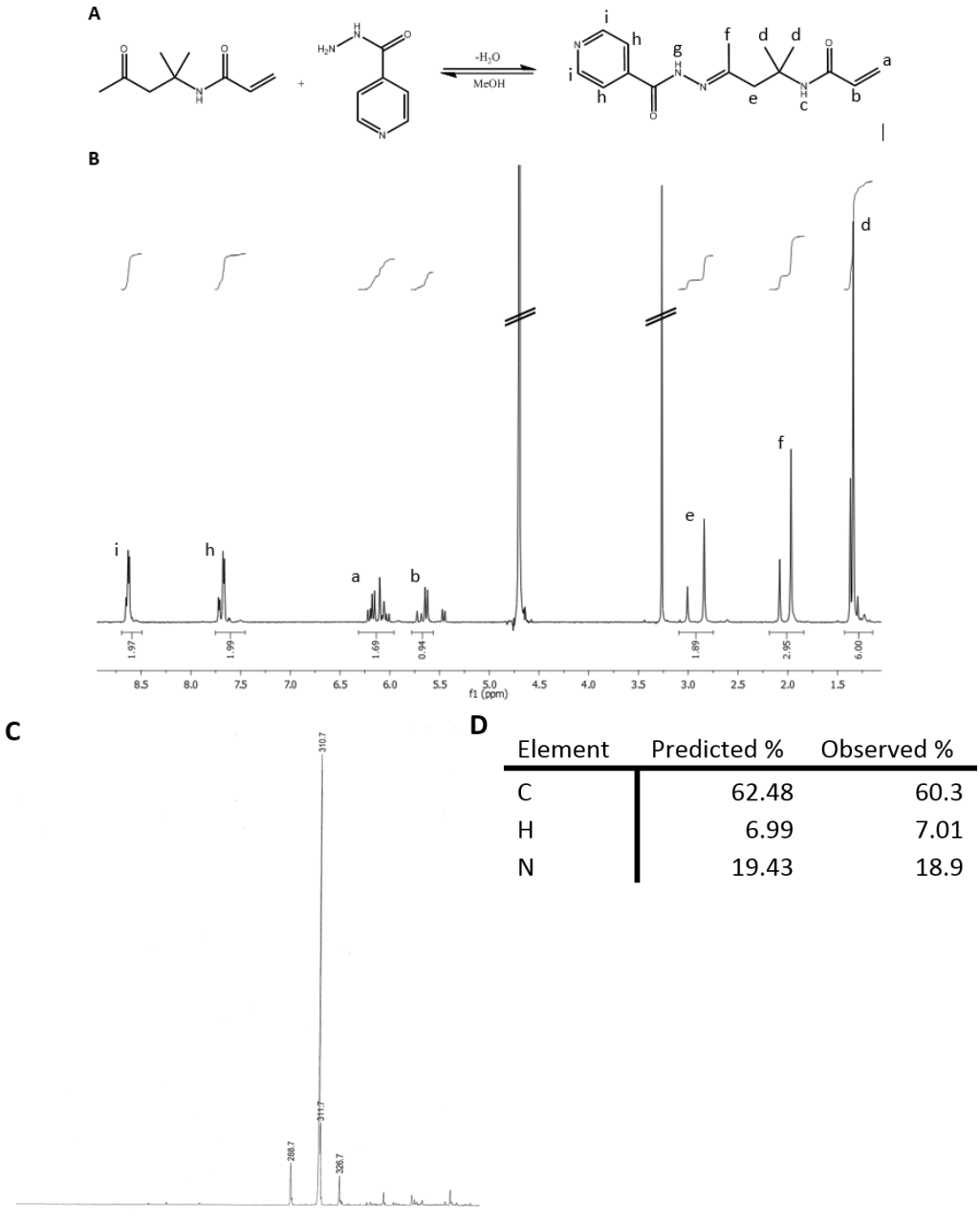


**Figure 4.1:** A) Reaction scheme for diacetone acrylamide-*hydrazone*-isoniazid monomer B) $^{1}H$ NMR spectrum confirming the structure of the monomer C) Mass spectrum showing the expected single peak at m/z= 310.7 $[Mwt + Na]^{+}$ and D) Elemental analysis of the monomer, showing percentages within the expected range of the proposed monomer structure

Isoniazid (5 g, 0.0365 mol, 1 eq.) and diacetone acrylamide (6.16 g, 0.0365 mol, 1 eq.) were dissolved in anhydrous methanol to a volume of 250 mL in a 500 mL round bottomed flask charged with a magnetic follower. Anhydrous magnesium sulphate (5g, 0.02 mol) was suspended in the reaction mixture to absorb water released by the condensation reaction, pushing the reaction equilibrium to the product. The flask was sealed with a rubber septum and left to stir at room temperature for 16 hours. The magnesium sulphate was then removed *via* Buchner filtration and methanol removed under vacuum using a rotary evaporator leaving behind a clear gel like solid, confirmed as the pure product by $^{1}$H NMR spectroscopy, mass spectrometry and elemental analysis. (Figure 4.10)

MS m/z = 310.7 $[M+Na]^+$ ($MS_{th}$: 311.06)

$^{1}$H NMR (300 MHz, $D_2O$) δ 8.63 (t, *J* = 7.1 Hz, 2H), 7.69 (dd, *J* = 18.0, 5.9 Hz, 2H), 6.31 – 5.96 (m, 2H), 5.67 (dd, *J* = 28.4, 13.5 Hz, 1H), 2.92 (d, *J* = 67.0 Hz, 2H), 2.02 (d, *J* = 45.2 Hz, 3H), 1.43 – 1.27 (m, 6H)

Melting point = 82°C

#### 4.5.3.2 Isoniazid-Diacetone Acrylamide Urea linked Non-Responsive Monomer (2-(2-isonicotinoylhydrazine-1-carboxamido)ethyl methacrylate) Synthesis

Isoniazid (804 mg, $5.86x10^{-3}$ mol, 1 eq.) and 2-icocyanatoethyl methacrylate (1g, $6.45x10^{-3}$ mol, 1.1 eq.) were dissolved in 50 mL of anhydrous methanol in a 100 mL round bottomed flask, charged with a magnetic follower. The flask was sealed with a rubber septum and left to stir. After four hours the product precipitated out of solution as a white powder. After cooling the reaction mixture to 8°C, full precipitation occurred and the precipitate was recovered by Buchner filtration using filter paper with pore size 11 μm. The powder was recrystallised using methanol as a solvent and confirmed as the product using $^{1}$H NMR spectroscopy, mass spectrometry and elemental analysis. (Figure 4.11)

MS: *m/z* = 315.2 $[M+Na]^+$ ($MS_{th}$: 315.11).

$^{1}$H NMR (300 MHz, DMSO) δ 10.44 (s, 1H), 8.75 (d, *J* = 5.7 Hz, 2H), 8.11 (s, 1H), 7.79 (d, *J* = 5.7 Hz, 2H), 6.74 (t, *J* = 4.9 Hz, 1H), 6.06 (s, 1H), 5.67 (s, 1H), 4.08 (t, *J* = 5.7 Hz, 2H), 2.50 (s, 4H), 1.88 (s, 3H).

Melting point =168°C

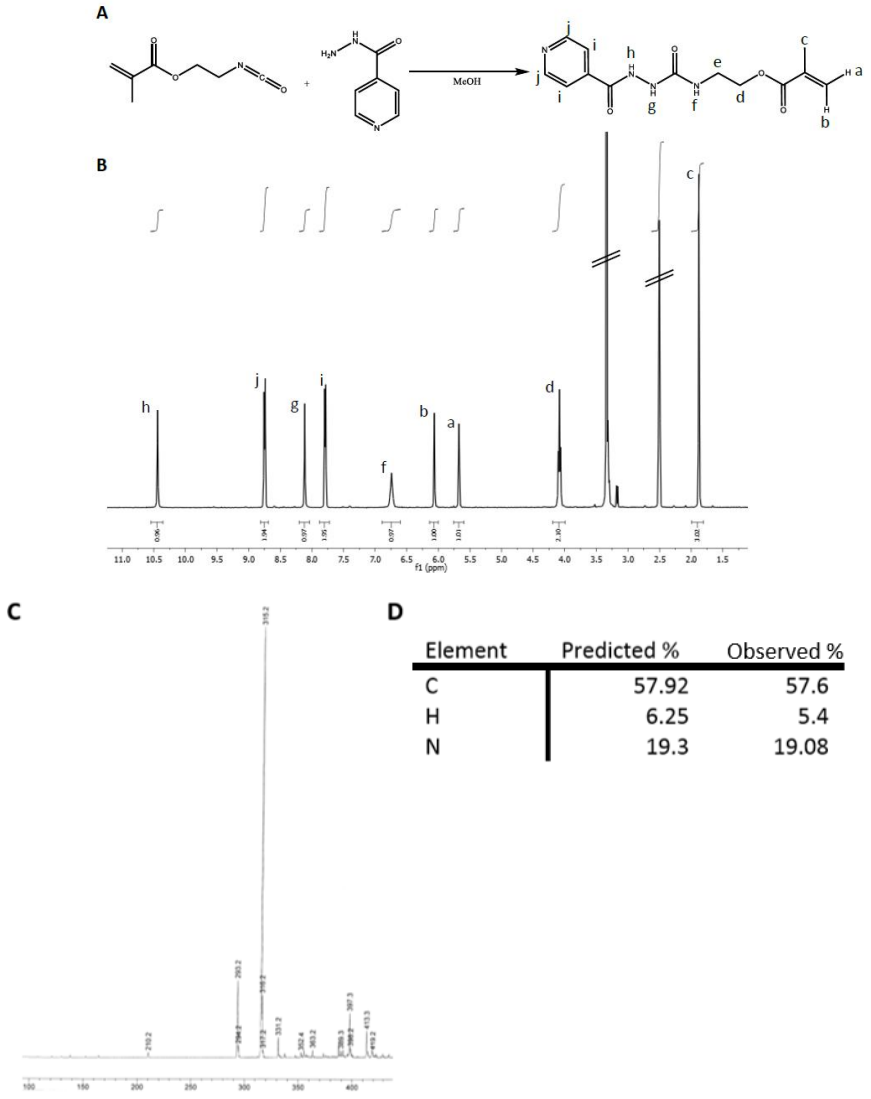


**Figure 4.2:** A) reaction scheme for non-hydrolysable isoniazid monomer (Diacetone acrylamide-*urea*-isoniazid), B) $^{1}$H NMR spectrum, C) mass spectrum showing major expected peak at m/z = 315.2 [Mwt + Na] and D) Elemental analysis of the monomer, showing percentages within the expected range of the proposed monomer structure

### 4.5.3.3 Cyanine 3 Acrylamide Synthesis

Cyanine 3 amine (5 mg, 7.965 mmol, 1 eq.), acryloyl chloride (0.793 mg, 8.76 mmol, 1.1 eq.) and N-methylmorpholine (NMM, 2.42 mg, 23.9 mmol, 3 eq.) were dissolved in 10 mL of chloroform in a 20 mL glass vial charged with a magnetic follower. The vial was sealed with a rubber septum and moved into a cold room to react at 8°C for six hours. The chloroform solvent and NMM was then removed under vacuum using a rotary evaporator, leaving a red crystalline powder. Due to the low mass of reactants, no purification or $^{1}$H NMR spectroscopy was performed, the product was confirmed

using high resolution mass spectrometry and HPLC, showing only the shifted monomer peak in HPLC and m/z in mass spectrometry. (Figure 4.12)

MS: m/z = 609.4 $[Mw]^+$ ($MS_{th}$: 609.42).

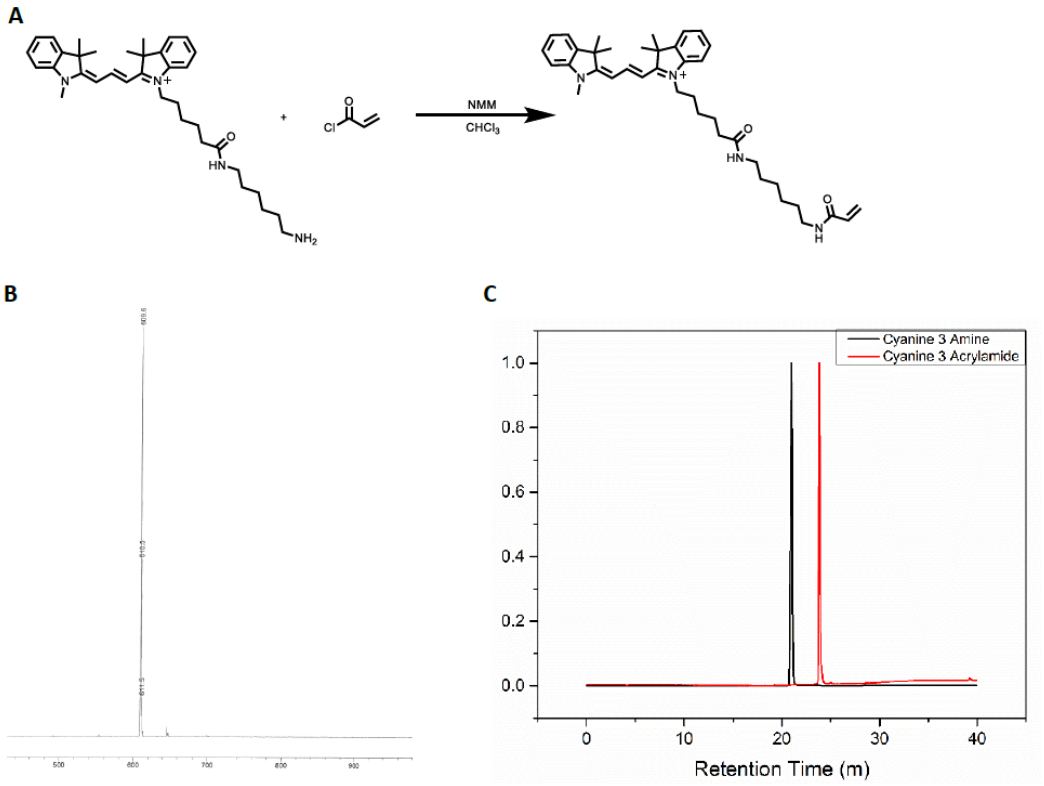


**Figure 4.3:** A) Synthetic scheme of Cy3Am B) Mass spectrum showing expected m/z = 609.6 [Mwt], C) HPLC fluorescence traces of cyanine 3 amine (black) and conjugate product (red) showing clear shift with no trace left of cyanine 3 amine

### 4.5.3.4 General Particle Synthesis Method

Nanoparticles of varying composition were synthesised by varying the monomers in the reaction mixture. The general method by which nanoparticles were prepared is represented by the following, using P(ManAm)-*co*-P(DAAm-*hydrazone*-INH)-*co*-P(DPAEMA) as an example. 50 mg VA-044 (1.6 x $10^{-4}$ mol) was added to 10 mL of deionised water to produce a 5 mg $mL^{-1}$ initiator stock solution. 13 mg of mannose acrylamide (4.67 x$10^{-5}$ M) and 13.5 mg (4.69 x$10^{-5}$ M) DAAm-*hydrazone*-INH was weighed into a tared 7.5 mL glass vial, 1.68 mL of deionised water was then added into the glass vial using an auto-pipette, to which 0.3 mL of the previously described stock solution of VA-044 was added. The glass vial was then charged with a 1 cm magnetic stirrer bar, sealed with a size 21 septum and purged of oxygen by bubbling nitrogen through the solution for 10 minutes. In a separate 20 mL glass vial, sealed

with a size 33 septum, DPAEMA was purged of oxygen by bubbling nitrogen through the liquid monomer for 10 minutes. After both solutions had been purged, 18 mg of DPAEMA ($8.4x10^{-5}$ moles, 0.02 mL)) was transferred into the 7.5 mL glass vial using a gas tight Hamilton syringe that had been purged of oxygen. The 7.5 mL vial was placed into an oil bath set to 50°C and stirred at a rate of 800 rpm for three hours. After approximately 5-10 minutes the reaction mixture turned a uniform white milky colour as the particles nucleated and the polymerisation proceeded. At the end of three hours the reaction was quenched by removing the vial from the oil bath and exposing it to oxygen by removing the septum. The resulting latex was analysed by DLS to determine particle size and dispersity (diameter = 212 nm, Pdi = 0.1) (Figure 4.13)

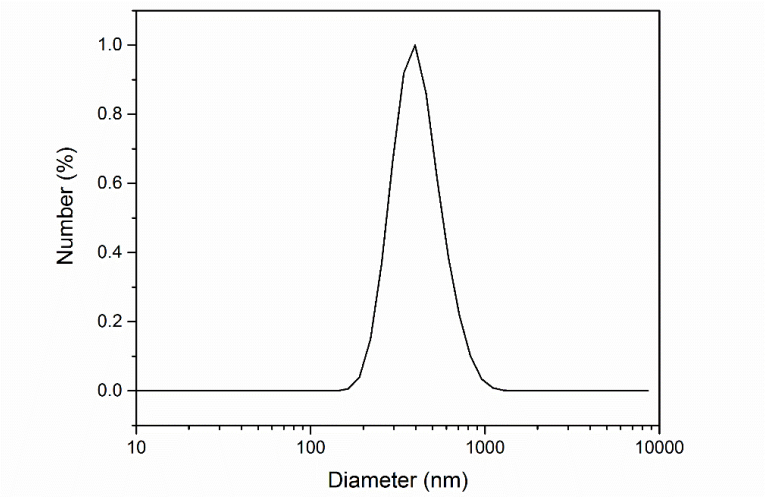


**Figure 4.4** Normalised size distribution by DLS for mannose-(DAAm-hydrazone-INH)-DPAEMA particle, diameter = 212 nm, Pdi = 0.01

## 4.6 References


1. Organization, W. H., Noncommunicable diseases: progress monitor 2017. **2017**.
2. García-Basteiro, A. L.; Brew, J.; Williams, B.; Borgdorff, M.; Cobelens, F., What is the true tuberculosis mortality burden? Differences in estimates by the World Health Organization and the Global Burden of Disease study. *International Journal of Epidemiology* **2018**.
3. Lee, J. Y., Diagnosis and treatment of extrapulmonary tuberculosis. *Tuberculosis Respiratory Diseases* **2015,** *78* (2), 47-55.
4. Glaziou, P.; Floyd, K.; Raviglione, M. C. In *Global Epidemiology of Tuberculosis*, Seminars in Respiratory and Critical Care Medicine, Thieme Medical Publishers: 2018; pp 271-285.
5. Shishido, Y.; Mitarai, S.; Otomo, K.; Seki, M.; Sato, A.; Yano, I.; Koyama, A.; Hattori, T., Anti-tuberculosis drug susceptibility testing of Mycobacterium bovis BCG Tokyo strain. *The International Journal of Tuberculosis Lung Disease* **2007,** *11* (12), 1334-1338.
6. Kolibab, K.; Derrick, S. C.; Morris, S. L., Sensitivity to isoniazid of Mycobacterium bovis BCG strains and BCG disseminated disease isolates. *Journal of Clinical Microbiology* **2011,** *49* (6), 2380-2381.
7. Gilpin, C.; Korobitsyn, A.; Migliori, G. B.; Raviglione, M. C.; Weyer, K., The World Health Organization standards for tuberculosis care and management. Eur Respiratory Soc: 2018.
8. Madigan, C. A.; Cameron, J.; Ramakrishnan, L., A zebrafish model of Mycobacterium leprae granulomatous infection. *The Journal of Infectious Diseases* **2017,** *216* (6), 776-779.
9. Conrad, W. H.; Osman, M. M.; Shanahan, J. K.; Chu, F.; Takaki, K. K.; Cameron, J.; Hopkinson-Woolley, D.; Brosch, R.; Ramakrishnan, L., Mycobacterial ESX-1 secretion system mediates host cell lysis through bacterium contact-dependent gross membrane disruptions. *Proceedings of the National Academy of Sciences* **2017,** *114* (6), 1371-1376.
10. Cambier, C.; O'Leary, S. M.; O'Sullivan, M. P.; Keane, J.; Ramakrishnan, L., Phenolic glycolipid facilitates mycobacterial escape from microbicidal tissue-resident macrophages. *Immunity* **2017,** *47* (3), 552-565. e4.
11. Hayashi, D.; Takii, T.; Mukai, T.; Makino, M.; Yasuda, E.; Horita, Y.; Yamamoto, R.; Fujiwara, A.; Kanai, K.; Kondo, M., Biochemical characteristics among Mycobacterium bovis BCG substrains. *FEMS Microbiology Letters* **2010,** *306* (2), 103-109.
12. Gill, W. P.; Harik, N. S.; Whiddon, M. R.; Liao, R. P.; Mittler, J. E.; Sherman, D. R., A replication clock for Mycobacterium tuberculosis. *Nature Medicine* **2009,** *15* (2), 211.
13. Gebremariam, M. K.; Bjune, G. A.; Frich, J. C., Barriers and facilitators of adherence to TB treatment in patients on concomitant TB and HIV treatment: a qualitative study. *BMC Public Health* **2010,** *10* (1), 651.
14. Kaona, F. A.; Tuba, M.; Siziya, S.; Sikaona, L., An assessment of factors contributing to treatment adherence and knowledge of TB transmission among patients on TB treatment. *BMC Public Health* **2004,** *4* (1), 68.
15. Diacon, A. H.; Dawson, R.; von Groote-Bidlingmaier, F.; Symons, G.; Venter, A.; Donald, P. R.; van Niekerk, C.; Everitt, D.; Winter, H.; Becker, P., 14-

day bactericidal activity of PA-824, bedaquiline, pyrazinamide, and moxifloxacin combinations: a randomised trial. *The Lancet* **2012,** *380* (9846), 986-993.
16. Diacon, A.; Donald, P.; Pym, A.; Grobusch, M.; Patientia, R.; Mahanyele, R.; Bantubani, N.; Narasimooloo, R.; De Marez, T.; Van Heeswijk, R., Randomized pilot trial of eight weeks of bedaquiline (TMC207) treatment for multidrug-resistant tuberculosis: long-term outcome, tolerability, and effect on emergence of drug resistance. *Antimicrobial Agents Chemotherapy* **2012,** *56* (6), 3271-3276.
17. Diacon, A. H.; Pym, A.; Grobusch, M. P.; de Los Rios, J. M.; Gotuzzo, E.; Vasilyeva, I.; Leimane, V.; Andries, K.; Bakare, N.; De Marez, T., Multidrug-resistant tuberculosis and culture conversion with bedaquiline. *New England Journal of Medicine* **2014,** *371* (8), 723-732.
18. Raju, R. M.; Unnikrishnan, M.; Rubin, D. H.; Krishnamoorthy, V.; Kandror, O.; Akopian, T. N.; Goldberg, A. L.; Rubin, E. J., Mycobacterium tuberculosis ClpP1 and ClpP2 function together in protein degradation and are required for viability in vitro and during infection. *PLoS Pathogens* **2012,** *8* (2), e1002511.
19. Gelperina, S.; Kisich, K.; Iseman, M. D.; Heifets, L., The potential advantages of nanoparticle drug delivery systems in chemotherapy of tuberculosis. *American Journal of Respiratory Critical Care Medicine* **2005,** *172* (12), 1487-1490.
20. Mignani, S.; Tripathi, R.; Chen, L.; Caminade, A.-M.; Shi, X.; Majoral, J.-P., New Ways to Treat Tuberculosis Using Dendrimers as Nanocarriers. *Pharmaceutics* **2018,** *10* (3), 105.
21. Su, F.-Y.; Chen, J.; Son, H.-N.; Kelly, A. M.; Convertine, A. J.; West, T. E.; Skerrett, S. J.; Ratner, D. M.; Stayton, P. S., Polymer-augmented liposomes enhancing antibiotic delivery against intracellular infections. *Biomaterials Science* **2018**.
22. Rao, M.; Streur, T. L.; Aldwell, F. E.; Cook, G. M., Intracellular pH regulation by Mycobacterium smegmatis and Mycobacterium bovis BCG. *Microbiology* **2001,** *147* (4), 1017-1024.
23. Ohkuma, S.; Poole, B., Fluorescence probe measurement of the intralysosomal pH in living cells and the perturbation of pH by various agents. *Proceedings of the National Academy of Sciences* **1978,** *75* (7), 3327-3331.
24. Su, F.-Y.; Srinivasan, S.; Lee, B.; Chen, J.; Convertine, A. J.; West, T. E.; Ratner, D. M.; Skerrett, S. J.; Stayton, P. S., Macrophage-targeted drugamers with enzyme-cleavable linkers deliver high intracellular drug dosing and sustained drug pharmacokinetics against alveolar pulmonary infections. *Journal of Controlled Release* **2018,** *287*, 1-11.
25. Crisan, D. N.; Creese, O.; Ball, R.; Brioso, J. L.; Martyn, B.; Montenegro, J.; Fernandez-Trillo, F., Poly (acryloyl hydrazide), a versatile scaffold for the preparation of functional polymers: synthesis and post-polymerisation modification. *Polymer Chemistry* **2017,** *8* (31), 4576-4584.
26. Prabaharan, M.; Grailer, J. J.; Pilla, S.; Steeber, D. A.; Gong, S., Amphiphilic multi-arm-block copolymer conjugated with doxorubicin via pH-sensitive hydrazone bond for tumor-targeted drug delivery. *Biomaterials* **2009,** *30* (29), 5757-5766.
27. Takeuchi, I.; Nobata, S.; Oiri, N.; Tomoda, K.; Makino, K., Biodistribution and excretion of colloidal gold nanoparticles after intravenous injection: Effects of particle size. *Bio-Medical Materials Engineering* **2017,** *28* (3), 315-323.
28. Madsen, J.; Madden, G.; Themistou, E.; Warren, N. J.; Armes, S. P., pH-Responsive diblock copolymers with two different fluorescent labels for simultaneous monitoring of micellar self-assembly and degree of protonation. *Polymer Chemistry* **2018,** *9* (21), 2964-2976.

29. Qiu, S.; Huang, H.; Dai, X. H.; Zhou, W.; Dong, C. M., Star-shaped polypeptide/glycopolymer biohybrids: Synthesis, self-assembly, biomolecular recognition, and controlled drug release behavior. *Journal of Polymer Science Part A: Polymer Chemistry* **2009,** *47* (8).
30. Boye, S.; Appelhans, D.; Boyko, V.; Zschoche, S.; Komber, H.; Friedel, P.; Formanek, P.; Janke, A.; Voit, B.; Lederer, A., pH-triggered aggregate shape of different generations lysine-dendronized maleimide copolymers with maltose shell. *Biomacromolecules* **2012,** *13* (12), 4222-4235.
31. Bae, Y.; Nishiyama, N.; Fukushima, S.; Koyama, H.; Yasuhiro, M.; Kataoka, K., Preparation and biological characterization of polymeric micelle drug carriers with intracellular pH-triggered drug release property: tumor permeability, controlled subcellular drug distribution, and enhanced in vivo antitumor efficacy. *Bioconjugate Chemistry* **2005,** *16* (1), 122-130.
32. Smith, A. E.; Xu, X.; McCormick, C. L., Stimuli-responsive amphiphilic (co) polymers via RAFT polymerization. *Progress in Polymer Science* **2010,** *35* (1-2), 45-93.
33. Yuan, W.; Yuan, J.; Zheng, S.; Hong, X., Synthesis, characterization, and controllable drug release of dendritic star-block copolymer by ring-opening polymerization and atom transfer radical polymerization. *Polymer* **2007,** *48* (9), 2585-2594.
34. Bütün, V.; Bennett, C. E.; Vamvakaki, M.; Lowe, A. B.; Billingham, N. C.; Armes, S. P., Selective betainisation of tertiary amine methacrylate blockcopolymers. *Journal of Materials Chemistry B* **1997,** *7* (9), 1693-1695.
35. Sun, X.; Jiang, G.; Wang, Y.; Xu, Y., Synthesis and drug release properties of novel pH-and temperature-sensitive copolymers based on a hyperbranched polyether core. *Colloid Polymer Science* **2011,** *289* (5-6), 677-684.
36. Chono, S.; Tanino, T.; Seki, T.; Morimoto, K., Efficient drug targeting to rat alveolar macrophages by pulmonary administration of ciprofloxacin incorporated into mannosylated liposomes for treatment of respiratory intracellular parasitic infections. *Journal of Controlled Release* **2008,** *127* (1), 50-58.
37. Wijagkanalan, W.; Kawakami, S.; Takenaga, M.; Igarashi, R.; Yamashita, F.; Hashida, M., Efficient targeting to alveolar macrophages by intratracheal administration of mannosylated liposomes in rats. *Journal of Controlled Release* **2008,** *125* (2), 121-130.
38. Chono, S.; Tanino, T.; Seki, T.; Morimoto, K., Uptake characteristics of liposomes by rat alveolar macrophages: influence of particle size and surface mannose modification. *Journal of Pharmacy Pharmacology* **2007,** *59* (1), 75-80.
39. Yilmaz, G.; Becer, C. R., Precision glycopolymers and their interactions with lectins. *European Polymer Journal* **2013,** *49* (10), 3046-3051.
40. Azad, A. K.; Rajaram, M. V.; Schlesinger, L. S., Exploitation of the macrophage mannose receptor (CD206) in infectious disease diagnostics and therapeutics. *Journal of Cytology Molecular Biology* **2014,** *1* (1).
41. Chono, S.; Tanino, T.; Seki, T.; Morimoto, K., Uptake characteristics of liposomes by rat alveolar macrophages: influence of particle size and surface mannose modification. *Journal of Pharmacy Pharmacology and Therapeutics* **2007,** *59* (1), 75-80.
42. Irache, J. M.; Salman, H. H.; Gamazo, C.; Espuelas, S., Mannose-targeted systems for the delivery of therapeutics. *Expert Opinion on Drug Delivery* **2008,** *5* (6), 703-724.

43. Taylor, M. E., Primary structure of the mannose receptor contains multiple motifs resembling carbohydrate-recognition domains. *The Journal of Biological Chemistry* **1990,** *265* (21), 12156-12162.
44. Ponader, D.; Maffre, P.; Aretz, J.; Pussak, D.; Ninnemann, N. M.; Schmidt, S.; Seeberger, P. H.; Rademacher, C.; Nienhaus, G. U.; Hartmann, L., Carbohydrate-lectin recognition of sequence-defined heteromultivalent glycooligomers. *Journal of the American Chemical Society* **2014,** *136* (5), 2008-2016.
45. Pieters, R. J., Maximising multivalency effects in protein–carbohydrate interactions. *Organic and Biomolecular Chemistry* **2009,** *7* (10), 2013-2025.
46. Gurnani, P.; Lunn, A. M.; Perrier, S., Synthesis of mannosylated and PEGylated nanoparticles via RAFT emulsion polymerisation, and investigation of particle-lectin aggregation using turbidimetric and DLS techniques. *Polymer* **2016,** *106*, 229-237.
47. Lunn, A. M.; Perrier, S., Synthesis of Sub-100 nm Glycosylated Nanoparticles via a One Step, Free Radical, and Surfactant Free Emulsion Polymerization. *Macromolecular Rapid Communications* **2018**, 1800122.
48. He, C.; Hu, Y.; Yin, L.; Tang, C.; Yin, C., Effects of particle size and surface charge on cellular uptake and biodistribution of polymeric nanoparticles. *Biomaterials* **2010,** *31* (13), 3657-3666.
49. Shang, L.; Nienhaus, K.; Nienhaus, G. U., Engineered nanoparticles interacting with cells: size matters. *Journal of Nanobiotechnology* **2014,** *12* (1), 5.
50. Banik, N.; Hussain, A.; Ramteke, A.; Sharma, H. K.; Maji, T. K., Preparation and evaluation of the effect of particle size on the properties of chitosan-montmorillonite nanoparticles loaded with isoniazid. *RSC Advances* **2012,** *2* (28), 10519-10528.
51. Pandey, R.; Zahoor, A.; Sharma, S.; Khuller, G., Nanoparticle encapsulated antitubercular drugs as a potential oral drug delivery system against murine tuberculosis. *Tuberculosis* **2003,** *83* (6), 373-378.
52. Rani, S.; Gothwal, A.; Khan, I.; Pachouri, P. K.; Bhaskar, N.; Gupta, U. D.; Chauhan, D. S.; Gupta, U., Smartly Engineered PEGylated Di-Block Nanopolymeric Micelles: Duo Delivery of Isoniazid and Rifampicin Against Mycobacterium tuberculosis. *AAPS PharmSciTech* **2018,** *19* (7), 3237-3248.
53. Shen, S.; Wu, Y.; Liu, Y.; Wu, D., High drug-loading nanomedicines: progress, current status, and prospects. *International Journal of Nanomedicine* **2017,** *12*, 4085.
54. WHO; Organization, W. H., *Guidelines on the Management of Latent Tuberculosis Infection*. World Health Organization: 2015.
55. Hwang, A. A.; Lee, B. Y.; Clemens, D. L.; Dillon, B. J.; Zink, J. I.; Horwitz, M. A., pH-Responsive Isoniazid-Loaded Nanoparticles Markedly Improve Tuberculosis Treatment in Mice. *Small* **2015,** *11* (38), 5066-5078.
56. Nkanga, C. I.; Walker, R. B.; Krause, R. W., pH-Dependent release of isoniazid from isonicotinic acid (4-hydroxy-benzylidene)-hydrazide loaded liposomes. *Journal of Drug Delivery Science Technology* **2018,** *45*, 264-271.
57. Nkanga, C. I.; Krause, R. W. M., Conjugation of isoniazid to a zinc phthalocyanine via hydrazone linkage for pH-dependent liposomal controlled release. *Applied Nanoscience* **2018**, 1-11.
58. Xu, X.; Smith, A. E.; Kirkland, S. E.; McCormick, C. L., Aqueous RAFT synthesis of pH-responsive triblock copolymer mPEO− PAPMA− PDPAEMA and formation of shell cross-linked micelles. *Macromolecules* **2008,** *41* (22), 8429-8435.

59. Kakwere, H.; Perrier, S., Design of complex polymeric architectures and nanostructured materials/hybrids by living radical polymerization of hydroxylated monomers. *Polymer Chemistry* **2011,** *2* (2), 270-288.
60. Hwang, S.-H.; Thielbeer, F.; Jeong, J.; Han, Y.; Chankeshwara, S. V.; Bradley, M.; Cho, W.-S., Dual contribution of surface charge and protein-binding affinity to the cytotoxicity of polystyrene nanoparticles in nonphagocytic A549 cells and phagocytic THP-1 cells. *Journal of Toxicology Environmental Health, Part A* **2016,** *79* (20), 925-937.
61. Kalluru, R.; Fenaroli, F.; Westmoreland, D.; Ulanova, L.; Maleki, A.; Roos, N.; Madsen, M. P.; Koster, G.; Jacobsen, W. E.; Wilson, S., Polylactide-co-glycolide-rifampicin-nanoparticles efficiently clear Mycobacterium bovis BCG infection in macrophages and remain membrane-bound in phago-lysosomes. *Cell Sci* **2013**, jcs. 121814.
62. Patel, B.; Gupta, N.; Ahsan, F., Particle engineering to enhance or lessen particle uptake by alveolar macrophages and to influence the therapeutic outcome. *European Journal of Pharmaceutics Biopharmaceutics* **2015,** *89*, 163-174.
63. Pei, Y.; Yeo, Y., Drug delivery to macrophages: Challenges and opportunities. *Journal of Controlled Release* **2016,** *240*, 202-211.
64. Filatova, L. Y.; Klyachko, N. L.; Kudryashova, E. V., Targeted delivery of anti-tuberculosis drugs to macrophages: targeting mannose receptors. *Russian Chemical Reviews* **2018,** *87* (4), 374.
65. Park, J. S.; Lee, J.-Y.; Lee, Y. J.; Kim, S. J.; Cho, Y.-J.; Yoon, H. I.; Lee, C.-T.; Song, J.; Lee, J. H., Serum levels of antituberculosis drugs and their effect on tuberculosis treatment outcome. *Antimicrobial Agents Chemotherapy* **2016,** *60* (1), 92-98.
66. Seth, V.; Beotra, A.; Seth, S.; Semwal, O.; Kabra, S.; Jain, Y.; Mukhopadhya, S., Serum concentrations of rifampicin and isoniazid in tuberculosis. *Indian Pediatrics* **1993,** *30* (9), 1091-1098.
67. Horváti, K.; Bacsa, B.; Kiss, E. v.; Gyulai, G.; Fodor, K.; Balka, G.; Rusvai, M. s.; Szabó, E. r.; Hudecz, F.; Bősze, S., Nanoparticle encapsulated lipopeptide conjugate of antitubercular drug isoniazid: in vitro intracellular activity and in vivo efficacy in a Guinea pig model of tuberculosis. *Bioconjugate Chemistry* **2014,** *25* (12), 2260-2268.
68. Toma, C. C.; Aloisi, A.; Bordoni, V.; Di Corato, R.; Rauner, M.; Cuniberti, G.; Delogu, L. G.; Rinaldi, R., Immune Profiling of Polysaccharide Submicron Vesicles. *Biomacromolecules* **2018,** *19* (8), 3560-3571.
69. Richards, S. J.; Jones, A.; Tomás, R. M.; Gibson, M. I., Photochemical "In-Air" Combinatorial Discovery of Antimicrobial Co-polymers. *Chemistry–A European Journal* **2018**.
70. Li, W.-J.; Tang, X.-F.; Shuai, X.-X.; Jiang, C.-J.; Liu, X.; Wang, L.-F.; Yao, Y.-F.; Nie, S.-P.; Xie, M.-Y., Mannose receptor mediates the immune response to Ganoderma atrum polysaccharides in macrophages. *Journal of Agricultural Food Chemistry* **2017,** *65* (2), 348-357.
71. Kuroki, A.; Sangwan, P.; Qu, Y.; Peltier, R.; Sanchez-Cano, C.; Moat, J.; Dowson, C. G.; Williams, E. G.; Locock, K. E.; Hartlieb, M., Sequence Control as a Powerful Tool for Improving the Selectivity of Antimicrobial Polymers. *ACS Applied Materials Interfaces* **2017,** *9* (46), 40117-40126.
72. Phillips, D. J.; Harrison, J.; Richards, S.-J.; Mitchell, D. E.; Tichauer, E.; Hubbard, A. T.; Guy, C.; Hands-Portman, I.; Fullam, E.; Gibson, M. I., Evaluation

of the antimicrobial activity of cationic polymers against mycobacteria: Toward antitubercular macromolecules. *Biomacromolecules* **2017,** *18* (5), 1592-1599.
73. Richards, S.-J.; Isufi, K.; Wilkins, L. E.; Lipecki, J.; Fullam, E.; Gibson, M. I., Multivalent Antimicrobial Polymer Nanoparticles Target Mycobacteria and Gram-Negative Bacteria by Distinct Mechanisms. *Biomacromolecules* **2017,** *19* (1), 256-264.
74. Passarini, I.; Rossiter, S.; Malkinson, J.; Zloh, M., In silico structural evaluation of short cationic antimicrobial peptides. *Pharmaceutics* **2018,** *10* (3), 72.
75. Varkouhi, A. K.; Scholte, M.; Storm, G.; Haisma, H. J., Endosomal escape pathways for delivery of biologicals. *Journal of Controlled Release* **2011,** *151* (3), 220-228.

## 4.7 Appendices

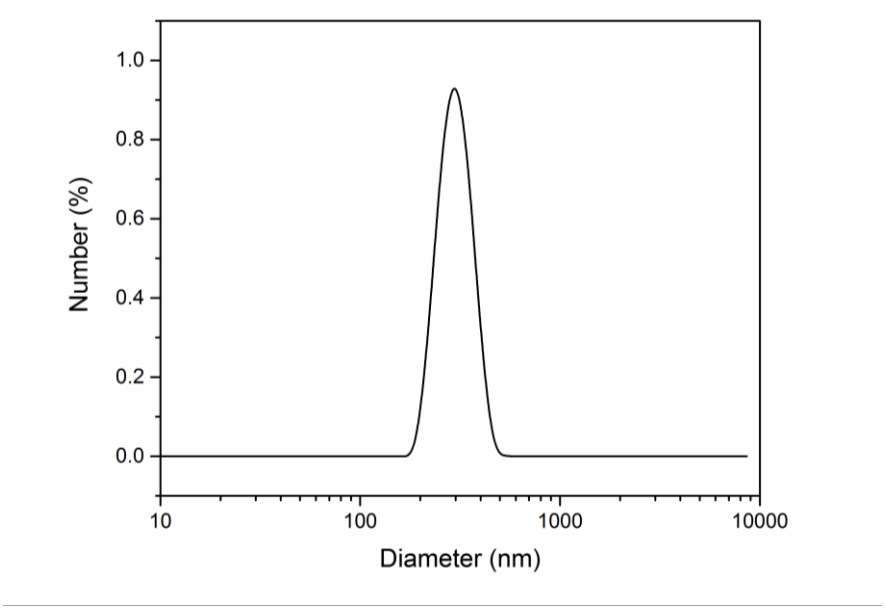


**A4.1**: Normalised size distribution by DLS for mannose-DPAEMA particle, diameter = 210 nm, Pdi = 0.08

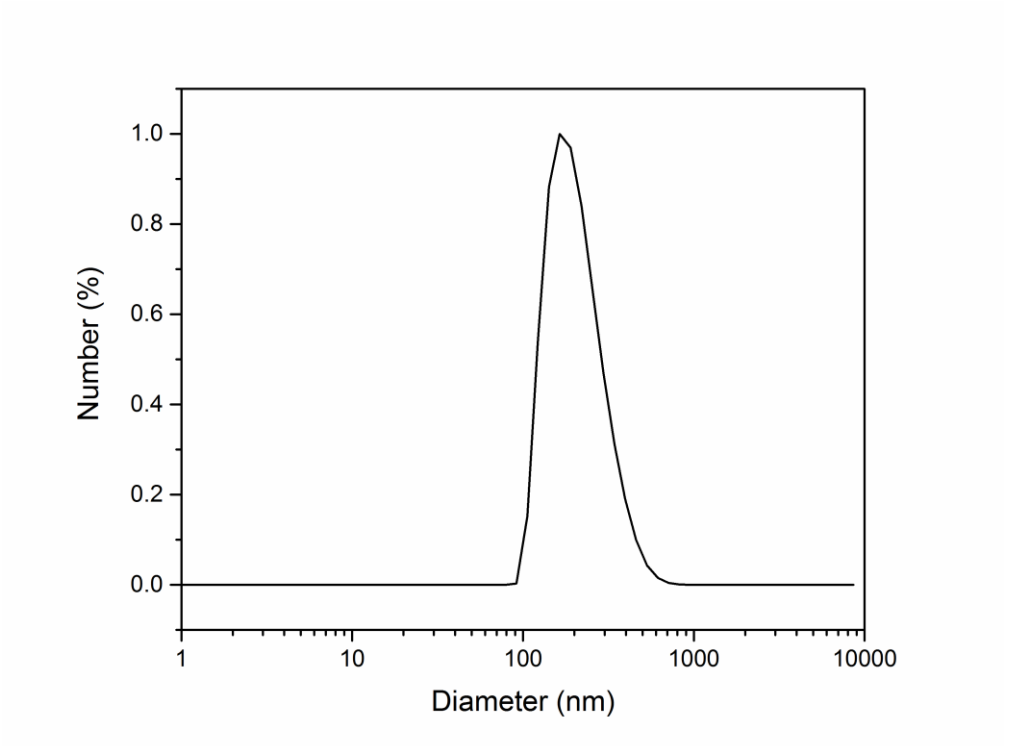


**A4.2**: Normalised size distribution by DLS for mannose-(*urea*-INH)-DPAEMA particle, diameter = 280 nm Pdi = 0.04

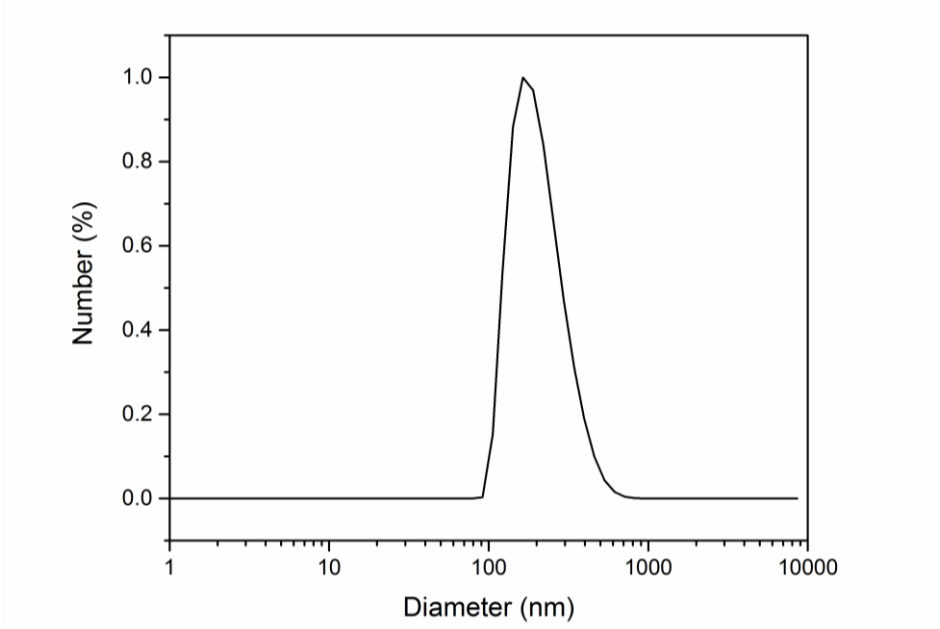


**A4.3**: Normalised size distribution by DLS for PEGA-DPAEMA particle, diameter = 212 nm, Pdi = 0.14

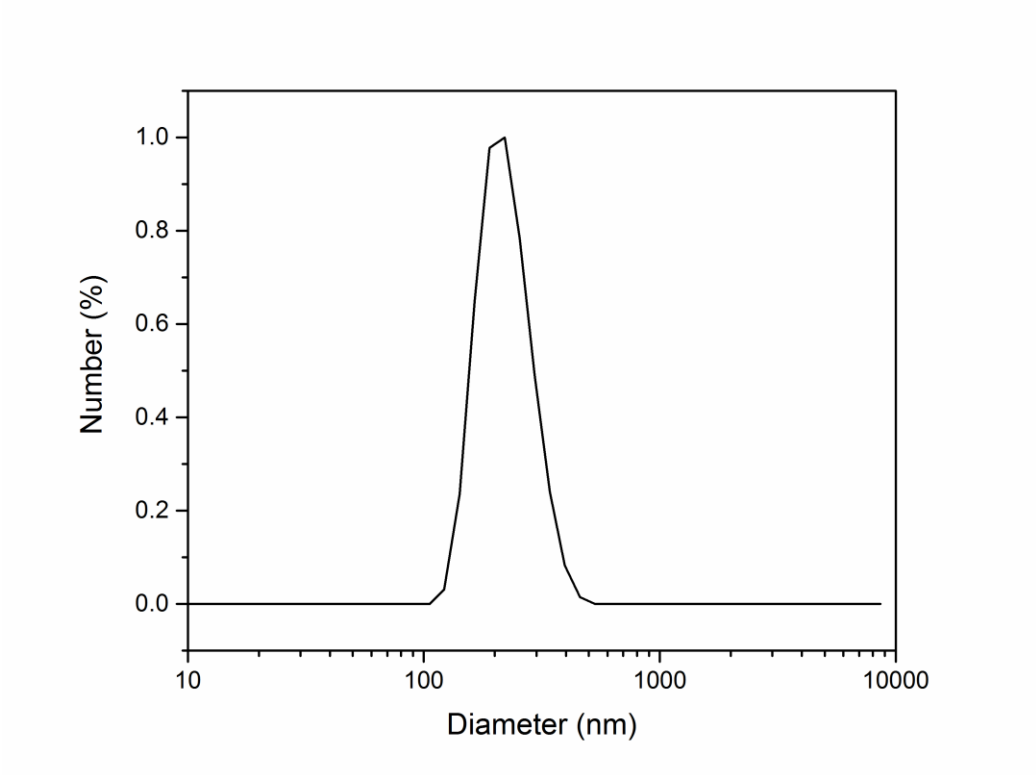


**A4.4**: Normalised size distribution by DLS for PEGA-(DAAm-*Hydrazone*-INH)-DPAEMA particle, diameter 225 nm, Pdi = 0.07

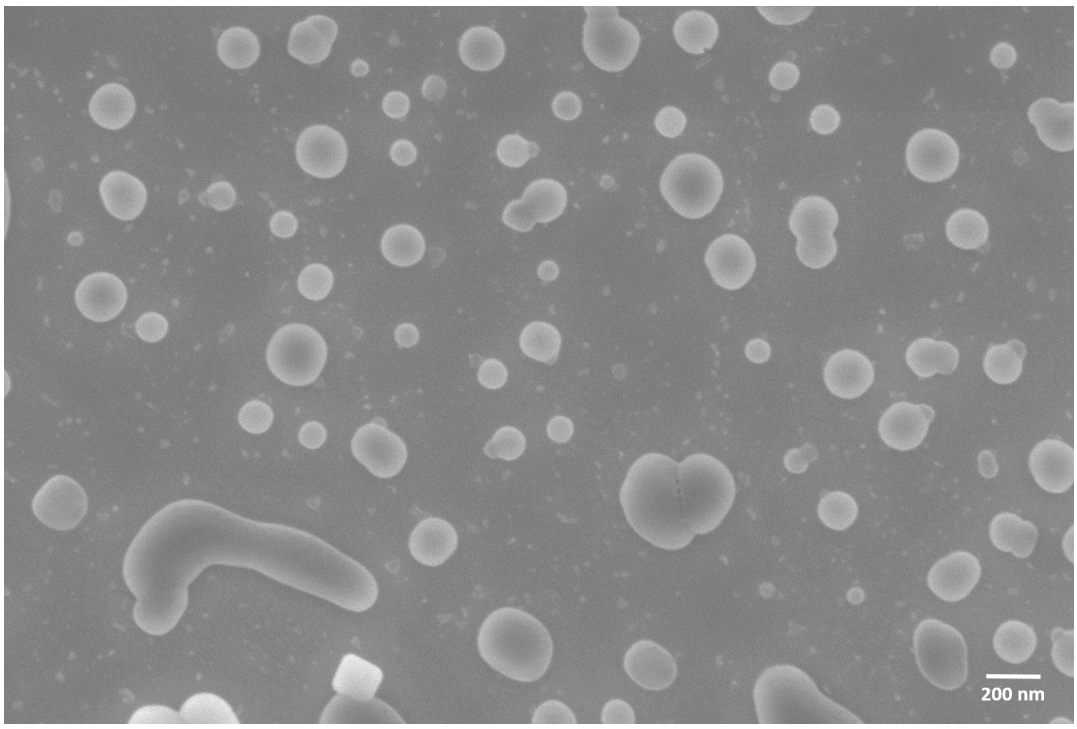


**A4.5**: Representative SEM Image of mannose-(DAAm-*hydrazone*-INH)-DPAEMA-Cy3Am particle, diameter = 175 nm Pdi = 0.1

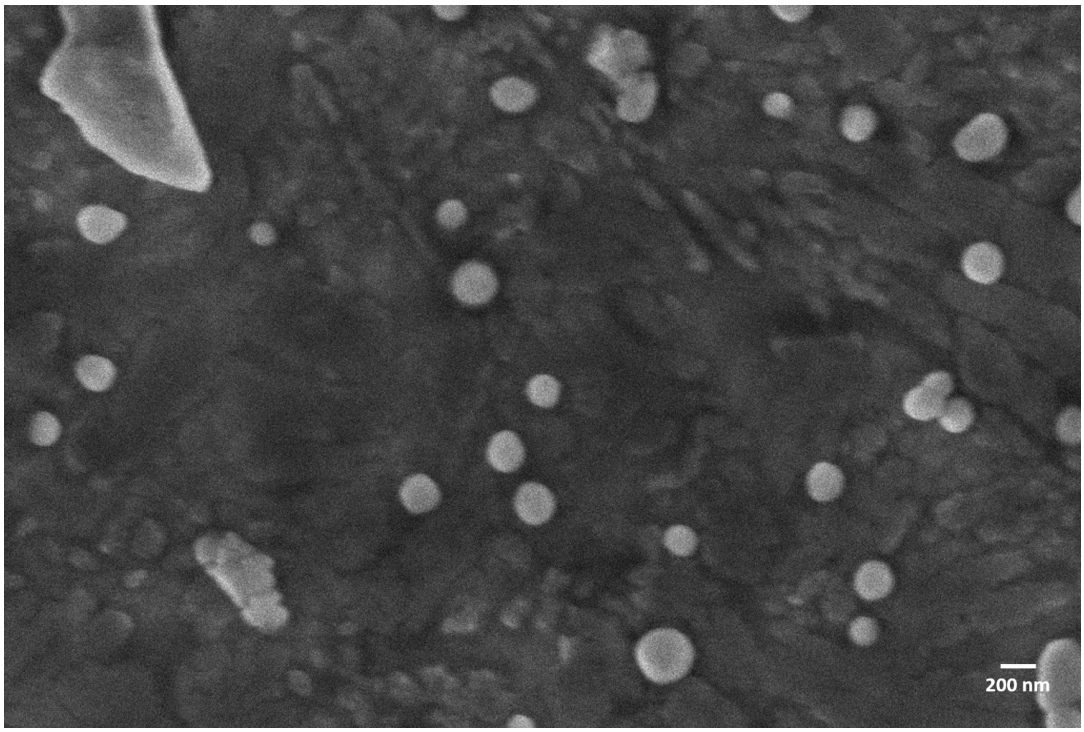


**A4.6:** Representative SEM Image of PEGA-(DAAm-*hydrazone*-INH)-DPAEMA-Cy3Am particle, diameter= 205 nm Pdi = 0.04

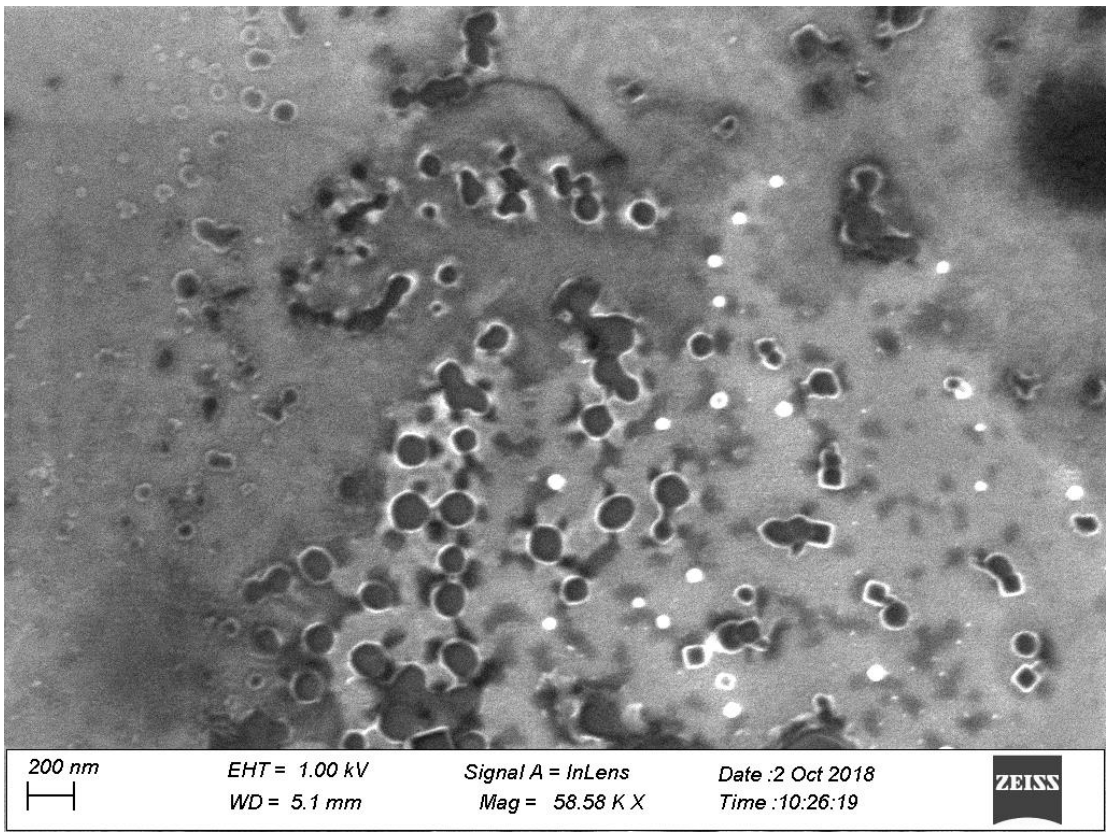


**A4.7**: Representative SEM Image of mannose-DPAEMA-Cy3Am particle, diameter = 231 nm Pdi = 0.03

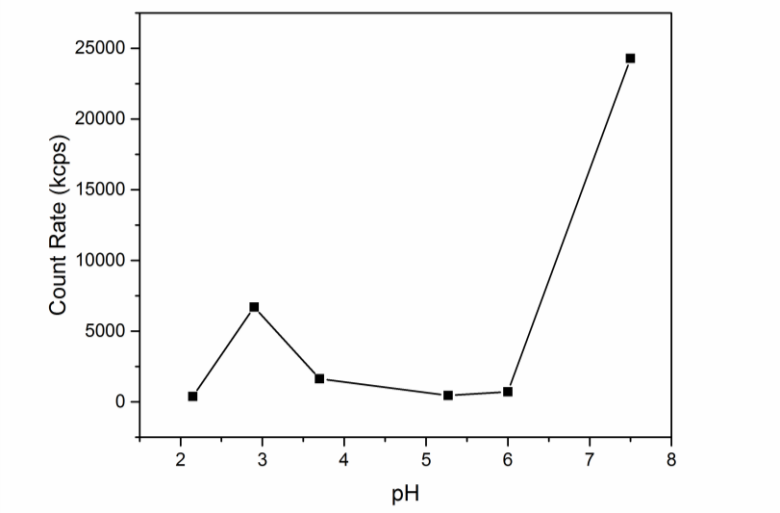


**A4.8:** DLS count rate of mannose-(DAAm-*hydrazone*-INH)-DPAEMA at different pHs, showing reduction at pH 6, indicative of particle break up due to protonation of tertiary amine on DPAEMA

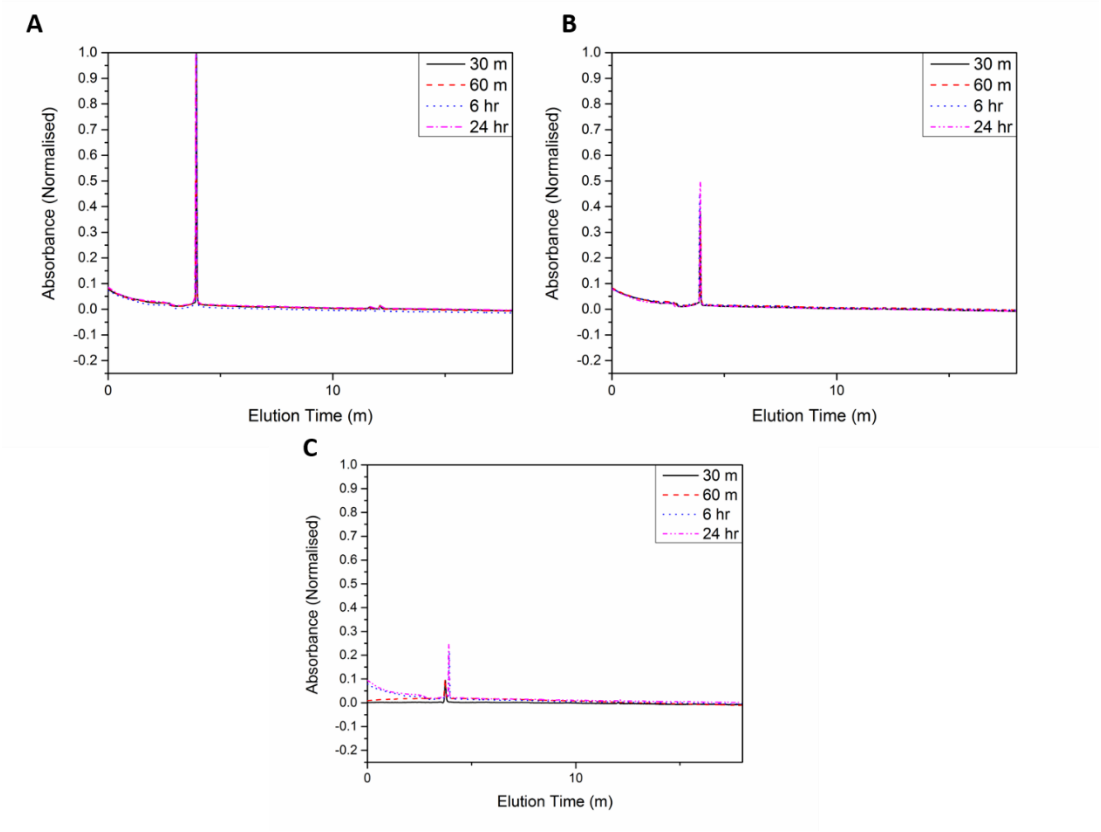


**A4.9:** Overlaid HPLC traces for mannose-(DAAm-*hydrazone*-INH)-DPAEMA, particle incubated at pH: 7 (A), 5(B) and 3(C) for 30 minutes, 60 minutes, 6 hours and 24 hours, showing increased isoniazid release at lower pH due to hydrolysis of hydrazone linker

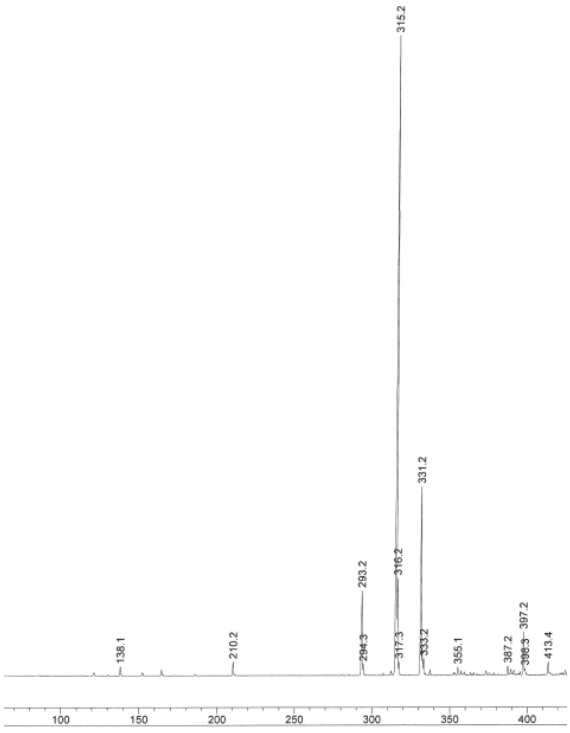


**A4.10**: Representative mass spectrum of non-responsive *urea*-isoniazid monomer at pH 3 for 24 hours, showing no peak from free isoniazid at an m/z of 160 [isoniazid+Na] indicating no hydrolysis of the urea linker.

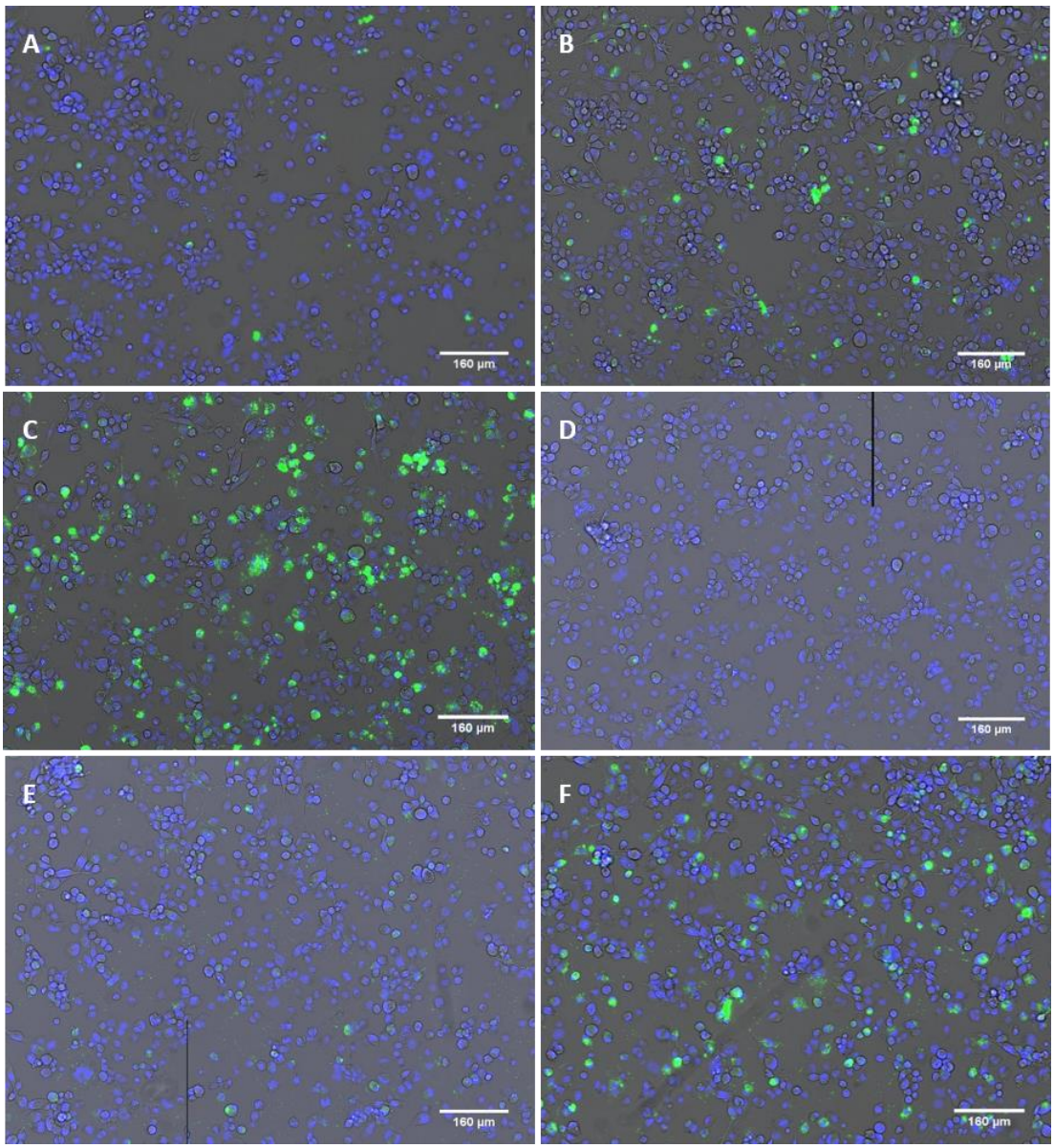


**A4.11**: Example images of particle uptake taken using a Cytation3 plate reader, and analysed to determine the level of endocytosis. In all images: green indicates Cy3Am labelled particles, blue indicates Hoechst 33342 stained nuclei and images are overlaid with greyscale light microscopy. A) mannose particles 2 hrs, B) mannose particles 6 hrs, C) mannose particles 24 hrs, D) PEGA particles 2 hrs, E) PEGA particles 6 hrs, F) PEGA particles 24 hrs.

| | A | B | C | D | E | F | G |
|---|---|---|---|---|---|---|---|
| A) 4 hr + control | | 0.278267 | 0.119908 | 0.033206 | 0 | 0 | 0 |
| B) 24 hr + control | 0.278267 | | 0.000208 | 0.000036 | 0 | 0 | 0 |
| C) Mannose-DPAEMA | 0.119908 | 0.000208 | | 0.9979 | 0 | 0 | 0 |
| D) Mannose-(DAAm-urea-Isoniazid)-DPAEMA | 0.033206 | 0.000036 | 0.9979 | | 0 | 0 | 0 |
| E) PEGA-(DAAm-hydrazone-Isoniazid)-DPAEMA | 0 | 0 | 0 | 0 | | 1 | 1 |
| F) Mannose-(DAAm-hydrazone-Isoniazid)-DPAEMA | 0 | 0 | 0 | 0 | 0 | | 1 |
| G) Isoniazid | 0 | 0 | 0 | 0 | 1 | 1 | |

**A4.12**: Full ANOVA-Tukey table of results for intracellular bacterial killing comparing ManAm-(DAAm-*hydrazone*-Isoniazid)-DPAEMA particles with controls

| | A | B | C | D | E |
|---|---|---|---|---|---|
| A) 4 hr + control | | 0.002 | 1.000 | 0.991 | 0.000 |
| B) 24 hr + control | 0.002 | | 0.001 | 0.006 | 0.000 |
| C) Mannose-DPAEMA | 1.000 | 0.001 | | 0.972 | 0.000 |
| D) PEGA-DPAEMA | 0.991 | 0.006 | 0.972 | | 0.000 |
| E) Isoniazid | 0.000 | 0.000 | 0.000 | 0.000 | |

**A4.13**: Full ANOVA-Tukey table of results for intracellular bacterial killing comparing ManAm-DPAEMA to PEGA-DPAEMA particles with an isoniazid control

# *Chapter 5*

**Conclusions and Outlook**

The overall aim of this thesis has been to explore the simplest methods to synthesise glyconanoparticles suitable for use both in fundamental studies, and as clinically scalable targeted drug delivery agents. The initial use of a RAFT emulsion polymerisation technique performed well in producing highly controlled particles, to develop a DLS based technique to track particle aggregation. The subsequent synthesis, using a free radical and surfactant free emulsion polymerisation, was shown to be suitable for use in aggregation studies and also applied to drug delivery with successful intracellular antibiotic delivery.

Chapter Two focussed on the synthesis of mannosylated nanoparticles *via* RAFT emulsion polymerisation. This was achieved with the initial synthesis of a poly(mannose acrylamide)$_{10}$-*b*-poly(butyl acrylate)$_{15}$ di-block used as a polymeric surfactant in an emulsion polymerisation with butyl acrylate producing a library of nanoparticles of varying diameter. The control of particle size was confirmed with a calibration of targeted molecular weight against the resulting particle volume. Using the characterised mannose-butyl acrylate particles an online DLS based system for tracking particle-lectin binding was developed. The system exploited a cannula injection system to introduce the lectin Con A causing aggregation, whilst the instrument was recording particle size. The technique was shown comparable to the standard UV-Vis turbidimetric experiments used for aggregation studies. Furthermore aggregate size data was applied to give an estimation of the number of particles present per aggregate (up to a sedimentation size limit). This allowed quantitative comparison of aggregation between particles, revealing that larger particles displayed increased aggregation. This finding was only possible using the developed DLS technique, as the increased scattering response from larger particles and aggregates could be separated from each other. RAFT emulsion polymerisation as a technique however has potential scale up and biocompatibility issues.

In efforts to address these issues, Chapter Three focussed on developing the simplest technique possible for synthesising glycoparticles with comparable properties to those produced by RAFT emulsion polymerisation. To do this a free radical and surfactant

free emulsion polymerisation was investigated. Previous studies had shown that stable particles could be produced using this technique using a highly charged initiator. It was shown that the initiator, 4,4'-azobis(4-cyanovaleric acid), could also be used and gave adequate particle stability. The potential for this technique to produce surface functionalised particles was also shown. Co-polymerisation of a hydrophilic monomer was shown to successfully incorporate c.50% of monomer onto the resulting nanoparticles. This allowed for the synthesis of glycosylated nanoparticles in a three hour synthesis from monomer to final latex. Furthermore the incorporation of monomer into the particle surface facilitated particle size control. By using a sterically large and highly water soluble monomer, particle diameters under 100 nm were reliably accessed without the need for time consuming controlled polymer synthesis or the addition of any potentially toxic surfactant. This technique does however leave a large amount of linear homopolymer in solution that is able to compete for lectin binding sites and is limited to a total solids content of around 15-20%. Particles synthesised using this technique were then used to investigate the effect of particle core glass transition temperature ($T_g$) on lectin induced aggregation. Using the previously developed DLS aggregation method and cryo-TEM, "soft" particles above their $T_g$ were shown to be able to deform and form larger aggregates, owing to the stronger multivalent interactions possible from the increased surface area between the particles.

Finally Chapter Four took the previously explored free radical, surfactant free emulsion polymerisation technique for producing glyconanoparticles and applied it to the delivery of an antibiotic. A system was designed and synthesised to target intracellular mycobacteria in macrophage cells, for the eventual treatment of tuberculosis. The particle system had a mannose surface, to target macrophages *via* sugar lectin interactions. A relevant antibiotic was covalently loaded into the particles, by co-polymerising a synthesised pH responsive monomer with a hydrazone linker between isoniazid and diacetone acrylamide. Finally the core of the particle was made with poly(2-(diisopropylamino)ethyl methacrylate) (P(DPAEMA)), to impart a second pH response, breaking up the particles in acidic pH. The synthesised particles were shown to be able to target the cell surface lectins on macrophages, and using *in vitro* techniques to release the bound isoniazid and break up into linear polymer at the reduced phagolysosomal pH. These particles were then shown superior in killing intracellular bacillus calmette guerin (BCG) in THP-1 derived macrophages, showing

significantly superior activity against controls. They were also shown to be statistically equivalent to free isoniazid at the same concentration as in the particles. Furthermore the mannose-isoniazid particle system was the only treatment that showed complete bacterial eradiation (within the resolution of the technique used).

In summary this thesis has presented two techniques for the synthesis of glycosylated nanoparticles. The first, RAFT emulsion polymerisation has been shown a reliable technique able to access a range of particle size. These particles are of particular use for fundamental studies as they have a known surface functionalisation and more controlled molecular weights, removing these as sources of error. The second, a simpler free radical and surfactant free technique, has been shown to be suited to the synthesis of glyconanoparticles for biological applications as it is cheaper, faster and uses fewer potentially toxic chemicals. A DLS based system for tracking and quantifying particle aggregation has been developed and used to show that larger glycoparticles undergo greater lectin induced aggregation, and that particles above their $T_g$ can deform under lectin induced aggregation to show closer packing than hard spheres and form larger aggregates. Finally a dual pH responsive glyconanoparticulate drug delivery system was developed, successfully delivering isoniazid intracellularly in macrophages to effectively eradicate intracellular BCG.

Going forward, the same tests bacterial killing test performed in Chapter Four would need to be repeated on *Mycobacterium tuberculosis* to show efficacy against the most prevalent TB causing pathogen. This would then lead to *in vivo* biological tests to determine the full benefit of delivering isoniazid with such a system, compared to a PEGylated equivalent and free isoniazid. The hypothesis being that intracellular concentrations of isoniazid would be increased compared to free isoniazid due to increased uptake owing to the particle size, and compared to the PEGylated system due to targeting of the macrophage through sugar-lectin interactions.

It would also be of interest to produce similar drug delivery systems with varying particle core $T_g$'s and explore the influence this has on cellular uptake and ultimately biological activity of a delivered drug.